Universidade de Brasília
Faculdade de Tecnologia
Departamento de Engenharia Mecânica

Roll-Off Displacement and Esophageal Protection in Hepatic and Cardiac Radiofrequency Ablation: Tissue Impedance and Temperature Control Based on Bioinspired PID Controller

Rafael Mendes Faria

TESE DE DOUTORADO

PROGRAMA DE PÓS-GRADUAÇÃO EM SISTEMAS MECATRÔNICOS

Brasília

2024

Universidade de Brasília
Faculdade de Tecnologia
Departamento de Engenharia Mecânica

Deslocamento do Roll-Off e Proteção Esofágica na Ablação por Radiofrequência Hepática e Cardíaca: Controle da Impedância Tecidual e Temperatura com Base no Controlador PID Bioinspirado

Rafael Mendes Faria

Tese de Doutorado submetida ao Departamento de Engenharia Mecânica da Universidade Brasília como parte dos requisitos necessários para a obtenção do grau de Doutor em Sistemas Mecatrônicos.

Orientadora: Profª. Drª. Suélia de Siqueira Rodrigues Fleury Rosa

Brasília
2024

Faria, Rafael Mendes .
F769r Roll-Off Displacement and Esophageal Protection in Hepatic and Cardiac Radiofrequency Ablation: Tissue Impedance and Temperature Control Based on Bioinspired PID Controller / Rafael Mendes Faria; orientadora Suélia de Siqueira Rodrigues Fleury Rosa. -- Brasília, 2024.
186 p.

Tese de Doutorado (Programa de Pós-Graduação em Sistemas Mecatrônicos) -- Universidade de Brasília, 2024.

1. Fibrilação Atrial. 2. Otimizador Lobo Cinzento. 3. Carcinoma Hepatocelular. 4. Otimização por Enxame de Partículas. I. Rosa, Suélia de Siqueira Rodrigues Fleury , orient. II. Título

Universidade de Brasília
Faculdade de Tecnologia
Departamento de Engenharia Mecânica

Roll-Off Displacement and Esophageal Protection in Hepatic and Cardiac Radiofrequency Ablation: Tissue Impedance and Temperature Control Based on Bioinspired PID Controller

Rafael Mendes Faria

Tese de Doutorado submetida ao Departamento de Engenharia Mecânica da Universidade Brasília como parte dos requisitos necessários para a obtenção do grau de Doutor em Sistemas Mecatrônicos.

Trabalho aprovado. Brasília, 07 de setembro de 2024:

Profª. Drª. Suélia de Siqueira Rodrigues Fleury Rosa, UnB/FGA
Orientador

Prof. Dr. Adson F. Rocha, UnB/FT/ENE
Examinador interno

Prof. Dr. Daniel Mauricio M. Arboleda, UnB/FGA
Examinador interno

Prof. Dr. Allisson L. de Oliveira, IFTM (Paracatu, Brazil)/Department of Electrical Engineering
Examinador externo

Prof. Dr. Ícaro dos Santos, MSOE (MKE, USA)/Depart. of Electrical Engineering
Examinador externo

Brasília
2024

Dedico este trabalho ao meu querido pai, que nunca
mediu esforços para me proporcionar uma educação de qualidade,
e à minha querida mãe, que está sempre de joelhos orando a Deus Pai
para que eu possa alcançar o título de Doutor.

Acknowledgements

First and foremost, I would like to express my gratitude to God for giving me the strength to overcome all battles, and with His mighty Arm, helped me triumph. Furthermore, I am thankful for the opportunity to be studying in the Postgraduate Programme in Mechatronic Systems at the University of Brasília.

I would also like to extend my immense gratitude to Drª. Suélia de Siqueira Rodrigues Fleury Rosa, UnB/FT/ENM, my dear advisor, for guiding me throughout the first half of this doctoral journey and for continuing to stand by my side, encouraging me, and holding my hand in this grand adventure. I consider you like a mother figure in the academic realm.

I am deeply thankful to my parents for all their support and prayers, enabling me to be here in this moment defending this qualification, and to my girlfriend Gabriela for her unwavering support and companionship.

I would also like to thank my great friend Allisson for encouraging me to enter this institution and pushing me forward. Similarly, I am grateful to my steadfast journey companion Kléríston for taking on this challenge with me and combining strengths, from the trips to the academic productions.

I express my gratitude to my close friend Ana Karoline for her partnership and assistance during this academic journey. May our partnership endure for a long time, and let's "go" on producing abundantly!

Lastly, I would like to thank all my colleagues at the BioEngLab for their companionship, especially the co-authors of the studies developed during this doctoral thesis.

“Mas os que esperam no Senhor
renovarão as suas forças, subirão com
asas como águias, correrão e não se
cansarão, caminharão e não se fadigarão.”
(Isaías 40:31)

Abstract

Introduction: Radiofrequency Ablation (RFA) is a widely used minimally invasive medical procedure for treating electrophysiological disorders and dysfunctional tissues, such as tumors. The method involves inserting a probe with an electrode into the patient's body, where the application of radiofrequency generates heat, causing necrosis in the tissue and resolving the disorder. However, RFA carries risks, such as overheating and complications related to temperature distribution in the target tissues and adjacent tissues, which can lead to severe outcomes like esophageal fistula in cardiac RFA. The roll-off phenomenon, characterized by the vaporization of tissue fluids and an increase in impedance, can compromise the success of the procedure, making it less effective and more dangerous. Given the critical nature of these procedures, the search for strategies employing controllers that prevent overheating and efficiently cover more tissue is of utmost importance. These technological advancements would not only improve the safety of the procedure but also increase its efficacy by reducing the risk of complications and providing a more comprehensive solution for treating cardiac and hepatic conditions. **Objectives:** This research proposes an innovative approach to mitigate the effects of roll-off by developing a bio-inspired dynamic control system. The strategy includes optimizing PID controllers using the Grey Wolf Optimizer (GWO) and Particle Swarm Optimization (PSO) algorithms. The main objective is to enhance cardiac and hepatic RFA by expanding the coagulation area, reducing procedure time, and decreasing tumor recurrence and the development of esophageal fistulas. **Methodology:** The research was structured into three main studies. The first study consisted of a systematic review, conducted following the PRISMA methodology, under the PROSPERO protocol registered under number CRD42022340100. The review was designed to identify gaps in the literature and gather the most current evidence on RFA, which served as the basis for the physiological data used in subsequent simulations. Studies involving liver, heart, or thyroid gland ablation using in vivo, ex vivo, or in silico techniques were considered. The databases searched included Pubmed (n = 958), Scopus (n = 581), Embase (n = 68), Science Direct (n = 21), Web of Science (n = 181), CINAHL Ebsco (n = 125), and IEEE (n = 333), and studies published in the last ten years, in English and Portuguese, were selected. The systematic review selected 29 studies after screening 1078, providing a comprehensive view of the electrical, thermal, and dynamic parameters in RFA procedures. The second study involved developing a PSO-tuned PID controller applied in ex vivo experiments with porcine liver, demonstrating efficacy in controlling tissue impedance during hepatic ablation, preventing roll-off, and ensuring greater precision in the procedure. The third study employed three-dimensional simulations in COMSOL® software to model temperature distribution during cardiac ablation, using a PID controller tuned by the GWO algorithm. This controller successfully regulated temperature, avoiding overheating of adjacent tissues, such as the esophagus, thereby reducing the risk of severe complications. **Results:** The thesis generated a systematic review that formed

the basis for subsequent experiments, identifying best practices and gaps in the literature. In the second study, the PSO-tuned PID controller proved effective in controlling impedance during hepatic ablation, preventing roll-off, and ensuring a larger ablation area. The third study, using GWO to tune the PID in cardiac ablation simulations, showed that the strategy was effective in controlling temperature distribution, especially in protecting against the emergence of esophageal fistulas. **Conclusion:** The research presented in this thesis not only advances knowledge on the optimization of RFA procedures but also introduces innovative solutions for the precise control of impedance and tissue temperature, critical aspects for the efficacy and safety of this procedure. The integration of computational modeling, PID controller optimization through advanced algorithms like GWO and PSO, along with experimental validation, results in a robust approach. The results promise to significantly expand the coagulation area, reduce procedure time, and minimize tumor recurrence. By avoiding severe complications such as overheating and the roll-off phenomenon, this research provides concrete advances that can be directly applied in cardiac and oncological applications, representing a valuable contribution to the development of safer and more effective approaches to treating complex medical conditions.

Keywords: Atrial Fibrillation. Grey Wolf Optimizer. Hepatocellular Carcinoma. Particle Swarm Optimization.

Resumo

Introdução: A Ablação por Radiofrequência (RFA) é um procedimento médico minimamente invasivo amplamente utilizado para tratar distúrbios eletrofisiológicos e tecidos disfuncionais, como tumores. O método envolve a inserção de uma sonda com um eletrodo no corpo do paciente, onde a aplicação de radiofrequência gera calor, causando necrose no tecido e resolvendo o distúrbio. No entanto, a RFA pode apresentar riscos, como o superaquecimento e complicações relacionadas à distribuição de temperatura nos tecidos alvos e tecidos adjacentes como, por exemplo, acarretar a fístula esofágica na RFA cardíaca. O fenômeno roll-off, caracterizado pela vaporização dos fluidos teciduais e aumento da impedância, pode comprometer o sucesso do procedimento, tornando-o menos eficaz e mais perigoso. Dada a natureza crítica desses procedimentos, a busca por estratégias que empreguem controladores que não provoquem superaquecimento e que possam abranger mais tecido de forma eficiente é de suma importância. Esses avanços tecnológicos não apenas melhorariam a segurança do procedimento, mas também aumentariam sua eficácia, reduzindo o risco de complicações e proporcionando uma solução mais abrangente para o tratamento de condições cardíacas e hepáticas. **Objetivos:** Esta pesquisa propõe uma abordagem inovadora para mitigar os efeitos do roll-off por meio do desenvolvimento de um sistema de controle dinâmico bioinspirado. A estratégia inclui a otimização de controladores PID utilizando os algoritmos Grey Wolf Optimizer (GWO) e Particle Swarm Optimization (PSO). O objetivo principal é aprimorar a RFA cardíaca e hepática, expandindo a área de coagulação, reduzindo o tempo de procedimento, diminuindo a recorrência tumoral e do desenvolvimento de fístulas esofágicas. **Metodologia:** A pesquisa foi estruturada em três estudos principais. O primeiro estudo consistiu em uma revisão sistemática, realizada seguindo a metodologia PRISMA, sob o protocolo PROSPERO registrado sob o número CRD42022340100. A revisão foi projetada para identificar lacunas na literatura e coletar as evidências mais atuais sobre a RFA, que serviram de base para os dados fisiológicos usados nas simulações subsequentes. Foram considerados estudos que envolvem ablação de fígado, coração ou glândula tireoide, utilizando técnicas in vivo, ex vivo ou in silico. As bases de dados pesquisadas incluíram Pubmed (n = 958), Scopus (n = 581), Embase (n = 68), Science Direct (n = 21), Web of Science (n = 181), CINAHL Ebsco (n = 125), and IEEE (n = 333), e foram selecionados estudos publicados nos últimos dez anos, em inglês e português. A revisão sistemática selecionou 29 estudos após triagem de 1078, proporcionando uma visão abrangente dos parâmetros elétricos, térmicos e dinâmicos em procedimentos de RFA. O segundo estudo envolveu o desenvolvimento de um controlador PID sintonizado pelo PSO, aplicado em experimentos ex vivo com fígado de porco, demonstrando eficácia no controle da impedância tecidual durante a ablação hepática, prevenindo o roll-off e garantindo maior precisão no procedimento. O terceiro estudo empregou simulações tridimensionais no software COMSOL® para modelar a distribuição de temperatura durante a

ablação cardíaca, utilizando um controlador PID sintonizado pelo algoritmo GWO. Este controlador foi capaz de regular a temperatura com sucesso, evitando o superaquecimento de tecidos adjacentes, como o esôfago, e, assim, reduzindo o risco de complicações graves. **Resultados:** A tese gerou uma revisão sistemática que formou a base para os experimentos subsequentes, identificando as melhores práticas e lacunas na literatura. No segundo estudo, o controlador PID sintonizado pelo PSO demonstrou ser eficaz em controlar a impedância durante a ablação hepática, prevenindo o roll-off e garantindo uma maior área de ablação. O terceiro estudo, utilizando o GWO para sintonização do PID em simulações de ablação cardíaca, mostrou que a estratégia foi eficaz em controlar a distribuição de temperatura, especialmente na proteção contra o surgimento da fístula esofágica. **Conclusão:** A pesquisa apresentada nesta tese não só avança o conhecimento sobre a otimização de procedimentos de RFA, como também introduz soluções inovadoras para o controle preciso da impedância e da temperatura tecidual, aspectos críticos para a eficácia e segurança desse procedimento. A integração de modelagem computacional, otimização de controladores PID através de algoritmos avançados como o GWO e o PSO, juntamente com a validação experimental, resulta em uma abordagem robusta. Os resultados prometem expandir significativamente a área de coagulação, reduzir o tempo de procedimento e minimizar a recorrência tumoral. Ao evitar complicações graves, como o superaquecimento e o fenômeno de roll-off, essa pesquisa proporciona avanços concretos que podem ser diretamente aplicados em aplicações cardíacas e oncológicas, representando uma contribuição valiosa para o desenvolvimento de abordagens mais seguras e eficazes no tratamento de condições médicas complexas.

Palavras-chave: Fibrilação Atrial. Otimizador Lobo Cinzento. Carcinoma Hepatocelular. Otimização por Enxame de Partículas.

List of Figures

List of Tables

List of abbreviations and acronyms

AF	Atrial fibrillation	90
AIOFL	Active Input-Output Sliding Mode Control	59
ANOVA	Analysis of variance	82
ARFACTA	Ablação por Radiofrequência com Ajuste de Frequência e Controle de Temperatura para Ablação Abrangente e Eficiente	29
ARX	Autoregressive representation with exogenous inputs	65
CAPES	Coordenação de Aperfeiçoamento de Pessoal de Nível Superior	35
EP	Electroporation	49
FEM	Finite Element Method	27
FIT	Fit estimation data	66
GWO	Grey Wolf Optimizer	28
HCC	Hepatocellular carcinoma	55
IAE	Integral of the absolute error	98
ISE	Integral of the squared error	98
ITAE	Integral of the absolute error weighted over time	98
ITSE	Integral of the absolute error weighted over time	98
LaB	Biomedical Engineering Laboratory	62
MFB	Modified Frequency Bat Algorithm	59
NNFOPID	Nonlinear fractional-order neural network-based controller	59
NNPID	Neural nonlinear PID controller	59
NP	Number of poles	97
NRMSE	Normalized root mean squared error	66
NUPITEC	Núcleo de Propriedade Intelectual	117
NZ	Numer of zeros	97
OF	Objective function	68
PEM	Prediction error minimization	64
PI	Proportional-integral	84

PICO Population, Intervention, Comparison, Outcome and Study Design 38

PID Proportional-integral-derivative 28

PID Proportional-integral-derivative 59

PRISMA Preferred Reporting Items for Systematic Reviews and Meta-Analyses 37

PROSPERO International prospective register of systematic reviews 37

PSO Particle Swarm Optmization 28

RF Radiofrequency 27

RFA Radiofrequency ablation 26

RFCA Radiofrequency Cardiac ablation 44

RMS Root mean square 64

ROB Risk of Bias 50

SI System Identification 64

SOFIA Software of Intense Ablation 29

SUS Sistema Único de Saúde 29

TF Transfer function 64

UnB University of Brasília 62

VERA Continuous monitoring system for hospital equipment 63

List of symbols

k	Time instant (ARX) or iteration index (PSO)	65
$k(s)$	PID controller TF	67
K_d	Derivative gain	61
K_i	Integral gain	61
K_p	Proportional gain	61
$MaxIter$	Maximum number of iterations	70
N	Number of samples (ARX) or number of dimensions (PSO)	65
na and nb	non-negative integers indicating the order of the model	65
p	$p = 1+\max(na,nb)$	65
$P(s)$	Plant continuous-time TF	74
$P_d(z)$	Plant discrete-time TF	74
$pbest$	Personal best position	70
Q_m	Metabolic heat generation rate	94
Q_p	Heat lost in blood perfusion	94
R^2	Coefficient of determination	66
r_1 and r_2	Rondom numbers	70
S	Number of the particles	70
$SysOvr$	System overshoot	68
T_q	Heat source generated by RF	94
T_s	Time sampling	97
u	Input Values	64
u_0	Blood velocity	94
V_{max}	Maximum velocity	70
V_{min}	Minimum coefficient	70
X_p	Position vector of the prey in GWO	100
X_{max}	Maximum position	70
X_{min}	Minimum position	70
y	Output Values	64
$\mathbf{E}$	Electric field	93
$\mathbf{J}$	Current density	93

a	GWO Parameter	100
c	Specific heat	94
F	Force	94
k	Thermal conductivity	94
P	Pressure	94
T	Temperature	94
V	Volts	61
W	Watts	63
Z	Impedance	28

Contents

1 Introduction

In the realm of minimally invasive thermo-surgical medicine, radiofrequency ablation (RFA) stands out as a widely employed technique, serving both primary and metastatic treatment of hepatic, renal, pulmonary, osseous, cerebral neoplasms, and even interventions for cardiac arrhythmias [1, 2]. This conventional methodology relies on the utilization of an active electrode, incorporated at the extremity of a percutaneous catheter, which is introduced into the affected area aided by imaging modalities such as ultrasound and computed tomography [3].

Hepatocellular carcinoma (HCC) is the most common type of primary liver cancer, accounting for approximately 75% of all liver cancer cases. It is estimated that HCC is the fourth most common cause of cancer-related death worldwide, with over 700,000 deaths annually . RFA has been widely used in treating HCC, particularly in patients who are not surgical candidates. Studies show that RFA can achieve local control rates of over 80% in small tumors, with a five-year survival rate of up to 60% . However, the procedure's efficacy may be limited by tumor size and proximity to critical vascular structures [4, 5].

In cardiology, RFA is an essential technique for managing atrial fibrillation (AF), the most common sustained cardiac arrhythmia, affecting approximately 33 million people worldwide. AF is associated with a significantly increased risk of stroke and heart failure, contributing to high morbidity and mortality rates. RFA treatment has proven effective in reducing AF recurrence, especially in patients with paroxysmal AF, where studies indicate success rates of 60% to 80% after one year. Additionally, using RFA for treating AF can significantly reduce long-term healthcare costs by decreasing the need for frequent hospitalizations and the risk of severe complications such as stroke [6–8].

By administering a high-frequency alternating current in RFA (approximately 500 kHz), a coagulative region is established, characterized by thermal lesion capable of eradicating malignant tissue through temperature elevation (above 50°C). This phenomenon stems from protein denaturation, compromising crucial mitochondrial enzymes and nucleosomal histone complexes [9, 10]. The current flows between the active electrode and a large dispersive electrode situated at the patient's posterior region, thereby completing the electrical circuit. However, the formation of the thermal lesion is confined to the target region due to the heightened current density in that locale [11]. In this scenario, the temperature in the tissue immediately adjacent to the active electrode tends to rapidly escalate until intracellular fluids transition to the vapor phase.

As the procedure progresses, tissue fluid vaporization occurs, signaling the critical roll-off point [12]. This realization highlights the importance of maintaining the maximum

temperature below 100°C during the intervention to prevent tissue carbonization, sudden impedance spikes, and the formation of undesirable vapor bubbles [13]. Procedural continuity is closely tied to tissue impedance, as a sharp increase in impedance results in a significant drop in power, potentially leading to an unintentional halt in the procedure. Additionally, vapor bubble formation poses substantial risks; when pressure from trapped vapor within the tissue becomes excessive, a dangerous rupture can occur. This is especially concerning when performing the procedure on the delicate myocardial wall during cardiac RFA, where there is also an increased risk of blood clot formation [14, 15].

In this context, the application of computational models has emerged as a pertinent tool for RFA research. The success of these studies derives from the incorporation of realistic models that holistically address electrical conduction, heat transfer, and fluid dynamics [14, 16]. The Finite Element Method (FEM) approach is extensively employed to model the propagation of thermal energy generated by Joule effect within tissues undergoing RFA. However, it's worth noting that several studies present models that don't faithfully replicate the power control algorithms employed in clinical devices [17, 18].

The delivery of power from the generators during RFA is guided by three control methodologies: power control, impedance control, and temperature control [13]. In the first case, a constant power is supplied to the electrode, requiring manual intervention for adjustment [19]. In contrast, impedance and temperature control are based on feedback from sensors and control systems. Temperature is regulated based on a reference value set by the operator, and the output power is adjusted to maintain it at the desired level [1].

Specifically, the impedance control mode is activated when the measured impedance between the active electrode and the dispersive electrode exceeds a predefined threshold, resulting in temporary shutdown of the radiofrequency (RF) generator, followed by a restart after a specified time interval [2]. In addition to control approaches, the roll-off point can be shifted through the use of electrodes irrigated with cooled saline solutions. This technique is an established clinical practice, facilitating a continuous flow of chilled saline solution through small orifices at the tip of the active electrode [15, 20].

Despite the substantial number of studies on cooled electrodes, many of these works do not sufficiently detail the protocols employed. Some studies reduce the applied power in the model until a limit is reached where tissue temperature does not reach the roll-off point [2]. Moreover, a literature analysis suggests that control methods, controller designs, and tuning are not adequately addressed in the context of RFA.

This present text, presented as a doctoral thesis, aims to conduct a systematic literature review, analyze, propose, and simulate effective control strategies for RFA techniques applied to cardiac and hepatic procedures. From an interdisciplinary perspective, Fig. 1 illustrates the proposed investigation, which will encompass all variables involved in the RFA process, supported by ex-vivo assays and in-silico simulations. Multifactorial analyses

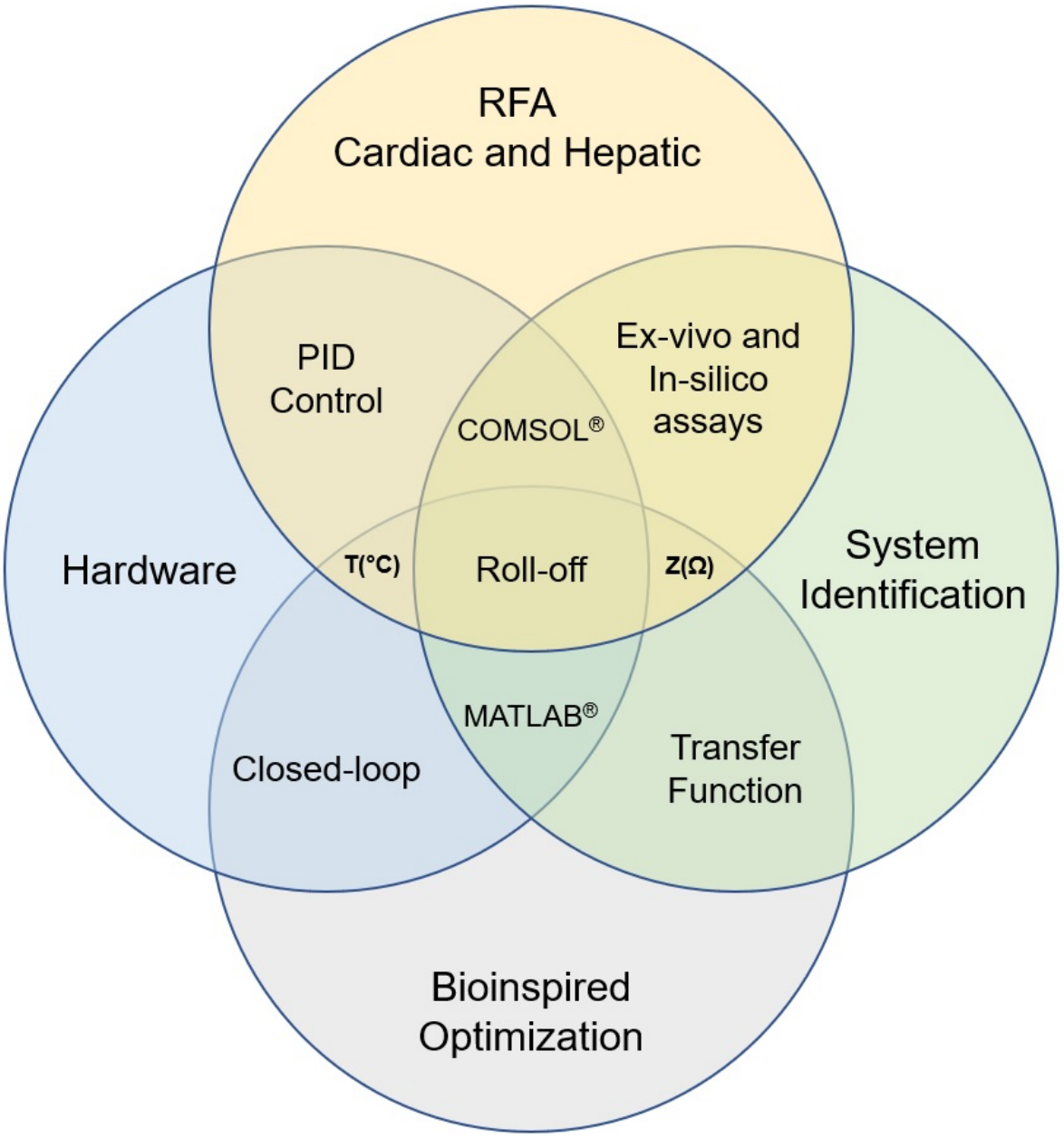

Figure 1 – Graphical Methodology.
Souce: Own authorship

will be conducted, covering electrical and thermal aspects, as well as fluid dynamics and mechanics related to computational modeling of blood perfusion and tissue movement, employing tools such as COMSOL® Multiphysics (COMSOL Inc., Burlington, MA, EUA)and MATLAB® (MathWorks, Natick, MA). Furthermore, system identification techniques will be applied to determine the most accurate mathematical model and to implement proportional-integral-derivative (PID) control, as well as bioinspired algorithms like Particle Swarm Optimization (PSO) and Grey Wolf Optimizer (GWO) to enhance control and mitigate the roll-off effect.

The present study materializes the culmination of the SOFIA® project (Software of Intense Ablation), conducted at the University of Brasília (UnB), whose results have been

remarkable and inspiring [21]. Stemming from a collaboration established with the Ministry of Health in 2015, the project led to the development of an RFA device, with the noble objective of integrating it into the Unified Health System (SUS). One of the foremost goals of this endeavor is to address the shortage of domestic RFA devices, thereby reducing the need for international dependence. The subsequent year, in 2016, SOFIA® underwent in vivo tests on pigs, in an effort to assess its performance in a real clinical context.

In this scenario, [22] undertook a detailed investigation of the equipment's performance concerning hepatic tumors in rats, simultaneously closely examining the cytotoxicity associated with the used electrode. SOFIA® not only represented a technological milestone but also gave rise to a diverse array of academic productions, encompassing scientific articles, master's dissertations, doctoral theses, undergraduate theses, undergraduate research projects, book chapters, and contributions to renowned congresses.

Initially conceived to tackle the challenges of hepatocellular carcinomas, the SOFIA® equipment has experienced notable progress, culminating recently in the creation of the ARFACTA system (Radiofrequency Ablation with Frequency Adjustment and Temperature Control for Comprehensive and Efficient Ablation). The ARFACTA, an evolution of SOFIA®, represents a significant leap aligned with innovation, becoming a benchmark instrument for ablation in cases of hepatic cancer and cardiac arrhythmia treatment. Endowed with advanced monitoring and control features, the ARFACTA enables the execution of precise ablations, centered on patient well-being.

2 Thesis Contributions and Textual Organization

The primary goal of this research is the optimization of the temperature and impedance control system in the ARFACTA device through the integration of bioinspired algorithms, with a particular focus on refining the PID controller's tuning process. This approach is designed to precisely regulate the variables linked to the roll-off phenomenon and the prevention of esophageal fistulas, addressing the critical challenges inherent to RFA.

The core contributions of this study are illustrated in Fig. 2 and are further detailed in Chapter 3. The comprehensive scope of this research is intended to drive significant advancements in the field of RFA, improving the precision, efficacy, and safety of treatments while adhering to the highest standards of patient care.

This research culminates in a thesis that directly explores the application of evolutionary algorithms, specifically PSO and GWO, within the hardware of the ARFACTA device, which includes components such as the ATmega®328 and ESP®-01. These enhancements are aimed at elevating the protocols for cardiac and hepatic ablation procedures. The expected outcomes include the creation of larger ablation volumes, shorter procedural times, reduced tumor recurrence and AF rates, and the prevention of esophageal fistulas and roll-off displacement. These improvements will be achieved through the stabilization of impedance and temperature during the ablation process.

The structure of this thesis is organized into six chapters, each contributing to a coherent and comprehensive presentation of the research. Chapter 1, the current chapter, and the subsequent one establish the context and outline the objectives of this study. Chapters 4, 5, and 6 present the findings of this investigation, each structured as independent sections supported by articles that have been submitted to and reviewed by experts in peer-reviewed scientific journals.

Specifically, Chapter 4 employs a systematic literature review approach to explore mathematical modeling techniques and the control of temperature and impedance in RFA. A thorough research process was conducted across major academic databases, initially yielding 828 articles. The selection process was guided by the PROSPERO protocol [23], with eligibility and exclusion criteria applied to refine this initial set into a more focused and relevant collection of studies, providing a robust foundation for the research presented in this thesis.

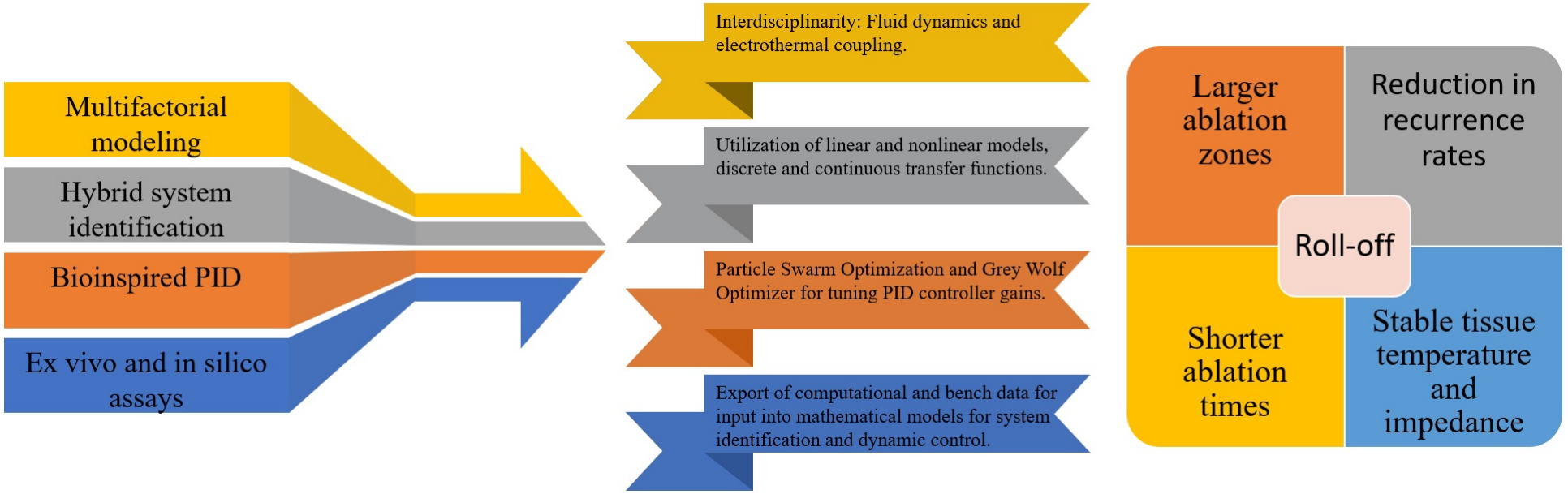

Figure 2 – Contributions of this thesis to the advancement of the control of variables directly related to the roll-off.
Source: Own authorship

Fig. 3 provides a visual representation of the research structure and flow, emphasizing the significance of each chapter in this comprehensive journey of exploration and discovery. The meticulous organization of these components ensures that every critical aspect of the study is thoroughly examined, thereby contributing meaningfully to the body of knowledge in the field of RFA and its clinical applications.

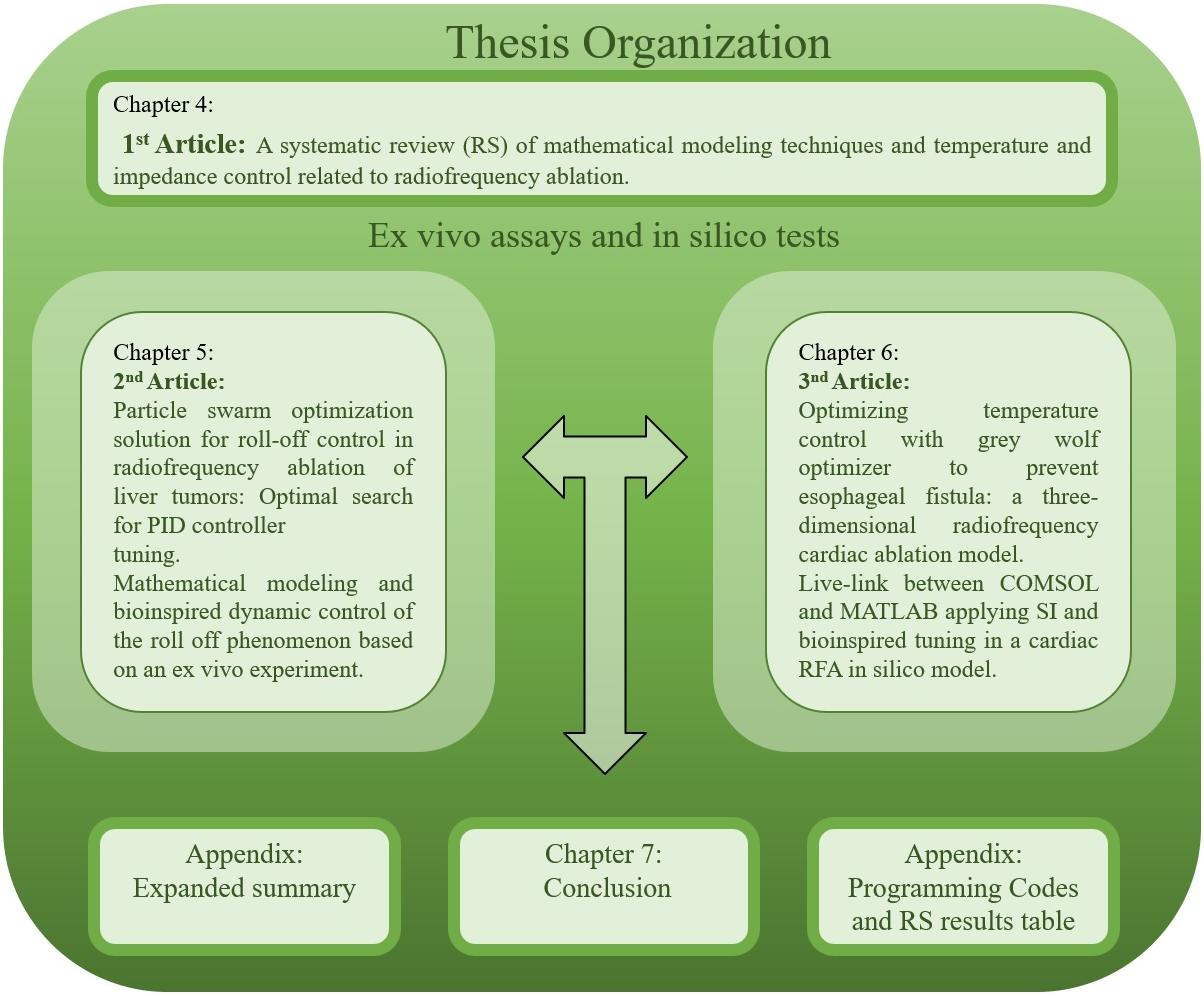

Figure 3 – Textual Organization.
Source: Own authorship

The chapter 5 delves into the phenomenon of roll-off in relation to RFA applied in the hepatic context. This section of the research aims to propose a mathematical model for the tissue impedance dynamics during the RFA procedure, with a specific focus on system identification techniques. Data obtained from ex vivo experiments provided the basis for constructing this model. Additionally, the implementation of dynamic control was explored by inserting a PID controller, whose tuning will be refined through the bioinspired PSO algorithm.

Chapter 6 delves into an in silico approach, employing COMSOL® and MATLAB® software to model a cardiac radiofrequency ablation (RFCA) environment. The primary objective was to explore potential scenarios in which the ablative procedure might result in

the formation of esophageal fistulas, a severe and undesirable complication. To achieve this, the environment was modeled using governing equations that describe electrical, thermal, and fluid dynamics phenomena. These equations were solved using the finite element method, generating a comprehensive dataset. This data was subsequently integrated into MATLAB® to facilitate system identification—a crucial step for analyzing and optimizing the ablative process.

Additionally, in chapter 6, a type K thermocouple was modeled within MATLAB® and incorporated into the closed-loop control system implemented in Simulink®. The GWO algorithm was then applied to fine-tune the PID controller parameters. This fine-tuning was essential to ensure the safety of the ablative procedure, preventing the creation of conditions that could lead to the formation of esophageal fistulas, thereby safeguarding the efficacy and safety of the treatment.

The culmination of this journey is presented in Chapter 7, where the results, insights, and achievements are skillfully condensed, reflecting the depth and significance of this study. For a detailed overview, the Extended Abstract is provided in Appendix A, offering readers an accessible and comprehensive synthesis of the research.

Additionally, the programming codes used, as well as the tables of results from the systematic review, are included in the subsequent appendices, ensuring transparency and providing additional technical support for the work conducted. The academic outputs associated with this research are duly documented in Annex A, contributing to a broader and more robust contextualization of this work within the academic and scientific landscape.

3 Objectives

The primary objective of this doctoral thesis was to develop a bioinspired dynamic control system aimed at managing roll-off displacement in hepatic ablation and preventing esophageal fistula during RFCA. This was achieved through ex vivo and in silico experiments, along with system identification techniques, to obtain larger ablation volumes, reduce procedure times, and maintain stable temperature and impedance at a predetermined set point.

3.1 Specific objectives

- **Systematic Literature Review:** Conduct a comprehensive literature review to investigate the current state of the art in mathematical modeling techniques and control systems specific to cardiac and hepatic RFA procedures;
- **Model Simulation:** Develop and simulate integrated models encompassing electrical, thermal and fluid dynamics, for both cardiac and hepatic RFA procedures, considering conditions of blood perfusion;
- **Mathematical Model Proposal:** Propose mathematical models through system identification techniques focusing on the behavior of tissue impedance and temperature during cardiac and hepatic RFA procedures, utilizing data derived from ex vivo and in silico experiments;
- **Dynamic Control Establishment:** Establish dynamic control by tuning a PID controller using the bioinspired PSO and GWO algorithm.
- **In Silico Reproduction:** Reproduce in silico assays by linking COMSOL® and MATLAB® software, employing FEM, system identification, and evolutionary algorithms to control temperature and impedance in cardiac and hepatic RFA procedures.

4 Systematic Review

This chapter presents the systematic review article titled "Advancements in Radiofrequency Ablation: A Systematic Analysis of Mathematical Modeling Techniques and Temperature Control Strategies," registered in the PROSPERO platform under the number CRD42022340100. This review constitutes a part of the studies developed throughout this doctoral research and is intended for submission to the "Computer Methods and Programs in Biomedicine" journal (Elsevier, ISSN 0169-2607), known for its A1 Qualis CAPES ranking, CiteScore of 10.1, and Impact Factor of 6.1.

The objective of this systematic review was to explore technological advancements in computational and mathematical modeling related to temperature control strategies in RFA procedures. Electronic databases utilized for the literature search included PubMed, IEEE, Cinalh/EBSCO, Scopus, Science Direct, and Web of Science. After eliminating duplicates, 828 articles were selected for the Phase 01 screening, which involved assessing the studies based on their titles and abstracts. Following this initial screening, 82 papers were chosen for full-text reading. Applying eligibility criteria, 29 studies were included in this review.

This study critically evaluated a plethora of research endeavors that employed computational simulations to analyze the RFA technique in medical procedures, with a particular focus on cardiac treatments and cancer therapies. This review stands as an integral bibliographical component of this qualification text, presenting the state of the art in pivotal studies focused on mathematical models elucidating RFA, alongside temperature and impedance control techniques.

4.1 Introduction

RFA is a minimally invasive medical procedure widely employed to address electrophysiological disorders and dysfunctional tissues. In this technique, a probe is inserted into the patient's body, with an electrode positioned in the target tissue. By applying RF energy through the electrode, heating occurs, leading to tissue necrosis and subsequent reduction or resolution of the specific disorder [24–26].

Despite being relatively safe, RFA presents risks related to tissue overheating, temperature and energy variation, potentially resulting in high mortality rates and unfavorable patient outcomes. According to [24], researchers investigated the effects of different active and grounding electrode lengths in bipolar RFA. Two scenarios were considered: Case 1 featured a longer active electrode than the grounding electrode, while Case 2 had the opposite configuration. It was observed that as the distance decreased, heating became faster,

exposing the tissue to elevated temperatures for more extended periods. The shorter active electrode length resulted in quicker heating, as the electric potential converged around this electrode, leading to more intense Joule heating.

In accordance with [24, 26–28], temperature distribution in tissue follows the gradients of electric potential, with higher temperatures around the shorter active electrode. Thermal coagulation is observed exclusively around this shorter active electrode. Increasing the initial applied voltage can enlarge the coagulation volume, except when probe lengths are equal. Hence, the lengths of electrodes and applicators play a crucial role in the efficacy and extent of thermal coagulation during bipolar RFA.

Particularly, the evaluation of temperature's impact in RFA is significant and influences various procedural aspects. Literature such as [29–31] highlights its therapeutic effect, as temperature is primarily responsible for tissue destruction during ablation. Controlled temperature elevation causes thermal coagulation, resulting in cellular death and the formation of a necrotic lesion at the desired site. Researchers have explored the potential to control the degree of thermal ablation, opening avenues for personalized cancer treatments and combined therapies that yield novel outcomes and aspects to investigate.

Indeed, temperature governs the coagulation volume, as temperature increments can lead to larger volumes, which is desirable for ensuring treatment efficacy [29]. Another factor is the safety of surrounding tissues, where rigorous temperature control is pivotal in avoiding risks during ablation. Tissue overheating can lead to severe complications such as bleeding, perforation, or fistula formation in adjacent structures and organs [24, 27, 30, 31]. Procedure duration, which induces heating rates and affects ablation efficacy, can influence the time taken for ablation completion. Higher temperatures can accelerate the coagulation process, reducing the required procedure time, but can lead to little clinically explored roll-off curves [25, 30–32].

From an application standpoint, predicting lesion formation through temperature control is essential for obtaining well-defined and predictable lesions. Improper temperatures can result in irregular or suboptimal lesions, affecting treatment efficacy [31, 32]. In terms of the procedure, the application of high temperatures may lead to increased discomfort and pain for the patient during and after the procedure.

A proper management of temperature can mitigate these undesirable effects. Hence, clinical outcomes derived from temperature application during ablation directly impact the procedure's success rate and disease recurrence. Through post-operative monitoring, the treated area can be assessed for ablation efficacy and potential complications [25–27, 30–32].

Further studies aim to deepen the understanding of precise temperature control, a critical element for ablation success, ensuring treatment effectiveness while minimizing patient risks. The demand for short-term interactions with the target tissue, allowing for

spatial-temporal-thermal targeting with minimal invasiveness in contrast to other treatments and interventions, is essential knowledge for appropriate utilization of techniques and monitoring equipment, ensuring safe and successful ablation.

The utilization of in silico computational modeling as a selected strategy stands as a powerful and alternative tool to enhance the reduction of therapeutic doses and minimize adverse effects of RFA. Particularly in analyses focused on the target temperature to be reached in the relevant biological tissue and the exposure time of the interaction, computational modeling presents significant benefits [11, 33]. Through computational modeling, it becomes possible to simulate and predict thermal interactions in the tissue, allowing for a more precise and personalized treatment planning. By adjusting parameters such as energy intensity and duration, researchers can optimize RFA efficacy, achieving the desired temperature in the target tissue while reducing unnecessary exposure of healthy tissues [34, 35].

Furthermore, computational modeling can account for tissue heterogeneity, commonly found in clinical scenarios, and consider the effect of neighboring organs or critical structures. This enables the anticipation of potential risk areas and avoidance of undesired damage during the procedure [33, 36]. Another advantage is the possibility of testing various therapeutic scenarios without subjecting patients to invasive experiments or unnecessary treatments. This leads to safer and more efficient planning, ensuring the selection of the most suitable and personalized approach for each patient [11, 36].

In this context, the present study was designed with the objective of investigating advancements through a systematic review, focusing on the analysis of technological progress in computational and mathematical modeling of temperature controllers in RFA procedures, highlighting their significance in enhancing procedure safety and efficacy. We anticipate that this study will contribute to a better understanding of the benefits of modeling and simulation technologies in RFA. It will examine the effects of temperature control during RFA procedures and discuss parameters such as temperature and time, which, when correlated, define the thermal dose, a fundamental determinant of RFA treatment efficacy.

4.2 Methodology

4.2.1 Protocol and Registration

This study was conducted in accordance with the PRISMA (Preferred Reporting Items for Systematic Reviews and Meta-Analyses) guidelines [37] [38]. The protocol for this systematic review was registered with the International Prospective Register of Systematic Reviews (PROSPERO) [23].

For the selection of studies, we employed the web-based reference management

platform Rayyan® (https://www.rayyan.ai), which facilitated the organization of folders corresponding to consulted databases such as Scopus, Science Direct, Cinahl Ebsco, IEEE Xplore, PubMed/MEDLINE, and Web of Science. The thorough examination of study titles and abstracts was carried out in pairs, utilizing the 'Blind ON' feature to ensure objectivity in the selection process.

To conduct bibliometric analysis on the selected studies, we utilized the Bibliometrix library within the RStudio® software, alongside VOSviewer® 1.6.8. These tools were employed for the assessment of scientific production, co-authorship network mapping, and identification of most prevalent keywords. The utilization of these tools facilitated a comprehensive and meticulous examination of the chosen studies.

4.2.2 Eligibility criteria

4.2.2.1 Inclusion Criteria

This systematic review employed the PICO (Population, Intervention, Comparison, Outcome, and Study Design) approach to establish the inclusion criteria for selected studies, adhering to the guidelines proposed by [39]. Studies encompassing adult populations, regardless of gender, with indications for liver, heart, or thyroid gland ablation procedures, as well as simulations involving biological models of the heart, liver, and thyroid, were considered eligible for inclusion.

For the intervention, studies encompassing in vivo and ex-vivo techniques were incorporated, which included aspects such as tissue thickness, temperature, catheter pressure on tissue, tissue characteristics, temperature gradient related to thermal energy dispersion, and ablation time. In silico studies exploring relevant physical quantities related to the studied tissue, such as volumetric density, specific heat, thermal conductivity, electrical conductivity, temperature, ablation procedure time, catheter pressure on tissue, operational voltage, and device power, were also included.

Selected studies also encompassed randomized clinical trials that addressed samples, intervention and control groups, target organs for ablation, post-procedure lesion rates, and types of catheters. In terms of comparison, studies utilizing 2D/3D catheter methods without contrast were included. The outcomes pertained to temperature reduction achieved through control actions on the dissipated energy during ablation. Temperature reduction was assessed both at the catheter and within the target tissue through mathematical modeling and the application of controllers.

The selected studies were published in English and Portuguese over a ten-year span, justified by recent advancements in technology and dedicated simulation tools within these contexts. The judicious selection of these criteria enabled a thorough and precise analysis of techniques, equations, and models applied in RFA over the past decade.

4.2.2.2 Exclusion Criteria

Stringent exclusion criteria were applied in the selection of studies included in this systematic review. Firstly, publications such as reviews, letters, personal opinions, book chapters, conference proceedings, and patents were excluded. Subsequently, studies that did not employ techniques to control temperature during the ablation procedure were excluded, as well as those that did not address mathematical modeling and simulations of the catheter's power delivery system and temperature control of tissues adjacent to the target.

Additionally, studies with incomplete computational models and studies on small animals that did not analyze temperature and thermal damage were excluded, along with articles that were not available in full or were not related to the topics of the systematic review. Studies not addressing in vivo, ex vivo models, and randomized clinical trials, as well as articles with low methodological quality, were also excluded. These criteria were employed to ensure the quality and relevance of the studies included in this systematic review.

4.2.3 Information Sources and Search Strategy

To conduct a comprehensive and rigorous investigation, tailored search strategies were developed for major bibliographic databases, including Scopus, Science Direct, Cinahl Ebsco, IEEE Xplore, PubMed/MEDLINE, and Web of Science. The search string can be found in Appendix B. Furthermore, similar studies registered in the PROSPERO database and Cochrane were consulted. The database search was performed without language restrictions in February 2023. To eliminate redundancy, duplicate references were removed using the web-based reference management platform Rayyan®.

4.2.4 Study and Selection

In pursuit of scientific accuracy, the primary author meticulously conducted the reference search in the selected databases and imported their records. Subsequently, a discussion group was organized on an instant messaging application to establish timelines, discuss strategies, and divide the team for the initiation of selection phases.

In the initial phase of reference selection, the authors were anonymously divided into four pairs, as determined by the primary author. The studies were equally distributed among the pairs, who reviewed the titles and abstracts of each article using the 'BLIND ON' feature of the Rayyan® web platform. Subsequently, we selected studies that met the inclusion criteria.

In this stage, we undertook: i) Importation of references from bibliographic databases and removal of duplicates, inaccessible works, and incomplete articles. These references were systematically stored for subsequent analysis; ii) Organization into review groups composed

of RF, SR, AKS, KS, AA, RP, GN, and LB (acronym of the authors' name); iii) Activation of blind study selection, allowing reviewers to analyze article titles and abstracts without knowledge of other authors or journals. This prevents selection bias during the review process; iv) Completion of the first phase involving discussions and resolution of inclusion or exclusion conflicts through the platform, allowing authors to make joint decisions on which studies to include in the review.

In the second phase, the same selection strategy was applied, with pairs anonymously redistributing studies. In this stage, authors read full articles and completed a form designed to extract information related to eligibility criteria. In both phases, pairs convened to discuss conflicts regarding study inclusion or exclusion. In cases of lack of consensus, a third reader was designated as the tiebreaker.

The third phase entailed the extraction of pertinent data, which were organized in a predefined table, describing key points related to the following aspects: study design (in vivo, ex vivo, or randomized controlled trial), studies based on computational simulations modeling cardiac, hepatic, or thyroid ablation, articles highlighting physical properties of tissues, catheters, mathematical modeling, and computational simulations that underpin tissue temperature distribution.

4.2.5 Research Network Analysis

Following the search and study selection process, the extracted data were meticulously tabulated in Excel® spreadsheets to facilitate impact analysis and the identification of research groups worldwide engaged in this field.

To store and manage the conducted bibliographic analyses, we chose to employ Mendeley® software, a robust and dependable tool for organizing references and research files. Additionally, we utilized RStudio® software (via the Bibliometrix library) and VOSviewer® 1.6.8 to conduct in-depth analyses, exploring data such as high-impact journals, influential authors, frequently recurring keywords, and other pertinent information that can be gleaned from the studies.

The central objective of these analyses is to maximize connections between researchers and link them with other prominent authors within this area of study. These tools and methodologies allow us to visually comprehend the research network, its interconnections, and the individual contributions of researchers, thereby providing a comprehensive overview of the scientific landscape at hand.

4.2.6 Data Summarization

The summarization of data from included studies was meticulously conducted by the authors, following a strategy of reading and highlighting, coupled with discussion meetings to

inform the data extraction form adapted from the Methodological Guidelines for Systematic Reviews proposed by the Brazilian Ministry of Health.

In this initial phase, authors, publication year, and the journal where the study was published were identified. Subsequently, study types were detailed, such as in-silico, in-vivo, and randomized clinical trial, alongside specifying the target organ for the ablative procedure and the type of computational tools employed.

Furthermore, data about the type of ablation equipment and accessories, such as electrode type, were added. Additionally, information about the model type, 2D or 3D, and the design in COMSOL® Multiphysics software were included, along with the equations and domains used in simulations.

Finally, the layout and data extraction followed the PRISMA 2009 verification protocol and were written by the study authors. This approach ensures the systematization and transparency of the summarized data, making them ready for analysis and interpretation of the results obtained in the systematic review.

4.2.7 Risk of Bias and Quality in Individual Studies

The quality of included articles was estimated by applying the 12-question tool from the GENERAL RoB Toll form to assess the risk of selection, performance, detection, attrition, and other biases. Items were answered for each study by two reviewers individually, and discrepancies were resolved by a third reviewer. Responses of LOW indicated a low risk of bias, HIGH indicated a high risk of bias, and NO INFORMATION or UNCLEAR indicated that attributing bias was not possible.

4.3 Results

In a bibliometric study conducted on January 24, 2023, using VOSviewer software version 1.6.17, we performed a search in the Pubmed, IEEE, Cinalh/EBSCO, Science Direct, and Web of Science databases using the MeSH terms "Mathematical Models," "Catheter Ablation," "Radiofrequency Ablation," "Ablation Techniques," and "Temperature OR Computer Simulation." A total of 1078 articles were found, excluding 260 duplicates. Fig. 4 illustrates the most frequent keywords found in the articles, categorized into three distinct groups. The lines connecting the terms depict the competitive relationships among them in the analyzed articles. It is evident that the located studies have limited relevance to the thematic focus of the current work. The co-occurrence threshold for these terms was set at a minimum of 30 occurrences.

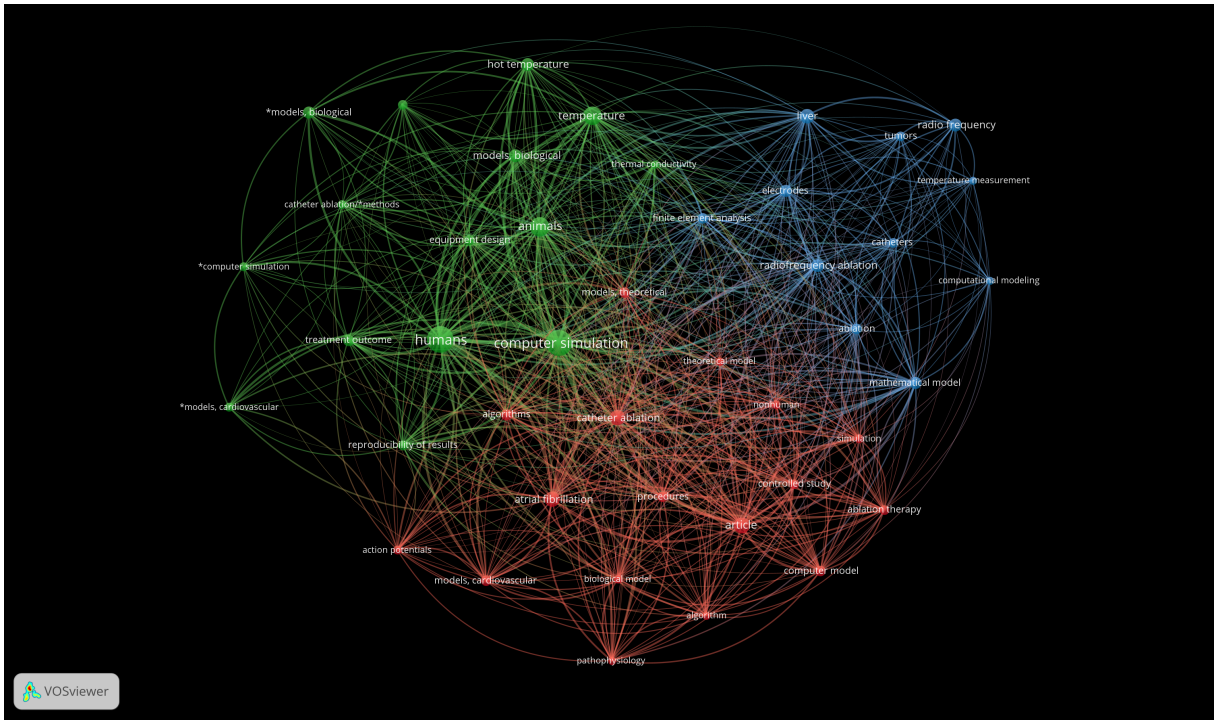

Figure 4 – **Bibliometric Analysis:** Word Map - Bibliometric analysis was conducted using the VOSviewer program version 1.6.17 [40] on 1,078 works published with the search string ("Atrial Fibrillation" AND "Catheter Ablation" OR "Radiofrequency Ablation" OR "Ablation Techniques" AND "Esophageal Fistula" OR "Temperature" AND "Computer Simulation") in the title, abstract, or keywords on January 24^{th}, 2023. The analysis was conducted using a minimum co-occurrence of terms of 30 times and binary counting.
Source: Own authorship

4.3.1 Synthesis of the Results

This systematic review aimed to investigate advancements in the field of temperature control within computational simulations for RFA procedures. A significant contribution of studies was derived from various databases: Pubmed (n = 958), Scopus (n = 581), Embase (n = 68), Science Direct (n = 21), Web of Science (n = 181), CINAHL Ebsco (n = 125), and IEEE (n = 333). After applying a filter to consider articles from the past 10 years, a total of 1088 works were retrieved. The titles and abstracts of these articles were independently reviewed in duplicate, and in cases of disagreement, a third author was consulted. Following the initial screening, 82 articles were selected for full-text reading, which was also done independently and in duplicate. Applying the pre-defined eligibility criteria, 29 articles were selected for inclusion in this review, as depicted in the PRISMA flowchart presented in Fig. 5. A comprehensive table detailing the results of the selected studies for this systematic review is provided in Appendix C (in silico studies) and Appendix D (ex vivo studies).

The execution of computational studies aimed at optimizing and understanding

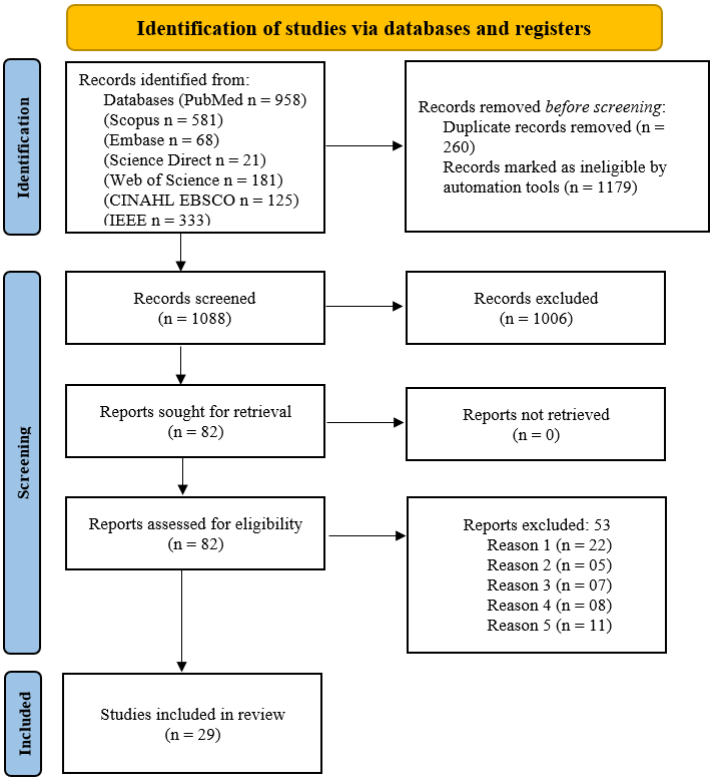

Figure 5 – **PRISMA Flowchart:** Flow diagram of literature search and selection criteria adapted from PRISMA.

Source: Own authorship

RFA processes is of paramount importance to enhance the efficacy and safety of clinical procedures. By analyzing the selected articles in this systematic review, a comprehensive view of the employed approaches, obtained results, and key conclusions related to RFA simulations has been acquired. Each article has provided valuable contributions to understanding the effects of parameter variations in ablation procedures, reflecting advances in the state of the art focused on temperature and impedance control in RFA.

In the study conducted by [41], the analysis of different electrical and thermal parameters revealed a direct influence on the ablation volume in tumors of varying sizes. The utilization of finite element method, along with the implementation of optimization techniques based on Taguchi matrices, facilitated the identification of correlations between parameters and ablation outcomes.

Conversely, the work by [16] addressed the importance of incorporating fluid dynamics into models of irrigated electrode cardiac ablation. By comparing simplified models with more complex approaches that consider fluid dynamics equations, it was demonstrated that the more precise method provides more consistent results in terms of thermal lesion width and tissue temperature.

[42] proposed a catheter model for RFCA, utilizing both experiments and computational simulations to validate the device's performance. A comparison between experimental

and simulated results underscored the relevance of incorporating intricate features, such as the presence of blood vessels, to achieve higher fidelity in the models.

The study by [43] conducted a sensitivity analysis of thermal and electrical parameters in RFA. The use of statistical methods and response surface techniques allowed for the identification of parameter influences throughout the ablation procedure.

Finally, the work by [16] investigated the inclusion of fluid dynamics in three-dimensional models of irrigated electrode cardiac ablation. The simulations enabled an understanding of how blood flow affects heat distribution during ablation.

In summary, the studies covered in this systematic review offer valuable insights into the influence of electrical, thermal, and fluid parameters in RFA. The combination of experimental and computational approaches, along with the application of control system techniques, provides a solid foundation for the development of more effective and safe ablation strategies in clinical procedures. The continuous improvement of these models and methods will contribute to the evolution of RFA techniques and, consequently, to better treatment for patients with medical conditions that require this type of procedure.

The study by [43] employed FEM-based simulations using COMSOL® Multiphysics software. They investigated the effects of thermal and electrical parameters on temperature during RFA, highlighting the significance of R and Sigma parameters at the distant point, as well as the variable sensitivity over time for Cp and rho. While the results are relevant, limitations such as the lack of consideration for blood vessel cooling and the need for more complex modeling persist.

[15] explored the inclusion of fluid dynamics in three-dimensional models of irrigated electrode cardiac ablation, utilizing COMSOL® Multiphysics software. Although the reduced model did not fully replicate the thermal lesions created by irrigated tip electrodes, this approach enabled the investigation of the saline irrigation effect on cardiac tissue. Limitations, such as overestimation of lesion width and blood temperature, should be considered when interpreting results in real clinical scenarios.

In the study by [44], liver RFA simulation addressed the effects of blood vessels using Minitab® software. The investigation of blood vessel influence on thermal lesions revealed that the distance between the RF needle and vessel, as well as blood coagulation, play crucial roles in determining lesion size and direction. However, study limitations, such as simplified representation of blood vessels and lack of coupling between blood coagulation and energy models, highlight the need for future research.

In the study conducted by [45], a two-compartment model was developed to analyze the relationship between target tissue size and resulting necrosis volume in RFA. The results indicated the need to adapt RFA protocols based on target tissue size, emphasizing the importance of personalized guidelines for hepatic tumor ablation.

[29] compared different methods of delineating atrial RFA lesions, exploring the use of thermal doses and hyperbolic equations. The results suggested that the CEM43°C method is more suitable for short-duration ablations, and the hyperbolic model better reflects the actual temperature distribution, contributing to a more accurate understanding of lesion contours.

The study by [46] examined the influences of electrical and thermal boundary conditions on liver cancer RFA models. The results emphasized the significance of appropriately choosing these conditions, illustrating that different impedance profiles and temperature distributions occur according to applied conditions.

These studies provide essential insights for adapting RFA procedures based on various variables and contexts. Continuous investigation through computational simulations is critical to enhancing the efficacy and safety of RFA techniques, benefiting patients with medical conditions that require this type of treatment. However, the limitations highlighted in each study underscore the need for future research and experimental validations to ensure the accuracy and clinical applicability of conclusions.

The detailed analysis of investigated articles provides a comprehensive view of computational simulations applied to the field of RFA for cancer and AF treatment. Each article addresses specific aspects related to different variables, electrode configurations, input voltage, ablation duration, among other factors. Through these simulations, researchers have the opportunity to explore different scenarios and virtually optimize treatment protocols (in silico) before conducting experiments in real environments.

The study by [47] examines the effects of electrode configuration, input voltage, and ablation duration on the efficacy of RFA for liver cancer treatment. Different electrode configurations and operational parameters resulted in varying thermal responses in tissues, highlighting the importance of carefully choosing these factors to optimize therapeutic outcomes.

The article by [48] investigates the influence of reversible and irreversible changes in tissue electrical conductivity during RFA. While the results show that irreversible changes in electrical conductivity do not significantly impact the size of the coagulation zone, the study provides valuable insights into the effects of tissue electrical properties on ablation efficacy.

The study by [49] focuses on unidirectional and alternating ablation in bipolar RF. The alternating approach shows promise in reducing undesirable thermal damage and increasing treatment efficacy, underscoring the importance of the ablation method in achieving desired outcomes.

[50] proposed a mathematical model to analyze and validate the electrical and thermal performance of externally irrigated electrodes for RFA. Ex vivo experiments were conducted

on bovine liver tissue to validate the model. The results indicated reasonable agreement between computational and experimental data regarding thermal lesion depth. The model demonstrated the influence of saline solution on thermal lesion creation, but the lesion width was larger in simulations than in experiments.

In this context, [2] presents theoretical and computational models explored for RFA using an internally cooled electrode with chilled saline solution. Electrical and thermal properties were analyzed, along with the evolution of the coagulation zone. The study compared different current and voltage pulse protocols and investigated their effects on coagulation zone formation. The study established a computational model to simulate an impedance-controlled pulse protocol used in clinical RFA practice.

The work by [51] employed the axiomatic design theory approach to evaluate existing RFA systems. The proposed protocol involved the use of an internally cooled cluster-shaped electrode to treat an ellipsoidal-shaped target tissue. A numerical model was developed in COMSOL® Multiphysics software to analyze temperature distribution during the RFA treatment session. The protocol proved to be feasible and allowed for the analysis of temperature distribution in the target tissue.

Overall, the limitations identified in each article indicate areas that require further investigation to enhance the accuracy and clinical applicability of simulations. The continued use of computational modeling can aid in the development of more effective and safer treatment protocols for patients undergoing RFA procedures.

the study of [52] presents a study that used COMSOL® software and Python® to simulate left atrial RFA under different scenarios. Two situations were considered: one with a collapsed esophagus in contact with the left atrium (Study 1) and another with the presence of an esophageal cooling device (Study 2). The goal was to analyze the effects of ablation under different conditions, such as ablation power, use of the cooling device, and cardiac wall anatomy. The results indicated that the esophageal cooling device was effective in protecting the esophagus during RFA. Furthermore, different RF powers resulted in different depths of myocardial lesions, highlighting the importance of adjusting the ablation duration to achieve appropriate outcomes.

[53] also used COMSOL® software to create a mathematical model simulating the effects of water evaporation during RFA. The study addressed how water evaporation creates barriers to the electric field and limits RF energy transmission, influencing ablation outcomes. Electrode cooling was highlighted as an important measure to reduce evaporation, and the study also discussed the use of internally cooled electrodes to improve thermal ablation outcomes.

The work by [54] focuses on simulating the temperature field during temperature-controlled RFA. The symmetric model was developed in COMSOL® and ANSYS®, including

a multipolar electrode. Experiments were conducted on a liver tissue-mimicking phantom. The study compared the accuracy of different simulation methods, such as using hyperbolic and parabolic bioheat equations, as well as variable voltage calibration with temperature. The results showed that variable voltage calibration with temperature was more accurate in simulating temperature-controlled thermal ablation.

In the article by [36], a computational model was developed to investigate the effects of RFCA using an open irrigated electrode. The influences of irrigation flow rate and electrode position on thermal lesion formation were analyzed. The study revealed that irrigation flow rate and electrode position impact thermal lesion dimensions and temperatures reached in tissue and blood.

In the study by [55], a 2D computational model was created using COMSOL® software to analyze thermal lesions resulting from cardiac ablation procedures. The study considered different distances between the ablation electrode and the external esophageal wall, as well as varying thicknesses of surrounding tissues. The results showed temperature distributions in tissue and blood, as well as lesion depths for different scenarios.

The article by [56] describes a computational modeling study using ANSYS® software to simulate RFCA. The model includes the consideration of various factors, such as electrode displacement due to cardiac motion, variation in contact force between the electrode and cardiac tissue, modeling of thermal and electrical properties of model elements, and other relevant parameters. The study focuses on predicting the effects of RFA on cardiac tissue, analyzing thermal and mechanical responses during the procedure. Some mentioned limitations include the absence of a mathematical model to predict vapor explosion phenomena, simplification in modeling the thermal effect of circulating blood, and lack of viscous behavior in the mechanical model.

[57] addresses the influence of uneven saline solution distribution on the development of thermal lesions during RFA. The study uses COMSOL® Multiphysics software to model 2D liver tissue with internally placed saline squares. The results demonstrate that increased electrical conductivity of tissue due to saline perfusion results in a larger ablation area, and increased blood perfusion causes temperature reduction. However, details about the limitations of this study were not provided.

The study by [1] presents a numerical investigation into the relationship between coagulation volume and electrode tip temperature during temperature-controlled RFA. The study uses COMSOL® and MATLAB® software for simulations and compares them with in vitro experiments on a phantom gel mimicking tissue. The results show agreement between computational and experimental results regarding coagulation volume. The simulations also explore the variation of applied input voltage across different tissues and the effect of target tip temperature on voltage. Proposed correlations between coagulation volume and treatment time have high accuracy ($R^2 > 0.99$). Among the study's limitations, a single-

compartment model is considered, and the effect of heat dissipation from large blood vessels is omitted.

The analytical work of [58] investigated the thermal performance of RF thermal ablation using different electrode geometries and types, as well as blood perfusion conditions. Four electrode types (dry spherical, cooled spherical, dry cylindrical, and cooled cylindrical) were modeled under two blood perfusion conditions. The results highlighted that temperature reaches a steady state in all cases except for cylindrical electrodes without blood perfusion. Spherical electrodes demonstrated a greater capacity to achieve steady temperatures due to more concentrated power distribution. Cooled electrodes showed lower temperatures but created larger lesions. Limitations included the lack of consideration of dynamic changes in tissue properties, such as electrical conductivity. Future studies should explore these conclusions considering such changes.

It's important to note that computational models are valuable tools for predicting and understanding the effects of complex medical procedures like RFCA. However, as mentioned in the limitations, these models have their own simplifications and limitations that can affect the accuracy of results. Experimental validation and consideration of specific clinical scenarios are essential to ensure the reliability and applicability of these models.

In the study by [59], researchers explored cardiac computational modeling as a tool to identify optimal RFA settings. Using ex vivo pig hearts and myocardial samples, they developed a computational model that replicates experimental setups to evaluate electrical potential during the ablation procedure. Time-harmonized Maxwell equations were employed to calculate the resulting electrical potential. Heat generated during ablation was treated with parabolic heat equations and the dual-phase-lag equation, considering different tissue regions. A three-state model of hyperthermic cell death was used to assess thermal damage to cardiac tissue. Processed fiber-optic data was used to create two-dimensional temperature maps, allowing a detailed understanding of thermal distribution during RFA. The dimensions of the damage were analyzed and compared with manual measurements, showing differences possibly due to measurement errors and temperature criteria. The study concludes that the model is sensitive to the alignment of fiber-optic arrays and myocardial fibers, emphasizing the importance of considering thermal anisotropy. However, the study presents some limitations, such as the simplification of the computational domain and the need to include electromechanical couplings, contact mechanics, and realistic geometries for greater clinical accuracy.

In this context, the study by [60] investigated temperature distribution during ex vivo hepatic tissue RFA. Researchers conducted infrared thermography measurements and numerical simulations to understand the heating process during ablation and contribute to improving medical techniques. Using ex vivo hepatic tissue, experiments were conducted at different power levels, kept constant in each test. The temperature distribution was

observed around the active electrode tip, with areas of more intense thermal increase. Tissue discoloration due to denaturation was observed when the temperature reached around 60°C. Temperature measurements along the active tip helped understand thermal kinetics. Numerical simulations confirmed temperature uniformity within the active tip, thanks to its high thermal diffusivity. The study contributed to a better understanding of thermal kinetics during ex vivo hepatic tissue RFA. However, the study recognizes the need for more research to optimize the effectiveness of RFA under different clinical conditions.

On the other hand, in the work by [61], a new in vitro method using direct thermography was developed to visualize temperature kinetics throughout the cross-section of myocardium during RFA, without the need for intramyocardial elements. Researchers used a standardized sample of pig myocardium and performed experiments with an active electrode at different power levels. Direct thermography measurements allowed visualization of temperature kinetics throughout the myocardium cross-section, offering valuable insights into thermal distribution during RFA. While the results were promising, the study acknowledges the need for further research for more precise temperature distribution measurement and to optimize the effectiveness of RFA under different clinical conditions.

The study by [62] investigated the effects of blood flow on cooling during RFA. They combined the heat transfer parameter 'Nu' with FEM. Samples of hepatic tissue and veins from freshly slaughtered pigs were used in the experiments. The methodology involved using FEM and the biological heat transfer equation to estimate temperature distribution during RFA in an in vitro container with hepatic tissue. The cooling effect of the blood vessel was considered. The results showed a gradual temperature increase after 200 seconds of RFA, with the cooling effect varying between samples due to tissue properties. The study had limitations, such as not considering factors beyond vessel cooling. Researchers plan to enhance the FEM model for complex clinical conditions.

Lastly, the study by [63] investigated a hybrid ablation technique that combines electroporation (EP) pulses with RFA. Conducted on Landrace breed pigs, the study involved 3 female pigs subjected to 4 procedures each. The methodology included theoretical and experimental evaluations of the hybrid technique, with theoretical models based on finite elements. However, the results showed that the combination of EP and RFA did not offer advantages over isolated RFA, as the electroporation effects were overshadowed by the thermal damage of RFA. Experiments on pigs also did not show significant differences in coagulation zones between the groups. The study faced limitations such as limited generalizability to humans due to the use of an animal model, small sample size, and lack of long-term evaluation. The analysis focused on macroscopic measurements, without exploring all parameter settings of the hybrid technique.

4.3.2 Outcome of Bias Risk Assessment

Upon subjecting the examined studies to a comprehensive assessment, guided by adapted inquiries from the generic Risk of Bias (ROB) tool, a majority of the scrutinized articles emerged with a commendably low susceptibility to bias. Notably, the in silico studies [2], [15], and [16] were observed to lack randomization within the simulation of parameters. The crucial tenet of allocation concealment, pivotal in curbing the undue influence of selection bias or prior awareness, remained unaddressed in the works authored by [41], [11], [36], [2], [16], [15], [42], and [56]. It is noteworthy that the blinding of investigators remained unexecuted in the investigations conducted by [50], [51], [41], [2], [36], [11], and [46], as meticulously delineated in Fig. 6.

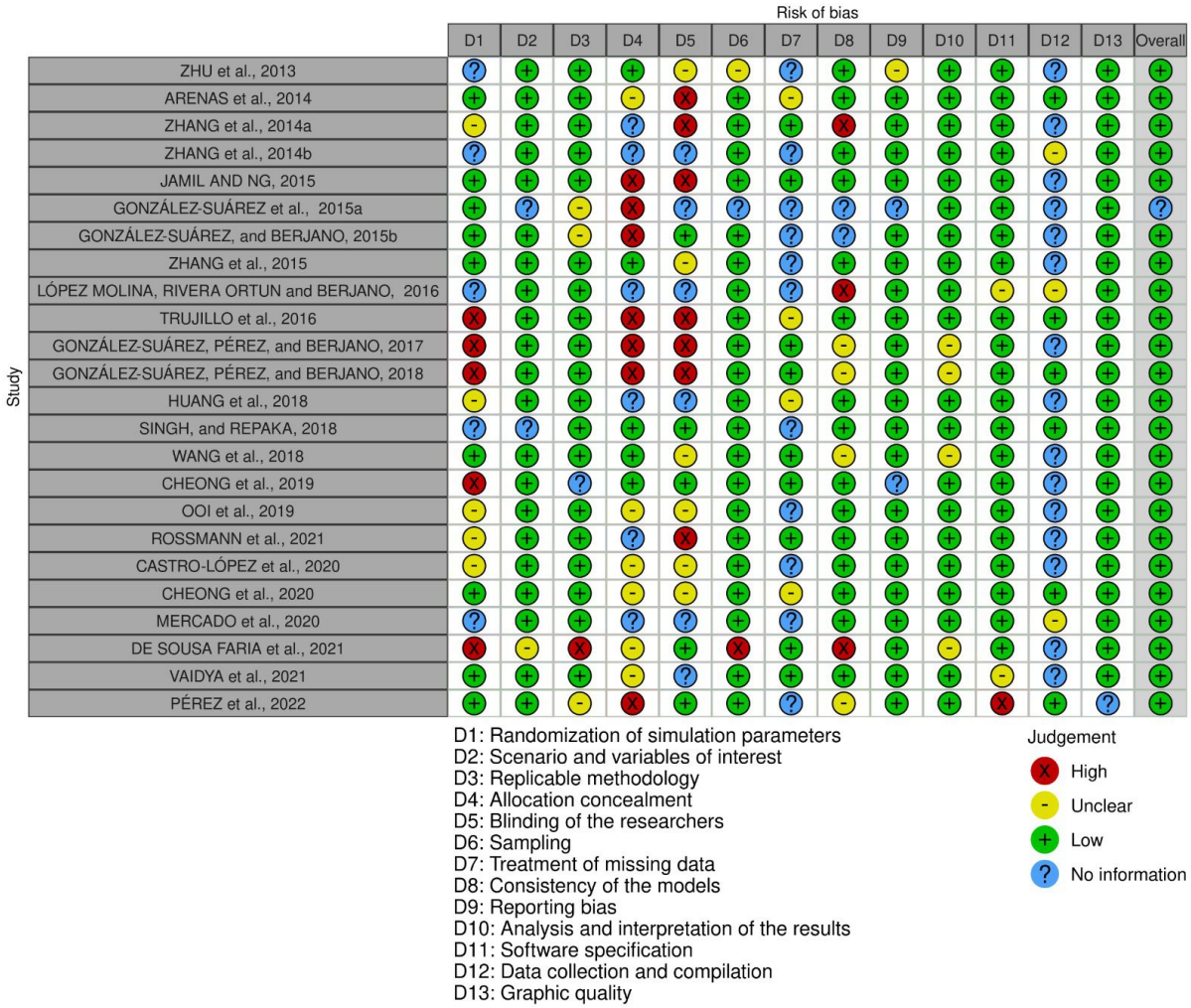

Figure 6 – Overall quality of the selected studies in silico.
Source: Own authorship

Fig. 7 showcases the bias risk assessment pertaining to the ex vivo studies, which, in turn, exhibited a similar trend of low susceptibility to bias. However, the study undertaken by [63] notably exhibited a high risk of bias, particularly in relation to randomization and blinding of researchers.

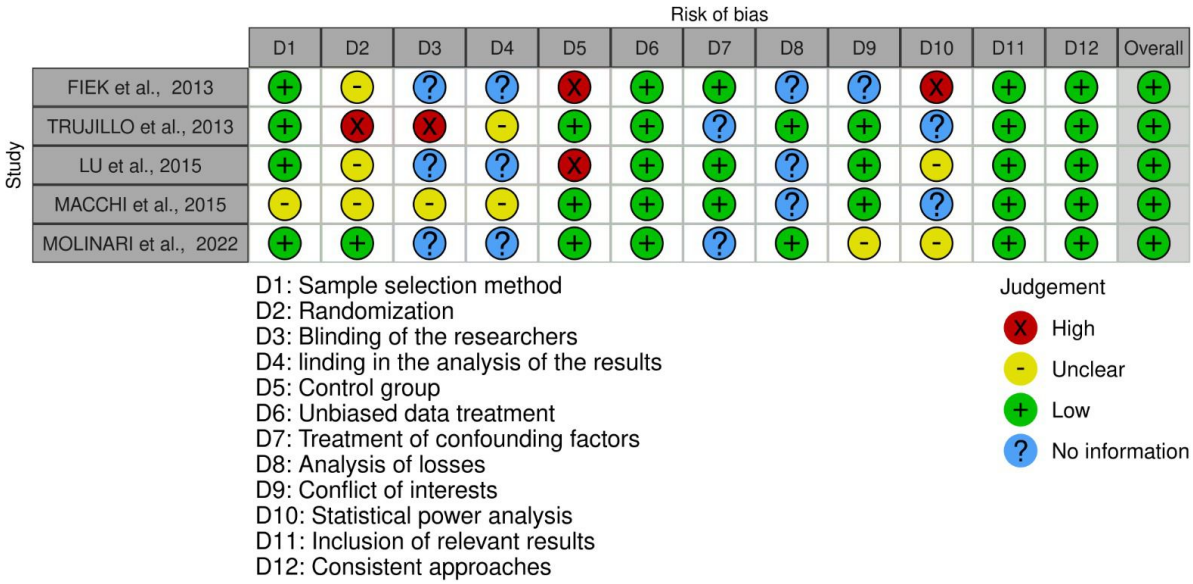

Figure 7 – Overall quality of the selected studies in vivo and ex vivo.
Source: Own authorship

These findings underscore the significance of a more rigorous approach in the execution and delineation of methods within research endeavors, particularly with regard to randomization, allocation concealment, and blinding. Enhancing these aspects has the potential to bolster the reliability and validity of the outcomes derived from the scrutinized studies, thereby advancing the foundational knowledge in the pertinent field.

4.4 Discussion

The pursuit of computational studies aimed at optimizing and comprehending RFA processes is of paramount importance in enhancing the efficacy and safety of clinical procedures. In this systematic review, a comprehensive overview of the employed methodologies, attained outcomes, and principal conclusions pertaining to RFA simulations was achieved through the analysis of selected articles. Each study contributed to the comprehension of parameter variations' effects on ablation procedures, manifesting advancements in the state of the art tailored towards temperature and impedance control.

For instance, the research conducted by [41] delved into diverse electrical and thermal parameters, discerning correlations between these parameters and ablation outcomes through finite element analysis and optimization based on Taguchi matrices. Meanwhile, the work by [16] underscored the fluid dynamics' significance in cardiac ablation models with irrigated electrodes, demonstrating that more intricate models incorporating fluid dynamics equations yield more consistent outcomes.

Model proposals, such as that of [42], validated ablation devices through computa-

tional simulations, emphasizing the necessity to consider complex features like the presence of blood vessels for greater model fidelity. Concurrently, [43] performed a sensitivity analysis on thermal and electrical parameters in RFA, employing statistical methods and response surface analysis.

Studies by [16] and [44] addressed fluid dynamics' influence in three-dimensional models of cardiac ablation with irrigated electrodes, accounting for the blood vessel effect on thermal lesions. [45] developed a two-compartment model to analyze the relationship between target tissue size and resulting necrosis volume from RFA, emphasizing protocol adaptation based on target tissue size.

Methods for delineating RFA lesions were compared by [29], while [46] examined the influences of electrical and thermal boundary conditions in liver cancer RFA models. The conclusions from these studies provide essential insights for adapting RFA procedures based on distinct variables and contexts.

The in-depth analysis of the investigated articles offers a comprehensive insight into computational simulations applied to RFA. Each article addresses specific facets related to different variables, electrode configurations, input voltage, ablation duration, and other factors. Through these simulations, researchers have the opportunity to explore diverse scenarios and virtually optimize treatment protocols (in silico) prior to conducting real-world experiments.

Furthermore, several studies employed COMSOL® Multiphysics software for their simulations, as evidenced by the works of [43], [16], [44], [45], and [2], underscoring the significance of this tool in RFA modeling. However, it is imperative to acknowledge that computational models possess limitations and necessitate experimental validation to ensure their accuracy and clinical applicability.

Additionally, ex vivo and in vitro studies have also contributed to understanding RFA effects. The study by [59] employed ex vivo porcine hearts and myocardial samples to develop a computational model mirroring experimental configurations, allowing a better comprehension of electrical and thermal distribution during RFA. The infrared thermography measurements and numerical simulations conducted by [60] and [61] also yielded valuable insights into thermal kinetics during RFA.

In summation, the amalgamation of computational and experimental studies has ushered significant advancements in the comprehension and optimization of RFA. However, it is pivotal to recognize the inherent limitations of these models and approaches, thereby encouraging ongoing research to refine the efficacy and safety of RFA techniques, ultimately benefiting patients with medical conditions necessitating such treatments.

4.5 Limitations

The main limitations encountered by the authors of this study are as follows:

Scope of the Research: This study exclusively focused on the systematic review of selected articles related to computational RFA simulations. As such, it did not encompass other ablation techniques or diagnostic methods that could provide a more comprehensive view of the approaches utilized in clinical practice.

Quality of Included Studies: Despite conducting a bias risk assessment for the included studies, it is important to acknowledge that the studies themselves might have methodological limitations that could impact the quality and reliability of the results.

Heterogeneity of Studies: The included studies addressed a wide array of approaches, models, and parameters, potentially leading to heterogeneity in results. This complexity made quantitative synthesis of results challenging.

Limited Experimental Validation: Many of the reviewed studies were based on computational simulations, and in some cases, these simulations might not have been experimentally validated.

Lack of Standardization: The lack of standardization in simulation methods, models, and parameters made it difficult to directly compare results across different studies.

Generalization: The results obtained from the reviewed studies may not be directly applicable to all patient populations, clinical conditions, or treatment settings.

4.6 Conclusion

In conclusion, the studies analyzed in this systematic review offer a comprehensive understanding of aspects related to radiofrequency ablation in medical procedures, particularly in the treatment of cancer and AF. The integration of experimental approaches and computational modeling has provided valuable insights into the influence of electrical, thermal, and fluid parameters on RFA outcomes. Each study addressed specific aspects, ranging from the analysis of electrical and thermal parameters to the incorporation of fluid dynamics in complex models.

Computational simulations play a pivotal role in investigating diverse scenarios, optimizing treatment protocols, and predicting effects under controlled conditions (in silico) before being applied in real experiments. However, it is essential to consider the inherent limitations of these models, such as simplifications in tissue representation and the absence of complex interactions and couplings occurring in the actual biological environment.

Furthermore, the analysis of bias risk revealed that most studies exhibit a low risk of bias, indicating a reliable methodological approach. Nevertheless, aspects like randomization,

allocation concealment, and blinding still need enhancement in some studies to strengthen internal validity and result robustness.

In light of the contributions from these studies, it becomes evident that research in the field of RFA continues to evolve, striving to enhance the efficacy and safety of clinical procedures. The ongoing use of computational modeling, in conjunction with experiments, offers a promising avenue for the development of personalized protocols and more effective treatment strategies. However, it is imperative for these approaches to be validated through in vivo experiments, with model limitations carefully considered when interpreting results in a clinical context.

In summary, the interplay between experimental studies and computational simulations has the potential to drive significant advancements in the field of RFA, benefiting patients with medical conditions requiring such treatment. The continuous refinement of methodologies and collaboration among researchers in medicine, engineering, and biomedical sciences are essential to propel this evolution and provide improved therapeutic options to patients in the future.

5 Particle Swarm Optimization for Roll-Off Control in RFA

This chapter presents the article entitled "Particle swarm optimization solution for roll-off control in radiofrequency ablation of liver tumors: Optimal search for PID controller tuning", which belongs to the studies developed during the course of the doctoral research and has been accepted to the scientific journal PLOS ONE (ISSN 1932-6203), boasting a QUALIS-CAPES A1 ranking, CiteScore of 6.2, and an Impact Factor of 2.9 (2023) [64]. In this study, we investigate a bio-inspired approach employing the evolutionary algorithm PSO for the design and tuning of a PID controller, enabling the delay of roll-off occurrence and potentially generating an extended ablation zone. The quantitative data collected from an ex-vivo experiment underwent behavioral modeling using system identification methods, and a dynamic model represented by a 9^{th}-order transfer function in the continuous-time domain was obtained. The results reveal satisfactory performances in all conducted simulations, notably the algorithm fine-tuned for 10 iterations and a swarm of 30 particles, yielding performance indices of 0.605% for overshoot at 0.314 s, 0.127 s for rise time, and 2.87 s for settling time concerning a unit step input.

5.1 Introduction

Cancer stands as a significant global concern, ranking among the top four leading causes of premature mortality before the age of 70 in many countries [65]. Worldwide, an estimated 18 million new cancer cases occur annually, with a higher incidence in the male population, accounting for approximately 53% of the total [65, 66]. Among various cancer types, liver tumors are the second most lethal, with an incidence rate of approximately 6.3% among newly diagnosed cases [5, 67].

Hepatocellular carcinoma (HCC), a form of liver cancer significantly influenced by the tumor stage, exhibits a five-year survival rate exceeding 70% for early-stage cases, while the average survival varies from 1 to 1.5 years for advanced and symptomatic cases treated with systemic therapies [67]. Accurate diagnosis distinguishing HCC from other liver diseases with similar clinical and radiological features is crucial for effective treatment planning [68].

The treatment of HCC presents challenges due to tumor resistance and recurrence [69]. Early stages are addressed through surgery, while advanced stages can be treated with chemotherapy, immunotherapy, oncolytic viruses, and nanotechnology to enhance effectiveness and reduce side effects [70, 71]. However, these methods face substantial

challenges that limit their effectiveness. Hepatic resection and liver transplantation are effective in early stages but are not options for most patients. Traditional chemotherapy is limited by drug resistance, and radiotherapy is constrained due to the liver's sensitivity to radiation. Immunotherapy and oncolytic viruses show promise but do not benefit all patients [71–74]. Additionally, RFA therapy, although effective in some cases, has its own limitations, including restrictions on the size and location of treatable tumors. Identifying risk factors and trends is crucial for developing effective strategies for prevention and intervention in the fight against liver cancer [74].

The importance of diversified techniques in the treatment of HCC is essential for enhanced treatment efficacy and safety. Thermal ablation is a minimally invasive medical procedure that utilizes microwave, laser, radiofrequency (RF), or ultrasound energy to perform tissue ablation [68, 75]. In RFA, the procedure entails the use of an ablation electrode that is navigated to the target region utilizing imaging techniques such as computed tomography or ultrasonography. Subsequently, the ablation is performed via the delivering of RF energy in the target region [9, 45, 76–78]. The Joule effect is the mechanism by which electromagnetic energy is converted into thermal energy during the RF ablation procedure [79]. As such, the intense heat generated through ionic agitation of molecules results in cellular demise and eventual necrosis of tumor cells. [80].

However, ablation procedures are subject to certain limitations, particularly in achieving precise and complete coagulation volumes that fully encompass larger tumors [12, 81]. The search for strategies aimed at enhancing the ablation volume ensued due to the occurrence of a limited coagulation zone in the target region [82]. The infusion of physiological solutions is currently utilized with the objective of augmenting tissue conductivity and promoting uniform energy propagation [83].

Research conducted by Jiang *et al.* [84] reveals that in the context of liver RFA, the adoption of internally cooled electrodes in conjunction with the injection of 10% hydrochloric acid (HCl) markedly augments the ablation zone volumes, thereby enabling the treatment of larger tumors. This increase in efficacy can be attributed to improved thermal conductivity, amplified electrical conductivity, and reduced impedance. Notwithstanding, other studies involving the utilization of infused saline solutions report a delayed onset of roll-off, which is postulated to be caused by the tissue hydration provided by the solution, leading to a reduction in dehydration and localized vaporization [9].

The liver comprises hepatic arteries, portal veins, and hepatic veins, each characterized by distinct diameters, flow rates, and spatial arrangements [12, 45, 81]. Although effective, RFA is hampered by certain technological constraints, resulting in complications such as local recurrences, deficient ablation zone control in the vicinity of the targeted field, risk of harm to non-tumoral tissues, and potential harm to vascular and biliary structures [28, 45, 76, 79, 85, 86].

As a consequence of ablative effects, a study conducted by [87] presents a significant reduction (44.4±14.6%) in tumor volume following RFA in HCC patients. In this context, ex vivo assays by [88] demonstrated a shrinkage in the coagulation zone in hepatic (15–31%) and pulmonary tissues. On the other hand, [89] conducted in silico assays applied to breast cancer and showed that with an increase in electrical potential, there was a significant growth in temperature and the value of the Arrhenius integral, which estimates the degree of tissue destruction. In this study, [89] also demonstrated that the optimal voltage level for the ablative procedure was between 12.5V and 15V. However, there was an impact on adjacent healthy tissues, for example, at a control point located in granular tissue, 5 mm from the tumor, where the Arrhenius integral showed a 60% probability of tissue destruction.

The use of techniques aimed at controlling RFA is well-explored in the literature. [90] investigated the effects of pulsating heat on thermal energy transfer in tumor-affected tissue subjected to hyperthermia. The study presented relevant results for the improvement of thermal ablation devices, avoiding temperature peaks and showing that tissue damage related to pulsating heat allows carbonizing the same tumor area as when using a non-pulsating heat source. In this scenario, [91] conducted a study to investigate the effects of different antenna arrangements on the thermal ablation of tumor tissue. Single, double, and triple antenna arrangements were analyzed. The results depict that the use of multiple antennas provides conditions for the expansion of ablation zones. Furthermore, it could be concluded that the use of multiple antennas resulted in lower maximum temperatures compared to simple arrangements.

To investigate the applications of roll-off time delay techniques, careful control of tissue impedance is paramount, whereby the RFA equipment modulates the output power in response to the designated set point established in the targeted tissue, which is diligently monitored throughout the procedure [92]. Manual temperature control of tissue involves maintaining a constant output voltage applied at the electrode tip and adjusting it manually through trial and error to ensure the temperature of the electrode tip remains below the predefined temperature threshold. It is a labor-intensive and time-consuming process that heavily relies on the operator's expertise [1]. On the other hand, automatic temperature control implemented in some RF generators offers a more advanced and reliable approach by utilizing temperature sensors and closed-loop control algorithms to maintain precise temperature control during the ablation procedure.

5.1.1 Related Works

Haemmerich *et al.* [93] reported that temperatures exceeding 50 °C induce intracellular protein denaturation and tumor cell membrane destruction, culminating in coagulative necrosis and consequent cell death [94]. Although tissue impedance decreases as heating begins, the dehydration of the target region caused by the vaporization of moisture leads

to an increase in impedance [80]. As a result of tissue carbonization, the expansion of the coagulation volume is limited, which compromises the effectiveness of the RFA procedure and exacerbates the roll-off phenomenon [95].

This phenomenon is closely associated with the increase in tissue temperatures, typically reaching 100 °C, leading to the fluctuation of tissue impedance throughout the RFA procedure [9]. Roll-off is typically observed during the ablation, after the tissue has been fully desiccated, and the flow and power of the generator have been reduced to zero [96]. Impedance gradual decrease is observed at the beginning of the RFA procedure. As the tissue temperature increases above 50°C and goes through the process of carbonization, impedance suddenly rises to values around 1000 Ω [12]. Consequently, the intervention is interrupted due to the inability to effectively conduct an electric current through the tissue [96].

Various strategies have been developed to delay the onset of roll-off, thereby prolonging the duration of RFA [76]. Alternative techniques have been developed to increase the size of coagulation zones, such as the use of internally cooled electrodes in conjunction with the infusion of a refrigerated saline solution [97]. The combined effect of increased tissue conductivity due to the presence of ions from the saline solution and the cooling of the ablation zone by hydration of the target region allows for impedance to be maintained at a reduced level for a prolonged period, thereby enhancing the efficiency of the RFA procedure [80].

In a similar vein, Trujillo and colleagues [9] conducted research utilizing both a theoretical model based on the finite element method and an ex-vivo experimental study. By utilizing porcine liver tissue, they were able to determine that the onset of roll-off is directly linked to the moment when the tissue reaches a point of severe dehydration. Their study demonstrated that infusion of a saline solution can effectively delay the onset of tissue carbonization, thereby postponing the occurrence of roll-off.

Global optimization is a field of applied mathematics and numerical analysis that is specifically concerned with minimizing and maximizing parameters in order to achieve the best possible values for meeting the global objective, while satisfying a set of mathematical modeling criteria, known as the objective function [98]. Bioinspired optimization stands out as one of the most promising methodologies for global optimization. It comprises a set of techniques in the field of computer science that rely on nature-inspired principles for the search of the global optimum. By drawing inspiration from biology and the natural world, bioinspired algorithms have been shown to achieve excellent results in a wide range of optimization problems [99].

The PSO can be applied in various industrial robotic applications. A study conducted by [100] synthesized research related to the motion control of robotic manipulators, with a focus on Super-Twisting Sliding Mode Control techniques. The article highlights the use

of optimization algorithms, such as PSO, for an effective approach to tuning these control parameters [100]. Other techniques, like Active Input-Output Sliding Mode Control (AIOFL), are also employed for similar purposes in nonlinear systems. AIOFL is an approach that cancels system disturbances in real-time, transforming it into a chain of integrators up to the relative degree of the system, requiring only knowledge of that degree [101].

In the same context, a study conducted by [102] utilized the PSO algorithm to tune a proportional-integral-derivative (PID) controller for controlling the speed of a permanent magnet direct current motor. Through experiments conducted at an educational level, the authors demonstrated the importance of the number of iterations for the algorithm's performance, which, for this plant and experimental setup, was 25 iterations. Overall, the study yielded promising results in terms of the desired dynamic response of the system concerning rise time, settling time, and overshoot control. The authors conclude this study with the expectation that this work may facilitate the efforts of young researchers and engineers interested in this field.

In the realm of potential optimization algorithms, the Bat Swarm has also been applied in robotics with the aim of finding the shortest path between the initial and final points while avoiding dynamic obstacles. An adaptation of the frequency parameter of the standard Bat algorithm was made to create an enhanced version called the Modified Frequency Bat Algorithm (MFB) [103]. The MFB operates in two modes: first, it generates the trajectory when there are no obstacles in the environment, and second, it avoids obstacles as soon as they are detected. Extensive simulations validated the effectiveness of the MFB, showing that it outperforms the standard Bat algorithm, finding shorter and collision-free trajectories [103, 104]. Research conducted by [105] reveals that the nonlinear fractional-order neural network-based controller (NNFOPID) is designed using nonlinear activation functions in hidden layers and linear functions in the output layers of a neural network, and its tuning is performed through a hybrid optimization algorithm called MAPSO-EFFO. Simulation results show that the NNFOPID surpasses a neural nonlinear PID controller (NNPID) in terms of trajectory tracking, minimizing mean square error, and reducing energy consumption during circular, linear, and lemniscate trajectories.

In the landscape of cancer research, particularly focusing on liver tumors, this paper distinguishes itself by addressing the limitations of RFA therapies through a comprehensive exploration of diverse techniques. While other studies have primarily concentrated on the thermal aspects of RFA, our work stands out by underscoring the critical role of tissue impedance control as a pivotal parameter in ensuring continuous and successful RFA. Furthermore, the integration of a PSO-tuned PID controller in our methodology demonstrates a novel approach to achieve precise and efficient control, setting our study apart from existing literature. By optimizing the PID controller with the PSO algorithm, we obtain robust results, showcasing low overshoot, rapid rise time, and efficient settling time, thereby contributing to

the development of more effective RFA procedures. This unique combination of techniques and emphasis on impedance control positions our work as a valuable contribution to the advancement of liver tumor treatment strategies.

5.1.2 Roll-off and Coagulation Zone

The analysis of the roll-off phenomenon in RF procedures is crucial to understand its correlation with the coagulated volume and investigate its potential connection with lesion recurrence. Hypotheses suggest that delaying the roll-off may lead to larger coagulation zones [9, 106]. In a study conducted by Arata *et al* [96], the observation of roll-off occurrence served as a significant predictor of local control after the procedure. Among 20 treated hepatic lesions, tissues that reached the roll-off exhibited a lower rate of local recurrence at 6 months (15%).

To address the issue of roll-off in RF procedures, several approaches have been proposed, including modifications to the mode of energy delivery to the tissue (continuous or pulsed), the use of feedback control laws employing a PID controller [107–109], real-time feedback information (such as tissue temperature, temperature at the active tip of the catheter, or impedance between the active tip and the grounding site), and adjustments for changes in tissue characteristics, such as dehydration. These approaches aim to maintain optimal conditions for the ablation process and avoid the negative consequences associated with roll-off, such as limited expansion of the coagulation volume and compromised therapeutic efficacy [110–112].

Temperature control is a critical aspect of many thermal therapies, and the PID controller is a commonly used method for achieving precise temperature control [110, 113]. This controller is widely utilized due to its ability to provide continuous output variation and high process precision. The PID controller works by measuring the error between the desired and actual temperature and modulating the input voltage in the circuit until the desired output temperature is achieved. It is a simple and easy-to-use control method that has found applications in a wide range of fields [41, 76].

Previous investigations have not incorporated a numerical model for tissue impedance control based on ex-vivo tests using system identification techniques to construct a data-driven dynamic model and apply a tuned controller using the PSO algorithm. The use of the PID controller stands out as a key strategy to mitigate the negative effects of the roll-off, enabling a more precise dynamic control of temperature during the RFA procedure. The implementation of swarm-based optimization techniques, such as the PSO algorithm, to adjust the parameters of the PID aims to optimize the system's performance.

The primary objective of this study is to establish dynamic control of tissue impedance for the RFA procedure by implementing a closed-loop PID controller. This control strategy

aims to delay the occurrence of roll-off and enhance the overall effectiveness of the intervention. This approach involves adjusting the PID controller to an optimal set of tuning parameters, including proportional gain (K_p), integral gain (K_i), and derivative gain (K_d). The optimization process is carried out using swarm intelligence-based techniques, specifically the PSO algorithm. By iteratively exploring and evaluating potential solutions, the PSO algorithm seeks to identify the most favorable combination of controller coefficients.

Compared to traditional methods like Ziegler-Nichols, this swarm intelligence-based optimization approach offers improved performance and superior results. It leverages the power of intelligent algorithms to fine-tune the PID controller, resulting in enhanced control over tissue impedance during the RFA procedure.

To construct the impedance curve model, ex-vivo experimental data obtained through system identification techniques is utilized. The resulting transfer function, which relates the input voltage (V) to the output impedance (Ω), is carefully analyzed and characterized. This data-driven model forms the basis for the dynamic control of tissue impedance in the RFA procedure.

This study addresses a gap in the literature by focusing on the lack of investigations into roll-off displacement with precise automatic adjustment control using bioinspired computational techniques such as PSO. Additionally, it aims to enable deployment of this control on hardware for real-time execution. In future work, we plan to integrate a dynamic actuation controller. This controller will receive information on tissue impedance variation and simultaneously adjust the PID controller to displace the roll-off, thus providing a more efficient ablation procedure.

5.2 Materials and Methods

The methodology of the study is graphically presented in Fig 8, which summarizes all the steps involved in the optimization process.

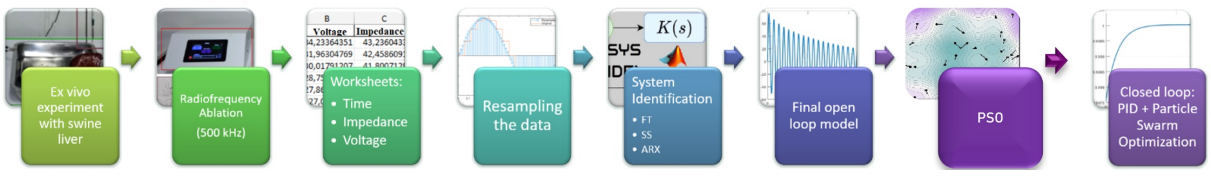

Figure 8 – **Methodological Flow of Theoretical-Experimental Procedure.** Initially, we conducted an ex-vivo experiment using porcine liver tissue, which was subjected to RFA using the SOFIA® equipment. The obtained data were organized in spreadsheets and resized. Next, SI was performed using the ARX method, and the model was converted to the TF domain. With the open-loop system, the PSO algorithm was applied (Fig 9), returning optimal gains for use in the PID controller.

Source: Own authorship

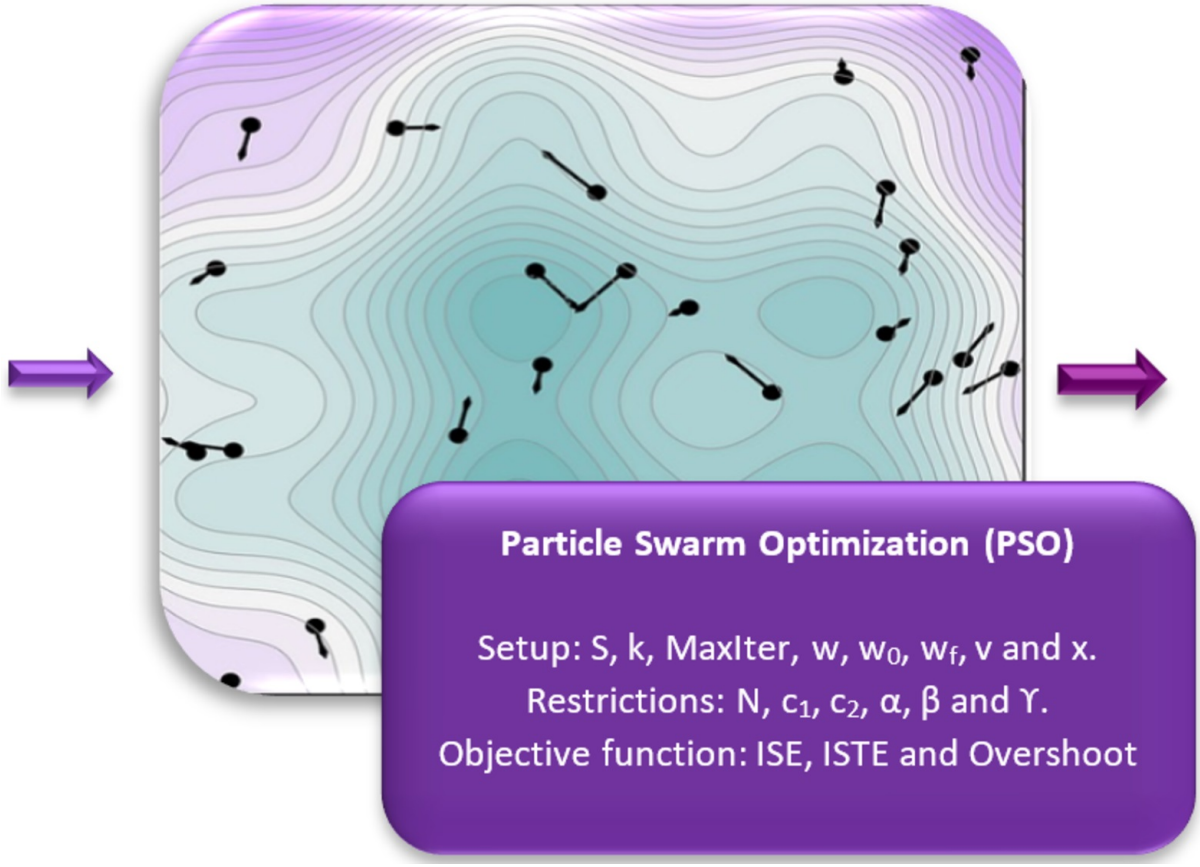

Figure 9 – **Expanded PSO (Fig 8)** In the open-loop system, the PSO algorithm was utilized, incorporating variable parameters such as the number of particles (S), iteration index (k), the maximum number of iterations (MaxIter), inertia factors calculated per iteration, initial and final (ω, ω_0, ω_f), and search intervals covering both position and velocity (x and v). On the other hand, fixed parameters, including the number of dimensions (N), cognitive and social coefficients (c_1 and c_2), as well as the weighting values of performance indicators α, β, and γ, remained constant throughout the process and were assessed through the objective functions of the integral of the squared error criterion (ISE), integral of the squared error weighted over time (ISTE), and overshoot. As a result, the achievement of optimal gains that can be employed in the PID controller was demonstrated.
Source: Own authorship

Experimental Protocolol

The experimental procedure utilized ex-vivo porcine liver tissue that was sourced from local markets and maintained at temperatures ranging from 18°C to 22°C. The organs were sectioned into cubes measuring approximately 6 cm on each side. The RFA equipment utilized in the experiment was developed by the Biomedical Engineering Laboratory (LaB) at the University of Brasilia (UnB). The equipment, named SOFIA®, has a patent request (BR 10 2017 002683 3) [21].

The Boston Scientific LeVeen® Standard 4.0 umbrella electrode (Marlborough, MA, USA) with a diameter of 2.5 cm was employed in all trials with the electrode in the semi-open position, following the RFA test protocol of the SOFIA® equipment [114, 115]. All components of the ex-vivo experiments are shown in Fig 10.

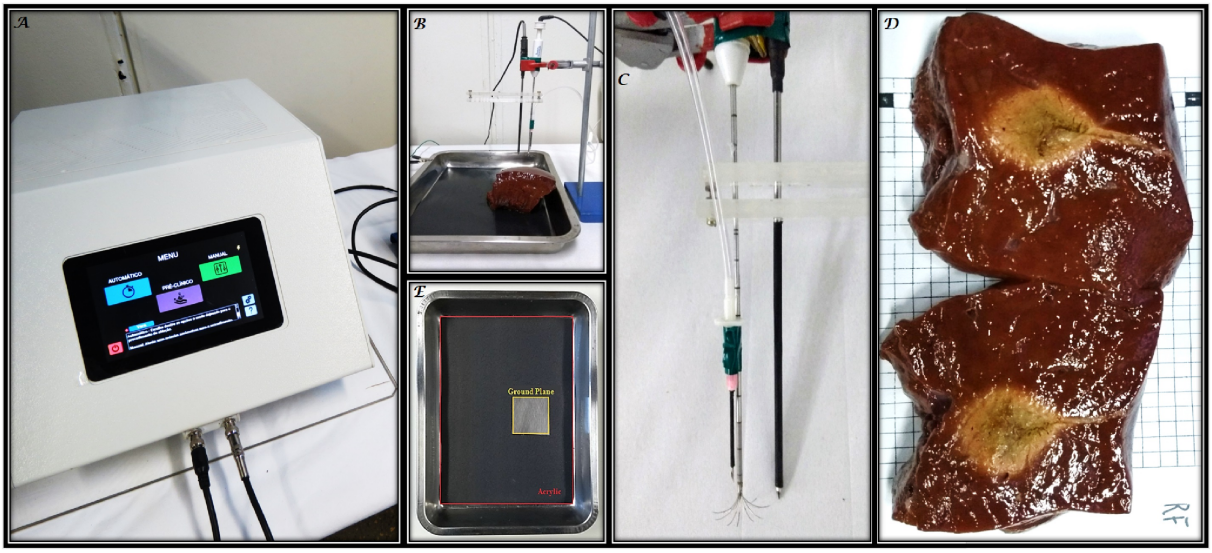

Figure 10 – **Experimental setup for ex-vivo tests.** Fig (A) shows the RFA equipment SOFIA® developed by the Biomedical Engineering Laboratory of the University of Brasília, adjusted to deliver an initial power of approximately 34 W through a 500 kHz sine wave electrical current. Fig (B) depicts the positioning of the piece of swine liver on the bench where the tray is connected to the dispersive electrode. In Fig (C) we have the Boston Scientific LeVeen Standard 4.0 umbrella electrode with a diameter of 2.5 cm responsible for supplying high-frequency energy for the procedure and a thermocouple sensor placed at a distance of 1.25 cm from the center of the electrode. In (D), we present the result of the RFA in one of the 6 cm cubic pieces of liver, which is sectioned in the middle, showing the region of hepatic tissue necrosis. In (E) we have the grounding plane that was connected to the dispersive electrode assembled from an aluminum tray coated with a layer of acrylic. A 6 cm x 6 cm window was cut out so that the pieces of hepatic tissue remained in contact with the grounding surface in a region with the same dimensions as the cubes. All procedures were based on the SOFIA® testing protocol, which can be consulted in references [114] and [115].
Source: Own authorship

The test was performed with an initial power of approximately 34 W applied by the monopolar electrode on the liver samples. The dispersive electrode was connected to an aluminum base covered by an acrylic plate, allowing only the section of the same dimensions as the liver sample to touch the ground terminal (see Fig 10 - E). The stopping criterion used was the detection of the first roll-off reached by the tissue, measured by the SOFIA® equipment. Maintaining a constant power level was necessary to ensure experiment reproducibility.

The temperature was measured using a thermocouple sensor provided with the SOFIA® equipment. The sensor was placed at a distance of 1.25 cm from the center of the electrode, located at the tip of one of the twelve electrode rods forming an "umbrella" geometry (see Fig 10 - C).

The VERA system, a continuous monitoring system connected to SOFIA® via serial communication, was used to monitor the parameters of the RFA signal. The system has a patent request (BR 10 2017 002919 0) [116].

5.2.1 System Identification - Roll Off

The application SI techniques to the dynamic modeling of the roll-off phenomenon enables the correlation of the applied voltage in the RFA procedure with the behavior of tissue impedance.

5.2.1.1 Data Acquisition

The open-loop SI is established by evaluating the input values u and output y. In this study, a 500 kHz sinusoidal voltage was utilized as input data, with effective RMS values measured in volts. The output data represents the impedance of the liver tissue, calculated from the voltage and current measurements obtained via the SOFIA® equipment. Only the real part of the impedance was considered as it is associated with Joule heating [117]. Reactances were neglected.

5.2.1.2 Model Structure

The data generated by the SOFIA® equipment were exported to MATLAB® R2021a for analysis. In order to overcome any data collection flaws, we conducted multiple experiments and selected one that exhibited measurements with the highest suitability for SI. Despite selecting the optimal experiment, the SOFIA® equipment exported measurements that did not possess constant time intervals Δt. Therefore, upon importing the data into MATLAB®, we utilized the resample function, which through data interpolation, eliminated the temporal gaps present in the measurement process, thus achieving uniformity in the voltage and impedance dataset with respect to Δt. The data was resampled at a rate of 1 measurement per second.

The acquired data was processed through the `iddata` command in MATLAB®, which enabled the creation of an object encapsulating the input/output data along with their respective properties such as labels, units of measure, and initial time. Subsequently, the System Identification Toolbox was utilized to load the data object into the environment where the identification of the system was performed.

After importing the data, we proceeded to identify discrete-time and continuous-time transfer function (TF) and state-space models of 2^{nd}, 3^{rd}, 4^{th}, 5^{th}, and 6^{th} order using the System Identification Toolbox in MATLAB®. To obtain the parameters for these models, we employed the prediction error minimization (PEM) method without perturbations. Although the results obtained were not satisfactory.

To process the data and obtain a more accurate model curve that closely fits the experimental data, we developed a MATLAB® script based on the autoregressive representation with exogenous inputs (ARX), which models the system as a linear combination of past outputs, past inputs, and system noise. This approach assumes that the data were collected

at defined instants of time and allows us to mathematically represent the system using (5.1) [118]:

$$A(z^{-1})y(k) = B(z^{-1})u(k) + \xi(k) \tag{5.1}$$

Where ($k = 1,2,...,N$), $y(k)$ represents the output signal at time instant k, $u(k)$ represents the input signal at time instant k, $\xi(k)$ represents the system noise (error in the model or in the measurements) at the time instant k and $A(z^{-1})$ e $B(z^{-1})$ are polynomials in the backward shift operator z^{-1}, representing the system dynamics:

- $A(z^{-1}) = 1 + a_1 z^{-1} + ... + a_{na} z^{-na}$;
- $B(z^{-1}) = 1 + b_1 z^{-1} + ... + b_{nb} z^{-nb}$;

where na, nb are non-negative integers indicating the order of the model.

From (5.1), we obtain the linear regression model (5.2):

$$\mathbf{y} = \phi\theta + \boldsymbol{\xi} \tag{5.2}$$

Where $u(k)$ and $y(k)$ are the sampled observations from the inputs and outputs of the system, respectively. ϕ is the regression matrix, with dimensions $(N - p + 1) \times (na + nb)$, θ are the model parameters, ξ is a vector of residues, distributed in an independent, uniform way, with zero average and finite variance and $p = 1+\max(na,nb)$. We present the expansion of the terms in (5.2) in sequence:

$$\phi(k) = \begin{bmatrix} -y(k-1) \\ -y(k-2) \\ . \\ . \\ . \\ -y(k-na) \\ u(k-1) \\ u(k-2) \\ . \\ . \\ . \\ u(k-nb) \end{bmatrix}, \theta = \begin{bmatrix} a_1 \\ a_2 \\ . \\ . \\ . \\ a_{na} \\ b_1 \\ b_2 \\ . \\ . \\ . \\ b_{nb} \end{bmatrix}$$

$$\begin{bmatrix} y(p) \\ y(p+1) \\ . \\ . \\ . \\ y(N) \end{bmatrix} = \begin{bmatrix} \phi^T(p) \\ \phi^T(p+1) \\ . \\ . \\ . \\ \phi^T(N) \end{bmatrix} \theta + \begin{bmatrix} \xi(p) \\ \xi(p+1) \\ . \\ . \\ . \\ \xi(N) \end{bmatrix}$$

To estimate the unknown parameters of the vector θ referring to the coefficients of the polynomials $A(z^{-1})$ and $B(z^{-1})$, we employed the least squares algorithm (5.3):

$$\hat{\theta} = (\phi^T \phi)^{-1} \phi^T \mathbf{y} \tag{5.3}$$

Once the SI was performed to depict the roll-off, the dataset generated using the ARX model with one-step forward prediction and $na = 20$ and $nb = 20$ (5.4) was converted to the discrete-time TF domain:

$$\begin{aligned} y(k) = &-a_1 y(k-1) - a_2 y(k-2) \cdots - a_{20} y(k-20) \\ &+ b_1 u(k-1) + b_2 u(k-2) \cdots + b_{20} u(k-20) \end{aligned} \tag{5.4}$$

We utilized the `tfest` command in MATLAB® to obtain the discrete-time TF model from the dataset. The initial model fit was retained, and subsequently, the model was converted from discrete to continuous time domain for utilization in the PSO algorithm for PID controller design.

5.2.1.3 Validation

The model validation procedure was performed based on the data obtained from the experiments conducted. The experiments were partitioned into two subsets: one for SI and the other for model validation. Initially, we assumed that all models were adequate. To determine the best experiment to include in the validation dataset, we conducted a thorough evaluation of the quality of fit by analyzing the observation and estimation data in both time and frequency domains, as well as analyzing residual plots and reliability regions.

To assess the robustness of the models to experimental data, we employed the "Fit to estimation data" (FIT) index, which is a performance measure commonly used to evaluate the quality of fit between the estimated and reference data for the analysis and validation of the identified models [119]. The FIT index was computed using the "Normalized root mean squared error" (NRMSE), which provides a quantitative measure of the accuracy of the model predictions (see 5.5):

$$FIT = \frac{\sqrt{\sum_{k=1}^{N}[\xi(k)]^2}}{\sqrt{\sum_{k=1}^{N}[y(k) - \bar{y}]^2}} \cdot 100 \tag{5.5}$$

In this context, we also considered the coefficient of determination R^2 (5.6):

$$R^2 = 1 - \frac{\sum_{k=1}^{N}[\xi(k)]^2}{\sum_{k=1}^{N}[y(k) - \bar{y}]^2} \tag{5.6}$$

Where y and $\bar{y}$ are the output data from the experiments and the mean of the experiments, respectively. This is a statistical measure of how well the estimated model fits the prediction data. This metric quantifies the degree of correlation between the estimated and predicted values and is commonly used to evaluate the accuracy of the identified model.

5.2.2 Control Design

5.2.2.1 PID Controller

To prevent roll-off, we propose incorporating a PID controller into the SI. The PID controller is a control technique that combines proportional, integral, and derivative actions to improve the dynamic response of a system. In our impedance control protocol, we use a closed control loop with negative feedback to measure the error, which is the difference between the current tissue impedance (in ohms) and the desired impedance (set point).

The controller takes the error as input and modulates an output voltage (in volts) applied between the active electrodes and the ground terminal using PID actions. Generally, the control loop is composed of two parts, in terms of TF relating the input and output signals: the controller itself, given in (5.7), and the system plant, given in (5.16). The plant is obtained from the SI and has the voltage modulated by the controller as input and the tissue impedance as output:

$$K(s) = K_p + \frac{K_i}{s} + K_d s \tag{5.7}$$

The modulated output voltage that is applied to the electrode tip in the continuous time domain can be represented by (5.8) [1]:

$$v(t) = K_p e(t) + K_i \int_0^t e(\tau)d\tau + K_d \frac{d}{dt} e(t) \tag{5.8}$$

In this work, we utilize the quadratic error integral criterion (5.9):

$$ISE = \int_0^\infty e^2(t)dt \tag{5.9}$$

and the time-weighted quadratic error integral (5.10):

$$ISTE = \int_0^\infty te^2(t)dt \tag{5.10}$$

These serve as performance measures to assess the effectiveness of the PID controller. These measures are assigned to the reduction of overshoot and accommodation time of the manipulated variable to the set point, respectively.

We determined the proportional K_p, integral K_i, and derivative K_d gains using the evolutionary PSO algorithm. In this context, the objective function (OF) we adopted was based on the linear combination of performance parameters in the continuous time domain.

To obtain performance indicators that provide good dynamic responses, we aimed to minimize the OF, given by (5.11):

$$argmin(OF = \alpha ISE + \beta SysOvr + \gamma ISTE) \tag{5.11}$$

Where the ISE, the overshoot of the system ($SysOvr$) and the $ISTE$ are parameters obtained from SIMULINK®. The values α, β and γ are weights referring to each of the performance indicators that should be reduced. Thus, according to the behavior of the system to be controlled, the weights were varied in order to point out to the algorithm which indicator needs more attention to obtain the optimal gains. The block diagram of the circuit designed in SIMULINK® is shown in Fig 11.

The stability analysis of the system is crucial to ensure the effectiveness of the controller design. To this end, we employed the Routh-Hurwitz criterion to analyze the stability of the system, represented by the TF obtained from SI and the PID controller. Specifically, we evaluated the characteristic polynomials and the distribution of the roots in the complex plane to ensure stability.

5.2.2.2 Particle Swarm Optimization

PID controllers are widely used to handle applications that require high precision, such as motion control, positioning, and heat treatment [120, 121]. Various controller tuning methodologies have been developed to achieve optimal performance, and among these, the Ziegler-Nichols method is considered to be one of the most well-known techniques [122, 123]. However, determining the optimal or near-optimal gains using the Ziegler-Nichols formula has a tendency to generate a large overshoot [124].

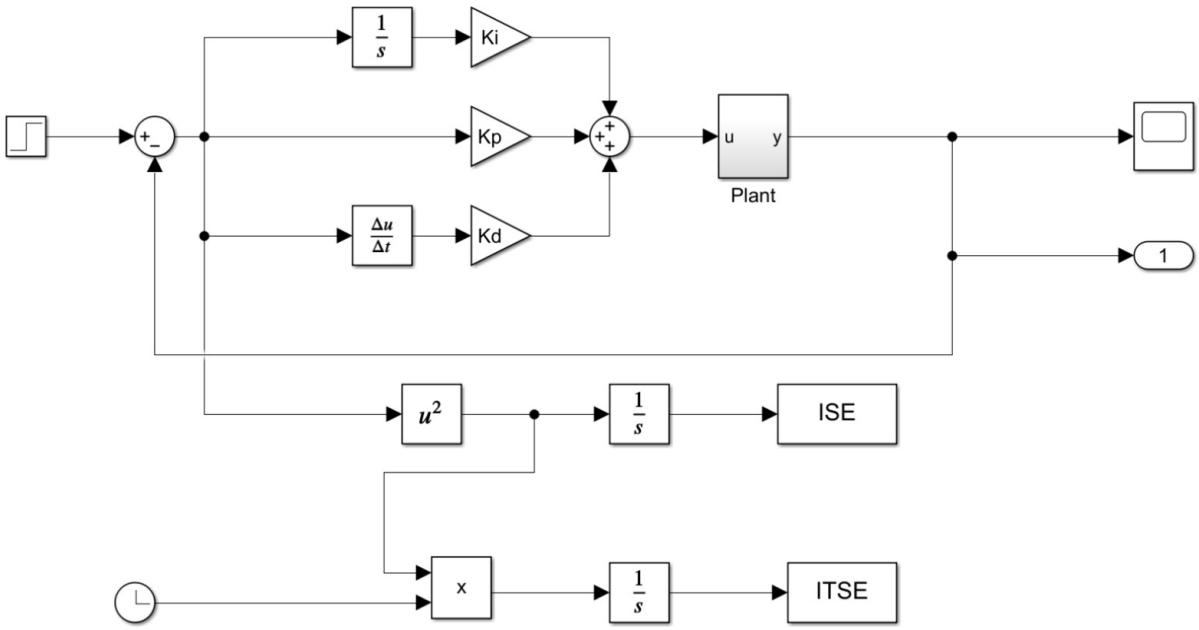

Figure 11 – **Block diagram of the circuit designed in SIMULINK®.** The block diagram highlights the circuit designed in Simulink software for determining the gains K_p, K_i, and K_d of the PID controller. Additionally, it shows the presence of the ISE and ISTE errors, which are calculated and sent to the script in MATLAB® software to compose the OF. Also visible are the presence of integrator blocks $\frac{1}{s}$, differentiator $\frac{\Delta u}{\Delta t}$, the system plant highlighted in 5.16, blocks performing quadratic calculations (u^2) and product (x) of variables besides the output variable (1) that returns values to the PSO algorithm for calculating the overshoot and being added to the OF.

Source: Own authorship

In this work, we use the PSO algorithm to tune the PID controller. The PSO algorithm was proposed by Eberhart and Kennedy [125] and is based on computational search and optimization techniques inspired by the collective intelligence of swarms, schools of fish, and the social behavior of birds when searching for food [126].

Each particle in the PSO algorithm is treated as a zero-volume element in an N-dimensional space [124], where N represents the number of tuning parameters of the controller. The particles work collaboratively and competitively to find the optimal solution, with each particle representing a possible potential solution [127, 128]. Each particle adjusts its search direction based on its own experience and the knowledge of its fellow swarm particles. It is attracted to the best solution that any particle in its neighborhood has found [122].

In this sense, the swarm is initiated by randomly distributing particles in the search space, represented by position and velocity vectors [129]. The i^{th} particle is then defined by three vectors:

- The coordinates of an individual particle in the N-dimentional search space $\vec{x}_i = (x_{i,1}, x_{i,2}, \cdots, x_{i,N})$;

- The rate of change in position (velocity)
  $\vec{v_i} = (v_{i,1}, v_{i,2}, \cdots, v_{i,N})$;
- The position of best fitness that each particle has achieved (*pbest*)
  $\vec{p_i} = (p_{i,1}, p_{i,2}, \cdots, p_{i,N})$.

The search for an optimal solution in the PSO algorithm involves determining the best overall fitness position, considering all elements globally. This is accomplished through the variable gbest. The velocity and position updates of each particle are then calculated based on the current velocity and the distance between the particle's personal best position (pbest) and the global best position (gbest). In an examination involving S particles, the position of the i^{th} particle in the j^{th} dimension is updated using (5.12) and (5.13):

$$v_{i,j}^{k+1} = \omega v_{i,j}^{k} + c_1 r_1 (pbest_{i,j} - x_{i,j}^{k}) + c_2 r_2 (gbest - x_{i,j}^{k}) \tag{5.12}$$

$$x_{i,j}^{k+1} = x_{i,j}^{k} + v_{i,j}^{k+1} \tag{5.13}$$

Where the iteration index is denoted by k, while the maximum number of iterations is represented by the variable MaxIter, which is used as a stopping criterion. Specifically, the algorithm continues to execute while the condition $0 < k \leq MaxIter$ is satisfied.

The values of c_1 and c_2 correspond to the cognitive and social coefficients, respectively, and are related to the degree of self-confidence and trust within the swarm. These values determine the influence of the particle's own experience and the collective knowledge of the swarm on its movement. They are usually set to constant values, although adaptive versions of PSO exist that dynamically adjust these coefficients during the optimization process. Additionally, the values of the maximum and minimum velocities (V_{max} and V_{min}, respectively) and positions (X_{max} and X_{min}, respectively) are pre-determined and constrain the particle's movements to remain within the search space.

The values of r_1 and r_2 are random numbers that are uniformly distributed in the range of 0 to 1. The variable ω represents the inertia factor, which is used to decrease the magnitude of the velocity during the iterations. The inertia factor is applied in the calculation of the velocity according to (5.14):

$$\omega^{(k+1)} = \omega^{k} + \frac{(\omega_f - \omega_0)}{MaxIter} \tag{5.14}$$

Where ω_f and ω_0 are the final and initial inertia factors, where we use the values 0.1 and 0.9, respectively.

In other words, the inertia factor is utilized as a scaling parameter to adjust the current velocity of each particle. A proper choice of ω can strike a balance between global and local

exploration, thereby reducing the number of iterations required to find a satisfactory solution [124].

Based on the simulation results, we have identified the parameters mentioned in this section that provide satisfactory performance. To ensure the validity of these parameters, we have conducted several validation tests. Our parameter selection was guided by research works cited in this paper, including [122, 124, 129–132], and [133]. The mentioned articles provide valuable information on PSO algorithm optimization, including the selection of appropriate values for its parameters based on swarm communication topologies and proposed modifications to the original algorithm. The flowchart has been appropriately included in the Appendix E.

5.3 Results

Despite being widely used for the treatment of HCC, RFA still requires parameter optimization and techniques that can provide better clinical outcomes, safety, and procedural efficacy. In this study, we demonstrate a System Identification (SI) technique to analyze tissue impedance behavior during RFA procedures through computer simulation. The impedance analysis, associated with the roll-off phenomenon, can result in a more effective procedure by extending the ablation time without damaging adjacent tissues. The data were derived from a previous ex vivo study conducted by our research group. In this study, we employed a PID controller to adjust the occurrence of the roll-off phenomenon using a PSO algorithm.

5.3.1 Ex vivo data obtained for simulation of parameters

The experiments were conducted with an initial power of approximately 34 W applied by the monopolar electrode to the liver samples. In Figure 12, for the estimation and validation experiment, we can observe that in the first 30 seconds of the ablation procedure, both the voltage and power decrease, stabilizing around 26 V and 16 W, respectively. This event is also observed in ex vivo liver experiments by [134]. The power and voltage exhibit this behavior due to the initiation of current circulation in the RF generator, causing a slight drop in power due to the applied load. In this scenario, at the beginning of the ablation procedure, the increase in temperature leads to an increase in the electrical conductivity of the tissue, causing the tissue impedance to drop slightly in the initial moments [135].

As we approach the moment of roll-off, there is a sharp drop in current and power, which can be attributed to the impedance behavior. According to [53], temperatures above 85°C result in a decrease in electrical conductivity due to progressive tissue dehydration. In this context, considering the relationship of Ohm's law, we can infer that the sudden increase in voltage is related to the increase in tissue impedance and decrease in current.

The decrease in power is associated with the relationship between power, impedance, and current, where the latter exhibits quadratic behavior in the mathematical expression.

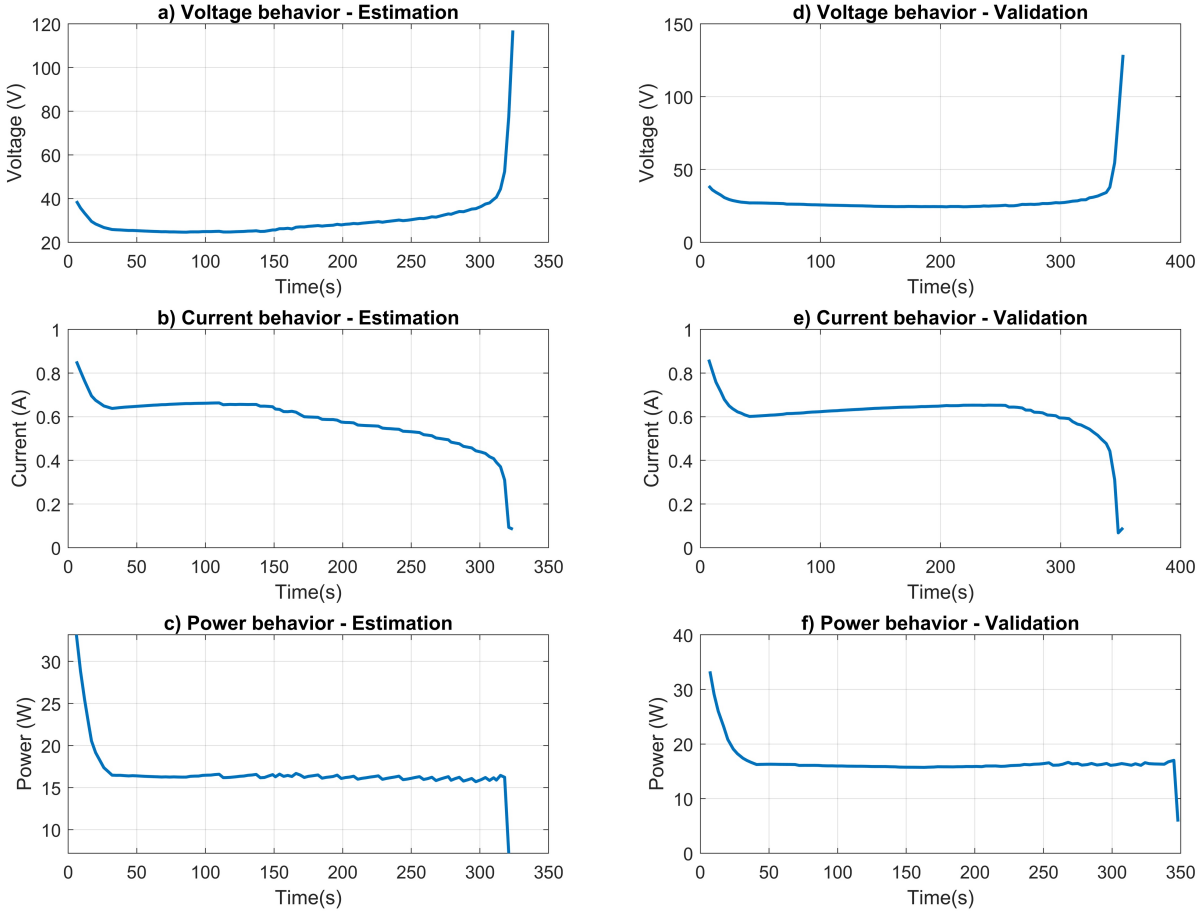

Figure 12 – **Voltage, current and power behavior.** The experimental setup involved initiating the procedure with a power of approximately 34 W using a monopolar electrode on the liver samples. Throughout the estimation phase (Figs a, b, and c), the behavior of voltage, current, and power was meticulously observed. The validation phase (Figs d, e, and f) mirrored these observations. The occurrence of roll-off, a crucial phenomenon in the ablation process, was clearly evidenced in both phases. Roll-off is characterized by a significant decrease in current and power, accompanied by a notable increase in voltage, indicating a sharp rise in impedance. This reduction in current and power can be attributed to the principle that the energy transferred per unit of time is directly proportional to the square of the current, highlighting its pivotal role in the procedure.
Source: Own authorship

5.3.2 System Identification

Based on the ex-vivo experiments conducted, we selected the most promising assays for use in SI for the estimation and validation phases of the model based on the comparison of obtained roll-off curves.

Firstly, we initiated the SI process using MATLAB® System Identification Toolbox. Several models such as TF, state-space representations, both in discrete and continuous-

time domain were applied to the experimental data, however, satisfactory results were not obtained, or the models did not converge. From this point, the next step was to use the ARX polynomial model.

Fig 13 displays the tissue impedance measurements obtained during the estimation and validation phases for the selected experiment at each time instant. In the following, we present the behavior of the data that we used for model estimation and validation.

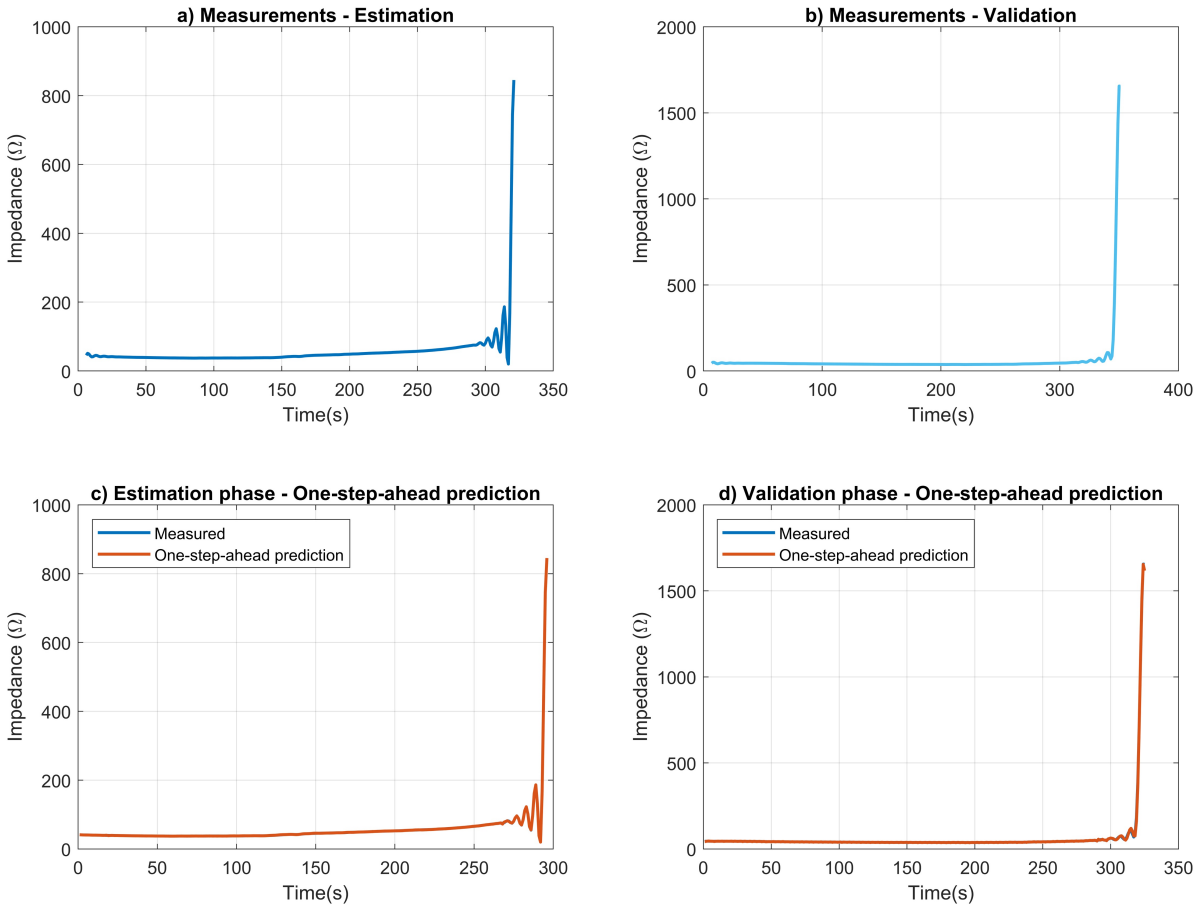

Figure 13 – **System identification graphs.** The tissue impedance measurement procedure in this study involved using the ARX model to measure tissue impedance (Ω) over time(s), with separate estimation and validation datasets. The procedure comprised four main steps: (a) displaying tissue impedance measurements related to SI, (b) displaying validation data measurements, (c) estimating phase using measurement and prediction curves one step ahead, and (d) validating the phase using measurement and prediction curves one step ahead. Plots for each step of the SI procedure are presented in corresponding subfigures (a), (b), (c), and (d), providing a detailed overview of the approach. As discussed in the previous subsection, the impedance behavior in both the estimation and validation datasets is clearly observable. Additionally, the graphs indicate that roll-off occurred at distinct time intervals, precisely at 318 s and 345 s, respectively. The prediction curves almost overlap with the measurement data, demonstrating the method's effectiveness for these experiments.

Source: Own authorship

After obtaining the measurements, we employed the SI procedure with a time interval of 316 seconds after resampling the data. During the simulation to determine the order of

the ARX model, we observed that higher order polynomials resulted in a better fit. However, when we transformed the model to continuous time TF representation, the FIT index was reduced, resulting in an unsatisfactory degree of accuracy.

Empirically, we determined the optimal orders of the polynomials $A(z^{-1})$ and $B(z^{-1})$ for the ARX model through computer simulations and verification of the FIT indices. We selected $na = 20$ and $nb = 20$ for the discrete-time model.

Figs 13(c) and 13(d) demonstrate the results of the one-step-ahead prediction using the model given in (5.4) for both the estimation and validation data, respectively, depicting the behavior of the tissue impedance. The FITs for the estimation and validation data were 99.628% and 97.872%, respectively. The correlation (R^2) values obtained were 0.99999 and 0.99955 for the estimation and validation data, respectively.

To ensure the adequacy of the ARX model, we conducted an analysis of the statistical properties of the residuals, in addition to selecting the best order of the model based on the fitting results. Fig 14 shows the autocorrelation and cross-correlation ranges of the residuals in relation to the input signal of the model. The plot indicates that the residuals exhibit low levels of autocorrelation and cross-correlation, and the dotted lines represent the threshold limits for adequacy of the model, where estimated residuals are approximately uncorrelated.

The bounded regions indicate the results of statistical validation tests, with 95% confidence, computed using the difference between the experimental impedance data and the one-step-ahead prediction of the input data (voltage).

Fig 14 comprises five representations. The first three show the autocorrelation and cross-correlation analysis from a linear point of view, which is the nature of the identification method used. The next two representations demonstrate an analysis carried out to check for any nonlinear correlations of the residuals.

It can be observed that a small portion of the correlation tests for the residuals falls outside the 95 percent confidence margin. This situation is attributed to the nonlinear behavior of the curve that describes the roll-off phenomenon. However, nonlinear tests were performed, but did not yield better FIT results than the adopted model. Additionally, the small extrapolations do not significantly affect the dynamic performance of the model [136].

From (5.4), we obtain the plant discrete-time TF $P_D(z^{-1})$ (5.15):

$$P_D(z) = \frac{33.37z^{-1} - 96.47z^{-2} + 120.6z^{-3}}{1 - 2.42z^{-1} + 2.72z^{-2} - 1.79z^{-3} + 0.45z^{-4}} \cdots \\ \cdots \frac{-80.08z^{-4} + 20.9z^{-5} + 1.71z^{-6}}{0.37z^{-5} - 0.68z^{-6} + 0.54z^{-7} - 0.17z^{-8}} \tag{5.15}$$

This representation maintained the polynomial model's good FIT. Then, we extracted the continuous-time TF representation to capture the behavior of the roll-off phenomenon,

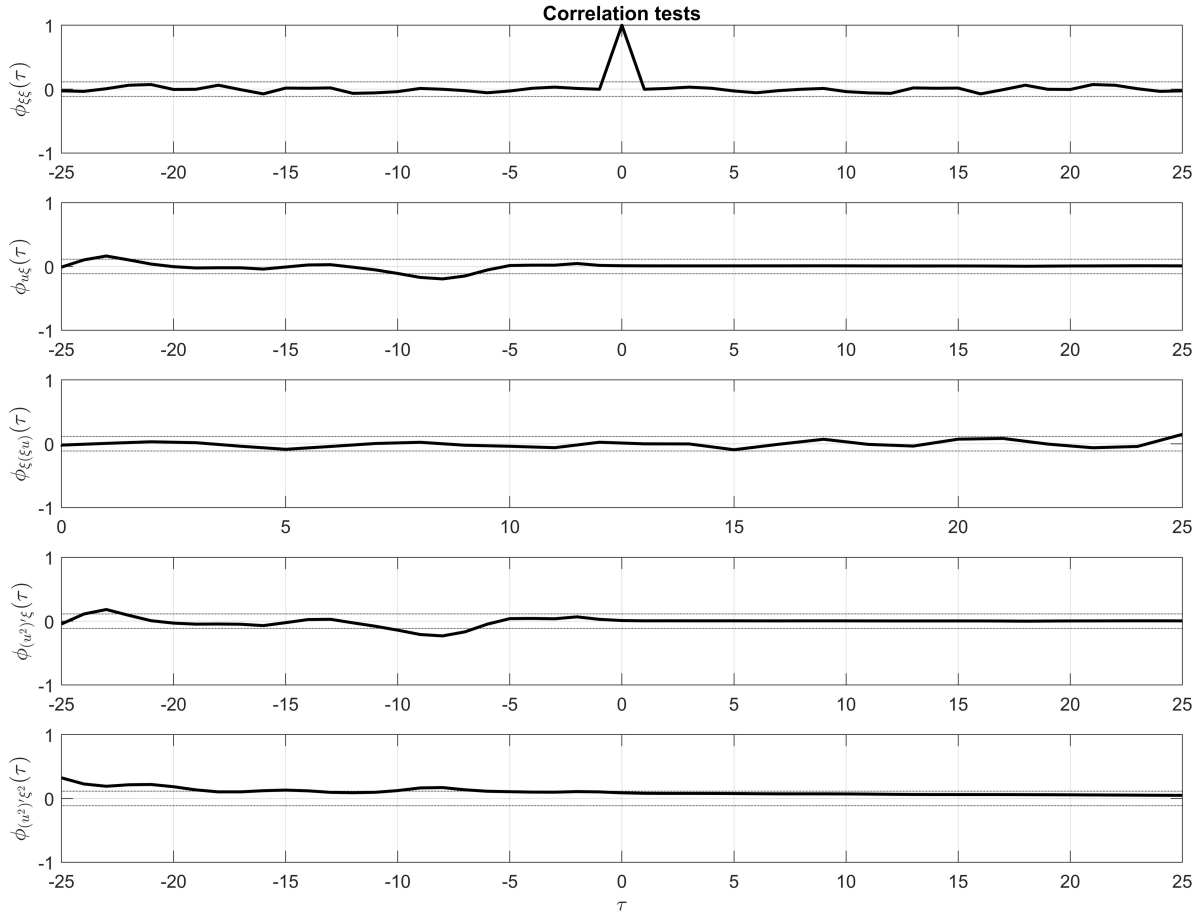

Figure 14 – **Correlation tests.** The graph displays the results of correlation tests conducted on the residuals. The first three plots depict the analysis of linear correlation, while the following two plots illustrate the analysis of non-linear correlation and autocorrelation. Dotted lines represent the 95% confidence level limits. It is worth noting that these residual tests are more concerned with the statistical performance of the estimator than with the dynamic performance of the identified system. Additionally, while the ARX method is linear, we employed non-linear correlation analysis due to the non-linear behavior exhibited in the impedance curves in both the estimation and validation phases.

Source: Own authorship

as shown in (5.16):

$$P(s) = \frac{32.43s^8 + 135s^7 + 510.3s^6 + 925.7s^5}{s^9 + 2.12s^8 + 15.76s^7 + 21.61s^6 + 55.28s^5} \cdots \\ \cdots \frac{1104s^4 + 829.7s^3 + 556.9s^2 + 58.83s + 0.81}{46.8s^4 + 49.14s^3 + 24.45s^2 + 7.28s + 0.5} \tag{5.16}$$

We conducted an empirical estimation of the TF by testing several model orders. The one with 9 poles and 8 zeros resulted in the best FIT, with an index of 85.29% and 64.16% for the estimation and validation data, respectively, as shown in Fig 15.

We proceeded to apply the Routh-Hurwitz criterion to verify the absolute stability of the open-loop system corresponding to the TF. This analysis avoids the need to factorize the

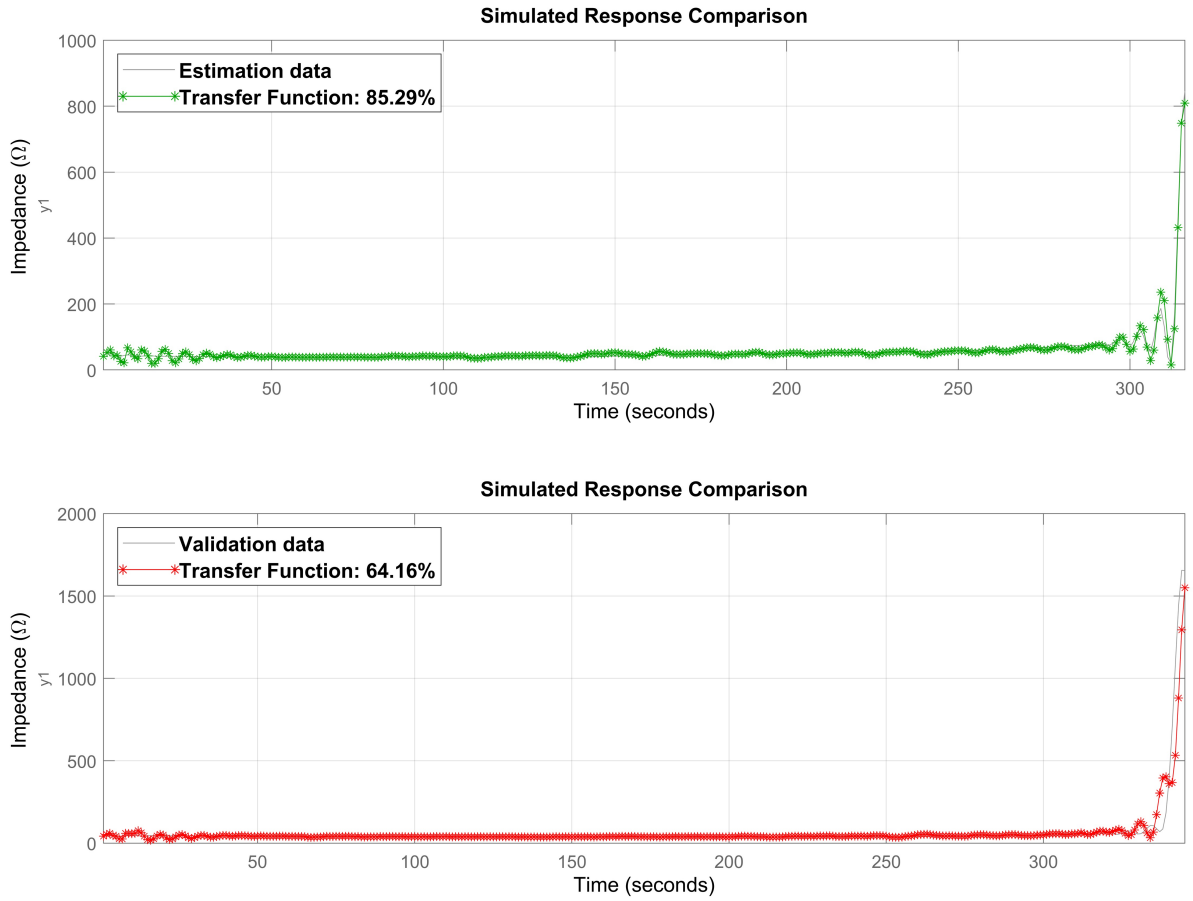

Figure 15 – **Transfer function camparison graphs.** These graphs depict the comparison between the data extracted from the ex-vivo experiment and the data belonging to the TF model, as presented in 5.16. The green curve represents the model fit to the estimation data (85.29%), while the red curve represents the fit to the validation data (64.16%). It is noteworthy that the system identification tests conducted directly from the measured data did not yield satisfactory results. The model fit obtained is due to the use of the ARX method with one-step-ahead prediction, which provided a new set of data from which the TF was derived.

Source: Own authorship

characteristic equation polynomial.

Table 1 shows the results of this analysis. The number of sign changes in the first column corresponds to the number of poles located on the right side of the complex plane. If all elements have the same sign, the system is considered stable.

After verifying the stability of the open loop system, we can now analyze the dynamic response of the model. Fig 16 shows the step response and the root locus of the system.

The step response shown in Fig 16 displays a significantly high overshoot of around 1980% for a unit input signal. Furthermore, the open-loop system's dynamic response exhibits a long settling time of 15.2 s and a final transfer function amplitude that differs from the expected value (1.61).

The Root Locus diagram, as depicted in Fig 16, illustrates the roll-off phenomenon,

Table 1 – **Routh-Hurwitz stability criterion for the $P(s)$ TF from SI: Open-loop roll-off system**.

s^9	1	15.7632	55.2829	49.1387	7.2780
s^8	2.1186	21.6147	46.7952	24.4473	0.5032
s^7	5.5608	33.1950	37.5992	7.0405	⋯
s^6	8.9679	32.4704	21.7650	0.5032	⋯
s^5	13.0608	24.1033	6.7285	⋯	⋯
s^4	15.9204	17.1450	0.5032	⋯	⋯
s^3	10.0379	6.3156	⋯	⋯	⋯
s^2	7.1282	0.5032	⋯	⋯	⋯
s^1	5.6070	⋯	⋯	⋯	⋯
s^0	0.5032	⋯	⋯	⋯	⋯

In summary, the Routh-Hurwitz criterion provides a useful tool for determining the stability of a TF obtained from SI, allowing for the analysis of its dynamic behavior and identification of the need for a controller to ensure stability.

indicating that any changes in the model parameters can induce a sudden increase in tissue impedance, interrupting the RFA procedure. The impending destabilization of the model requires the presence of a controller to modify the Root Locus and ensure a stable dynamic response of the RFA model.

The evaluation of the system's Root Locus diagram in Fig 16, linked to the system's transient response, reveals the representation of the open-loop poles and zeros, noting the absence of a control process in the control parameters. As it is a qualitative method, it is possible to observe that the dominant poles, close to the y-axis, have very short branches that, when varying any parameter, affect the root locus branch.

To make adjustments in this system, it is necessary to carefully evaluate the ideal positions for the inclusion of parameters, in order to meet stability and sensitivity criteria. This analysis provides an understanding of the best control strategy to be selected for the system, the need for simplifications in the extracted mathematical model, and the limitations of the model. This justifies the inclusion of a method for constructing a controller that generates a mathematical precision of adjustment and design made by using bioinspired systems techniques. This leads us to believe that controllers incorporated into ablation systems should be adjusted using techniques like those presented in this article. Table 5 presents the roots of the open-loop system.

5.3.3 PSO Results

We performed all simulations on a computer with a 2.2 GHz Intel® Core I5-5200 processor and 8 GB of RAM. We used MATLAB® / SIMULINK® 2021a. The computational cost will be presented in the following sections.

Table 2 presents the parameters used to obtain the best results. The performance of the PID controller was estimated using the PSO algorithm, and the results are shown in Fig

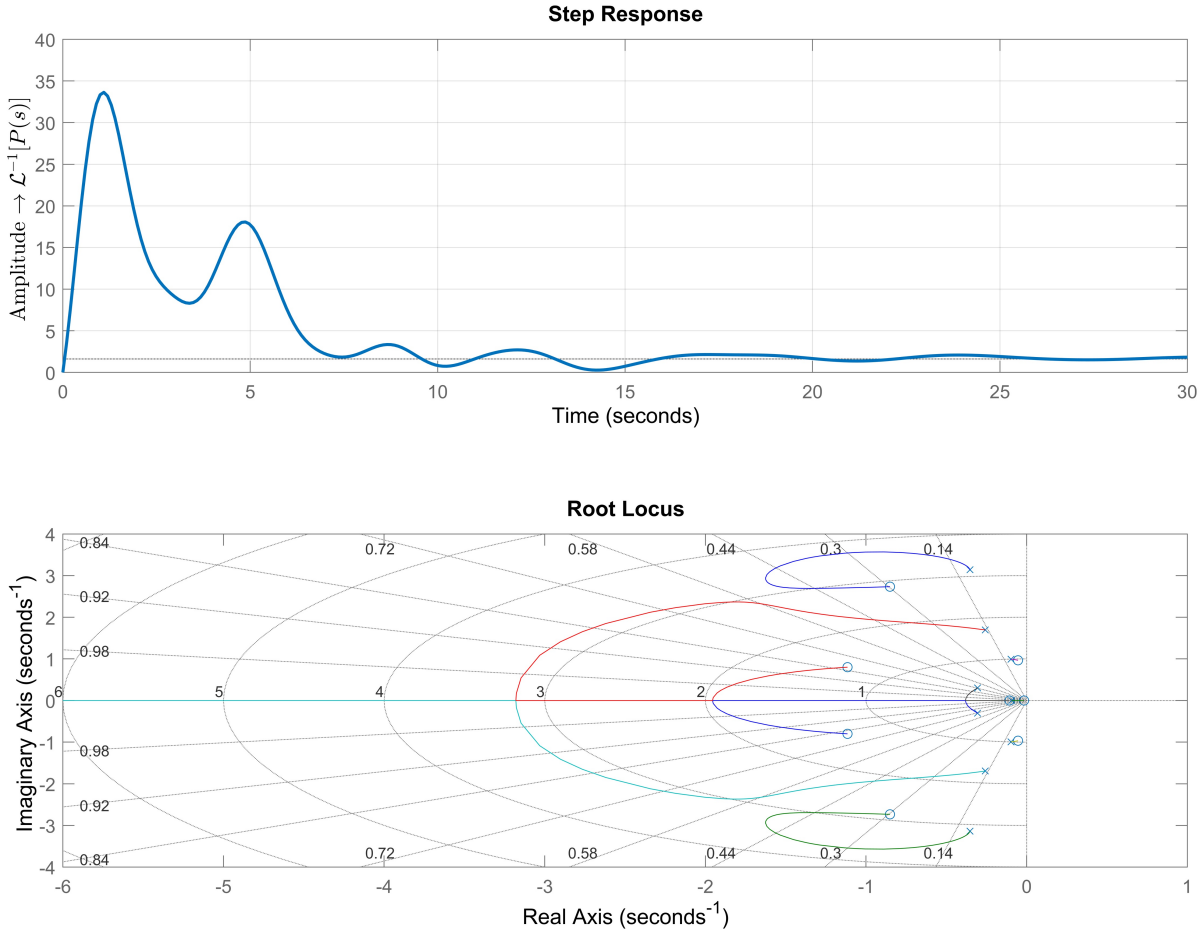

Figure 16 – **Step response and root locus.** The dynamic step response of the open-loop model, where the input is voltage and the output is impedance, is presented. Along with the root locus plot, the figures demonstrate that the system response is composed of several terms that promote oscillatory behavior and does not reach the desired setpoint. The step response exhibits a rise time of 0.0364 s, a peak amplitude of 33.6, a settling time of 15.2 s, and a final value of 1.61. From the characteristic equation in (5.16), it can be observed that the system has nine poles in the left-half plane of the complex plane, indicating stability. However, dominant complex conjugate poles close to the imaginary axis are present. These poles exhibit oscillatory behavior, which is reflected in the oscillations and long settling time of the system. Such characteristics make the system highly susceptible to disturbances, which can lead to instability. In the context of this work, the root locus represents the roll-off phenomenon, where any changes in the model parameters can cause a sudden increase in tissue impedance, potentially disrupting the RFA procedure. The impending destabilization of the model highlights the need for a controller to modify the root locus and sustain a stable dynamic response of the RFA model.
Source: Own authorship

17 and Table 3. Points A, B and C in the step response graph indicate the rise time, overshoot and settling time, respectively. The step response illustrate the behavior of the PID controller described in (5.7), applied to the plant described in (5.16).

Additionally, the convergence curve of the PSO algorithm is displayed in Fig 18, demonstrating that the algorithm converged to the solution after 7 iterations, with a precision of 10^{-2}.

Table 2 – **Parameters applied to PSO**

⋯	Min. value	Max. value
S	30	⋯
N	3	⋯
x	0.01	10
ω	0.1	0.9
c_1	2.05	⋯
c_2	2.05	⋯
v	$\frac{v_{max}}{3}$	$(x_{max} - x_{min}) \times 2$
$MaxIter$	⋯	10
α	0.5	⋯
β	0.6	⋯
γ	0.8	⋯

Table 3 – **Simulation PID gains and performance indexes**

⋯	K_p	K_i	K_d
⋯	5.0594	10.0	0.4959
Peak amplitude	1.007(B)		
Overshoot	0.605 % at 0.314s (B)		
Rise time (s)	0.127 (A)		
Settling time (s)	2.87(C)		
Elapsed time (s)	832		

By implementing the PID controller and introducing negative feedback, we confirmed that the system still satisfies the Routh-Hurwitz stability criterion, as described in Table 4. In contrast to the open-loop system, where the poles of the characteristic equation are considerably close to the zeros of the transfer function (TF), the introduction of the controller significantly influences the TF of the model. This influence can result in the poles experiencing negligible displacement towards their respective zeros with the variation of gain. This transformation can change a system that initially exhibited a long settling time into a critically damped system, as shown in the root locus diagram (see Fig 17).

With the introduction of the controller, the branches of the root locus were repositioned, notably in the interval between [x = -6 and -7] and [x = -2.5 and -3], optimizing their decay. These branches, when located on the real axis, contribute to adjusting the steady-state

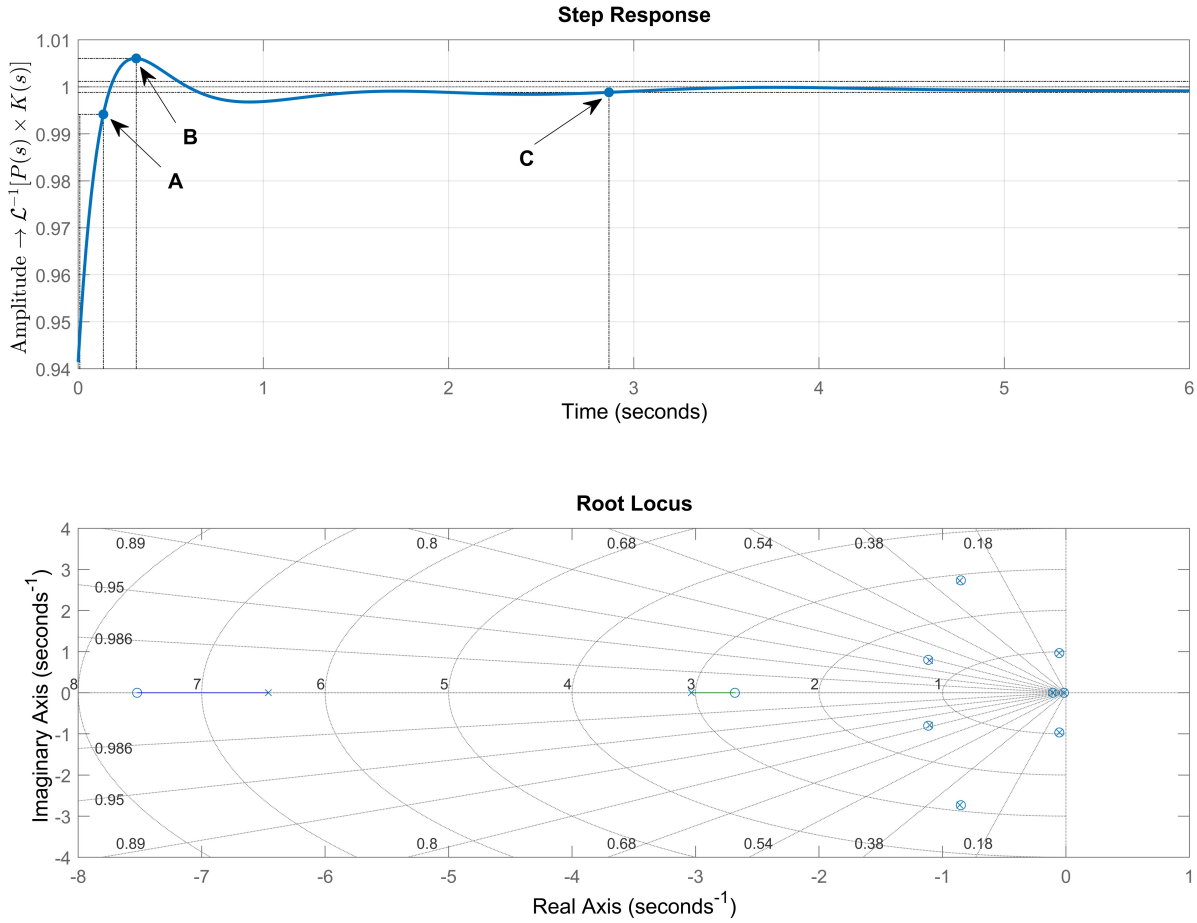

Figure 17 – **Step response and root locus after PSO PID tuning.** The plots depict the response of the PSO algorithm with the parameters presented in Table 3. The step response illustrate the effect of the applied PID controller on P(s) (see (5.16)), where the input is voltage and the output is impedance, represented by the tuned TF K(s) (see (5.7)). Points A, B, and C highlight the instants where the rise time, peak amplitude, and settling time of the step response are measured, respectively. Additionally, the root locus after PID controller implementation is displayed. The poles of the characteristic equation are considerably close to the zeros of the TF. This indicates the significant influence of the controller on the TF of the model in such a way that the poles underwent a minimal displacement towards their respective zeros with the variation of the gain, transforming an underdamped system into a critically damped one.

Source: Own authorship

response to reach the desired threshold. As for the other poles, especially the complex conjugate pairs (see Table 5), they were precisely adjusted with a precise branching locus, thanks to the presence of the PSO. This was done to ensure that performance indicators achieved the best possible response. The individual contributions of each pair, in terms of stability, were evenly distributed in the plane. By analyzing the angular contributions of each one, we can observe the balance that a PID controller adjusted by PSO can promote.

Consequently, we deduce that the RFA procedure moves away from the realm of imminent instability, allowing control of the roll-off by adjusting the input voltage while preserving the tissue impedance at a predetermined value.

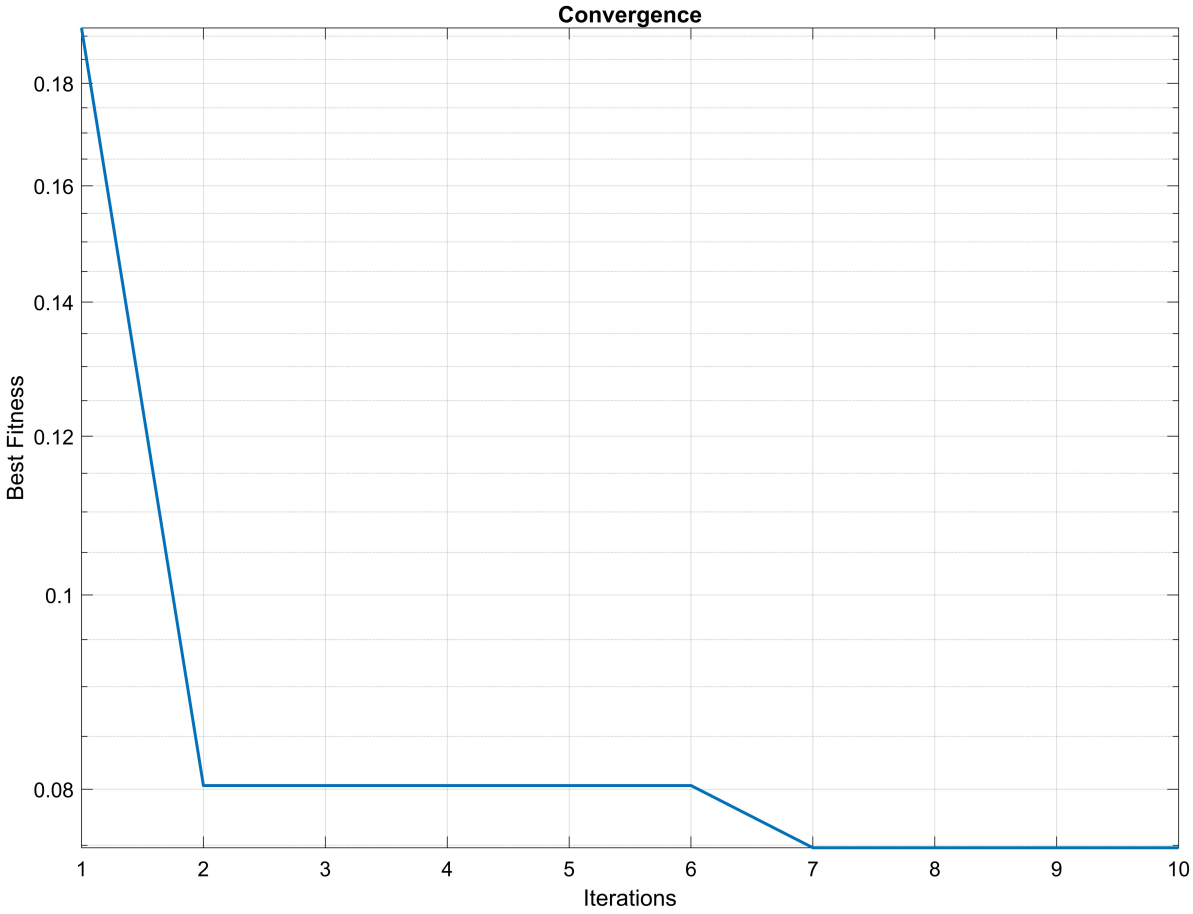

Figure 18 – **PSO convergence curve.** The convergence curve of the PSO algorithm is displayed, demonstrating that the algorithm converged to the solution after 10 iterations, with a precision of 10^{-2}.

Source: Own authorship

Table 4 – **Routh-Hurwitz stability criterion for the $P(s)+K(s)$ TF: Closed-loop roll-off system**

s^{10}	17.08	1276.1	10389	15563	5874.3	8.12
s^9	233.14	4412.4	15301	11168	592.91	⋯
s^8	952.84	9268.2	14745	5830.9	8.12	⋯
s^7	2144.7	11693	9741.5	590.93	⋯	⋯
s^6	4073.3	10417	5568.4	8.12	⋯	⋯
s^5	6208.2	6809.6	586.65	⋯	⋯	⋯
s^4	5949.1	5183.4	8.12	⋯	⋯	⋯
s^3	1400.4	578.17	⋯	⋯	⋯	⋯
s^2	2727.3	8.12	⋯	⋯	⋯	⋯
s^1	574	⋯	⋯	⋯	⋯	⋯
s^0	8.12	⋯	⋯	⋯	⋯	⋯

In an additional set of 19 simulations using a swarm of 30 particles and 10 iterations, the proportional gain (K_p) exhibited a mean of 5.86, variance of 4.22, and a standard deviation of 2.05. The integral gain (K_i) showed values of 9.89, 0.048, and 0.22, respectively. Conversely, the derivative gain (K_d) displayed a mean of 0.57, variance of 0.021, and a standard deviation of 0.14, as we can see in Table 6. Furthermore, the analysis of variance (ANOVA) across

Table 5 – **Root locus for the open-loop and closed-loop system**

Open-loop system roots		**Closed-loop system roots**	
Zeros	**Poles**	**Zeros**	**Poles**
-0.8509 + 2.7340i	-0.3521 + 3.1406i	-7.5226 + 0.0000i	-6.4591 + 0.0000i
-0.8509 - 2.7340i	-0.3521 - 3.1406i	-0.8509 + 2.7340i	-3.0329 + 0.0000i
-1.1152 + 0.8003i	-0.2576 + 1.6943i	-0.8509 - 2.7340i	-0.8595 + 2.7274i
-1.1152 - 0.8003i	-0.2576 - 1.6943i	-2.6809 + 0.0000i	-0.8595 - 2.7274i
-0.0538 + 0.9654i	-0.0979 + 0.9935i	-1.1152 + 0.8003i	-1.1037 + 0.7842i
-0.0538 - 0.9654i	-0.0979 - 0.9935i	-1.1152 - 0.8003i	-1.1037 - 0.7842i
-0.1067 + 0.0000i	-0.3052 + 0.3021i	-0.0538 + 0.9654i	-0.0540 + 0.9654i
-0.0162 + 0.0000i	-0.3052 - 0.3021i	-0.0538 - 0.9654i	-0.0540 - 0.9654i
⋯	-0.0934 + 0.0000i	-0.1067 + 0.0000i	-0.1067 + 0.0000i
⋯	⋯	-0.0162 + 0.0000i	-0.0162 + 0.0000i

the 19 experiments yielded a p-value $\ll 0.05$, suggesting non-normality among the means. Detailed results and statistical analyses can be found in the supplementary materials.

Table 6 – **Statistical Analysis of Controller Gains**

Parameter	Mean	Variance	Standard Deviation
Kp	5.86	4.22	2.05
Ki	9.89	0.048	0.22
Kd	0.57	0.021	0.14

We also explored different parameter settings to optimize the PID controller design and assess the computational cost. Due to the random search nature of the PSO algorithm, each execution returns different controller parameters. We present the results of these simulations for the PID gains in Table 7. The execution time (in seconds) of the algorithm is closely related to the swarm population and the number of iterations, as well as the fixed TF of the plant. The simulation results show that the best trade-off between performance indices and execution time was obtained in Table 3.

Table 7 – **Additional simulations**

S	10	20	20	50	30	100
$MaxIter$	50	30	50	10	50	100
K_p	3.7047	3.1824	10.0	10.0	10.0	4.0299
K_i	10.0	9.9105	10.0	10.0	10.0	10.0
K_d	0.4453	0.4477	0.8001	0.8005	0.8116	0.4698
Elapsed time (s)	1713	2018	3221	1704	4536	29737

In this table, we investigated other possible outcomes for the tuning of the PID controller parameters. From the perspective of PSO, the meta-heuristic returns different results for each simulation. Therefore, we varied the number of swarm individuals and the number of iterations to show the convergence level of the meta-heuristic and compare the computational cost for each initial condition application.

In the last column of Table 7, we present a simulation with a significantly larger particle swarm, along with the algorithm being executed a hundred times. In this scenario,

it can be inferred that the simulation time grew considerably and did not demonstrate an improved result compared to a swarm of 30 particles executing 10 iterations. The performance indices of this simulation for a step response were: 0.768% overshoot at 0.325 s, 0.138 s rise time, and 2.82 s settling time. More details on the simulation results can be found in the supplementary material.

5.4 Discussion

The integration of control systems into RFA procedures for monitoring tissue impedance plays a crucial role in expanding the ablative volume and, consequently, in combating HCC. Enhancing the necrosis region beyond 3 cm has been the focus of numerous studies. However, the roll-off phenomenon, intrinsic to the carbonization of affected tissue in RFA, makes it crucial to regulate the power applied to the target region. One of the primary objectives in the RFA procedure is to avoid any disruption of the energy flow and heat propagation through the tissue.

In this study, we emphasized the application of a PID controller tuned using the PSO technique. Our focus is on managing tissue impedance to delay the occurrence of roll-off and indirectly regulate temperature. We highlighted the real-time management of the manipulated variable by exploring the best performance indicators for the control system. The use of SI based on the experiments described in this paper has yielded satisfactory results for the application of the PID controller. The analysis of various SI techniques resulted in varying levels of accuracy. In this work, we have addressed the combination of methodologies to obtain the best model fit over the experimental data.

The experimental data used in this study were also applied in the work of Da Fonseca *et al* [95]. Using the Box-Jenkins SI technique, [95] concluded that the dynamic response of the system led to abrupt variations in impedance and exhibited a long settling time, in agreement with the ex vivo experiments. This study demonstrated that the mathematical model used revealed that the transient response of the system could be improved by performing the infusion of 0.9% saline solution at 5°C. On the other hand, the incorporation of a properly tuned PID controller yields enhanced results compared to the saline infusion technique. In addition to the prolonged settling time, their system exhibited considerable overshoot.

In the current scientific landscape, only a few authors have presented studies that apply control methods targeting specific variables to enhance RFA procedures. In this context, Cheng *et al* [113] implemented temperature control in RFA interventions based on Fuzzy-PID control. Using voltage as the system input and temperature as the output, this study yielded significant results. By working with a third-order TF, the authors achieved commendable performance indices for the dynamic model. Although this study did not describe the values of gains applied in the tuned PID.

To address the lack of systematic methods for calculating the parameters of the PID controller in control systems applied to RFA, we began by identifying experimental data using the ARX polynomial method, which we then transformed into the TF domain. This approach differs from that of Haemmerich and Webster [137], who identified the model using a discrete TF and the software ANA 2.52 (Freeware, Dept. of Control Engineering, Tech. Univ. Vienna/Austria), and determined the model parameters using the recursive least squares algorithm, as in the ARX method.

To model the RFA procedure more faithfully to the laboratory setting, where energy transfer and impedance variation occur in the continuous-time domain, we designed the PID controller from a continuous-time TF. This approach stands in contrast to that of [137], who used a discrete TF. It is noteworthy that while several theoretical studies on control systems applied to RFA exist, few offer systematic methods for calculating the PID parameters K_p, K_i, and K_d [138]. This underscores the need for further research to develop more systematic approaches for designing PID controllers in RFA systems.

Alba-Martínez *et al* [138], recognizing that most commercial RFA equipment utilize a PI (Proportional Integral) controller, applied this model to control a dynamic system derived from a biological study simulated in COMSOL® Multiphysics software (COMSOL Inc., Burlington, MA, USA), and identified using MATLAB®. Similarly, Webster *et al* [137] employed a PI controller in their study. They, too, used the error between the current temperature of the active electrode and the set point temperature as the input signal of the controller. This error modulated the voltage applied between the active and dispersive electrodes, determining the output of the controller. The temperature measured at the active electrode served as the output signal of the system.

Using the PSO algorithm to determine the controller tunings resulted in significant outcomes. Alba-Martínez *et al* [138] utilized the geometric root locus technique to determine the PI controller gains, while Webster *et al* [137] chose the gains empirically to minimize overshoot and achieve a temporal behavior akin to in vivo experiments. The results found by [138] for the gains of the PI controller have values equal to $K_p = 4.78$ and $K_i = 3.39$. This study does not provide further details regarding performance indices. In the case of [137], the values are $K_p = 0.02$ and $K_i = 0.0064$, obtaining an overshoot of 11%, which was reached after 148 s.

Although the output variable of the dynamic system in our study differs, our simulations yielded significant results. Specifically, after conducting several simulations, the calculated controller gains shared a notable characteristic: the magnitude of the K_d parameter was reduced when compared to the other gains (as shown in Table 7), bringing us closer to a PI controller.

This finding aligns with our expectations, as it suggests that the dynamic system model that describes the roll-off phenomenon based on tissue impedance exhibits clear

similarities with previously studied models based on the active electrode temperature [84, 96]. The model presented in this paper offers the capability to simulate various conditions encountered during RFA interventions by utilizing a bioinspired search topology. It effectively avoids local minima in the objective function, which is strongly connected to the TF of the model.

From a computational simulation perspective, the controller's response suggests that there will be an effective shift in the roll-off curve or, conversely, the prevention of the phenomenon's occurrence. The next steps in this research will involve incorporating the control system into the SOFIA® equipment, along with the optimization algorithm, in the hope of obtaining a system that can be used in RFA of other tissues [95]. In this context, when the ex-vivo tests were conducted, we only have data regarding the ablation volume without the implementation of the controller in the SOFIA device. The citations related to the coagulation volume were based on references that suggest that with the displacement of the roll-off curve, the procedure would not terminate, leading to a more extensive treatment.

The results of this study have the potential to significantly influence clinical guidelines for the treatment of hepatic tumors through RFA. The application of the PSO technique for tuning the PID controller may have a direct impact on the accuracy and effectiveness of RFA. This improvement may result in enhanced clinical outcomes for patients, including more effective tumor ablation, reduced associated complications, and possibly an increase in survival.

The optimized procedure that has emerged from this study comprises a series of well-defined steps intended to guide healthcare professionals in its implementation. Initially, it is crucial to ensure that the RFA equipment is properly calibrated and sterilized. Next, the administration of local anesthesia and correct patient positioning are performed. High-precision imaging techniques are employed for the precise localization of the tumor. The specific settings of the PID controller optimized by PSO are then applied, taking into consideration tissue impedance dynamics. The RFA procedure is initiated, with continuous monitoring of impedance and tissue temperature. Adjustments to the PID controller settings are made as necessary to maintain optimal ablation. Following ablation, an evaluation is conducted to determine the extent of tumor treatment and ensure patient stability.

By optimizing the PID controller, the procedure aims to minimize risks for both patients and the medical team during RFA treatments. The control precision provided by the PID optimized by PSO reduces the potential for complications. Additionally, there are considerations related to potential cost savings. However, specific data and cost estimates require further in-depth analysis. To facilitate the effective implementation of this method, it is important for medical professionals to acquire the necessary training and education.

Comparing the PID controller optimized by PSO approach with existing methods highlights its advantages. This approach offers precise control, minimizing the roll-off

phenomenon and enhancing practical effectiveness compared to other techniques in use. To promote continuous improvement, it is crucial to establish a feedback mechanism that allows professionals to share their experiences and suggestions for procedure optimization. While real case studies or specific success stories of this approach may be limited in number, ongoing research and clinical trials can provide valuable practical evidence. These studies offer insights into the technique's effectiveness in terms of improving patient outcomes and optimizing the RFA procedure.

Through a thorough analysis of our model's dynamics, we can uncover valuable insights into the intricate interplay among tissue impedance, ablation temperature, and electrical factors in RFA. This model offers substantial benefits to both researchers and clinicians working in the realm of RFA, facilitating a comprehensive grasp of the fundamental dynamics that govern the ablation process.

5.4.1 Limitations and future work

One limitation of the proposed model is related to the ex-vivo experiments, which did not take into account the effects of blood perfusion and the heating generated by metabolism, which are present in in vivo RFA scenarios and are also represented in the Pennes' equation. Additionally, the laboratory tests were performed on liver sections rather than the entire organ, which may not fully capture the behavior of electrothermal heating in a complete liver inside the body. Therefore, while the proposed model provides valuable insights into the dynamics of RFA, its applicability to in vivo scenarios may be limited and should be further validated in future studies.

As a prospective avenue for future research, the authors intend to explore the adoption of different objectives in the optimization of RFA procedures. One of these objectives could be to minimize the impact on the ablation zone in healthy tissue, with the aim of avoiding necrosis in the surrounding non-tumor tissue. This approach would prioritize the preservation of healthy liver tissue, which is essential for the patient's overall liver function.

Furthermore, an intriguing prospect for future research involves performing a multi-objective optimization analysis of RFA procedures, which, in addition to minimizing damage to healthy tissue, would also consider factors such as exposure time during the procedure. Multi-objective optimization would allow several parameters to be adjusted simultaneously, providing a more comprehensive assessment of the procedure's effectiveness.

In addition, we plan to investigate the effect of blood perfusion and metabolic heating on the RFA procedure and include these factors in our model. We will also explore the behavior of the RFA procedure in different organs and tissues, such as lung, pancreas, and kidney. Furthermore, we aim to develop a real-time control system that will allow us to monitor and adjust the RFA parameters during the procedure, based on feedback from the

tissue impedance and temperature measurements. Finally, we will investigate the use of other types of controllers, such as adaptive and robust controllers, to improve the performance and robustness of the RFA procedure.

The authors believe that by exploring these future research directions, they can contribute to the advancement of RFA techniques, making them more precise, patient-centered and efficient. This approach has the potential to produce better outcomes for patients with liver tumors while minimizing the impact on healthy liver tissue, which is a critical consideration in the context of RFA.

5.5 Conclusion

This paper presents a novel approach for controlling tissue impedance during RFA procedures based on porcine liver ex-vivo experiments. Our methodology combines three system identification techniques, yielding superior results compared to individual methods.

The implementation of a PID control technique effectively regulates the voltage at the active catheter tip relative to the dispersive one, thereby maintaining tissue impedance at a user-defined preset value to prevent roll-off. The PSO algorithm optimizes the controller gains, resulting in satisfactory performance indicators: a mere 0.605% overshoot, 0.314 seconds rise time, and 2.87 seconds settling time for a unit step input. This showcases the robustness of our PSO-tuned PID controller design in achieving precise and efficient control.

Unlike previous studies that primarily focus on modeling RFA based on tissue temperature or use trial and error techniques to determine the optimal voltage for roll-off delay, our work highlights the importance of controlling tissue impedance as a critical parameter for ensuring continuous and successful RFA.

Moreover, our results demonstrate that the PSO-tuned PID controller design is robust and adaptable to variations in liver tissue properties and environmental conditions. The statistical analysis of 19 simulations revealed PID gains: Kp (mean: 5.86, variance: 4.22, standard deviation: 2.05), Ki (mean: 9.89, variance: 0.048, standard deviation: 0.22), and Kd (mean: 0.57, variance: 0.021, standard deviation: 0.14). The clinical implications of this study are significant and can lead to the development of more effective RFA procedures with reduced complications.

Future research should explore hardware implementations of the proposed PID controller and validate its performance in in-vivo animal models. Additionally, investigating the impact of controlled tissue impedance on the coagulation zone size and conducting clinical trials will further enhance the understanding and applicability of our approach in real-world scenarios.

Overall, this study contributes to advancing the field of RFA by introducing a bioin-

spired solution for roll-off control, offering improved outcomes and expanding the possibilities for liver tumor treatment.

6 Temperature Control to Prevent Esophageal Fistula in RFCA

This chapter presents the article entitled "Optimizing Temperature Control With Particle Swarm Optimization To Prevent Esophageal Fistula: A Three-Dimensional Radiofrequency Cardiac Ablation Model", which belongs to the studies developed during the course of the doctoral research and has been submitted to the scientific journal PLOS ONE (ISSN 1932-6203), boasting a QUALIS-CAPES A1 ranking, CiteScore of 5.3, and an Impact Factor of 3.752.

RFCA is a widely used treatment for AF and other cardiac arrhythmias, where targeted tissue destruction is achieved through the application of radiofrequency energy. Despite its effectiveness, RFCA presents significant challenges, particularly regarding the unintended heating of surrounding tissues, which can lead to severe complications. One of the most concerning complications is the formation of esophageal fistulas, a potentially fatal outcome caused by excessive thermal exposure to the esophagus during the procedure. Therefore, precise control of tissue temperature, especially in critical areas adjacent to the ablation site, is essential for the safety and success of RFCA procedures.

Building on the successes of previous studies, particularly the development of a PSO-tuned PID controller for hepatic ablation, this study aims to extend the application of bio-inspired optimization techniques by employing the GWO algorithm to optimize temperature control in RFCA. The GWO algorithm, known for its robust performance in handling complex optimization problems, will be used to fine-tune the PID controller parameters to manage the dynamic thermal environment of RFCA, similar to how the PSO algorithm was previously used to delay roll-off in hepatic ablation and expand the ablation zone.

In this study, a three-dimensional computational model of RFCA is developed using COMSOL Multiphysics® to simulate the thermal effects of the ablation process, with a particular focus on the temperature distribution in the esophagus. The GWO algorithm will optimize the PID controller parameters to achieve precise temperature regulation, minimizing the risk of esophageal overheating. By leveraging the strengths of the GWO algorithm in optimizing control systems, this research aims to offer a novel solution to one of the most pressing challenges in RFCA, ultimately enhancing the safety and efficacy of the procedure.

6.1 Introduction

AF is the most common type of cardiac arrhythmia, affecting about 50 million people worldwide and is associated with high health costs [6]. The evidence related to its appearance points to the involvement of abnormalities in the conduction of nerve impulses, electrical refractoriness, molecular factors, and unbalance in gene transcription [139, 140].

The AF constitutes a progressive disorder that significantly impacts the patient's functional capacity and quality of life. In the long term, it is associated with high risks of heart failure, cardiovascular failure, and ischemic stroke [141, 142]. However, the available treatments, including antiarrhythmic drugs and ablation surgery, have limitations, potentially leading to adverse effects, complications, or recurrence [139, 143].

RFCA stands as the foremost recommended approach in addressing AF due to its minimally invasive nature and efficacy in restoring heart rhythm control [6, 144]. This technique involves introducing an intravascular catheter housing a RF emitting electrode [145]. When an arrhythmia is detected, the active electrode emits an RF wave, typically around 500 kHz, to a dispersive one positioned on the patient's back [139]. The resulting Joule effect transforms this current into heat, forming a lasting lesion in the cardiac tissue. Cellular necrosis occurs when the temperature reaches approximately 50°C [143]. Despite its effectiveness, RFCA carries potential complications, including cardiac tissue and blood overheating, as well as the potential warming of adjacent organs like the esophagus during the procedure [145].

The efforts to minimize such injuries involve highly complex technological advancements, including the use of computational simulations and mathematical modelling [146]. The *in silico* modelling is a tool used to simulate RFCA aiming to: (i) maintain control of variables; (ii) complement experimental studies; (iii) analyze conditions that would not be easily obtainable *in vivo*; and (iv) predict potential complications during the procedure [145].

The catheters used in the RFCA procedure have undergone technological improvements to allow for more accurate mapping, stimulation, and delivery of RF energy [147]. Some control models are used to measure the electromagnetic power reaching the tissue, such as voltage, temperature or impedance control [147]. In temperature-controlled RFCA, the electrode tip is maintained at a predefined temperature, thus preventing other involved tissue from overheating [147, 148].

To achieve greater precision in the entry temperature of the ablation electrode, it is crucial to control this variable. This equipment improvement could prevent tissue overheating and the formation of clots. In this context, the aim of this article was to develop a three-dimensional computational model for temperature stabilization and precision during RFCA procedures. The study aims to simulate and control the entry temperature of the ablation electrode through a closed-loop controller. The model was devised considering elec-

trical, thermal, and fluid coupling, mathematically solving this intricate interaction using the FEM. This study seeks to precisely control the entry temperature of the ablation electrode using a GWO-tuned PID controller, with the specific goal of preventing the temperature from reaching critical levels in the esophagus, thus preventing fistula formation. The Identification Systems tool was employed to develop the controller, utilizing data obtained from the three-dimensional simulation as the system's input and output. We hope to contribute to enhancing the effectiveness and safety of RFCA procedures, mitigating risks associated with therapy, and improving clinical outcomes for patients with AF.

6.2 Materials and methods

Three-dimensional theoretical models are proposed herein to simulate cardiac ablation procedures with the objective of analytically resolving or minimizing issues related to tissue overheating during RFCA procedures. The methodologies, software implementations, equations, geometries, and convection coefficients at simulation interfaces exhibit a complex and diverse landscape in the existing literature. Leveraging computational simulation data, we employ SI techniques to extract the requisite transfer functions for controller design. In culmination, we introduce the design and implementation of a controller, aimed at refining and optimizing the intricate processes inherent in RFCA.

6.2.1 Computational Model

6.2.1.1 Description of the Three-Dimensional Model

The model was developed adhering to common standards in RFCA, with the myocardium considered as a homogeneous structure devoid of irregularities. The simulated measurements were meticulously selected to mitigate edge effects and were extracted in accordance with the references provided in Table 8 [145, 149].

A three-dimensional computational model was proposed, represented by a cubic fragment measuring 15 mm in width, 15 mm in thickness, and 22.5 mm in height concerning the YZ symmetry plane, considering the actual volume, as depicted in Fig 19. This structure encompasses the myocardium (with a thickness of 2.5 mm), a layer of adipose tissue (with a thickness of 2 mm), the esophageal wall (with a thickness of 3 mm), and represents the blood volume (with a thickness of 15 mm).

The ablation electrode utilized in the simulation is non-irrigated, with a radius of 1.165 mm, and positioned perpendicular to the surface. To simulate the pressure force exerted on the cardiac tissue during RFCA, the electrode is inserted to a depth of 0.5 mm and positioned at 90^{o} in relation to the myocardium, disregarding variations in movement and position [150, 151]. This electrode representation includes a probe to monitor temperature

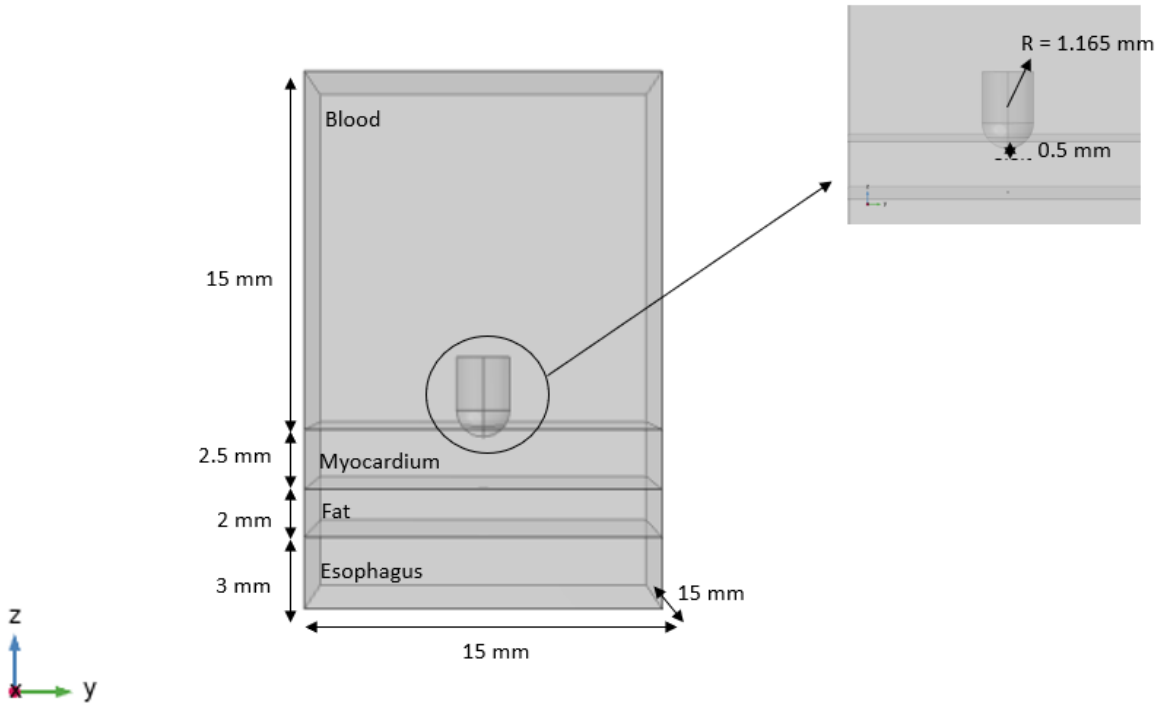

Figure 19 – Parameters of dimensions and geometry employed in the 3D computational model for radiofrequency cardiac ablation (RFCA) simulation.
Source: Own authorship

variations, a fundamental parameter in the modeling and control of this study. Point P_c, illustrated in Fig 20, is the location for temperature measurement.

6.2.1.2 Simulation in COMSOL® Multiphysics Software

The proposed model was implemented and simulated using COMSOL® Multiphysics software. In developing the system, three distinct physical aspects were integrated: electrical, thermal, and fluid dynamics. Specific modules within COMSOL® were employed to address each of these aspects, namely the *Heat Transfer in Solids and Fluids* module, the *Laminar Flow* module, and the *Electrical Currents* module. Additionally, multiphysics coupling modules were utilized to connect these studies, including the *Nonisothermal Flow*, which integrates *Heat Transfer in Solids and Fluids* with *Laminar Flow*, and *Electromagnetic Heating*, coupling *Heat Transfer in Solids and Fluids* with *Electrical Currents*.

It is noteworthy that, owing to its unique characteristics, blood exhibits electrical, thermal, and fluid properties, being the sole fluid considered in the simulation. The mathematical solution to integrate the electrical, thermal, and fluid systems was also resolved within the COMSOL® software.

The numerical solution obtained through COMSOL® software employs the finite element method, utilizing specific governing equations for each physical domain. Initially,

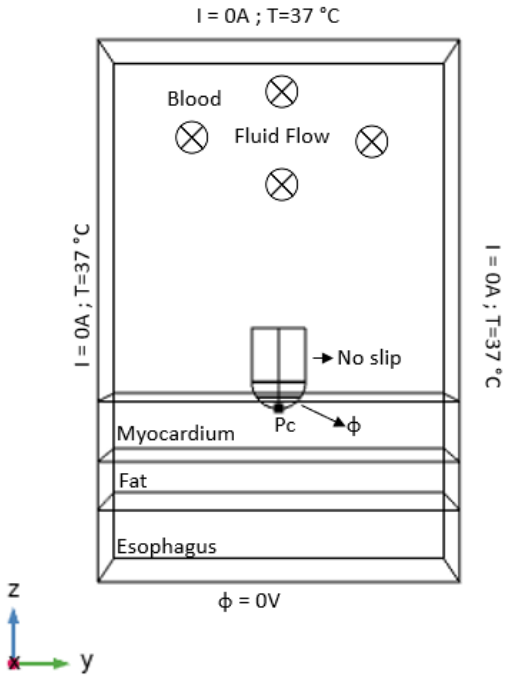

Figure 20 – Geometry of the electrode used in the simulation of RFCA, with emphasis on the temperature measurement point (P_c).
Source: Own authorship

the electrical problem is resolved, where 6.1 represents the Laplace's Equation:

$$\nabla \cdot (\sigma \nabla \phi) = 0 \, . \tag{6.1}$$

In this equation, σ represents electrical conductivity (S/m), and ϕ represents voltage (V).

In RFCA simulations, the model is treated as quasi-static due to the simulated distance, where the ablation electrode impacts a small area around the ablated point. Considering a frequency around 500 kHz, the tissue is considered practically resistive [141, 145]. The distribution of the heat source is determined by the Joule Effect, expressed by 6.2.

$$q = \mathbf{J} \cdot \mathbf{E} \, , \tag{6.2}$$

where $\mathbf{J}$ is the current density (A/m^2), and $\mathbf{E}$ is the electric field (V/m).

The calculation of the electric field stems from the voltage gradient, based on Ohm's second law, expressed by 6.3:

$$\mathbf{J} = \sigma \cdot \mathbf{E} \, . \tag{6.3}$$

This results in 6.4:

$$\mathbf{E} = -\nabla \phi \, . \tag{6.4}$$

To address the thermal problem, we employ the Pennes Equation, also known as the Bioheat Transfer Equation [145, 146]. This equation models heat transfer in living organisms, considering the effects of blood flow on temperature [145, 146, 152]. Its formulation, presented in Equation 6.5, involves parameters such as density, specific heat, and thermal conductivity of the tissue.

$$\rho \, c \frac{\partial T}{\partial t} = k \nabla^2 T_q - Q_p + Q_m - \rho c \boldsymbol{u_0} \nabla T \, , \tag{6.5}$$

where ρ is the density (kg/m^3), c is the specific heat (J/kg·K), and k is the thermal conductivity (W/m·K).

Here, Q_m (W/m^3) represents the metabolic heat generation rate, Q_p (W/m^3) indicates heat lost in blood perfusion, and T (°C) refers to temperature. Additionally, T_q (W/m^3) is the heat source generated by RF, and u_0 (m/s) is the blood velocity field. Due to the insignificance of the values of Q_m and Q_p compared to other terms, they are considered negligible in 6.5.

As this equation addresses the thermal problem, it is incorporated in the option for heat transfer between solids and fluids. The necessary data for these calculations were inputted into the material properties, as shown in Table 8.

The fluid part pertains to blood flow and is governed by the Continuity Equation:

$$\rho \frac{\partial \boldsymbol{u_0}}{\partial t} + \rho \boldsymbol{u_0} \cdot \nabla \boldsymbol{u_0} = -\mu \nabla P + \nabla^2 \boldsymbol{u_0} + \mathbf{F} \, , \tag{6.6}$$

where P represents pressure (Pa), μ is the viscosity of blood (cm/s), and F (N/m^3) are the applied forces. Additionally, we have the incompressible Navier-Stokes flow equation [152–154]:

$$\nabla \boldsymbol{u_0} = 0 \, . \tag{6.7}$$

In this case, F is null, as there is no presence of forces [153, 154]. Therefore, the Navier-Stokes equation can be represented by 6.8:

$$\frac{\partial \boldsymbol{u_0}}{\partial t} = \frac{-P}{\rho} \, . \tag{6.8}$$

6.8 is a combination of a momentum equation (principle of momentum or force balance) and a mass equation (mass conservation) [153].

6.2.1.3 Boundary Conditions

Fig 20 illustrates the electrical boundary conditions applied in the simulation. The electrode was initialized with a voltage of 15 V for 30 s. For temperature analysis aimed at control, the simulation was conducted using a protocol with constant voltage. The initial voltage of the active electrode was set at $\phi = 0$ V.

To maintain realistic conditions, a current of 0 A was adopted, representing zero electrical flux, i.e., a Neumann boundary condition applied to the sides, the top, and the contact point between blood and cardiac tissue during the simulation [152]. An exception was made at the bottom of the model, where the dispersive electrode ($\phi = 0$ V) was located, simulating a monopolar configuration in which the current flows from the active electrode to the dispersive one.

In the context of solving the thermal problem, a Dirichlet condition was applied, fixing the temperature at T = 37°C throughout the entire model [145, 152]. This procedure aims to simulate a constant body temperature throughout the RFCA procedure. The initial temperatures of the tissues were considered as 37°C.

Considering the dynamic properties of blood, its viscosity was set at 0.0021 Pa.s [152, 153]. Blood flow was modeled as laminar, flowing in the negative X-axis direction (see Fig 21), with a velocity of 0.085 m/s [153]. In Fig 20, the circles with a cross in the center indicate that blood flow is directed into the plane of visualization. For the outflow surface, a zero-pressure outlet boundary condition (P = 0 Pa) was set [152, 153].

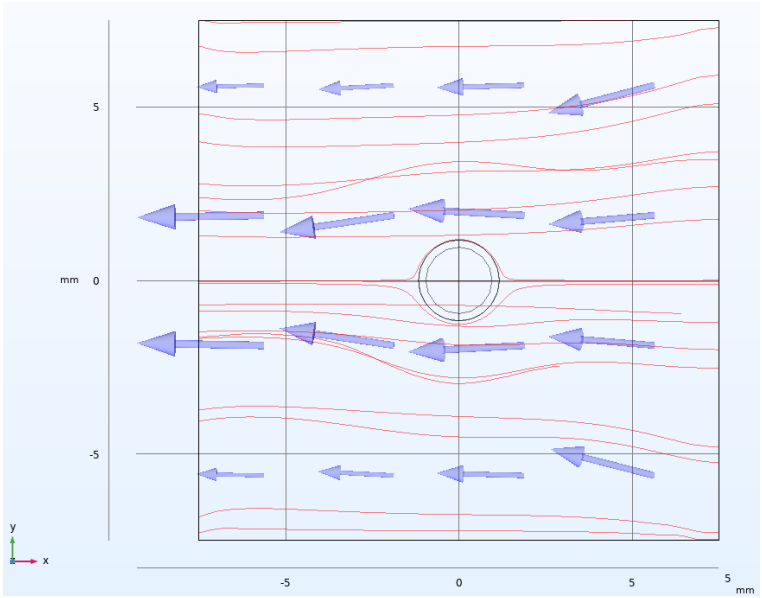

Figure 21 – Direction of blood flow in the negative X-axis direction. The flow velocity was defined as 0.085 m/s with zero pressure at the outlet surface.
Source: Own authorship

6.2.2 Material Properties

Through an extensive literature review, thermal and electrical properties of materials were extracted and presented in Table 8. For properties with distinct values in the literature, the average was used. The lateral boundary conditions were matched so that the average body temperature was 37°C, the voltage of the active electrode was 15 V, and the average duration of the procedure was 30 seconds. Table 8 is divided into two parts: the first with data from the literature review, and subsequently, the data used in COMSOL® simulations.

Table 8 – **Thermal and electrical properties of the model elements**

Literature Review								
		Electric conductivity (σ) [S/m]	**Thermal Conductivity (k) [W/m.k]**	**Density (ρ) [kg/m^3]**	**Specific Heat (c) [J/kg.K]**	**Temperature (T) (°C)**	**Tissue type**	**Power (W) / Voltage (V)**
Domain	**Myocardium**	**0.540** [155] **0.222** [156] **0.222** [157]	**0.53** [155] **0.55** [156] **0.55** [157]	**1060** [155] **1200** [156] **1200** [157]	**3111** [155] **3200** [156] 3200 [157]	**37** [155] **37** [156]	**In silico** [155] [156] [157]	**30** [155] **10** [156] **30** [157]
	Blood	**0.667** [157] **0.99** [151]	**0.543** [157] **0.54** [151]	**1000** [157] **1000** [151]	**4180** [157] **4180** [151]	**36** [151]		
	Electrode	**4.6x10^{-6}** [155]	**71** [155]	**21500** [155]	**132** [155]	**37** [155]		
	Cable	**10^{-5}** [155]	**0.026** [155]	**70** [155]	**1045** [155]	**37** [155]		
	Fat[1]	**0.09**	**0.21**	**911**	**2348**	**37**		
	Esophagus	**0.127** [151]	**0.4** [151]	**1000** [151]	**3700** [151]	**36** [151]		
	Simulation Time	**60s** [155]; **10-130ms** [156]; **30s** [157]						
	Blood velocity	**0.085 m/s** [153]						
Properties used in COMSOL® simulations								
Domain	**Myocardium**	0.541	0.531	1060	3111	37	In silico	
	Blood	0.667	0.541	1000	4180	37		15 V
	Electrode	4.6x10^{6}	71	21500	132	37		20 V
	Cable	10^{-5}	0.026	70	1045	37		
	Fat	0.09	0.21	911	2348	37		
	Esophagus	0.127	0.4	1000	3700	37		
	Simulation Time	30 s						
	Blood velocity	0.085 m/s						

[1] The properties of fat were extracted from the *Bioheat* material library in COMSOL®.

6.2.3 System identification from COMSOL® Multiphysics data

The data employed for modeling originated from simulations conducted in the COMSOL® software. Simulated parameters were exported to MATLAB® R2021a, executed on a computer equipped with a 2.2GHz Intel® I5-5200 processor and 8GB of RAM. Input parameters consisted of voltage values, while output parameters corresponded to temperature measurements, both sampled at a rate of 0.1 seconds.

Simulated data generated an Excel® spreadsheet (Microsoft, Redmond, WA), which was imported into MATLAB® and utilized for SI. The objective was to derive a representative transfer function from this simulation, conducting identification with one dataset for modeling and another for validation.

By applying the `iddata(Y,U,Ts)` function, which creates a data object with output Y, input U, and sampling time T_s, data from COMSOL® were concatenated and utilized in the `tfest(DATA, NP, NZ)` function. This function estimates a transfer function using data in the time or frequency domain, with NP and NZ representing the number of poles and zeros, respectively. This strategy was adopted based on the implementation of SI techniques for dynamic modeling, focusing specifically on the heat transfer phenomenon to the esophageal tissue during cardiac ablation procedures.

For the selection of the transfer function, an order previously used in the literature was chosen, ensuring that the function possesses performance indices that can be evaluated and adjusted through controller design [147].

The `tfest` command in the MATLAB® environment was employed to derive the discrete-time model from the dataset, subsequently converting it to the continuous domain for application in controller design.

Validation of the transfer function model followed the same data generation procedure used for its creation, introducing a 5 V variation in the input voltage. Specifically, the model was initially generated with a 15 V input, and validation data were obtained with a 20 V input. The selection of the most robust model was guided by the FIT index, providing a comprehensive evaluation of the quality of the simulated models.

6.2.4 PID Control Design Methods to Enhance Cardiac Ablation and Prevent Esophageal Fistulas

To prevent esophageal fistulas and optimize the execution of cardiac ablation procedures, we propose the integration of a PID controller into the SI. The PID is a control technique that combines proportional, integral, and derivative actions to enhance the dynamic response of a system. In the configuration of our temperature control protocol, we implemented a closed-loop control system with negative feedback, using a temperature transduction system to voltage, employing a thermocouple through its respective transfer function to measure the error. The error is defined as the difference between the current tissue temperature, obtained in degrees Celsius, and the desired temperature (setpoint). The goal of the controller is to make the procedure more gradual, with controlled heat regulation, as abrupt changes can result in irreversible damage.

The TF of the thermocouple in the feedback loop was estimated through SI (see 6.20), using data collected from the datasheet of a type K thermocouple manufacturer and

adjusting them to our model. Thus, in Fig 22, the block diagram of the complete closed-loop system was obtained with negative feedback. The controller, represented in the diagram by gains K_p, K_i, and K_d together with the integrator and differentiator blocks, has a transfer function given by 5.7.

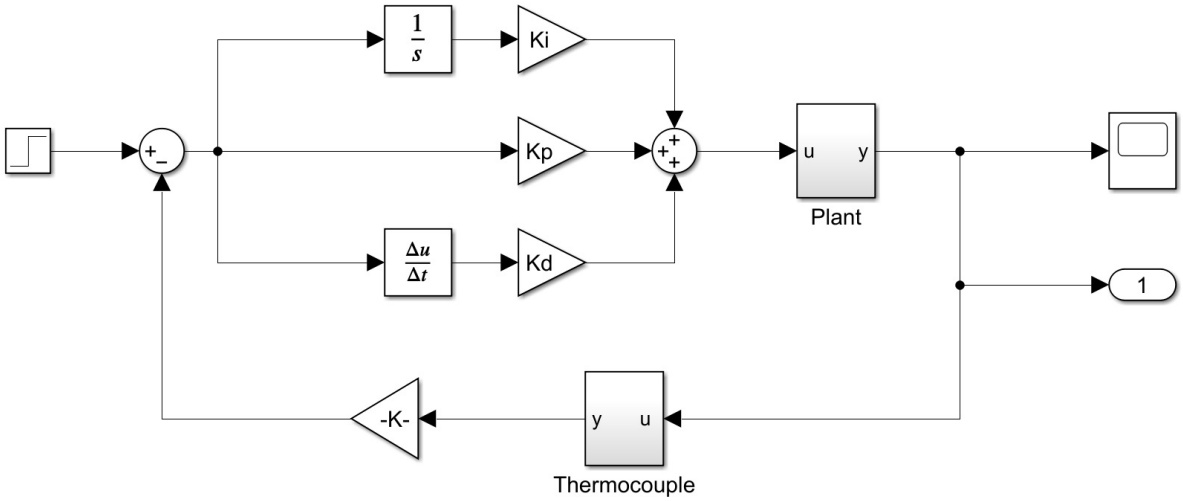

Figure 22 – Block diagram of the complete closed-loop system with negative feedback. The controller is represented by the gains K_p, K_i, and K_d, accompanied by the integrator and differentiator blocks.

Source: Own authorship

The plant obtained through SI (see 6.19) takes the modulated voltage from the controller as an input parameter, with the output being the temperature adjusted to reach the setpoint. This output voltage applied to the electrode tip in the continuous-time domain is given by 5.8 [1].

Another conducted analysis included performance measures to assess the effectiveness of the PID controller. These measures were associated with reducing overshoot and the settling time of the manipulated variable to the setpoint, respectively. In this work, we utilized performance indices based on integral-of-error criteria for controller tuning through the PSO algorithm. We employed the integral of the squared error (5.9), integral of the squared error weighted over time (5.10), integral of the absolute error (6.9), and integral of the absolute error weighted over time (6.10) [158, 159]. These indices quantitatively depict the dynamic control performance of the temperature variable during RFCA. The integration limits are related to instants $t = 0$, when the controller is activated, and T, corresponding to the settling time.

$$IAE = \int_0^T |e(t)|dt \ , \tag{6.9}$$

$$ITAE = \int_0^T t|e(t)|dt \ . \tag{6.10}$$

In the ISE index, it yields high values for significant errors and low magnitudes for small errors, thus reducing critical errors, especially in the initial instants. However, this index demonstrates low selectivity, and the system tends to exhibit a rapid response but with low relative stability, inducing oscillations. The IAE considers the absolute value of the error and shows acceptable damping, meaning a transient response with low oscillations. However, like the previous case, it does not demonstrate significant selectivity regarding the variation of controller parameters. The ITSE index exhibits greater selectivity compared to the ISE criterion, which works in a weighted manner concerning the large initial error with low weight. Near stabilization, this index penalizes transient response errors extremely. Finally, the ITAE works similarly to the ITSE in terms of error weighting and selectivity, showing, in addition, low overshoot in transient response and effective damping of oscillations.

For the determination of proportional gains K_p, integral gains K_i, and derivative gains K_d, we applied the GWO evolutionary algorithm to minimize the OF_{RFCA} presented in 6.11. This OF_{RFCA} is a linear combination of performance indices in the continuous-time domain.

$$argmin(OF_{RFCA} = \alpha SysOvr + \beta ISE + \gamma ITSE + \omega IAE + \lambda ITAE) \tag{6.11}$$

Where the overshoot ($SysOvr$), ISE, $ITSE$, IAE, and $ITAE$ are values obtained from the SIMULINK® dynamic systems analysis tool. The values of α, β, γ, ω, and λ are weights corresponding to each performance index that should be minimized. Thus, according to the system's behavior after each simulation, the weights were varied to highlight a specific dynamic response behavior resulting from the system. In other words, for example, if the overshoot presented an unsatisfactory result, the parameter α would be increased so that the GWO algorithm could emphasize the reduction of this performance index.

The stability analysis of the system is crucial in the controller design to ensure that the esophageal temperature does not reach dangerous levels. For this purpose, we employed the use of the Routh-Hurwitz criterion. This methodology is crucial for refining the cardiac ablation procedure, contributing significantly to the prevention of esophageal complications and ensuring controlled heat regulation.

6.2.5 Grey Wolf Optimizer

In this study, we opted to employ the GWO algorithm to adjust the parameters of the PID controller. The GWO algorithm offers several advantages, including simplicity, flexibility, and the ability to escape local minima, making it a promising choice for optimization problems in various fields such as engineering, finance, and medicine. Additionally, its application in multi-objective optimization problems has demonstrated robust and competitive results, especially when combined with other optimization techniques [160].

Proposed by Mirjalili et al. [161], the GWO algorithm is inspired by the social hunting behavior of grey wolves (*Canis lupus*). This bio-inspired optimization algorithm is distinguished by its simulation of the social hierarchy and cooperative hunting strategies of wolves, which are organized into a leadership structure composed of four main groups: alpha, beta, delta, and omega. In the context of GWO, these hierarchical positions are used to guide the search for optimal solutions within the search space [162].

In the GWO algorithm, the alpha wolves represent the most promising solution found so far, while the beta and delta wolves correspond to the next best solutions. The remaining wolves, designated as omega, follow and contribute to the exploration of the search space [161, 163]. The movement of the wolves toward the prey (the ideal solution) is modeled through three main operations: approaching, encircling, and attacking the prey.

Considering that the wolves encircle the prey, from a mathematical modeling perspective, the position of each wolf is updated based on the positions of the alpha, beta, and delta wolves, as shown in 6.12 and 6.13 [164]:

$$\vec{D} = |\vec{C} \cdot \vec{X}_p(k) - \vec{X}(k)| \tag{6.12}$$

$$\vec{X}(k+1) = \vec{X}_p(k) - \vec{A} \cdot \vec{D} \tag{6.13}$$

Where k denotes the current iteration, $\vec{A}$ and $\vec{C}$ are coefficient vectors, $\vec{X}_p$ and $\vec{X}$ represent the position vector of the prey and the position vector of a grey wolf, respectively. $\vec{A}$ and $\vec{C}$ are calculated according to 6.14 and 6.15.

$$\vec{A} = 2\vec{a} \cdot \vec{r}_1 - \vec{a} \tag{6.14}$$

$$\vec{C} = 2 \cdot \vec{r}_2 \tag{6.15}$$

Here, $\vec{r}_1$ and $\vec{r}_2$ are random vectors uniformly distributed in the range [0,1], and $\vec{a}$ is a parameter that decreases linearly from 2 to 0 over the course of the iterations. The vector $\vec{A}$ regulates the impact of the positions of the alpha, beta, and delta wolves on the position update of each wolf, while $\vec{C}$ influences the chasing distance from the prey [165].

After encircling the prey, the wolves begin the hunting and attacking phase. To mathematically represent this process, the three best positions are saved, and the remaining agents update their positions relative to the positions of the best search agents (alpha), with an average being extracted to account for the contributions of the beta and delta wolves, as represented in 6.16, 6.17, and 6.18 [161, 164]:

$$\vec{D}_\alpha = |\vec{C}_1 \cdot \vec{X}_\alpha(k) - \vec{X}(k)|, \quad \vec{D}_\beta = |\vec{C}_2 \cdot \vec{X}_\beta(k) - \vec{X}(k)|, \quad \vec{D}_\delta = |\vec{C}_3 \cdot \vec{X}_\delta(k) - \vec{X}(k)| \quad (6.16)$$

$$\vec{X}_1(t+1) = \vec{X}_\alpha(k) - \vec{A}_1 \cdot \vec{D}_\alpha, \quad \vec{X}_2(t+1) = \vec{X}_\beta(k) - \vec{A}_2 \cdot \vec{D}_\beta, \quad \vec{X}_3(t+1) = \vec{X}_\delta(k) - \vec{A}_3 \cdot \vec{D}_\delta \quad (6.17)$$

$$\vec{X}(k+1) = \frac{\vec{X}_1(k+1) + \vec{X}_2(k+1) + \vec{X}_3(k+1)}{3} \quad (6.18)$$

In summary, the GWO algorithm divides the search for the optimal solution into three main phases, which mirror the social and hunting behaviors of wolves:

- **Encircling:** Initially, the wolves encircle the prey based on the positions of alpha, beta, and delta.
- **Approaching:** The wolves adjust their positions towards the prey. If $|\vec{A}| < 1$, the prey is attacked, and the position is updated; otherwise, the wolves continue to encircle.
- **Attacking:** Finally, the approach culminates in an attack when $|\vec{A}| < 1$, leading the wolves to the prey's position and, consequently, to the optimal solution.

The algorithm flowchart has been appropriately included in the Appendix F.

6.3 Results

6.3.1 Bibliometric Review

Aiming to analyze the current state of research and identify trends, predominant themes and knowledge gaps in the field of computer simulation, a bibliometric review was carried out on the article's theme.

It was conducted in the bibliographic databases: Cochrane Library, Prospero, LILACS/BVS, EMBASE, MEDLINE/Pubmed, The Institute of Electrical and Electronics Engineers (IEEE), Scopus, CINAHL/EBSCO and Web of Science, using the terms "Atrial Fibrillation"; "Catheter Ablation"; "Radiofrequency Ablation"; "Ablation Techniques"; "Esophageal Fistula"; "Temperature" and "Computer Simulation".

The studies included after filtering 1 and 2 (n= 39) were considered and in the RStudio software we used the Bibliometrix package to evaluate the titles and abstracts of the selected works. We plot the word clouds shown in Fig 23 for better viewing. They have the 80 most frequent words, with the term "ablation" appearing the most, totaling 37 times in study titles and 129 times in abstracts.

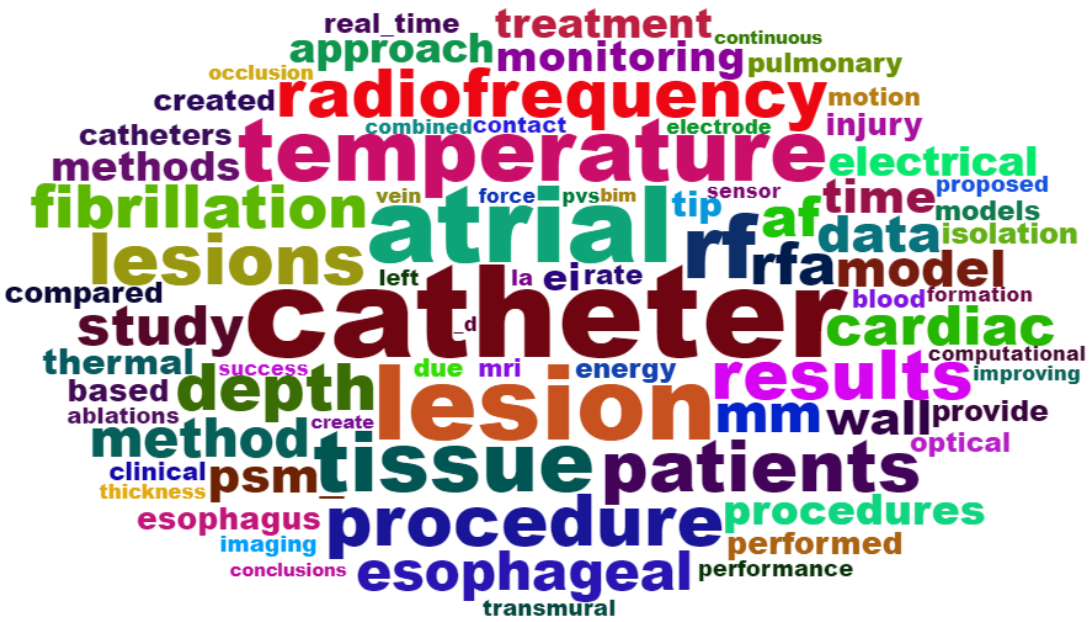

Figure 23 – Bibliometric analysis, with the Bibliometrix Program Rstudio, of the 80 works published with the search string ("Atrial Fibrillation AND Catheter Ablation OR Radiofrequency Ablation OR Ablation Techniques AND Esophageal Fistula OR Temperature AND Computer Simulation"), in title/abstract/words-keys, on June 28, 2022, with a minimum co-occurrence of terms of 4 times and "binary counting".
Source: Own authorship

6.3.2 Simulation of the three-dimensional model in COMSOL®

The computational simulation of RFCA was first performed by applying a constant voltage to evaluate the temperature distribution in the tissues. The Fig 24 presents this temperature distribution in the myocardium, fat and esophagus, highlighting the maximum temperature reached in 74.56°C, detected at the tip of the electrode, located at the central point with coordinates x = 0, y = 0 e z = - 0 .05 mm.

During the simulation, the isothermal lines show an increase in temperature in the esophagus, reaching 41.58°C. This increase, even in a short simulation period, points to heat dissipation in regions adjacent to the RFCA application.

Fig 25 illustrates the spatial distribution of temperature in the simulated tissues, showing the temperatures recorded at the borders of each tissue. It demonstrates the effectiveness of the procedure in increasing the temperature in the myocardium, the target tissue of the treatment, highlighting, however, the need for additional strategies to mitigate the increase in temperature in neighboring tissues, such as the esophagus.

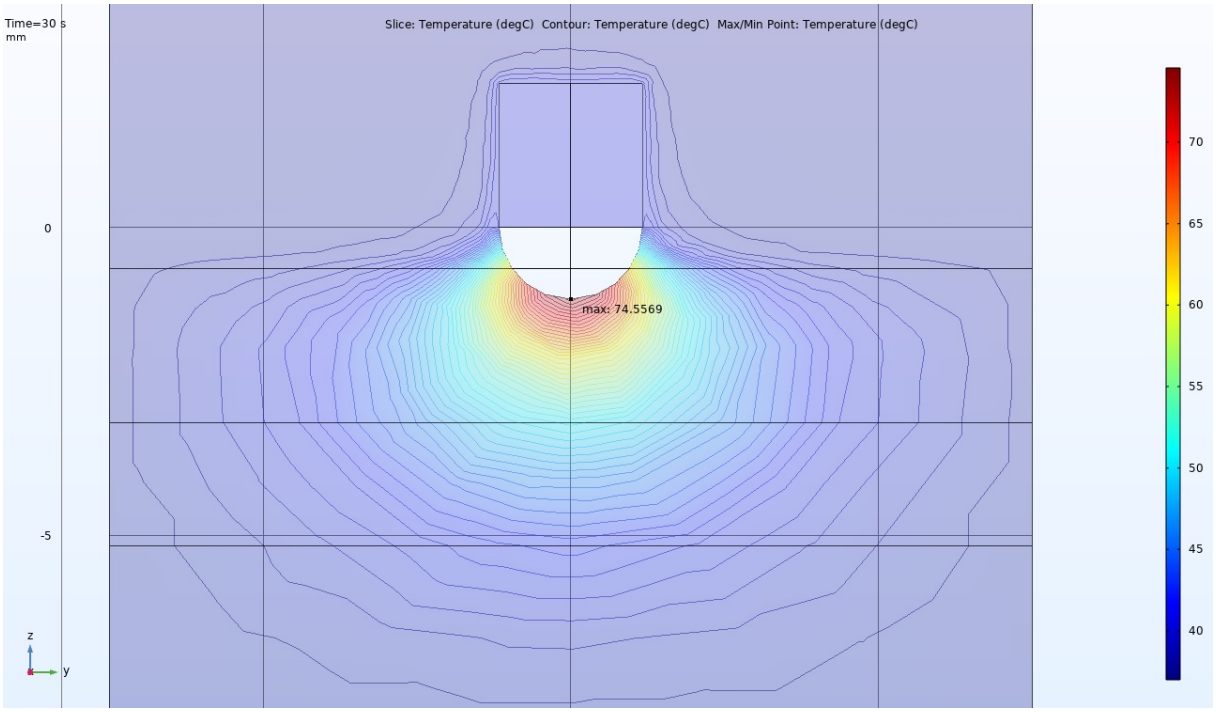

Figure 24 – This image shows the temperature distribution in the myocardial tissue, fat and esophagus, without the use of any temperature control technique. Temperature distribution in myocardial, fat and esophageal tissues during simulation of cardiac radiofrequency ablation without temperature control.

Source: Own authorship

6.3.3 System Identification and Control Design

6.3.3.1 Plant's SI

The data generated by the simulation carried out in COMSOL® allowed the analysis of the warming of the esophagus over time. The analysis point was strategically selected between the border of the adipose tissue and the esophagus, positioned in the central part of the model geometry with coordinates x = 0, y = 0, z = -5.165 mm. Through processing this data, the SI method was used to estimate a third-order transfer function, presented in 6.19. This function presented an estimation rate of 99.73%. The selection of the function order took into account the balance between a high estimation rate and a good result obtained when tuning the PID controller.

$$P(s) = \frac{5133.63s^2 + 158.81s + 22.46}{s^3 + 2080.31s^2 + 60.03s + 8.278}\,. \tag{6.19}$$

To validate this estimate, data generated from a new simulation carried out by COMSOL® was used with the same model geometry but with an input voltage of 20 V. In this way, a validation FIT of 42.02% was obtained. Fig 26 illustrates the behavior of the model obtained by computer simulation and the comparison with the system identified for the proposed plant for the control system.

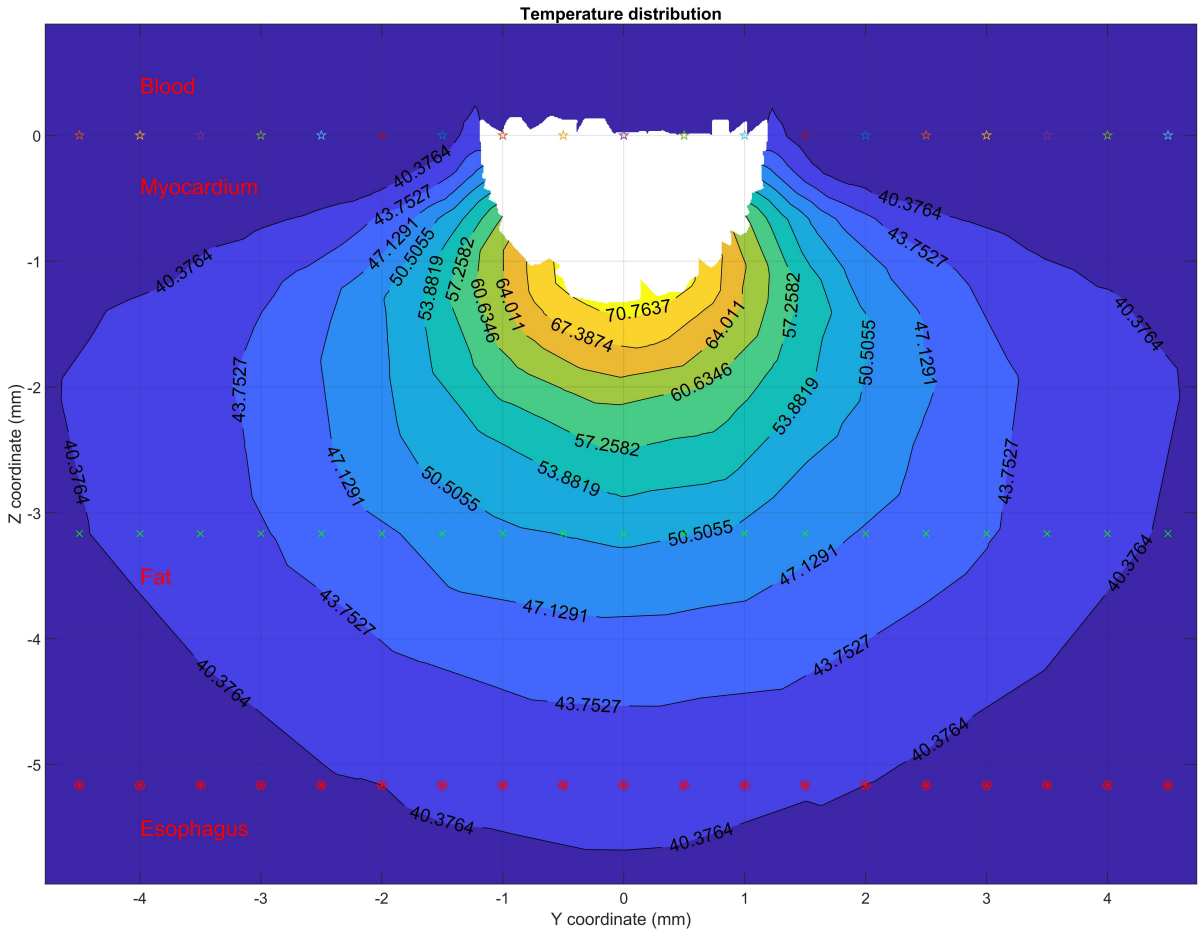

Figure 25 – Detailed representation of the temperature field and the boundaries between the internal regions of the heart, myocardium, fat and esophagus, showing the thermal distribution during the simulation of cardiac radiofrequency ablation.
Source: Own authorship

We used the Routh-Hurwitz criterion to verify the absolute stability of the open-loop system, opting for this strategy to avoid the need to factorize the system's characteristic equation.

The Routh-Hurwitz criterion is a fundamental tool for evaluating the stability of dynamic systems. By examining the number of sign changes in the first column of the resulting table, we can determine the number of system poles located on the right side of the complex plane. These poles on the right side indicate the presence of unstable components in the system. Table 9 presents the results of this analysis, demonstrating, based on the Routh-Hurwitz criterion, that the system is stable in open loop.

Table 9 – **Routh-Hurwitz stability criterion for the transfer function** $P(s)$.

s^3	1	60.03
s^2	2080.31	8.28
s^1	60.03	⋯
s^0	8.28	⋯

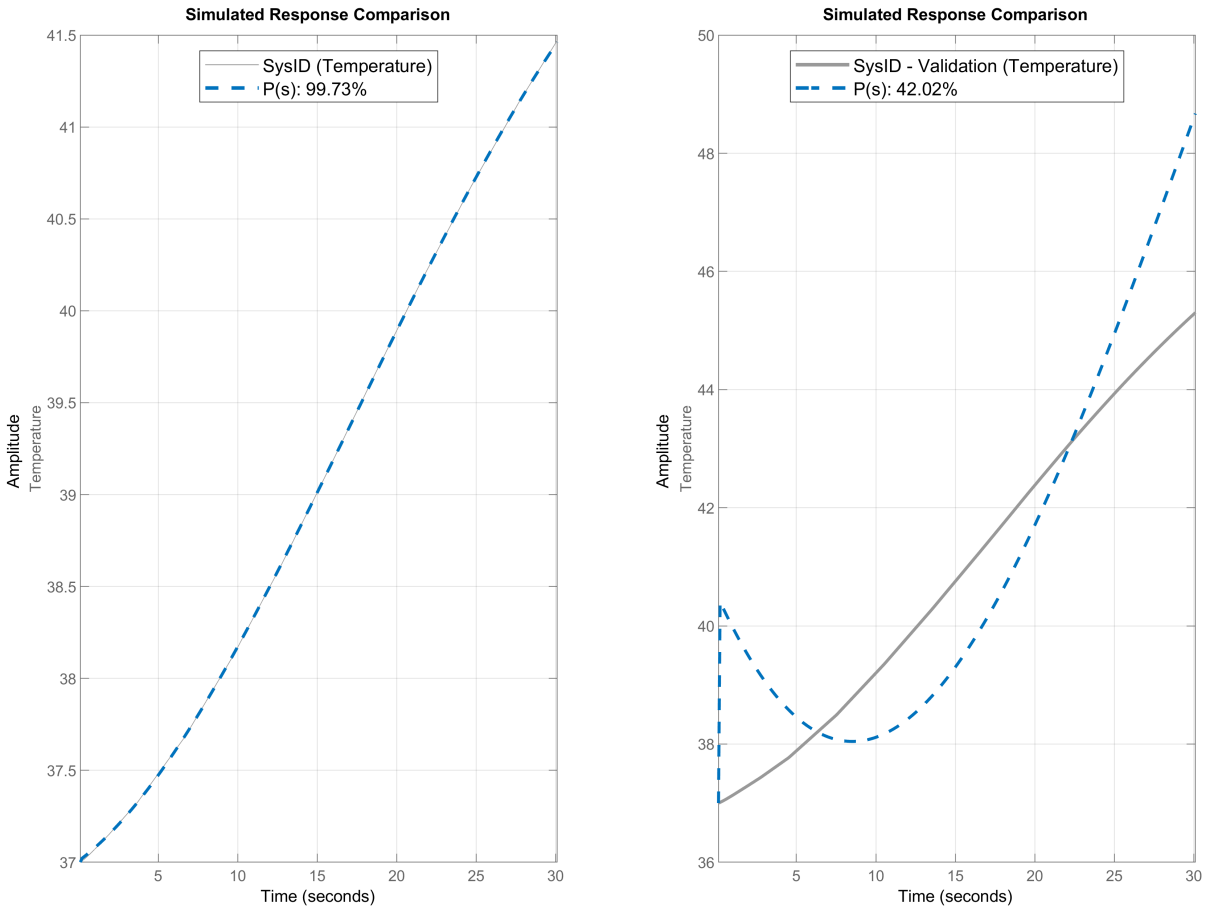

Figure 26 – The image graphically shows the data corresponding to the evolution from heating on the esophagus were extracted and manipulated to identify the system in question. A third order transfer function was estimated presenting a fit equivalent to 99.73%.
Source: Own authorship

The analysis of poles and zeros of the open-loop dynamic system modeled by a third-order transfer function (see 6.19) is crucial for understanding the system's dynamic behavior. In this case, the poles and zeros are presented in Table 10.

Table 10 – **Root locus for the open-loop system**

Zeros	Poles
-1.5469e-02 + 6.4310e-02i	-2.0803e+03
-1.5469e-02 - 6.4310e-02i	-1.4427e-02 + 6.1409e-02i
⋯	-1.4427e-02 - 6.1409e-02i

The poles of a system determine its time response characteristics, including stability, response time, and transient behavior. The first pole, which is real, negative, and has a large magnitude (≈ -2080), suggests that this component of the system's response stabilizes very quickly due to its rapid exponential decay. The second and third poles are complex conjugates with a real part of -1.4427×10^{-2} and an imaginary part of $\pm 6.1409 \times 10^{-2}$. The negative real part indicates stability, but with a slower decay compared to the first pole. The presence of the imaginary component indicates that the system exhibits oscillatory behavior,

with a natural frequency associated with the magnitude of the imaginary part ($\omega_n \approx 0.0614$). These oscillations occur at a low frequency, and their attenuation is relatively slow due to the small value of the real part.

The zeros of a system influence its frequency response and transient behavior. The location of the zeros can introduce cancellations or reinforcements of certain response components. The complex conjugate zeros are located around a small negative real part with a frequency associated with the imaginary part ($\omega_n \approx 0.0643$). These zeros may partially cancel the components associated with poles that have similar characteristics (the poles $-1.4427 \times 10^{-2} \pm 6.1409 \times 10^{-2}i$, impacting the oscillatory response of the system.

Regarding the dynamic behavior of the system, it is stable in open-loop operation since all poles are in the left half of the complex plane. The transient response is characterized by damped oscillations due to the complex conjugate poles, which occur at low frequency and have relatively slow attenuation, as indicated by the small negative real part of the complex poles. The rapid stabilization of the response, indicated by the fast pole, will be followed by a slower and more prolonged oscillatory response dominated by the low-frequency oscillations of the complex poles, which are partially canceled by the nearby zeros. Understanding this behavior is crucial for designing controllers that effectively manage the esophageal wall temperature, ensuring safety and efficacy in the context of radiofrequency ablation procedures.

Fig 27 displays the dynamic response of the open-loop model, revealing an instantaneous signal growth with a rise time of 0.0112 s and an overshoot of 64.79% for the unitary input signal. The presence of two dominant conjugate poles stands out, located very close to the imaginary axis in the left half plane. Although these poles have tiny imaginary parts, they exert a great influence on the dynamic response of the system.

6.3.3.2 Thermocouple's SI

Fig 22 represents the system's control loop, which handles the voltage input and temperature output. To carry out the negative feedback necessary in this context, we use a type K thermocouple (Chromel/Alumel) to transduce the quantities. This thermocouple has a well-defined relationship between the temperature measured in degrees Celsius and the voltage in millivolts. To equate the units and obtain a reading in volts, we incorporated a gain of 1000 units in the feedback stage [166].

The thermocouple data was imported into MATLAB® where SI was performed. This resulted in obtaining the following first-order transfer function:

$$T(s) = \frac{0.2519}{s + 6.158}\,. \tag{6.20}$$

Fig 28 presents the comparison between the thermocouple data and the identified

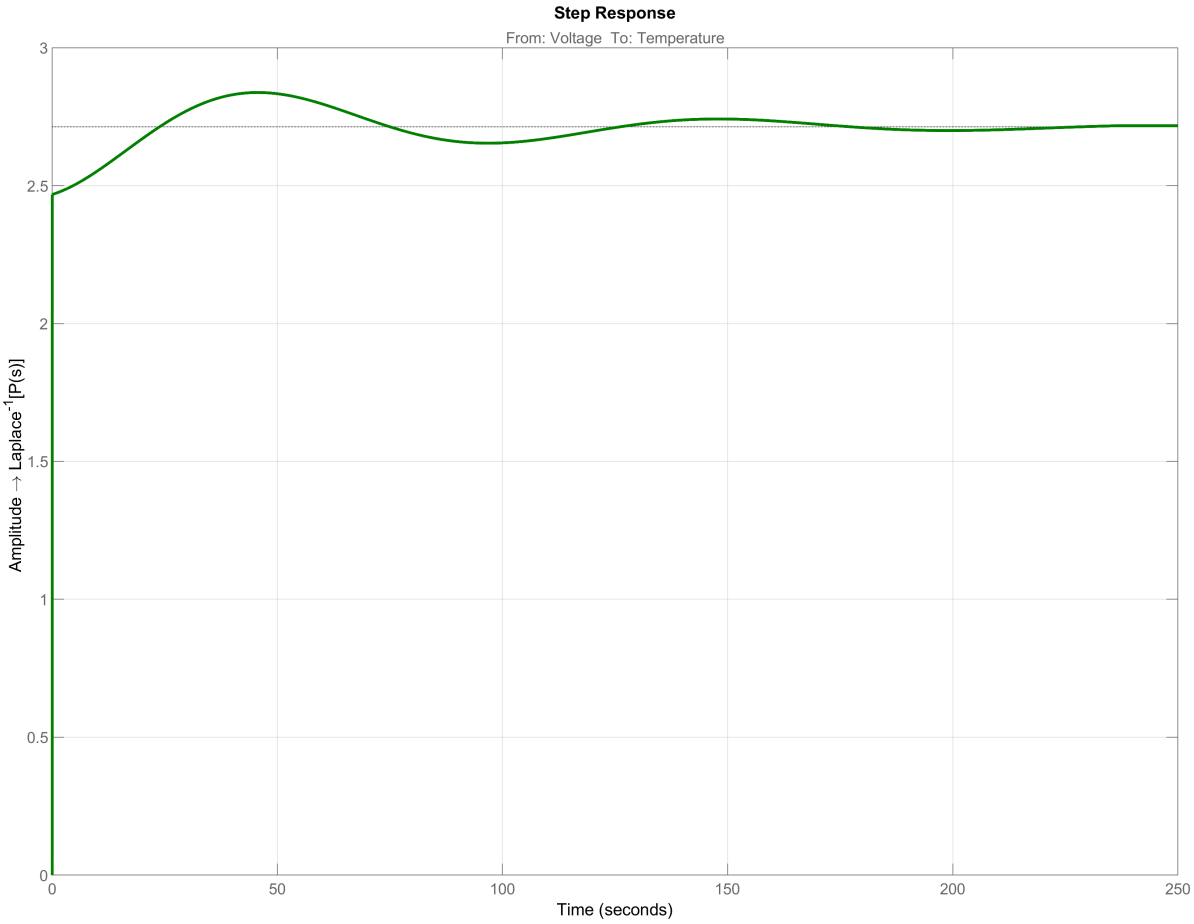

Figure 27 – Dynamic response of the open-loop model. The image shows instantaneous growth of the signal which has a rise time of 0.0112 s and reaching an overshoot of 64.79% for the unitary input signal.

Source: Own authorship

model, which presented an adjustment of 95.42%.

6.3.4 COMSOL® in closed-loop: application of PID and GWO

We integrate all identified transfer functions into SIMULINK® (Fig 22). In Table 11, we present the parameters used in the GWO algorithm simulations carried out in the MATLAB ® software.

Fig 29 illustrates the dynamic response for the closed-loop system with controller. Table 12 presents the performance indices obtained. Additionally, the convergence curve of the GWO algorithm is displayed in Fig 30, demonstrating that the algorithm converged to the solution after 100 iterations, with a precision of 10^0.

Table 13 presents the analysis of the Routh-Hurwitz stability criterion for the closed-loop system with PID controller. Compared to the open-loop system, the poles of the transfer function are considerably close to zero. This indicates the controller's influence on the model's transfer function, along with the other components of the mesh. Therefore, the

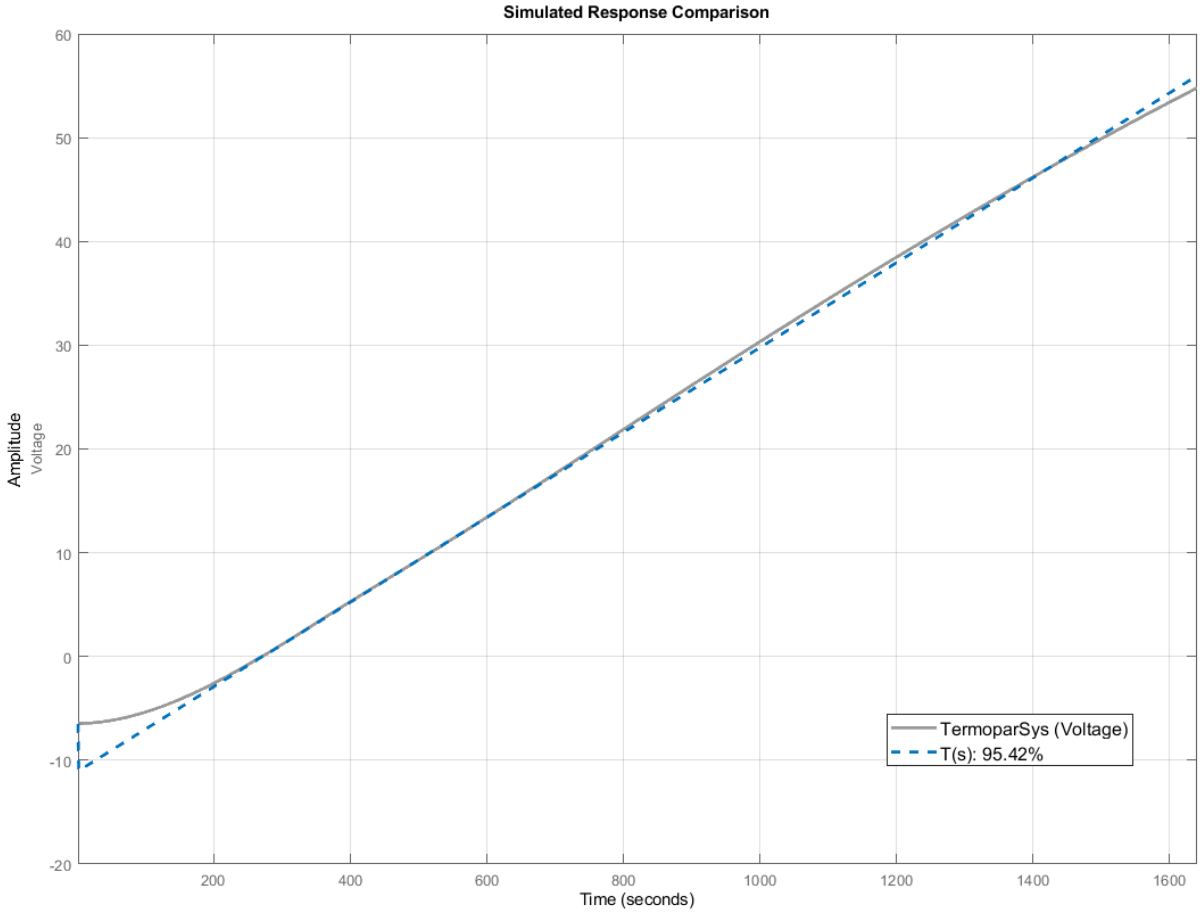

Figure 28 – The Figure shows a 95.42% fit of the transfer function on the corresponding data between temperature and voltage.

Source: Own authorship

Table 11 – **Parameters used in the GWO algorithm**

Variable	**Value**
Number of wolves	12
Number of dimensions	3
Lower bound	0
Upper bound	0.1
$MaxIter$	100
α	1
β	0.02
γ	0.06
ω	0.06
λ	0.01

poles may have only insignificant shifts towards their respective zeros with variations in gain, reflecting a stable system and less susceptible to disturbances.

The analysis of the poles and zeros of a third-order dynamic system, now including a PID controller reveals important insights into the system's behavior. The poles and zeros for the system with the PID controller are presented in Table 14.

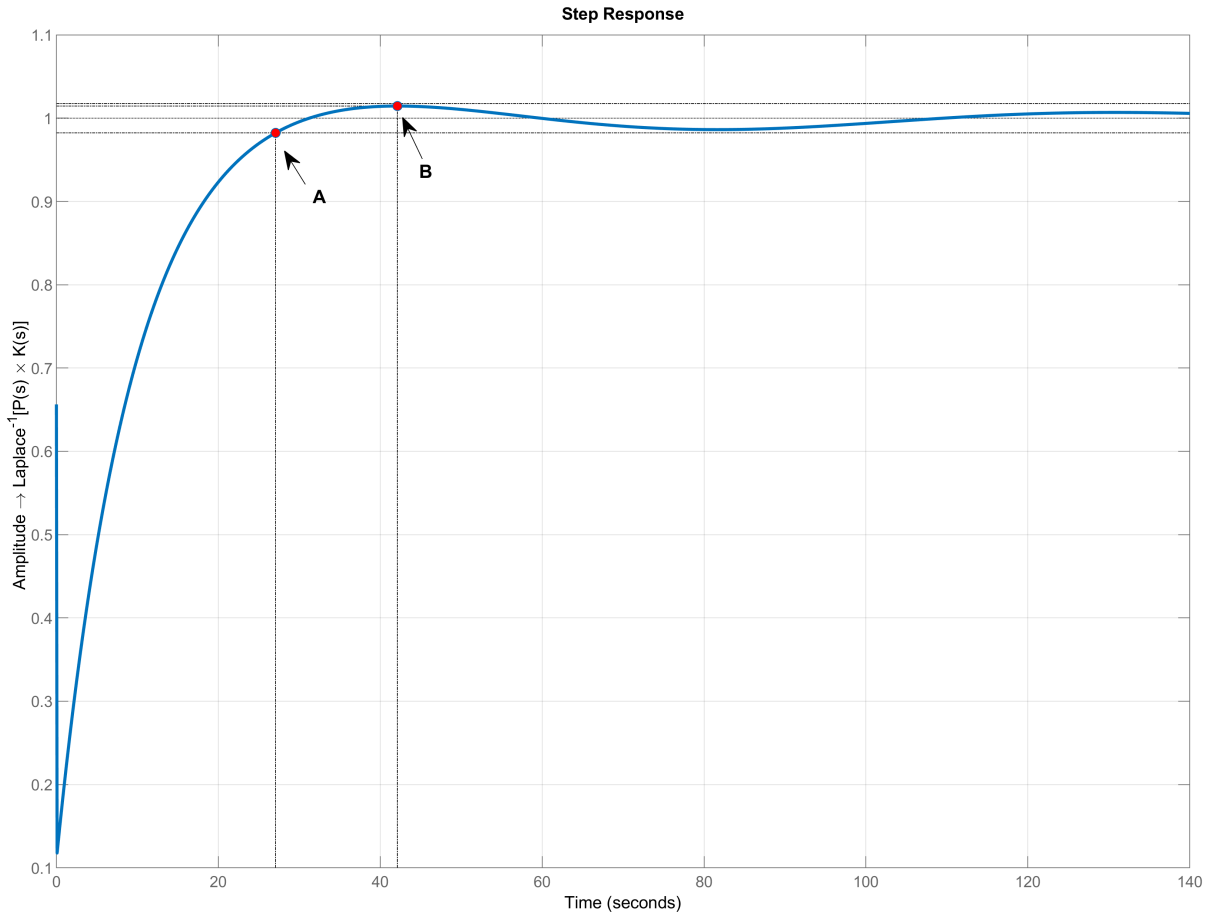

Figure 29 – The image shows that the application of the optimized controller significantly reduced the system overshoot in addition to providing smoother growth so that in RFCA, this will be reflected in the temperature of the myocardium and adjacent tissues.
Source: Own authorship

Table 12 – K_p, K_i, K_d **and performance indices**

⋯	K_p	K_i	K_d
⋯	**0.047498**	**0.05**	**0.00022132**
Peak amplitude	1.01(B)		
Overshoot	1.48% at 42 s (B)		
Rise time (s)	16.1		
Settling time (s)	27.1 (A)		
Elapsed time (s)	483.233		

The introduction of the PID controller significantly alters the system's dynamics. The first pole, with a large negative real part (-1.0878×10^3), indicates a very fast response component that will stabilize quickly, similar to the behavior observed in the uncontrolled system, but even more rapidly due to the pole's increased magnitude. The second pole, located at -1.1167×10^{-1}, is a real pole with a small negative value, suggesting a slow decaying component that contributes to the overall stability of the system but might also introduce a slower transient response.

The complex conjugate poles $-1.3927 \times 10^{-2} \pm 6.4291 \times 10^{-2}i$ introduce oscillatory

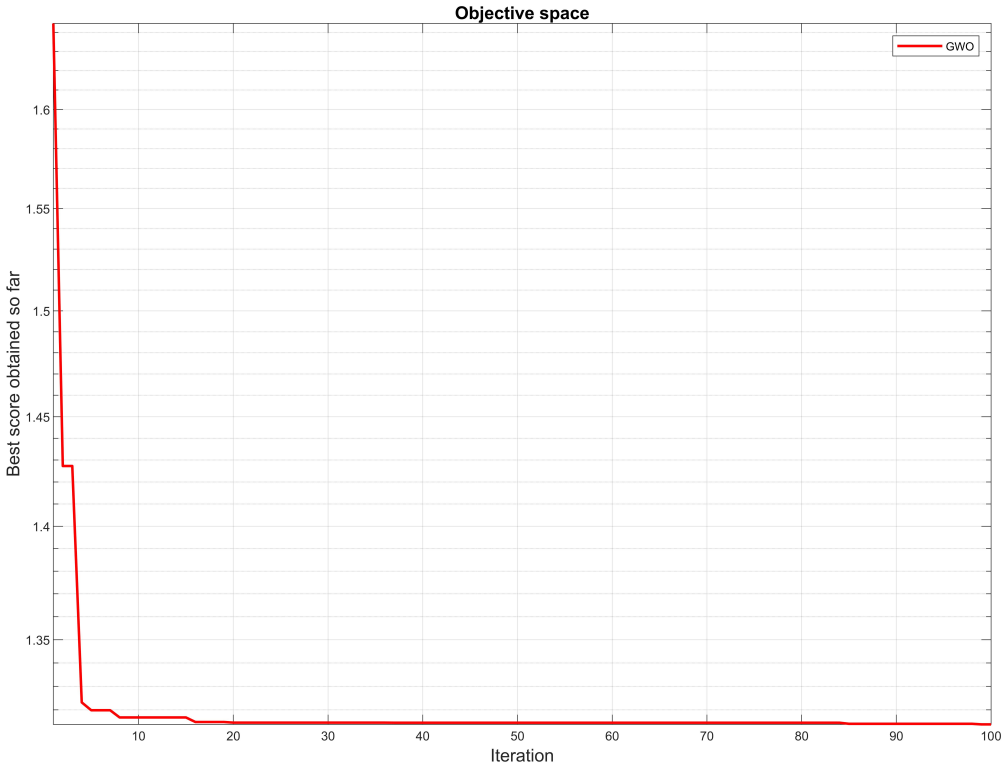

Figure 30 – Convergence curve of the GWO algorithm
Source: Own authorship

Table 13 – **Routh-Hurwitz stability criterion for the closed-loop system.**

s^4	2.13	324.260	1.123
s^3	2324.182	17.285	⋯
s^2	324.244	1.123	⋯
s^1	9.236	⋯	⋯
s^0	1.123	⋯	⋯

Table 14 – **Root locus for the closed-loop system**

Zeros	**Poles**
-2.1355e+02	-1.0879e+03
-1.0579e+00	-1.1167e-01
-1.5469e-02 + 6.4310e-02i	-1.3927e-02 + 6.4291e-02i
-1.5469e-02 - 6.4310e-02i	-1.3927e-02 - 6.4291e-02i

behavior to the system. These poles, with their small negative real parts, indicate low-frequency oscillations with slow attenuation, which contribute to the transient response of the system. However, these oscillations are more damped compared to the system without the PID controller, suggesting that the controller improves the system's stability and reduces the magnitude of oscillations.

The zeros of the system, introduced by the PID controller, include a large negative real

zero (-2.1355×10^2) and another real zero at -1.0579, both of which influence the system's frequency response. These zeros can introduce cancellations or reinforce certain dynamics within the system, potentially improving the transient response by reducing overshoot or adjusting the response speed. The complex conjugate zeros $-1.5469 \times 10^{-2} \pm 6.4310 \times 10^{-2}i$, similar to those in the uncontrolled system, indicate an influence on the system's oscillatory behavior, likely contributing to the partial cancellation of the oscillatory poles.

Overall, the PID controller introduces significant improvements to the system's dynamic behavior. The faster stabilization due to the rapid pole and the improved damping of oscillations from the complex poles suggest a more controlled and stable system response. The presence of additional zeros further enhances the system's transient response, reducing the likelihood of overshoot and improving the precision of temperature control in the context of esophageal wall temperature management during radiofrequency ablation procedures. These adjustments lead to a more effective and safer system, which is critical for clinical applications.

Nineteen experiments were conducted to determine the parameters of the PID controller. The results showed in Table 15 that the proportional gain had an average of 0.049736, with a variance of 6.4115×10^{-7} and a standard deviation of 0.008. K_i remained constant at 0.05, with an extremely low variance of 2.03×10^{-34} and an insignificant standard deviation of 1.43×10^{-17} indicating high consistency in the values. The derivative gain had an average of 8.45×10^{-5}, with a variance of 6.29×10^{-9} and a standard deviation of 7.93×10^{-5}, showing greater variability compared to the other parameters, but still maintaining a relatively stable pattern. These results highlight the effectiveness of the GWO in tuning the PID parameters, ensuring precise and consistent control under different experimental conditions. Additionally, an ANOVA conducted across the 19 experiments produced a p-value significantly less than 0.05, indicating a strong likelihood that the differences among the means are not due to chance and that the data do not follow a normal distribution. The p-value is a statistical measure that helps determine the significance of the results; in this case, a p-value much smaller than 0.05 suggests that there is a statistically significant difference between the groups. Further details and comprehensive statistical analyses are provided in Fig 35.

Table 15 – **Statistical Analysis of RFCA Controller Gains**

Parameter	Mean	Variance	Standard Deviation
Kp	0.049736	6.415×10^{-7}	0.000800
Ki	0.05	2.03×10^{-34}	1.43×10^{-17}
Kd	8.45×10^{-5}	6.29×10^{-9}	7.93×10^{-5}

After completing the PID controller project, we conducted new simulations in the COMSOL® to evaluate the effects on the temperature of the esophageal region. In this context, we include the control library in the software and adjust the gains based on the results obtained by the GWO algorithm.

The setpoint was adjusted to 38°C at the starting point of the esophageal tissue, in the same coordinates as in the simulations without a controller. In Fig 31, it can be seen that the temperature at the electrode tip was controlled, reaching a maximum of 50.31°C at 10.4 s, which is suitable for carrying out the RFCA procedure. Furthermore, at the end of the simulation (30 s), the temperature reduced to 48°C.

The temperature reached by the esophagus was effectively controlled, reaching its peak of 38.63°C at the end of the simulation. At 10.4 s, when the electrode temperature reached its maximum, the esophageal temperature was 37.51°C. In Fig 32 we can observe the temperature distribution after implementing the optimized controller, at 30 s.

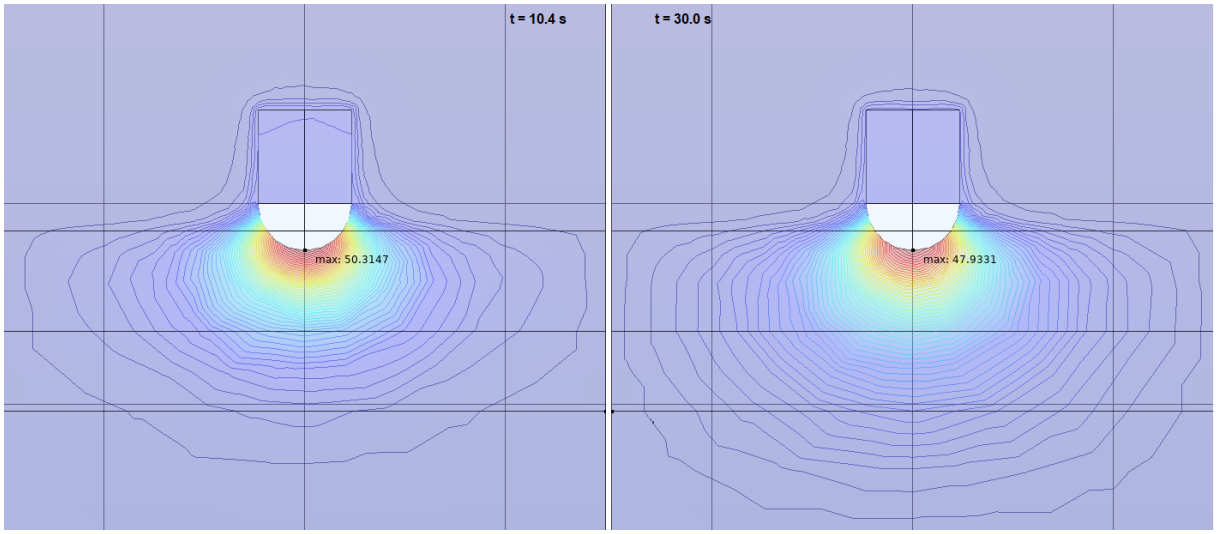

Figure 31 – In this Fig we see the results related to temperature in the esophagus region, where the control library was added to the software and we parameterized the gains according to the results obtained by the GWO algorithm. It is also possible to observe that the temperature at the electrode tip was controlled, reaching a maximum value of 50.31°C at 10.4 s, which is sufficient to carry out the RFCA procedure.
Source: Own authorship

6.4 Discussion

The three-dimensional model simulation for RFCA application revealed a concerning trend: the esophageal temperature during the procedure exceeded safety limits. When simulating the model without implementing any control mechanism, applying a voltage of 15 V led to a temperature of 75°C around the electrode tip. This heat transferred to adjacent tissues, resulting in a temperature of 42°C in the esophagus, a value considered risky for the development of an esophageal fistula.

Prospective study conducted by [167], 185 patients underwent radiofrequency catheter ablation for left atrial arrhythmias. The study aimed to investigate the incidence, endoscopic characterization, and dependency of endoluminal temperature on esophageal thermal lesions following RFCA. Upper gastrointestinal endoscopy was performed on all patients

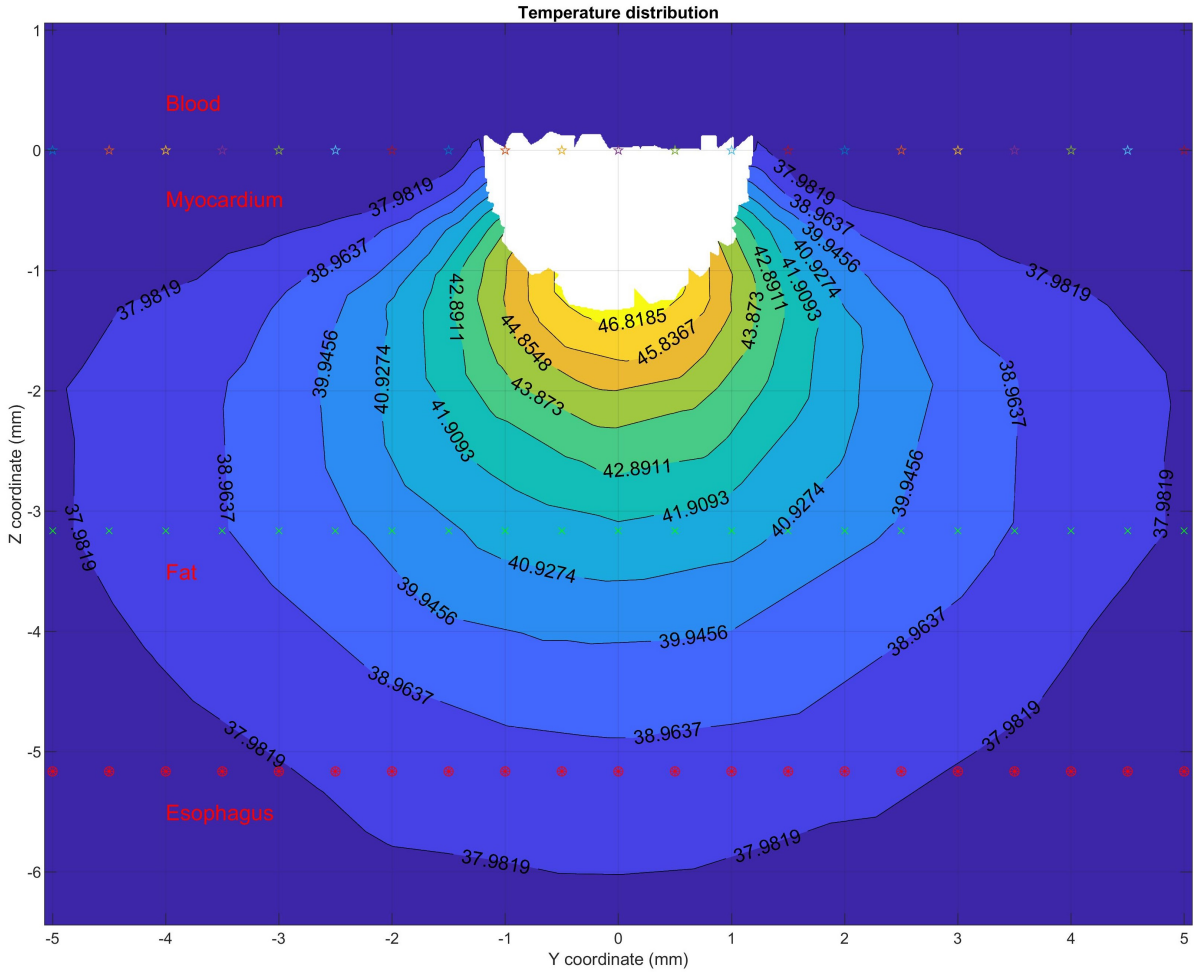

Figure 32 – The image shows the temperature distribution after implementing the optimized controller, at 30 s.

Source: Own authorship

during the ablation procedure, with real-time monitoring of intraluminal esophageal temperature. Twenty-seven asymptomatic esophageal thermal lesions, ranging from 2 to 16 mm in diameter, were observed, all above an intraluminal esophageal temperature of 41°C. The maximum esophageal temperature was significantly higher in patients with thermal lesions than in those without lesions (42.6 ± 1.7°C vs. 41.4 ± 1.7°C, $P = 0.003$). Each 1°C increase in endoluminal temperature increased the odds of esophageal injury by 1.36 times.

In a similar study, it was investigated whether limiting the delivery of RF energy by monitoring luminal esophageal temperature (LET) is associated with a reduction in esophageal injuries during AF ablation compared to a strategy that solely limits RF power. The study involved 81 patients undergoing AF ablation, followed by esophageal endoscopy. RF applications in the posterior left atrium were capped at 35 W. In a subset of 67 patients, an esophageal sensor was used to monitor temperature during ablation. When the temperature reached 38.5°C, applications were either halted or reduced. Post-procedure endoscopy revealed ablation-related esophageal ulcers in 11% of patients, more prevalent in those without esophageal temperature monitoring. The findings suggest that monitoring esophageal

temperature during ablation may decrease the risk of esophageal injuries compared to mere RF power limitation [168].

Given this concerning trend, there arose the need to explore control strategies to mitigate the excessive temperature increase in the esophagus during RFCA. When we tuned the PID controller using the GWO algorithm, there was a notable improvement in the thermal regulation of the simulations. Applying the obtained parameters reduced the maximum temperature reached by the console during the simulation to around 50°C, considerably safer than the initial scenario. Furthermore, by adjusting the setpoint to 38°C in the esophagus, the simulation resulted in a maximum temperature very close to this value, indicating the controller's ability to maintain a safe temperature level, thus avoiding damage to adjacent tissues.

Compared to earlier research, like that conducted by [137] and [138], which concentrated on PI controllers, our investigation, employing a PID controller, showcased a prevalence of the proportional and integral components over the derivative element. While we observed resemblances to these studies, our utilization of the PI components demonstrated superior efficiency within our system. This emphasizes the significance of tailoring controller parameters and considering the distinct dynamics of the plant to attain optimal outcomes.

In this scenario, when we removed the derivative component of the controller for the present study, we observed a considerably reduced rise time, as evidenced in Fig 27 of the uncontrolled system. In the system with the controller present (Fig 29), we noticed, in the initial instants, a sharp increase in amplitude, reflecting the alteration in the derivative gain of the controller. By adjusting the GWO parameters, we were able to attenuate this initial impulse resulting in a more gradual heating, making the RFCA procedure safer.

Implementing the PID controller, tuned through GWO, led to a significant reduction in the maximum temperature reached during the ablation. The new configuration, with a setpoint of 38°C, allowed the myocardium to be heated to the point of tissue necrosis for the treatment of AF without reaching dangerous conditions for the esophagus, resulting in a maximum temperature of about 38°C [143]. This demonstrates the effectiveness of PID control in preventing damage to the esophagus during the ablation procedure.

The study outlines several limitations that warrant consideration. The computational model's simplifications might not comprehensively capture the intricate and diverse nature of tissues and actual human body structures. Moreover, the absence of validation through real experiments or clinical studies limits its generalizability, given individual anatomical disparities or specific circumstances within the population. While the focus remains on esophageal temperature, the study might overlook the potential impact on adjacent anatomical structures during RFCA. These limitations stress the necessity for additional research, experimental validations, and careful clinical assessments before widespread clinical

adoption.

A perspective for future work involves incorporating a multi-objective analysis into the RFCA procedure, enabling optimization of both temperature control in the esophageal region and the volume of cardiac tissue lesion. Additionally, we plan to explore other algorithms, seeking more promising solutions compared to GWO. In the same context, implementing the live-link feature between MATLAB® and COMSOL® will be of great importance in upcoming studies, allowing real-time optimization and facilitating data exchange between the software, resulting in more promising findings.

6.5 Conclusion

The three-dimensional simulation conducted in COMSOL® allowed the assessment of temperature distribution within tissues. Results highlighted a maximum temperature of 74.56°C at the electrode tip, while the esophagus showed a significant temperature rise, reaching 41.58°C during the simulation. This revealed heat dissipation in regions neighboring the RFCA application. Despite effectively raising myocardial temperature, the treatment's target, there was a recognized need for additional strategies to control temperature elevation in adjacent tissues, such as the esophagus.

Employing the SI method enabled the estimation of a transfer function for control. This function, in conjunction with the implementation of the PID with GWO controllers, effectively regulated esophageal temperature, maintaining it below critical levels. Implementing this model holds significant potential for enhancing the safety and efficiency of RFCA procedures by precisely controlling tissue temperature adjacent to the treatment area, thereby mitigating complications such as the formation of esophageal fistulas. The results obtained through the proposed control highlight the viability of this model as a promising tool to enhance procedure safety.

7 Conclusion

This thesis integrates advancements in RFA, focusing on optimizing procedures through computational modeling, tissue impedance control, and temperature management strategies. The three studies presented in this research significantly contribute to the understanding and improvement of RFA techniques for both oncological and cardiac applications.

In Study 1 (Chapter 4), a systematic review provides a comprehensive overview of various aspects related to RFA, emphasizing the importance of combining experimental approaches with computational modeling. This study reviewed 29 key research papers that explored electrical, thermal, and fluid dynamics parameters in RFA procedures. It highlighted the importance of optimizing electrode configuration and ablation duration to enhance treatment efficacy. Computational modeling was identified as a crucial tool for personalizing treatments and predicting potential complications, although the review also noted the limitations of oversimplified models and the challenges of addressing more complex clinical factors. Additionally, the need for validating computational models through in vivo experiments was underscored.

Study 2 (Chapter 5) focused on the development of a PSO-tuned PID controller to regulate tissue impedance during ex vivo hepatic ablation procedures. The controller exhibited remarkable robustness in maintaining impedance within predefined levels, thereby preventing the phenomenon of roll-off, which occurs when tissue impedance spikes abruptly, interrupting the procedure. The simulation results were impressive, with an overshoot of 0.605%, a rise time of 0.314 seconds, and a settling time of 2.87 seconds. These outcomes reflect the controller's efficacy in minimizing complications such as incomplete tumor ablation. The study suggests that PSO-based controllers may play a pivotal role in improving clinical outcomes in hepatic ablations, offering a more precise and controlled procedural approach.

Study 3 (Chapter 6) utilized three-dimensional simulations in COMSOL® to investigate temperature distribution during RFCA. A PID controller, tuned by the GWO, was employed to manage myocardial temperature, ensuring it reached desired levels while maintaining the esophageal temperature below critical thresholds. The results demonstrated that the controller effectively kept the esophageal temperature under 38.63°C, significantly reducing the risk of esophageal fistula formation, a severe complication associated with RFCA. The findings underscore the importance of precise temperature control to protect adjacent tissues, suggesting this approach has the potential to enhance the safety and efficacy of cardiac ablation procedures.

Collectively, these studies highlight the importance of multidisciplinary approaches

that combine computational modeling, precise control of critical parameters, and experimental validation. This thesis advances knowledge in the field of RFA by proposing innovative solutions that improve the efficacy and safety of these procedures. The continuous development and refinement of these techniques, alongside collaboration across medicine, engineering, and biomedical sciences, are essential for the evolution of ablation therapies and for enhancing patient care. Furthermore, the application of bioinspired algorithms, such as PSO and GWO, has brought innovative contributions to the control of RFA parameters, as demonstrated by the studies presented. The ARFACTA device, currently under patent application number 78-1123-ARFACTA at the Intellectual Property Center of the University of Brasília (NUPITEC), will incorporate the technical advancements described in this thesis into its hardware.

References

[1] S. Singh and R. Repaka. “Temperature-controlled radiofrequency ablation of different tissues using two-compartment models”. In: *International Journal of Hyperthermia* 33.2 (2017), pp. 122–134 (cit. on pp. 26, 27, 47, 57, 67, 98, 158).

[2] M. Trujillo, J. Bon, M. Jose Rivera, F. Burdío, and E. Berjano. “Computer modelling of an impedance-controlled pulsing protocol for RF tumour ablation with a cooled electrode”. In: *International Journal of Hyperthermia* 32.8 (2016), pp. 931–939 (cit. on pp. 26, 27, 46, 50, 52, 156).

[3] G. S. Gazelle, S. N. Goldberg, L. Solbiati, and T. Livraghi. “Tumor ablation with radio-frequency energy”. In: *Radiology* 217.3 (2000), pp. 633–646 (cit. on p. 26).

[4] A. Forner, M. Reig, and J. Bruix. “Hepatocellular carcinoma”. In: *The Lancet* 391.10127 (2018), pp. 1301–1314. ISSN: 0140-6736. DOI: https://doi.org/10.1016/S0140-6736(18)30010-2. URL: https://www.sciencedirect.com/science/article/pii/S0140673618300102 (cit. on p. 26).

[5] A. Villanueva. “Hepatocellular Carcinoma”. eng. In: *The New England journal of medicine* 380.15 (2019), pp. 1450–1462. ISSN: 0028-4793 (cit. on pp. 26, 55).

[6] R. Cardoso, G. B. Justino, F. P. Graffunder, L. Benevides, L. Knijnik, L. M. Sanchez, and A. d’Avila. “Catheter Ablation is Superior to Antiarrhythmic Drugs as First-Line Treatment for Atrial Fibrillation: a Systematic Review and Meta-Analysis”. In: *Arquivos Brasileiros de Cardiologia* (2022) (cit. on pp. 26, 90).

[7] P. Kirchhof, S. Benussi, D. Kotecha, A. Ahlsson, D. Atar, B. Casadei, M. Castella, H.-C. Diener, H. Heidbuchel, J. Hendriks, et al. “2016 ESC Guidelines for the management of atrial fibrillation developed in collaboration with EACTS”. In: *Polish Heart Journal (Kardiologia Polska)* 74.12 (2016), pp. 1359–1469 (cit. on p. 26).

[8] H. Calkins, G. Hindricks, R. Cappato, Y.-H. Kim, E. B. Saad, L. Aguinaga, J. G. Akar, V. Badhwar, J. Brugada, J. Camm, et al. “Temporary removal: 2017 hrs/ehra/ecas/aphrs/solaece expert consensus statement on catheter and surgical ablation of atrial fibrillation”. In: *Heart rhythm* (2017), e275–e444 (cit. on p. 26).

[9] M. Trujillo, J. Alba, and E. Berjano. “Relationship between roll-off occurrence and spatial distribution of dehydrated tissue during RF ablation with cooled electrodes”. In: *International Journal of Hyperthermia* 28.1 (2012), pp. 62–68 (cit. on pp. 26, 56, 58, 60).

[10] M. W. Miller and M. C. Ziskin. “Biological consequences of hyperthermia”. In: *Ultrasound in medicine & biology* 15.8 (1989), pp. 707–722 (cit. on p. 26).

[11] A. González-Suárez and E. Berjano. “Comparative analysis of different methods of modeling the thermal effect of circulating blood flow during RF cardiac ablation”. In: *IEEE Transactions on Biomedical Engineering* 63.2 (2015), pp. 250–259 (cit. on pp. 26, 37, 50, 160).

[12] N. Yamazaki, Y. Kobayashi, H. Kikuchi, Y. Isobe, X. Lu, T. Miyashita, and M. G. Fujie. “Modeling of lung’s electrical impedance using fractional calculus for analysis of heat generation during RF-ablation”. In: *2014 36th Annual International Conference of the IEEE Engineering in Medicine and Biology Society*. IEEE. 2014, pp. 5323–5328 (cit. on pp. 26, 56, 58).

[13] S. Singh and R. Repaka. “Numerical study to establish relationship between coagulation volume and target tip temperature during temperature-controlled radiofrequency ablation”. In: *Electromagnetic biology and medicine* 37.1 (2018), pp. 13–22 (cit. on p. 27).

[14] A. González-Suárez, E. Berjano, J. M. Guerra, and L. Gerardo-Giorda. “Computational modeling of open-irrigated electrodes for radiofrequency cardiac ablation including blood motion-saline flow interaction”. In: *PloS one* 11.3 (2016), e0150356 (cit. on p. 27).

[15] A. González-Suárez, J. J. Pérez, and E. Berjano. “Should fluid dynamics be included in computer models of RF cardiac ablation by irrigated-tip electrodes?” In: *Biomedical engineering online* 17.1 (2018), pp. 1–14 (cit. on pp. 27, 44, 50, 152).

[16] A. González-Suárez, J. J. Pérez, and E. Berjano. “Computer modeling of irrigated-tip electrodes during RF cardiac ablation: Comparative analysis between including and excluding the problem of fluid dynamics”. In: *2017 Computing in Cardiology (CinC)*. IEEE. 2017, pp. 1–4 (cit. on pp. 27, 43, 44, 50–52, 150).

[17] D. Haemmerich. “Mathematical modeling of impedance controlled radiofrequency tumor ablation and ex-vivo validation”. In: *2010 Annual International Conference of the IEEE Engineering in Medicine and Biology*. IEEE. 2010, pp. 1605–1608 (cit. on p. 27).

[18] C.-C. R. Chen, M. I. Miga, and R. L. Galloway. “Optimizing electrode placement using finite-element models in radiofrequency ablation treatment planning”. In: *IEEE transactions on biomedical engineering* 56.2 (2008), pp. 237–245 (cit. on p. 27).

[19] B. Zhang, M. A. Moser, E. M. Zhang, Y. Luo, C. Liu, and W. Zhang. “A review of radiofrequency ablation: Large target tissue necrosis and mathematical modelling”. In: *Physica Medica* 32.8 (2016), pp. 961–971 (cit. on p. 27).

[20] K. Yokoyama, H. Nakagawa, F. H. Wittkampf, J. V. Pitha, R. Lazzara, and W. M. Jackman. “Comparison of electrode cooling between internal and open irrigation in radiofrequency ablation lesion depth and incidence of thrombus and steam pop”. In: *Circulation* 113.1 (2006), pp. 11–19 (cit. on p. 27).

[21] U. of Brasília Foundation and T. D. Center. “Radiofrequency Hepatic Ablation System Containing Equipment with Electronic Controland Electrode in Umbrella Format Made in Alloy with Memory of Formand Its Method of Processing and Analysis of Medical Images”. In: *Patent BR 10 2017 002 683 3* (2017). URL: https://gru.inpi.gov.br (cit. on pp. 29, 62).

[22] M. S. Monteiro. “Avaliação da biocompatibilidade e eficácia terapêutica da ablação térmica utilizando um eletrodo de níquel-titânio em modelo de carcinossarcoma hepático”. In: (2018) (cit. on p. 29).

[23] N. I. for Health and C. Research. *PROSPERO - International prospective register of systematic reviews*. Centre for Reviews and Dissemination, University of York. Disponível em: https://https://www.crd.york.ac.uk/prospero/ – acesso em 09 fev. 2022. 2022 (cit. on pp. 30, 37).

[24] J. K. Cheong, S. Yap, E. T. Ooi, and E. H. Ooi. “A computational model to investigate the influence of electrode lengths on the single probe bipolar radiofrequency ablation of the liver”. In: *Computer methods and programs in biomedicine* 176 (2019), pp. 17–32 (cit. on pp. 35, 36, 159).

[25] Z. Fang, H. Wei, H. Zhang, M. A. Moser, W. Zhang, Z. Qian, and B. Zhang. “Radiofrequency ablation for liver tumors abutting complex blood vessel structures: treatment protocol optimization using response surface method and computer modeling”. In: *International Journal of Hyperthermia* 39.1 (2022), pp. 733–742 (cit. on pp. 35, 36).

[26] B. Zhang, M. A. Moser, E. M. Zhang, Y. Luo, and W. Zhang. “Numerical analysis of the relationship between the area of target tissue necrosis and the size of target tissue in liver tumours with pulsed radiofrequency ablation”. In: *International Journal of Hyperthermia* 31.7 (2015), pp. 715–725 (cit. on pp. 35, 36).

[27] P. C. d. Souza. “Módulo esofágico para resfriamento durante cirurgia de ablação cardíaca por radiofrequência”. In: (2019) (cit. on p. 36).

[28] M. A. F. Ribeiro Jr, R. P. Colaneri, B. d. S. Nunes, E. Chaib, G. D’Ipolitto, J. J. Gama-Rodrigues, W. A. Saad, and I. Cecconello. “Radiofrequency ablation of primary and metastatic liver tumors: 113 cases experience”. In: *ABCD. Arquivos Brasileiros de Cirurgia Digestiva (São Paulo)* 20 (2007), pp. 38–44 (cit. on pp. 36, 56).

[29] Z. Tian, Q. Nan, X. Nie, T. Dong, and R. Wang. “The comparison of lesion outline and temperature field determined by different ways in atrial radiofrequency ablation”. In: *Biomedical engineering online* 15 (2016), pp. 439–449 (cit. on pp. 36, 45, 52, 153).

[30] J. H. Yoon, J. M. Lee, S. Woo, E. J. Hwang, I. Hwang, W. Choi, J. K. Han, and B. I. Choi. "Switching bipolar hepatic radiofrequency ablation using internally cooled wet electrodes: comparison with consecutive monopolar and switching monopolar modes". In: *The British Journal of Radiology* 88.1050 (2015). PMID: 25873479, p. 20140468. DOI: 10.1259/bjr.20140468. URL: https://doi.org/10.1259/bjr.20140468 (cit. on p. 36).

[31] S. Woo, J. M. Lee, J. H. Yoon, I. Joo, S. H. Kim, J. Y. Lee, J. H. Yoon, Y. J. Kim, J. K. Han, and B. I. Choi. "Small-and medium-sized hepatocellular carcinomas: monopolar radiofrequency ablation with a multiple-electrode switching system—mid-term results". In: *Radiology* 268.2 (2013), pp. 589–600 (cit. on p. 36).

[32] A. S. Kho, E. H. Ooi, J. J. Foo, and E. T. Ooi. "The effects of vaporisation, condensation and diffusion of water inside the tissue during saline-infused radiofrequency ablation of the liver: A computational study". In: *International Journal of Heat and Mass Transfer* 194 (2022), p. 123062. ISSN: 0017-9310. DOI: https://doi.org/10.1016/j.ijheatmasstransfer.2022.123062. URL: https://www.sciencedirect.com/science/article/pii/S001793102200535X (cit. on p. 36).

[33] L. González-Rodríguez, S. Pérez-Davila, M. López-Álvarez, S. Chiussi, J. Serra, and P. González. "Review article laser-induced hyperthermia on graphene oxide composites". In: *Journal of Nanobiotechnology* 21.1 (2023), p. 196 (cit. on p. 37).

[34] X. Zhang, S. Wang, G. Cheng, P. Yu, and J. Chang. "Light-responsive nanomaterials for cancer therapy". In: *Engineering* 13 (2022), pp. 18–30 (cit. on p. 37).

[35] U. Sorgucu and I. Develi. "Thermal Analysis of Biological Tissues Exposed To Electromagnetic Fields by Using Pennes' Bio-Heat Transfer Equation". In: *2021 IEEE International Conference on Electronics, Computing and Communication Technologies (CONECCT)*. IEEE. 2021, pp. 01–06 (cit. on p. 37).

[36] A. González-Suárez, E. Berjano, J. M. Guerra, and L. Gerardo-Giorda. "A computational model of open-irrigated electrode for endocardial RF catheter ablation". In: *2015 Computing in Cardiology Conference (CinC)*. IEEE. 2015, pp. 73–76 (cit. on pp. 37, 47, 50, 159).

[37] D. Moher, A. Liberati, J. Tetzlaff, D. G. Altman, and T. P. Group. "Preferred Reporting Items for Systematic Reviews and Meta-Analyses: The PRISMA Statement". In: *PLOS Medicine* 6.7 (July 2009), pp. 1–6. DOI: 10.1371/journal.pmed.1000097. URL: https://doi.org/10.1371/journal.pmed.1000097 (cit. on p. 37).

[38] B. Hutton, G. Salanti, D. M. Caldwell, A. Chaimani, C. H. Schmid, C. Cameron, J. P. Ioannidis, S. Straus, K. Thorlund, J. P. Jansen, et al. "The PRISMA extension statement for reporting of systematic reviews incorporating network meta-analyses

of health care interventions: checklist and explanations". In: *Annals of internal medicine* 162.11 (2015), pp. 777–784 (cit. on p. 37).

[39] M. Li, X. Liu, P. Bradbury, J. Yu, Y.-M. Zhang, R. J. Todhunter, E. S. Buckler, and Z. Zhang. "Enrichment of statistical power for genome-wide association studies". In: *BMC biology* 12 (2014), pp. 1–10 (cit. on p. 38).

[40] N. J. Van Eck and L. Waltman. "VOSviewer manual". In: *Manual for VOSviewer version* 1.0 (2011) (cit. on p. 42).

[41] M. Jamil and E. Ng. "Quantification of the effect of electrical and thermal parameters on radiofrequency ablation for concentric tumour model of different sizes". In: *Journal of Thermal Biology* 51 (2015), pp. 23–32 (cit. on pp. 43, 50, 51, 60, 150).

[42] C. Rossmann, A. Motamarry, D. Panescu, and D. Haemmerich. "Computer simulations of an irrigated radiofrequency cardiac ablation catheter and experimental validation by infrared imaging". In: *International Journal of Hyperthermia* 38.1 (2021), pp. 1149–1163 (cit. on pp. 43, 50, 51, 151).

[43] X. Wang, H. Gao, S. Wu, Y. Bai, and Z. Zhou. "RF ablation thermal simulation model: Parameter sensitivity analysis". In: *Technology and Health Care* 26.S1 (2018), pp. 179–192 (cit. on pp. 44, 52, 151).

[44] N. Vaidya, M. Baragona, V. Lavezzo, R. Maessen, and K. Veroy. "Simulation study of the cooling effect of blood vessels and blood coagulation in hepatic radio-frequency ablation". In: *International Journal of Hyperthermia* 38.1 (2021), pp. 95–104 (cit. on pp. 44, 52, 152).

[45] B. Zhang, M. A. Moser, E. M. Zhang, Y. Luo, H. Zhang, and W. Zhang. "Study of the relationship between the target tissue necrosis volume and the target tissue size in liver tumours using two-compartment finite element RFA modelling". In: *International Journal of Hyperthermia* 30.8 (2014), pp. 593–602 (cit. on pp. 44, 52, 56, 154).

[46] E. H. Ooi, K. W. Lee, S. Yap, M. A. Khattab, I. Y. Liao, E. T. Ooi, J. J. Foo, S. R. Nair, and A. F. M. Ali. "The effects of electrical and thermal boundary condition on the simulation of radiofrequency ablation of liver cancer for tumours located near to the liver boundary". In: *Computers in biology and medicine* 106 (2019), pp. 12–23 (cit. on pp. 45, 50, 52, 154).

[47] J. K. Cheong, E. H. Ooi, and E. T. Ooi. "Thermal and thermal damage responses during switching bipolar radiofrequency ablation employing bipolar needles: A computational study on the effects of different electrode configuration, input voltage and ablation duration". In: *International journal for numerical methods in biomedical engineering* 36.9 (2020), e3374 (cit. on pp. 45, 155).

[48] D. L. Castro-López, M. Trujillo Guillen, E. Berjano, and R. Romero-Mendez. “Two-compartment mathematical modeling in RF tumor ablation: New insight when irreversible changes in electrical conductivity are considered”. In: *Mathematical Biosciences and Engineering* 17.6 (2020), pp. 7980–7993 (cit. on pp. 45, 155).

[49] E. H. Ooi and E. T. Ooi. “Unidirectional ablation minimizes unwanted thermal damage and promotes better thermal ablation efficacy in time-based switching bipolar radiofrequency ablation”. In: *Computers in biology and medicine* 137 (2021), p. 104832 (cit. on p. 45).

[50] J. Arenas, J. J. Perez, M. Trujillo, and E. Berjano. “Computer modeling and ex vivo experiments with a (saline-linked) irrigated electrode for RF-assisted heating”. In: *BioMedical Engineering OnLine* 13.1 (2014), pp. 1–16 (cit. on pp. 45, 50, 153).

[51] B. Zhang, M. A. Moser, Y. Luo, E. M. Zhang, and W. Zhang. “Evaluation of the current radiofrequency ablation systems using axiomatic design theory”. In: *Proceedings of the Institution of Mechanical Engineers, Part H: Journal of Engineering in Medicine* 228.4 (2014), pp. 397–408 (cit. on pp. 46, 50, 156).

[52] M. Mercado, L. Leung, M. Gallagher, S. Shah, and E. Kulstad. “Modeling esophageal protection from radiofrequency ablation via a cooling device: an analysis of the effects of ablation power and heart wall dimensions”. In: *BioMedical Engineering OnLine* 19.1 (2020), pp. 1–17 (cit. on pp. 46, 157).

[53] Q. Zhu, Y. Shen, A. Zhang, and L. X. Xu. “Numerical study of the influence of water evaporation on radiofrequency ablation”. In: *Biomedical engineering online* 12.1 (2013), pp. 1–16 (cit. on pp. 46, 71, 157).

[54] M. Zhang, Z. Zhou, S. Wu, L. Lin, H. Gao, and Y. Feng. “Simulation of temperature field for temperature-controlled radio frequency ablation using a hyperbolic bioheat equation and temperature-varied voltage calibration: a liver-mimicking phantom study”. In: *Physics in Medicine & Biology* 60.24 (2015), p. 9455 (cit. on pp. 46, 158).

[55] S. de Sousa Faria, P. C. de Souza, G. P. Souza, C. F. da Justa, A. F. da Rocha, and S. d. S. R. F. Rosa. “Analysis of the Depth of Thermal Injuries Caused during the Cardiac Ablation Procedure with the Cooling of the Esophageal Wall”. In: *IEEE Latin America Transactions* 19.7 (2021), pp. 1121–1128 (cit. on p. 47).

[56] J. J. Pérez, E. Nadal, E. Berjano, and A. González-Suárez. “Computer modeling of radiofrequency cardiac ablation including heartbeat-induced electrode displacement”. In: *Computers in Biology and Medicine* 144 (2022), p. 105346 (cit. on pp. 47, 50, 161).

[57] H.-W. Huang, L. Hui, J. C. Hung, and K. M. Wang. “Illustrating the impact of uneven saline distribution on thermal lesion during radiofrequency ablation using computer simulation for smarter healthcare treatment planning”. In: *Journal of Medical and Biological Engineering* 38 (2018), pp. 880–888 (cit. on pp. 47, 161).

[58] J. A. López Molina, M. J. Rivera Ortun, and E. Berjano. “Electrical-thermal analytical modeling of monopolar RF thermal ablation of biological tissues: determining the circumstances under which tissue temperature reaches a steady state”. In: *Mathematical biosciences and engineering* 13.2 (2016), pp. 281–301 (cit. on pp. 48, 157).

[59] L. Molinari, M. Zaltieri, C. Massaroni, S. Filippi, A. Gizzi, and E. Schena. “Multiscale and multiphysics modeling of anisotropic cardiac RFCA: experimental-based model calibration via multi-point temperature measurements”. In: *Frontiers in Physiology* 13 (2022), p. 845896 (cit. on pp. 48, 52, 162).

[60] E. G. Macchi, M. Gallati, G. Braschi, A. Cigada, and L. Comolli. “Temperature distribution during RF ablation on ex vivo liver tissue: IR measurements and simulations”. In: *Heat and Mass Transfer* 51 (2015), pp. 611–620 (cit. on pp. 48, 52, 162).

[61] M. Fiek, F. Gindele, C. von Bary, D. Muessig, A. Lucic, E. Hoffmann, C. Reithmann, and G. Steinbeck. “Direct thermography—a new in vitro method to characterize temperature kinetics of ablation catheters”. In: *Journal of Interventional Cardiac Electrophysiology* 38 (2013), pp. 53–59 (cit. on pp. 49, 52, 163).

[62] X. Lu, H. Kikuchi, K. Hirooka, Y. Isobe, H. Watanabe, Y. Kobayashi, T. Miyashita, and M. G. Fujie. “Method for estimating the temperature distribution associated with the vessel cooling effect in radio frequency ablation”. In: *2015 37th Annual International Conference of the IEEE Engineering in Medicine and Biology Society (EMBC)*. IEEE. 2015, pp. 4836–4839 (cit. on pp. 49, 163).

[63] M. Trujillo, Q. Castellví, F. Burdío, P. Sanchez Velazquez, A. Ivorra, A. Andaluz, and E. Berjano. “Can electroporation previous to radiofrequency hepatic ablation enlarge thermal lesion size? A feasibility study based on theoretical modelling and in vivo experiments”. In: *International Journal of Hyperthermia* 29.3 (2013), pp. 211–218 (cit. on pp. 49, 50, 164).

[64] R. M. Faria, S. d. S. R. F. Rosa, G. A. M. d. A. Nunes, K. S. Santos, R. P. de Souza, A. D. I. Benavides, A. K. d. O. Alves, A. K. A. da Silva, M. F. Rosa, A. A. d. A. Cardoso, et al. “Particle swarm optimization solution for roll-off control in radiofrequency ablation of liver tumors: Optimal search for PID controller tuning”. In: *Plos one* 19.6 (2024), e0300445 (cit. on p. 55).

[65] H. Rumgay, J. Ferlay, C. de Martel, D. Georges, A. S. Ibrahim, R. Zheng, W. Wei, V. E. Lemmens, and I. Soerjomataram. “Global, regional and national burden of primary liver cancer by subtype”. In: *European Journal of Cancer* 161 (2022), pp. 108–118 (cit. on p. 55).

[66] J. Ferlay, M. Colombet, I. Soerjomataram, T. Dyba, G. Randi, M. Bettio, A. Gavin, O. Visser, and F. Bray. “Cancer incidence and mortality patterns in Europe: Estimates

for 40 countries and 25 major cancers in 2018". In: *European journal of cancer* 103 (2018), pp. 356–387 (cit. on p. 55).

[67] J. M. Llovet, R. K. Kelley, A. Villanueva, A. G. Singal, E. Pikarsky, S. Roayaie, R. Lencioni, K. Koike, J. Zucman-Rossi, and R. S. Finn. "Hepatocellular carcinoma." In: *Nature reviews. Disease primers* 7.1 (2021), pp. 6–6 (cit. on p. 55).

[68] X. Li, Y. Zhong, A. Subic, R. Jazar, J. Smith, and C. Gu. "Prediction of tissue thermal damage". In: *Technology and Health Care* 24.s2 (2016), S625–S629 (cit. on pp. 55, 56).

[69] D. Anwanwan, S. K. Singh, S. Singh, V. Saikam, and R. Singh. "Challenges in liver cancer and possible treatment approaches". In: *Biochimica et Biophysica Acta (BBA)-Reviews on Cancer* 1873.1 (2020), p. 188314 (cit. on p. 55).

[70] B. Alawyia and C. Constantinou. "Hepatocellular Carcinoma: a Narrative Review on Current Knowledge and Future Prospects". In: *Current Treatment Options in Oncology* (2023), pp. 1–14 (cit. on p. 55).

[71] C. A. Philips, S. Rajesh, D. C. Nair, R. Ahamed, J. K. Abduljaleel, P. Augustine, and J. Abduljaleel. "Hepatocellular carcinoma in 2021: an exhaustive update". In: *Cureus* 13.11 (2021) (cit. on pp. 55, 56).

[72] H. Enomoto, T. Nishimura, S. Fukunushi, H. Shiomi, and H. Iijima. "Determination of the Possible Target Genes of Hepatoma-derived Growth Factor in Hepatoma Cells". In: *in vivo* 37.5 (2023), pp. 1975–1979 (cit. on p. 56).

[73] S. Chidambaranathan-Reghupaty, P. B. Fisher, and D. Sarkar. "Hepatocellular carcinoma (HCC): Epidemiology, etiology and molecular classification". In: *Advances in cancer research* 149 (2021), pp. 1–61 (cit. on p. 56).

[74] P. Dasgupta, C. Henshaw, D. R. Youlden, P. J. Clark, J. F. Aitken, and P. D. Baade. "Global trends in incidence rates of primary adult liver cancers: a systematic review and meta-analysis". In: *Frontiers in oncology* 10 (2020), p. 171 (cit. on p. 56).

[75] S. Tungjitkusolmun, S. T. Staelin, D. Haemmerich, J.-Z. Tsai, H. Cao, J. G. Webster, F. T. Lee, D. M. Mahvi, and V. R. Vorperian. "Three-dimensional finite-element analyses for radio-frequency hepatic tumor ablation". In: *IEEE transactions on biomedical engineering* 49.1 (2002), pp. 3–9 (cit. on p. 56).

[76] S. Singh and R. Repaka. "Numerical study to establish relationship between coagulation volume and target tip temperature during temperature-controlled radiofrequency ablation". In: *Electromagnetic biology and medicine* 37.1 (2018), pp. 13–22 (cit. on pp. 56, 58, 60).

[77] A. González-Suárez, J. J. Pérez, R. M. Irastorza, A. D'Avila, and E. Berjano. "Computer modeling of radiofrequency cardiac ablation: 30 years of bioengineering research". In: *Computer Methods and Programs in Biomedicine* (2021), p. 106546 (cit. on p. 56).

[78] H. K. Lim, D. Choi, W. J. Lee, S. H. Kim, S. J. Lee, H.-J. Jang, J.-H. Lee, J. H. Lim, and I. W. Choo. “Hepatocellular carcinoma treated with percutaneous radio-frequency ablation: evaluation with follow-up multiphase helical CT”. In: *Radiology* 221.2 (2001), pp. 447–454 (cit. on p. 56).

[79] E. Berjano, W. Franco, et al. “Radiofrequency based hyperthermia therapy: A centennial technique serving modern surgery”. In: *Revista Mexicana de Ingenier a Biom dica* 31.2 (2010), pp. 142–153 (cit. on p. 56).

[80] E. Ewertowska, R. Quesada, A. Radosevic, A. Andaluz, X. Moll, F. G. Arnas, E. Berjano, F. Burdío, and M. Trujillo. “A clinically oriented computer model for radiofrequency ablation of hepatic tissue with internally cooled wet electrode”. In: *International Journal of Hyperthermia* 35.1 (2018), pp. 194–204 (cit. on pp. 56, 58).

[81] M. Nakai, M. Sato, S. Sahara, N. Kawai, H. Tanihata, M. Kimura, and M. Terada. “Radiofrequency ablation in a porcine liver model: effects of transcatheter arterial embolization with iodized oil on ablation time, maximum output, and coagulation diameter as well as angiographic characteristics”. In: *World Journal of Gastroenterology: WJG* 13.20 (2007), p. 2841 (cit. on p. 56).

[82] M. Habibi, R. D. Berger, and H. Calkins. “Radiofrequency ablation: technological trends, challenges, and opportunities”. In: *EP Europace* 23.4 (2021), pp. 511–519 (cit. on p. 56).

[83] M. R. DeWitt, E. L. Latouche, J. D. Kaufman, C. C. Fesmire, J. H. Swet, R. C. Kirks, E. H. Baker, D. Vrochides, D. A. Iannitti, I. H. McKillop, et al. “Simplified non-thermal tissue ablation with a single insertion device enabled by bipolar high-frequency pulses”. In: *IEEE Transactions on Biomedical Engineering* 67.7 (2019), pp. 2043–2051 (cit. on p. 56).

[84] X.-Y. Jiang, T.-Q. Zhang, G. Li, Y.-K. Gu, F. Gao, W. Yao, Y.-y. Zhang, and J.-h. Huang. “Increasing radiofrequency ablation volumes with the use of internally cooled electrodes and injected hydrochloric acid in ex vivo bovine livers”. In: *International Journal of Hyperthermia* 35.1 (2018), pp. 37–43 (cit. on pp. 56, 85).

[85] L. O. O. Kikuchi. “Análise da sobrevida de pacientes com carcinoma hepatocelular atendidos no Instituto do Câncer do Estado de São Paulo”. PhD thesis. Universidade de São Paulo, 2015 (cit. on p. 56).

[86] G. C. Cavalcante, F. F. Lima, M. Venturin, R. P. Jacobi, and S. d. S. R. F. Rosa. “Development of radiofrequency ablation device for surgical hepatocellular carcinoma treatment in agreement with Brazilian standards”. In: *Research on Biomedical Engineering* 34 (2018), pp. 115–126 (cit. on p. 56).

[87] M. H. Yu, Y. J. Kim, H. S. Park, S. I. Jung, and H. J. Jeon. “Shrinkage of hepatocellular carcinoma after radiofrequency ablation following transcatheter arterial chemoembolization: Analysis of contributing factors”. In: *Plos one* 14.2 (2019), e0210667 (cit. on p. 57).

[88] C. L. Brace, T. A. Diaz, J. L. Hinshaw, and F. T. Lee Jr. “Tissue contraction caused by radiofrequency and microwave ablation: a laboratory study in liver and lung”. In: *Journal of Vascular and Interventional Radiology* 21.8 (2010), pp. 1280–1286 (cit. on p. 57).

[89] M. Paruch. “Mathematical modeling of breast tumor destruction using fast heating during radiofrequency ablation”. In: *Materials* 13.1 (2019), p. 136 (cit. on p. 57).

[90] A. Andreozzi, L. Brunese, M. Iasiello, C. Tucci, and G. P. Vanoli. “Numerical analysis of the pulsating heat source effects in a tumor tissue”. In: *Computer Methods and Programs in Biomedicine* 200 (2021), p. 105887 (cit. on p. 57).

[91] A. Andreozzi, L. Brunese, M. Iasiello, C. Tucci, and G. P. Vanoli. “A novel local thermal non-equilibrium model for biological tissue applied to multiple-antennas configurations for thermal ablation”. In: *Numerical Heat Transfer, Part A: Applications* 79.2 (2020), pp. 111–121 (cit. on p. 57).

[92] S. Singh, A. Bhowmik, and R. Repaka. “Thermal analysis of induced damage to the healthy cell during RFA of breast tumor”. In: *Journal of thermal biology* 58 (2016), pp. 80–90 (cit. on p. 57).

[93] D. Haemmerich, T. Staelin, S. Tungjitkusolmun, F. Lee, D. Mahvi, and J. Webster. “Hepatic bipolar radio-frequency ablation between separated multiprong electrodes”. In: *IEEE Transactions on Biomedical Engineering* 48.10 (2001), pp. 1145–1152. DOI: 10.1109/10.951517 (cit. on p. 57).

[94] M. W. Dewhirst, J. Abraham, and B. Viglianti. “Evolution of thermal dosimetry for application of hyperthermia to treat cancer”. In: *Advances in heat transfer*. Vol. 47. Elsevier, 2015, pp. 397–421 (cit. on p. 57).

[95] R. D. da Fonseca, M. S. Monteiro, M. P. Marques, B. C. Motta, G. dos Anjos Guimarães, P. R. do Santos, R. P. Jacobi, and S. d. S. R. F. Rosa. “Roll-off displacement in ex vivo experiments of RF ablation with refrigerated saline solution and refrigerated deionized water”. In: *IEEE Transactions on Biomedical Engineering* 66.5 (2018), pp. 1390–1401 (cit. on pp. 58, 83, 85).

[96] M. A. Arata, H. L. Nisenbaum, T. W. Clark, and M. C. Soulen. “Percutaneous radiofrequency ablation of liver tumors with the LeVeen probe: is roll-off predictive of response?” In: *Journal of Vascular and Interventional Radiology* 12.4 (2001), pp. 455–458 (cit. on pp. 58, 60, 85).

[97] S. Mulier, Y. Miao, P. Mulier, B. Dupas, P. Pereira, T. D. Baere, R. Lencioni, R. Leveillee, G. Marchal, L. Michel, et al. “Electrodes and multiple electrode systems for radio frequency ablation: a proposal for updated terminology”. In: *Liver and Pancreatic Diseases Management*. Springer, 2006, pp. 57–73 (cit. on p. 58).

[98] X. Fan, W. Sayers, S. Zhang, Z. Han, L. Ren, and H. Chizari. “Review and classification of bio-inspired algorithms and their applications”. In: *Journal of Bionic Engineering* 17.3 (2020), pp. 611–631 (cit. on p. 58).

[99] S. Binitha, S. S. Sathya, et al. “A survey of bio inspired optimization algorithms”. In: *International journal of soft computing and engineering* 2.2 (2012), pp. 137–151 (cit. on p. 58).

[100] A. Q. Al-Dujaili, A. Falah, A. J. Humaidi, D. A. Pereira, and I. K. Ibraheem. “Optimal super-twisting sliding mode control design of robot manipulator: Design and comparison study”. In: *International Journal of Advanced Robotic Systems* 17.6 (2020), p. 1729881420981524 (cit. on pp. 58, 59).

[101] W. R. Abdul-Adheem, I. K. Ibraheem, A. J. Humaidi, and A. T. Azar. “Model-free active input–output feedback linearization of a single-link flexible joint manipulator: An improved active disturbance rejection control approach”. In: *Measurement and Control* 54.5-6 (2021), pp. 856–871 (cit. on p. 59).

[102] E. Kumru and N. F. O. Serteller. “DC motor Analysis Based on Improvement of PID Coefficients Using PSO Algorithm for Educational Use”. In: *International Conference on Interactive Collaborative Learning*. Springer. 2022, pp. 901–909 (cit. on p. 59).

[103] S. Ali, G. Yang, and C. Huang. “Performance optimization of linear active disturbance rejection control approach by modified bat inspired algorithm for single area load frequency control concerning high wind power penetration”. In: *ISA transactions* 81 (2018), pp. 163–176 (cit. on p. 59).

[104] F. H. Ajeil, I. K. Ibraheem, A. J. Humaidi, and Z. H. Khan. “A novel path planning algorithm for mobile robot in dynamic environments using modified bat swarm optimization”. In: *The Journal of Engineering* 2021.1 (2021), pp. 37–48 (cit. on p. 59).

[105] G. A. R. Ibraheem, A. T. Azar, I. K. Ibraheem, and A. J. Humaidi. “A novel design of a neural network-based fractional PID controller for mobile robots using hybridized fruit fly and particle swarm optimization”. In: *Complexity* 2020 (2020), pp. 1–18 (cit. on p. 59).

[106] R. D. da Fonseca, M. S. Monteiro, M. P. Marques, B. C. Motta, G. dos Anjos Guimaraes, P. R. do Santos, R. P. Jacobi, and S. d. S. R. F. Rosa. “Roll-off displacement in ex vivo experiments of RF ablation with refrigerated saline solution and refrigerated deionized water”. In: *IEEE Transactions on Biomedical Engineering* 66.5 (2018), pp. 1390–1401 (cit. on p. 60).

[107] M. R. Najjari and M. W. Plesniak. “PID controller design to generate pulsatile flow rate for in vitro experimental studies of physiological flows”. In: *Biomedical Engineering Letters* 7 (2017), pp. 339–344 (cit. on p. 60).

[108] A. Orrico, S. Korganbayev, L. Bianchi, M. De Landro, and P. Saccomandi. “Feedback-controlled laser ablation for cancer treatment: comparison of On-Off and PID control strategies”. In: *2022 44th Annual International Conference of the IEEE Engineering in Medicine & Biology Society (EMBC)*. IEEE. 2022, pp. 5012–5015 (cit. on p. 60).

[109] D. Haemmerich and J. G. Webster. “Automatic control of finite element models for temperature-controlled radiofrequency ablation”. In: *Biomedical engineering online* 4.1 (2005), pp. 1–8 (cit. on p. 60).

[110] B. Zhang, M. A. Moser, E. M. Zhang, Y. Luo, and W. Zhang. “A new approach to feedback control of radiofrequency ablation systems for large coagulation zones”. In: *International Journal of Hyperthermia* 33.4 (2017), pp. 367–377 (cit. on p. 60).

[111] S. B. Joseph, E. G. Dada, A. Abidemi, D. O. Oyewola, and B. M. Khammas. “Meta-heuristic algorithms for PID controller parameters tuning: Review, approaches and open problems”. In: *Heliyon* (2022) (cit. on p. 60).

[112] A. Daraz, S. A. Malik, I. U. Haq, K. B. Khan, G. F. Laghari, and F. Zafar. “Modified PID controller for automatic generation control of multi-source interconnected power system using fitness dependent optimizer algorithm”. In: *PloS one* 15.11 (2020), e0242428 (cit. on p. 60).

[113] Y. Cheng, Q. Nan, R. Wang, T. Dong, and Z. Tian. “Fuzzy proportional integral derivative control of a radiofrequency ablation temperature control system”. In: *2017 10th International Congress on Image and Signal Processing, BioMedical Engineering and Informatics (CISP-BMEI)*. IEEE. 2017, pp. 1–5 (cit. on pp. 60, 83).

[114] R. D. da Fonseca Campos. “Modelagem Bond Graph e Controlador Discreto de um Equipamento Médico Assistencial de Ablação por Radiofrequência”. PhD thesis. Brasília: Universidade de Brasília, Mar. 2022 (cit. on pp. 62, 63).

[115] M. P. Marques. “Desenvolvimento de eletrodo expansível de níquel-titânio para ablação por radiofrequência”. MA thesis. Brasília: Universidade de Brasília, Sept. 2016 (cit. on pp. 62, 63).

[116] U. of Brasília Foundation and T. D. Center. “Continuous monitoring system for hospital equipment”. In: *Patent BR 10 2017 002 919 0* (2017). URL: https://gru.inpi.gov.br (cit. on p. 63).

[117] Q. Chen, S. Müftü, F. C. Meral, K. Tuncali, and M. Akcakaya. “Pre-treatment planning for hepatic radiofrequency ablation”. In: *2015 IEEE Signal Processing in Medicine and Biology Symposium (SPMB)*. IEEE. 2015, pp. 1–6 (cit. on p. 64).

[118] S. A. Billings. *Nonlinear system identification: NARMAX methods in the time, frequency, and spatio-temporal domains*. John Wiley & Sons, 2013 (cit. on p. 65).

[119] MATLAB. *version 7.10.0 (R2010a)*. Natick, Massachusetts: The MathWorks Inc., 2020 (cit. on p. 66).

[120] Y. Shi. "Particle swarm optimization". In: *IEEE connections* 2.1 (2004), pp. 8–13 (cit. on p. 68).

[121] D. Wang, D. Tan, and L. Liu. "Particle swarm optimization algorithm: an overview". In: *Soft computing* 22 (2018), pp. 387–408 (cit. on p. 68).

[122] M. I. Solihin, L. F. Tack, and M. L. Kean. "Tuning of PID controller using particle swarm optimization (PSO)". In: *Proceeding of the international conference on advanced science, engineering and information technology*. Vol. 1. 2011, pp. 458–461 (cit. on pp. 68, 69, 71).

[123] T. M. Shami, A. A. El-Saleh, M. Alswaitti, Q. Al-Tashi, M. A. Summakieh, and S. Mirjalili. "Particle swarm optimization: A comprehensive survey". In: *IEEE Access* 10 (2022), pp. 10031–10061 (cit. on p. 68).

[124] Z.-L. Gaing. "A particle swarm optimization approach for optimum design of PID controller in AVR system". In: *IEEE transactions on energy conversion* 19.2 (2004), pp. 384–391 (cit. on pp. 68, 69, 71).

[125] R. Eberhart and J. Kennedy. "A new optimizer using particle swarm theory". In: *MHS'95. Proceedings of the sixth international symposium on micro machine and human science*. Ieee. 1995, pp. 39–43 (cit. on p. 69).

[126] S. Ribeiro and L. G. Lopes. "PSO Performance for Solving Nonlinear Systems of Equations: Comparing Segmentation of Search Space and Increase of Number of Particles". In: *International Conference on Computational Science and Its Applications*. Springer. 2022, pp. 261–272 (cit. on p. 69).

[127] E. H. Houssein, A. G. Gad, K. Hussain, and P. N. Suganthan. "Major advances in particle swarm optimization: theory, analysis, and application". In: *Swarm and Evolutionary Computation* 63 (2021), p. 100868 (cit. on p. 69).

[128] F. Wang, H. Zhang, and A. Zhou. "A particle swarm optimization algorithm for mixed-variable optimization problems". In: *Swarm and Evolutionary Computation* 60 (2021), p. 100808 (cit. on p. 69).

[129] D. Bratton and J. Kennedy. "Defining a standard for particle swarm optimization". In: *2007 IEEE swarm intelligence symposium*. IEEE. 2007, pp. 120–127 (cit. on pp. 69, 71).

[130] T.-H. Kim, I. Maruta, and T. Sugie. "Robust PID controller tuning based on the constrained particle swarm optimization". In: *Automatica* 44.4 (2008), pp. 1104–1110 (cit. on p. 71).

[131] Y. Shi and R. Eberhart. “A modified particle swarm optimizer”. In: *1998 IEEE international conference on evolutionary computation proceedings. IEEE world congress on computational intelligence (Cat. No. 98TH8360)*. IEEE. 1998, pp. 69–73 (cit. on p. 71).

[132] M. Clerc and J. Kennedy. “The particle swarm-explosion, stability, and convergence in a multidimensional complex space”. In: *IEEE transactions on Evolutionary Computation* 6.1 (2002), pp. 58–73 (cit. on p. 71).

[133] F. Van den Bergh and A. P. Engelbrecht. “A new locally convergent particle swarm optimiser”. In: *IEEE International conference on systems, man and cybernetics*. Vol. 3. IEEE. 2002, 6–pp (cit. on p. 71).

[134] S. Mulier, Y. Jiang, J. Jamart, C. Wang, Y. Feng, G. Marchal, L. Michel, and Y. Ni. “Bipolar radiofrequency ablation with 2× 2 electrodes as a building block for matrix radiofrequency ablation: Ex vivo liver experiments and finite element method modelling”. In: *International Journal of Hyperthermia* 31.6 (2015), pp. 649–665 (cit. on p. 71).

[135] U. Zurbuchen, C. Holmer, K. S. Lehmann, T. Stein, A. Roggan, C. Seifarth, H.-J. Buhr, and J.-P. Ritz. “Determination of the temperature-dependent electric conductivity of liver tissue ex vivo and in vivo: Importance for therapy planning for the radiofrequency ablation of liver tumours”. In: *International journal of hyperthermia* 26.1 (2010), pp. 26–33 (cit. on p. 71).

[136] L. A. Aguirre. *Introdução à identificação de sistemas–Técnicas lineares e não-lineares aplicadas a sistemas reais*. Editora UFMG, 2004 (cit. on p. 74).

[137] D. Haemmerich and J. G. Webster. “Automatic control of finite element models for temperature-controlled radiofrequency ablation”. In: *Biomedical engineering online* 4.1 (2005), pp. 1–8 (cit. on pp. 84, 114).

[138] J. Alba-Martínez, M. Trujillo, R. Blasco-Giménez, and E. Berjano. “Could it be advantageous to tune the temperature controller during radiofrequency ablation? A feasibility study using theoretical models”. In: *International Journal of Hyperthermia* 27.6 (2011), pp. 539–548 (cit. on pp. 84, 114).

[139] B. D. de Oliveira. “Estudo sobre o efeito de técnicas preventivas na incidência de lesões esofageanas após ablação do átrio esquerdo para tratamento de fibrilação atrial”. PhD thesis. Faculdade de Medicina, Universidade de São Paulo, 2015 (cit. on p. 90).

[140] S. B. de Cardiologia. “Arquivos Brasileiros de Cardiologia”. In: 106.4 (Apr. 2016), p. 35 (cit. on p. 90).

[141] C. Berkmortel, H. Avari, and E. Savory. “Computational Modelling Of Radiofrequency Cardiac Ablation To Study The Effect Of Cooling On Lesion Parameters”. In: *Proceedings of The Canadian Society for Mechanical Engineering International Congress 2018, CSME International Congress 2018: 27-30 May 2018; Toronto; Canada*. 2018 (cit. on pp. 90, 93).

[142] S. Salmasi, P. S. Loewen, R. Tandun, J. G. Andrade, and M. A. D. Vera. “Adherence to oral anticoagulants among patients with atrial fibrillation: a systematic review and meta-analysis of observational studies”. In: *BMJ Open* 10 (2020), e034778 (cit. on p. 90).

[143] E. Ewertowskaa, R. Quesadab, A. Radosevicc, A. Andaluzd, X. Molld, F. G. Arnas, E. Berjano, F. Burdío, and M. Trujillo. “A clinically oriented computer model for radiofrequency ablation of hepatictissue with internally cooled wet electrode”. In: *International Journal of Hyperthermia* 35 (2018), pp. 194–204 (cit. on pp. 90, 114).

[144] P. Calvert, G. Y. Lip, and D. Gupta. “Radiofrequency catheter ablation of atrial fibrillation: A review of techniques”. In: *Trends in Cardiovascular Medicine* (2022) (cit. on p. 90).

[145] A. González-Suárez, J. J.Pérez, R. M.Irastorza, A. D’Avila, and E. Berjano. “Computer modeling of radiofrequency cardiac ablation: 30 years of bioengineering research”. In: *Computer Methods and Programs in Biomedicine* 2014 (2022), p. 106546 (cit. on pp. 90, 91, 93–95).

[146] E. J. Berjano and F. Hornero. “What affects esophageal injury during radiofrequency ablation of the left atrium? An engineering study based on finite-element analysis”. In: *Physiological Measurement* 26 (2005), pp. 837–848 (cit. on pp. 90, 94).

[147] D. Haemmerich and J. G. Webster. “Automatic control of finite element models for temperature-controlled radiofrequency ablation”. In: *Biomedical engineering online* 4.1 (2005), pp. 1–8 (cit. on pp. 90, 97).

[148] M. Selmi, A. Bajahzar, and H. Belmabrouk. “Effects of target temperature on thermal damage during temperature-controlled MWA of liver tumor”. In: *Case Studies in Thermal Engineering* 31 (2022), p. 101821 (cit. on p. 90).

[149] F. de Sousa Faria, P. C. de Souza, G. P. Souza, J. F. da Justa, R. F. da Rocha, and S. de Siqueira Rodrigues Fleury Rosa. “Analysis of the Depth of Thermal Injuries Caused during the Cardiac Ablation Procedure with the Cooling of the Esophageal Wall”. In: *IEEE Latin America Transactions* 19 (2021), pp. 1121–1128 (cit. on p. 91).

[150] A. González-Suárez, E. Berjano, J. M. Guerra, and L. Gerardo-Giorda. “Computational Modeling of Open-Irrigated Electrodes for Radiofrequency Cardiac Ablation Including Blood Motion-Saline Flow Interaction”. In: *Plos One* 11 (2016), pp. 1–18 (cit. on p. 91).

[151] J. J. Pérez, A. D'Avila, A. Aryana, and E. Berjano. "Electrical and Thermal Effects of Esophageal Temperature Probes on Radiofrequency Catheter Ablation of Atrial Fibrillation: Results from a Computational Modeling Study". In: *Journal of Cardiovascular Electrophysiology* 26 (2015), pp. 556–564 (cit. on pp. 91, 96).

[152] A. González-Suárez, J. J. Pérez, and E. Berjano. "Should fluid dynamics be included in computer models of RF cardiac ablation by irrigated-tip electrodes?" In: *BioMedical Engineering OnLine* 17 (2018) (cit. on pp. 94, 95).

[153] A. González-Suárez and E. Berjano. "Comparative Analysis of Different Methods of Modeling the Thermal Effect of Circulating Blood Flow During RF Cardiac Ablation". In: *IEEE Transactions on Biomedical Engineering* 63 (2016), pp. 250–259 (cit. on pp. 94–96).

[154] A. Petras, M. Leoni, J. M. Guerra, J. Jansson, and L. Gerardo-Giorda. "A computational model of open-irrigated radiofrequency catheter ablation accounting for mechanical properties of the cardiac tissue". In: *International Journal for Numerical Methods in Biomedical Engineering* 35 (2019), e3232 (cit. on p. 94).

[155] S. Yan, X. Wu, and W. Wang. "A simulation study to compare the phase-shift angle radiofrequency ablation mode with bipolar and unipolar modes in creating linear lesions for atrial fibrillation ablation". In: *International Journal of Hyperthermia* 32.3 (2016), pp. 231–238 (cit. on p. 96).

[156] N. Soor, R. Morgan, M. Varela, and O. V. Aslanidi. "Towards patient-specific modelling of lesion formation during radiofrequency catheter ablation for atrial fibrillation". In: *2016 38th Annual International Conference of the IEEE Engineering in Medicine and Biology Society (EMBC)*. IEEE. 2016, pp. 489–492 (cit. on p. 96).

[157] M. Pasternak, E. Samset, J. D'hooge, and G. U. Haugen. "Temperature monitoring by channel data delays: Feasibility based on estimated delays magnitude for cardiac ablation". In: *Ultrasonics* 77 (2017), pp. 32–37 (cit. on p. 96).

[158] E. H. C. G. Teixeira et al. *Controles típicos de equipamentos e processos industriais*. Editora Blucher, 2010 (cit. on p. 98).

[159] Y. Nishikawa, N. Sannomiya, T. Ohta, and H. Tanaka. "A method for auto-tuning of PID control parameters". In: *Automatica* 20.3 (1984), pp. 321–332 (cit. on p. 98).

[160] S. Mirjalili, S. Saremi, S. M. Mirjalili, and L. d. S. Coelho. "Multi-objective grey wolf optimizer: a novel algorithm for multi-criterion optimization". In: *Expert systems with applications* 47 (2016), pp. 106–119 (cit. on p. 99).

[161] S. Mirjalili, S. M. Mirjalili, and A. Lewis. "Grey wolf optimizer". In: *Advances in engineering software* 69 (2014), pp. 46–61 (cit. on pp. 100, 181).

[162] S. Khodadoost, M. Saraee, S. Talatahari, and P. Sareh. “Optimal design of fractional-order proportional integral derivative controllers for structural vibration suppression”. In: *Scientific Reports* 14.1 (2024), p. 17207 (cit. on p. 100).

[163] S. Mirjalili. “How effective is the Grey Wolf optimizer in training multi-layer perceptrons”. In: *Applied intelligence* 43 (2015), pp. 150–161 (cit. on p. 100).

[164] S. Oladipo, Y. Sun, and Z. Wang. “Optimization of FOPID controller with hybrid Particle Swarm and Grey Wolf optimization for AVR System”. In: *2020 12th International Conference on Computational Intelligence and Communication Networks (CICN)*. IEEE. 2020, pp. 273–279 (cit. on p. 100).

[165] C. Muro, R. Escobedo, L. Spector, and R. Coppinger. “Wolf-pack (Canis lupus) hunting strategies emerge from simple rules in computational simulations”. In: *Behavioural processes* 88.3 (2011), pp. 192–197 (cit. on p. 100).

[166] E. T. Industrial. *Type K Thermocouples*. Last accessed 28 November 2023. 2023. URL: https://ecil.com.br/pirometria-2/termopares/termopar-tipo-k/ (cit. on pp. 106, 181).

[167] U. Halm, T. Gaspar, M. Zachäus, S. Sack, A. Arya, C. Piorkowski, I. Knigge, G. Hindricks, and D. Husser. “Thermal esophageal lesions after radiofrequency catheter ablation of left atrial arrhythmias”. In: *Official journal of the American College of Gastroenterology| ACG* 105.3 (2010), pp. 551–556 (cit. on p. 112).

[168] S. M. Singh, A. d’Avila, S. K. Doshi, W. R. Brugge, R. A. Bedford, T. Mela, J. N. Ruskin, and V. Y. Reddy. “Esophageal injury and temperature monitoring during atrial fibrillation ablation”. In: *Circulation: Arrhythmia and Electrophysiology* 1.3 (2008), pp. 162–168 (cit. on p. 114).

[169] M. Silva, A. A. d. Mattos, P. R. O. Fontes, F. L. Waechter, and L. Pereira-Lima. “Avaliação da ressecção hepática em pacientes cirróticos com carcinoma hepatocelular”. In: *Arquivos de Gastroenterologia* 45 (2008), pp. 99–105 (cit. on p. 160).

[170] J. Oliveira, M. Bergamini, M. Bonfim, and G. Leandro. “Identification of nonlinear system using evolutionary differential and grey wolf optimizer”. In: *24th ABCM International Congress of Mechanical Engineering, Curitiba, Brazil*. 2017, pp. 1–9 (cit. on p. 166).

Appendix

APPENDIX A – Resumo Estendido em Língua Portuguesa

Título: Deslocamento do Roll-Off e Proteção Esofágica na Ablação por Radiofrequência Hepática e Cardíaca: Controle da Impedância Tecidual e Temperatura Fundamentado no Controlador PID Bioinspirado
Autor: Rafael Mendes Faria
Orientador: Suelia de Siqueira Rodrigues Fleury Rosa
Programa de Pós-Graduação em Sistemas Mecatrônicos
Brasília, 07 de setembro de 2024

Palavras-chave: Fibrilação atrial. Carcinoma Hepatocelular. Otimizador lobo cinzento. Otimização por enxame de partículas.

Introdução

No campo da medicina termo-cirúrgica minimamente invasiva, a ablação por radiofrequência (RFA) destaca-se como uma técnica amplamente utilizada no tratamento de neoplasias hepáticas, renais, pulmonares, ósseas, cerebrais e arritmias cardíacas [1, 2]. O procedimento utiliza um eletrodo ativo incorporado em um cateter percutâneo, inserido na área afetada com auxílio de imagens de ultrassom ou tomografia computorizada [3]. A aplicação de uma corrente alternada de alta frequência (cerca de 500 kHz) cria uma lesão térmica que destrói o tecido maligno ao elevar a temperatura acima de 50°C, resultando na desnaturação de proteínas e comprometimento de enzimas mitocondriais [4, 5]. No entanto, a formação da lesão térmica é limitada à área alvo devido à alta densidade de corrente local, e a temperatura no tecido adjacente ao eletrodo tende a subir rapidamente até a vaporização dos fluidos intracelulares.

A vaporização dos fluidos do tecido marca o ponto crítico conhecido como roll-off [6]. Manter a temperatura máxima abaixo de 100°C durante a intervenção é fundamental para evitar a carbonização do tecido, picos súbitos de impedância e a formação de bolhas de vapor indesejáveis [7]. A continuidade do procedimento depende diretamente da impedância do tecido, que, ao aumentar bruscamente, pode levar à interrupção do processo [8]. Bolhas de vapor também apresentam riscos significativos, especialmente em procedimentos realizados na delicada parede miocárdica durante a RFA cardíaca, onde há maior risco de formação de coágulos sanguíneos [9].

Modelos computacionais tornaram-se ferramentas essenciais na pesquisa sobre RFA, permitindo simulações que integram condução elétrica, transferência de calor e dinâmica dos fluidos [8, 10]. O Método dos Elementos Finitos (FEM) é amplamente utilizado para modelar a propagação de energia térmica gerada pelo efeito Joule nos tecidos. No entanto, muitos estudos não replicam fielmente os algoritmos de controle de potência utilizados em dispositivos clínicos [11, 12]. A entrega de potência durante a RFA é guiada por três metodologias de controle: potência, impedância e temperatura [7], com a última sendo ajustada para manter a segurança e eficácia do procedimento.

O controle de impedância, por exemplo, é ativado quando a impedância entre o eletrodo ativo e o eletrodo dispersivo excede um limiar predefinido, levando à interrupção temporária do gerador de radiofrequência (RF) [2]. Para aprimorar o procedimento e evitar o roll-off, eletrodos irrigados com soluções salinas resfriadas são frequentemente utilizados, uma prática clínica consolidada [9, 13].

Este trabalho de doutorado tem como objetivo revisar sistematicamente a literatura, analisar, propor e simular estratégias de controle eficazes para a RFA aplicada a procedimentos cardíacos e hepáticos. A investigação abrange todos os aspectos envolvidos no processo de RFA, conforme ilustrado na Fig. 1, e utiliza ferramentas como COMSOL® Multiphysics e MATLAB® para modelagem e simulação. Técnicas de identificação de sistemas serão aplicadas para determinar o modelo matemático mais preciso e implementar algoritmos bioinspirados, como a Otimização por Enxame de Partículas (PSO) e o Otimizador de Lobo Cinzento (GWO), visando aprimorar o controle e mitigar o efeito de roll-off.

Este estudo é parte do projeto SOFIA® (Software of Intense Ablation), realizado na Universidade de Brasília (UnB), que resultou no desenvolvimento de um dispositivo de RFA com o objetivo de integrá-lo ao Sistema Único de Saúde (SUS) [14]. O projeto, em colaboração com o Ministério da Saúde, resultou em testes in vivo bem-sucedidos em porcos, avaliando o desempenho do equipamento em um contexto clínico real.

O equipamento SOFIA®, inicialmente concebido para o tratamento de carcinomas hepatocelulares, evoluiu para o sistema ARFACTA (Ablação por Radiofrequência com Ajuste de Frequência e Controle de Temperatura para Ablação Abrangente e Eficiente), que se tornou uma referência no tratamento de câncer hepático e arritmias cardíacas. Este sistema, com monitoramento e controle avançados, possibilita ablações precisas, centradas no bem-estar do paciente.

O objetivo principal desta pesquisa é a otimização do sistema de controle de temperatura e impedância no dispositivo ARFACTA, integrando algoritmos bioinspirados para refinar o processo de ajuste do controlador PID. A abordagem visa regular com precisão as variáveis relacionadas ao fenômeno de roll-off e à prevenção de fístulas esofágicas, abordando desafios críticos inerentes à RFA.

As principais contribuições deste estudo são ilustradas na Fig. 2 e detalhadas no Capítulo 3. A estrutura da tese inclui sete capítulos que apresentam uma visão abrangente da pesquisa. O Capítulo 1 estabelece o contexto e os objetivos, enquanto os Capítulos 4, 5 e 6 apresentam as descobertas, suportadas por artigos submetidos a periódicos científicos revisados por pares.

O Capítulo 4 explora técnicas de modelagem matemática e controle de temperatura e impedância na RFA, utilizando uma revisão sistemática da literatura baseada no protocolo PROSPERO [15], como mostrado na Fig. 3. O Capítulo 5 propõe um modelo matemático para a dinâmica da impedância tecidual durante a RFA hepática, utilizando técnicas de identificação de sistemas e controle dinâmico com um controlador PID otimizado pelo algoritmo PSO.

No Capítulo 6, uma abordagem in silico modela o ambiente da ablação cardíaca por radiofrequência (RFCA) com o uso de COMSOL® e MATLAB®, buscando prevenir complicações como fístulas esofágicas. As equações que governam os fenômenos elétricos, térmicos e dinâmicos dos fluidos foram resolvidas pelo método dos elementos finitos, gerando um conjunto de dados que foi integrado ao MATLAB® para a identificação do sistema e otimização do processo ablativo.

Finalmente, o Capítulo 7 resume os resultados e as realizações do estudo, enquanto os apêndices contêm esse resumo estendido, códigos de programação e tabelas de resultados, proporcionando suporte técnico adicional. As produções acadêmicas associadas a esta pesquisa são documentadas no Anexo A, contribuindo para uma contextualização mais ampla do trabalho no cenário acadêmico e científico.

Materiais e Métodos

Capítulo 4

Este estudo foi conduzido de acordo com as diretrizes PRISMA [16] [17] e registrado no PROSPERO [15]. A seleção dos estudos utilizou a plataforma Rayyan® (`https://www.rayyan.ai`), permitindo uma análise objetiva por meio da funcionalidade *'Blind ON'*. Para a análise bibliométrica dos estudos selecionados, foram utilizados o RStudio® com a biblioteca Bibliometrix e o VOSviewer® 1.6.8.

Os critérios de inclusão seguiram a abordagem PICO, contemplando estudos sobre ablação em fígado, coração ou glândula tireoide, além de simulações de modelos biológicos desses órgãos. Foram incluídos estudos que empregaram técnicas in vivo, ex vivo, e in silico, focando em parâmetros físicos e de controle de temperatura durante o procedimento de ablação.

Foram excluídos estudos que não abordaram o controle de temperatura, modelos com-

putacionais incompletos, ou que não estavam relacionados ao tema da revisão sistemática. Além disso, foram excluídas publicações como revisões, cartas, opiniões pessoais, capítulos de livros, e conferências.

Para a busca nas bases de dados principais, como Scopus, Science Direct, Cinahl Ebsco, IEEE Xplore, PubMed/MEDLINE e Web of Science, foram desenvolvidas estratégias específicas, com a remoção de duplicatas realizada na plataforma Rayyan®. A *string* de busca pode ser encontrada no apêndice B. O processo de seleção foi dividido em três fases, com revisores trabalhando em pares de forma anônima para garantir a imparcialidade.

Após a seleção dos estudos, os dados foram organizados em planilhas Excel®, e as análises de impacto e rede de pesquisa foram realizadas utilizando Mendeley®, RStudio® e VOSviewer®. Essas ferramentas permitiram uma compreensão visual da rede de pesquisa e das contribuições individuais dos pesquisadores.

A sumarização dos dados foi feita de forma meticulosa, seguindo as diretrizes do PRISMA 2009 e as orientações metodológicas do Ministério da Saúde do Brasil. Os autores identificaram o tipo de estudo, o órgão alvo do procedimento ablativo, as ferramentas computacionais utilizadas, e os equipamentos de ablação.

Por fim, a qualidade dos estudos foi avaliada usando a ferramenta GENERAL RoB, com 12 questões aplicadas por dois revisores independentes, resolvendo discrepâncias com a intervenção de um terceiro revisor.

Capítulo 5

A metodologia utilizada neste estudo, apresentada graficamente na Fig. 8, envolve uma série de etapas no processo de otimização. Foram utilizados tecidos de fígado suíno ex-vivo, adquiridos em mercados locais e mantidos entre 18°C e 22°C. Esses tecidos foram cortados em cubos de aproximadamente 6 cm de lado. O experimento empregou o equipamento de RFA SOFIA®, desenvolvido pelo Laboratório de Engenharia Biomédica da UnB, com patente requerida (BR 10 2017 002683 3) [14], utilizando o eletrodo LeVeen® Standard 4.0 da Boston Scientific [18, 19]. Todos os componentes dos experimentos ex-vivo estão ilustrados na Fig. 10.

O experimento foi conduzido com uma potência inicial de aproximadamente 34 W aplicada pelo eletrodo monopolar nas amostras de fígado, e o critério de parada foi o primeiro roll-off detectado pelo equipamento SOFIA®. A temperatura foi medida utilizando um sensor termopar a 1,25 cm do centro do eletrodo (Fig. 10 - C). A uniformidade dos dados foi garantida através da reamostragem dos dados exportados para o MATLAB® R2021a, onde o intervalo de tempo Δt foi ajustado para 1 medição por segundo.

Para a identificação do sistema, foram gerados modelos de função de transferência e de espaço de estados de 2^{nd}, 3^{rd}, 4^{th}, 5^{th} e 6^{th} ordem, utilizando a Toolbox de Identificação

de Sistemas no MATLAB®, e aplicando o método de minimização do erro de previsão (PEM). Além disso, foi utilizado o modelo ARX para obter uma curva mais precisa que se ajustasse aos dados experimentais (Eq. 5.1) [20].

A validação dos modelos foi realizada com base em dados experimentais, divididos em conjuntos para a identificação e validação do modelo. O índice de ajuste (FIT) foi utilizado para avaliar a qualidade do ajuste entre os dados estimados e de referência, sendo calculado através do erro quadrático médio normalizado (NRMSE) (Eq. 5.5).

Para prevenir o roll-off, propôs-se a inclusão de um controlador PID no SI, ajustado pelo algoritmo PSO, o qual otimizou os ganhos K_p, K_i, e K_d. O algoritmo PSO, inspirado no comportamento social de enxames e cardumes, foi empregado para garantir a precisão do controle de impedância durante o procedimento, minimizando o overshoot e o tempo de acomodação [21]. A aplicação de controladores PID é essencial em processos que exigem alta precisão, como controle de movimento e tratamento térmico [22, 23], e a utilização do PSO proporcionou uma alternativa eficaz ao método de Ziegler-Nichols, que tende a gerar overshoots elevados [24].

Capítulo 6

Modelos tridimensionais foram desenvolvidos para simular procedimentos de RFCA em tecido cardíaco, visando melhorar a eficácia do tratamento e evitar cenários de fístula esofágica. Utilizando o COMSOL® Multiphysics, técnicas de Identificação de Sistemas (SI) foram aplicadas para extrair funções de transferência que orientam o projeto de um controlador para otimizar o procedimento de RFCA.

Um modelo computacional tridimensional foi proposto, representado por um fragmento cúbico de 15 mm de largura, 15 mm de espessura e 22,5 mm de altura em relação ao plano de simetria YZ, considerando o volume real, conforme representado na Fig 19. Essa estrutura engloba o miocárdio (com espessura de 2,5 mm), uma camada de tecido adiposo (com espessura de 2 mm), a parede esofágica (com espessura de 3 mm), e representa o volume de sangue (com espessura de 15 mm).

O eletrodo de ablação utilizado na simulação é não irrigado, com um raio de 1,165 mm, posicionado perpendicularmente à superfície. Para simular a força de pressão exercida sobre o tecido cardíaco durante a RFCA, o eletrodo é inserido a uma profundidade de 0,5 mm e posicionado a 90º em relação ao miocárdio, desconsiderando variações de movimento e posição [25, 26]. A representação do eletrodo inclui uma sonda para monitorar variações de temperatura, um parâmetro fundamental na modelagem e controle deste estudo. O ponto P_c, ilustrado na Fig 20, é o local de medição da temperatura.

O modelo proposto foi implementado e simulado utilizando o software COMSOL® Multiphysics. No desenvolvimento do sistema, três aspectos físicos distintos foram integrados:

elétrico, térmico e dinâmica dos fluidos. Módulos específicos dentro do COMSOL® foram empregados para abordar cada um desses aspectos, incluindo o módulo *Heat Transfer in Solids and Fluids*, o módulo *Laminar Flow* e o módulo *Electrical Currents*. Além disso, módulos de acoplamento multifísico foram utilizados para conectar esses estudos, como o *Nonisothermal Flow*, que integra *Heat Transfer in Solids and Fluids* com *Laminar Flow*, e *Electromagnetic Heating*, que acopla *Heat Transfer in Solids and Fluids* com *Electrical Currents*.

Vale destacar que, devido às suas características únicas, o sangue exibe propriedades elétricas, térmicas e de fluido, sendo o único fluido considerado na simulação. A solução matemática para integrar os sistemas elétrico, térmico e de fluidos também foi resolvida dentro do software COMSOL®.

Propriedades dos materiais foram definidas conforme a literatura (Tabela 8), e as condições de contorno incluíram uma voltagem inicial de 15 V por 30 s, temperatura corporal constante de 37°C, e fluxo sanguíneo laminar a 0,085 m/s [27]. A Equação de Laplace (6.1) foi usada para resolver o problema elétrico, e a Equação de Fourier (6.2) para o problema térmico, ambos resolvidos pelo método dos elementos finitos.

Para prevenir fístulas esofágicas e otimizar a execução de procedimentos de ablação cardíaca, propomos a integração de um controlador PID no SI. O PID é uma técnica de controle que combina ações proporcionais, integrais e derivativas para melhorar a resposta dinâmica de um sistema. Na configuração do nosso protocolo de controle de temperatura, implementamos um sistema de controle em malha fechada com feedback negativo, usando um sistema de transdução de temperatura para voltagem, empregando um termopar através de sua respectiva função de transferência para medir o erro. O erro é definido como a diferença entre a temperatura atual do tecido, obtida em graus Celsius, e a temperatura desejada (setpoint). O objetivo do controlador é tornar o procedimento mais gradual, com regulação de calor controlada, pois mudanças bruscas podem resultar em danos irreversíveis.

Para o ajuste do dos parâmetros do controlador PID, foi empregado o Algoritmo GWO. Proposto por Mirjalili et al. [28], o algoritmo GWO é inspirado no comportamento de caça social dos lobos cinzentos (*Canis lupus*). Este algoritmo de otimização bioinspirado se distingue por sua simulação da hierarquia social e estratégias de caça cooperativa dos lobos, que são organizados em uma estrutura de liderança composta por quatro grupos principais: alfa, beta, delta e ômega. No contexto do GWO, essas posições hierárquicas são usadas para orientar a busca por soluções ótimas dentro do espaço de busca [29].

Resultados e Discussões

Capítulo 4

No estudo bibliométrico realizado em 24 de janeiro de 2023, utilizando o software VOSviewer versão 1.6.17, foi realizada uma busca nas bases de dados Pubmed, IEEE, Cinalh/EBSCO, Science Direct e Web of Science, utilizando os termos MeSH "Mathematical Models", "Catheter Ablation", "Radiofrequency Ablation", "Ablation Techniques" e "Temperature OR Computer Simulation". Um total de 1078 artigos foram encontrados, sendo excluídos 260 duplicados. A Fig. 4 ilustra as palavras-chave mais frequentes nos artigos, categorizadas em três grupos distintos, com as linhas conectando os termos representando as relações competitivas entre eles nos artigos analisados. Fica evidente que os estudos localizados têm relevância limitada para o foco temático do presente trabalho. O limiar de coocorrência para esses termos foi estabelecido em um mínimo de 30 ocorrências.

Esta revisão sistemática teve como objetivo investigar os avanços no campo do controle de temperatura em simulações computacionais para procedimentos de ablação por radiofrequência (RFA). Um número significativo de estudos foi derivado de várias bases de dados: Pubmed (n = 958), Scopus (n = 581), Embase (n = 68), Science Direct (n = 21), Web of Science (n = 181), CINAHL Ebsco (n = 125) e IEEE (n = 333). Após aplicar um filtro para considerar artigos dos últimos 10 anos, um total de 1088 trabalhos foram recuperados. Os títulos e resumos desses artigos foram revisados independentemente em duplicata e, em casos de discordância, um terceiro autor foi consultado. Após a triagem inicial, 82 artigos foram selecionados para leitura completa, realizada também de forma independente e em duplicata. Aplicando os critérios de elegibilidade predefinidos, 29 artigos foram selecionados para inclusão nesta revisão, conforme ilustrado no fluxograma PRISMA apresentado na Fig. 5. Uma tabela abrangente detalhando os resultados dos estudos selecionados para esta revisão sistemática é fornecida no Apêndice C (estudos in silico) e no Apêndice D (estudos ex vivo).

A execução de estudos computacionais com o objetivo de otimizar e compreender os processos de RFA é de suma importância para melhorar a eficácia e a segurança dos procedimentos clínicos. Ao analisar os artigos selecionados nesta revisão sistemática, foi adquirida uma visão abrangente das abordagens empregadas, dos resultados obtidos e das principais conclusões relacionadas às simulações de RFA. Cada artigo contribuiu de maneira valiosa para a compreensão dos efeitos da variação de parâmetros nos procedimentos de ablação, refletindo os avanços no estado da arte focados no controle de temperatura e impedância em RFA.

Capítulo 5

O estudo apresentou uma aplicação do PSO para ajuste dos parâmetros de um controlador PID, visando melhorar o controle do roll-off durante a ablação por radiofrequência (RFA) de tumores hepáticos. Foram realizados experimentos ex-vivo, resultando em uma função de transferência de 9ª ordem (ver 5.16). Os resultados da simulação utilizando o controlador PID otimizado pelo PSO mostraram um desempenho excelente: um sobressinal de 0,605%, tempo de subida de 0,314 segundos e tempo de acomodação de 2,87 segundos para uma entrada de degrau unitário (ver Tabela 3). Análises estatísticas dos 19 experimentos realizados revelaram ganhos médios de $K_p = 5{,}86$, $K_i = 9{,}89$ e $K_d = 0{,}57$. A análise de variância (ver Tabela 6) indicou significância estatística com p-valor inferior a 0,05. Os resultados alcançados demonstram que a utilização do algoritmo PSO para ajuste dos parâmetros do controlador PID é uma estratégia eficaz para controlar o roll-off durante o procedimento de RFA. A baixa taxa de sobressinal e o rápido tempo de acomodação são indicativos de um sistema bem ajustado, capaz de realizar ablações mais precisas e eficientes. A significância estatística dos resultados reforça a confiabilidade da abordagem. A aplicação desta técnica pode ter implicações clínicas significativas, especialmente na redução das taxas de recorrência tumoral e danos colaterais. No entanto, para a implementação clínica em larga escala, seria interessante realizar estudos adicionais que considerem a variabilidade dos tecidos humanos e possíveis adaptações do modelo.

Capítulo 6

Neste estudo, foi desenvolvido um modelo tridimensional para controlar a temperatura durante procedimentos de RFCA, utilizando um controlador PID ajustado por GWO. O objetivo principal foi evitar o superaquecimento do esôfago e, consequentemente, a formação de fístulas esofágicas. Os resultados demonstraram que o controlador GWO-PID foi eficaz em manter a temperatura do esôfago abaixo de níveis críticos. Os resultados da sintonia do controlador apresentam índices de desempenho promissores para uma função de transferência de 3 ordem (ver 6.19) realimentada com a função de transferência de 1 ordem (ver 6.20) proveniente do termopar tipo K. Com $K_p = 0.0474$, $K_i = 0.05$ e $K_d = 0.000221$, o sistema apresentou um sobresinal de 1,48%, tempo de subida de 16,1 s e tempo de acomodação de 21,1 s (ver Tabela 12). Durante simulações no ambiente do COMSOL® com o controlador PID implementado e ajustado com os parâmetros devolvidos pelo GWO, a temperatura esofágica máxima atingiu 38,63°C. No instante (10,4 s) em que a temperatura máxima foi atingida pelo eletrodo, a temperatura no esôfago foi de 37,51°C. Comparado ao sistema de malha aberto, a aplicação do controlador otimizado reduziu significativamente o sobresinal e proporcionou um crescimento mais suave da temperatura, protegendo melhor os tecidos adjacentes ao miocárdio durante o procedimento. A capacidade do controlador de manter a temperatura esofágica em níveis seguros pode reduzir a incidência de complicações

graves, como a formação de fístulas, que são eventos adversos críticos em ablações cardíacas. Além disso, o controle preciso da temperatura pode contribuir para a eficácia do tratamento, assegurando que as lesões desejadas no tecido cardíaco sejam criadas sem causar danos excessivos. Em comparação com abordagens tradicionais, o uso de um controlador fechado, como o proposto neste estudo, oferece uma regulação mais robusta da temperatura, o que é essencial para procedimentos clínicos mais seguros e eficazes. Contudo, estudos adicionais são necessários para validar esses resultados em modelos experimentais e, eventualmente, em ensaios clínicos.

Conclusão

Esta tese aborda, de forma integrada, os avanços no campo da ablação por radiofrequência (RFA), com foco na otimização de procedimentos através de modelagem computacional, controle de impedância tecidual e estratégias de controle de temperatura. Os três estudos que compõem esta pesquisa contribuem significativamente para o entendimento e aprimoramento das técnicas de RFA, tanto em aplicações oncológicas quanto cardíacas.

O Estudo 1 (Capítulo 4), uma revisão sistemática, oferece uma visão abrangente dos diferentes aspectos relacionados à RFA, destacando a relevância da integração entre abordagens experimentais e modelagem computacional. A análise dos parâmetros elétricos, térmicos e fluidodinâmicos, bem como a avaliação dos riscos de viés, reforça a importância de metodologias robustas e a necessidade de validação dos modelos computacionais em experimentos in vivo. Os resultados sugerem que a combinação de estudos experimentais com simulações computacionais pode promover avanços significativos na personalização de protocolos e estratégias de tratamento.

No Estudo 2 (Capítulo 5), foi desenvolvido e testado um controlador PID sintonizado por PSO para regular a impedância tecidual durante procedimentos de ablação hepática ex vivo. Este trabalho destacou a importância do controle preciso da impedância como um parâmetro crucial para a efetividade da RFA, demonstrando a robustez do controlador em manter a impedância dentro dos níveis pré-definidos e, assim, evitar o fenômedo roll off. O estudo mostrou que essa abordagem pode ser um passo importante para reduzir complicações e melhorar os resultados clínicos em ablações hepáticas, sugerindo que futuras pesquisas explorem implementações em hardware e validações em modelos in vivo.

Por fim, o Estudo 3 (Capítulo 6) investigou, por meio de simulações tridimensionais no COMSOL®, a distribuição de temperatura durante RFCA, utilizando um controlador PID sintonizado pelo algoritmo GWO. Os resultados indicaram que, embora o controlador tenha sido eficaz em elevar a temperatura do miocárdio ao nível desejado, o controle da temperatura em tecidos adjacentes, como o esôfago, é essencial para evitar complicações graves. A modelagem proposta mostrou potencial para aprimorar a segurança dos procedimentos de

RFCA, mitigando riscos como a formação de fístulas esofágicas.

Em conjunto, esses estudos evidenciam a importância de abordagens multidisciplinares que combinam modelagem computacional, controle de parâmetros críticos e validação experimental. A tese contribui para o avanço do conhecimento no campo da ablação por radiofrequência, propondo soluções inovadoras para melhorar a eficácia e a segurança desses procedimentos. O contínuo desenvolvimento e refinamento dessas técnicas, aliados à colaboração entre áreas da medicina, engenharia e ciências biomédicas, são fundamentais para a evolução das terapias de ablação e o aprimoramento dos cuidados aos pacientes.

Referências

[1] S. Singh and R. Repaka. “Temperature-controlled radiofrequency ablation of different tissues using two-compartment models”. In: *International Journal of Hyperthermia* 33.2 (2017), pp. 122–134 (cit. on p. 136).

[2] M. Trujillo, J. Bon, M. Jose Rivera, F. Burdío, and E. Berjano. “Computer modelling of an impedance-controlled pulsing protocol for RF tumour ablation with a cooled electrode”. In: *International Journal of Hyperthermia* 32.8 (2016), pp. 931–939 (cit. on pp. 136, 137).

[3] G. S. Gazelle, S. N. Goldberg, L. Solbiati, and T. Livraghi. “Tumor ablation with radio-frequency energy”. In: *Radiology* 217.3 (2000), pp. 633–646 (cit. on p. 136).

[4] M. Trujillo, J. Alba, and E. Berjano. “Relationship between roll-off occurrence and spatial distribution of dehydrated tissue during RF ablation with cooled electrodes”. In: *International Journal of Hyperthermia* 28.1 (2012), pp. 62–68 (cit. on p. 136).

[5] M. W. Miller and M. C. Ziskin. “Biological consequences of hyperthermia”. In: *Ultrasound in medicine & biology* 15.8 (1989), pp. 707–722 (cit. on p. 136).

[6] N. Yamazaki, Y. Kobayashi, H. Kikuchi, Y. Isobe, X. Lu, T. Miyashita, and M. G. Fujie. “Modeling of lung’s electrical impedance using fractional calculus for analysis of heat generation during RF-ablation”. In: *2014 36th Annual International Conference of the IEEE Engineering in Medicine and Biology Society*. IEEE. 2014, pp. 5323–5328 (cit. on p. 136).

[7] S. Singh and R. Repaka. “Numerical study to establish relationship between coagulation volume and target tip temperature during temperature-controlled radiofrequency ablation”. In: *Electromagnetic biology and medicine* 37.1 (2018), pp. 13–22 (cit. on pp. 136, 137).

[8] A. González-Suárez, E. Berjano, J. M. Guerra, and L. Gerardo-Giorda. “Computational modeling of open-irrigated electrodes for radiofrequency cardiac ablation including blood motion-saline flow interaction”. In: *PloS one* 11.3 (2016), e0150356 (cit. on pp. 136, 137).

[9] A. González-Suárez, J. J. Pérez, and E. Berjano. “Should fluid dynamics be included in computer models of RF cardiac ablation by irrigated-tip electrodes?” In: *Biomedical engineering online* 17.1 (2018), pp. 1–14 (cit. on pp. 136, 137).

[10] A. González-Suárez, J. J. Pérez, and E. Berjano. “Computer modeling of irrigated-tip electrodes during RF cardiac ablation: Comparative analysis between including and excluding the problem of fluid dynamics”. In: *2017 Computing in Cardiology (CinC)*. IEEE. 2017, pp. 1–4 (cit. on p. 137).

[11] D. Haemmerich. “Mathematical modeling of impedance controlled radiofrequency tumor ablation and ex-vivo validation”. In: *2010 Annual International Conference of the IEEE Engineering in Medicine and Biology*. IEEE. 2010, pp. 1605–1608 (cit. on p. 137).

[12] C.-C. R. Chen, M. I. Miga, and R. L. Galloway. “Optimizing electrode placement using finite-element models in radiofrequency ablation treatment planning”. In: *IEEE transactions on biomedical engineering* 56.2 (2008), pp. 237–245 (cit. on p. 137).

[13] K. Yokoyama, H. Nakagawa, F. H. Wittkampf, J. V. Pitha, R. Lazzara, and W. M. Jackman. “Comparison of electrode cooling between internal and open irrigation in radiofrequency ablation lesion depth and incidence of thrombus and steam pop”. In: *Circulation* 113.1 (2006), pp. 11–19 (cit. on p. 137).

[14] U. of Brasília Foundation and T. D. Center. “Radiofrequency Hepatic Ablation System Containing Equipment with Electronic Controland Electrode in Umbrella Format Made in Alloy with Memory of Formand Its Method of Processing and Analysis of Medical Images”. In: *Patent BR 10 2017 002 683 3* (2017). URL: https://gru.inpi.gov.br (cit. on pp. 137, 139).

[15] N. I. for Health and C. Research. *PROSPERO - International prospective register of systematic reviews*. Centre for Reviews and Dissemination, University of York. Disponível em: https://https://www.crd.york.ac.uk/prospero/ – acesso em 09 fev. 2022. 2022 (cit. on p. 138).

[16] D. Moher, A. Liberati, J. Tetzlaff, D. G. Altman, and T. P. Group. “Preferred Reporting Items for Systematic Reviews and Meta-Analyses: The PRISMA Statement”. In: *PLOS Medicine* 6.7 (July 2009), pp. 1–6. DOI: 10.1371/journal.pmed.1000097. URL: https://doi.org/10.1371/journal.pmed.1000097 (cit. on p. 138).

[17] B. Hutton, G. Salanti, D. M. Caldwell, A. Chaimani, C. H. Schmid, C. Cameron, J. P. Ioannidis, S. Straus, K. Thorlund, J. P. Jansen, et al. “The PRISMA extension statement for reporting of systematic reviews incorporating network meta-analyses of health care interventions: checklist and explanations”. In: *Annals of internal medicine* 162.11 (2015), pp. 777–784 (cit. on p. 138).

[18] R. D. da Fonseca Campos. “Modelagem Bond Graph e Controlador Discreto de um Equipamento Médico Assistencial de Ablação por Radiofrequência”. PhD thesis. Brasília: Universidade de Brasília, Mar. 2022 (cit. on p. 139).

[19] M. P. Marques. “Desenvolvimento de eletrodo expansível de níquel-titânio para ablação por radiofrequência”. MA thesis. Brasília: Universidade de Brasília, Sept. 2016 (cit. on p. 139).

[20] S. A. Billings. *Nonlinear system identification: NARMAX methods in the time, frequency, and spatio-temporal domains*. John Wiley & Sons, 2013 (cit. on p. 140).

[21] S. Ribeiro and L. G. Lopes. “PSO Performance for Solving Nonlinear Systems of Equations: Comparing Segmentation of Search Space and Increase of Number of Particles”. In: *International Conference on Computational Science and Its Applications*. Springer. 2022, pp. 261–272 (cit. on p. 140).

[22] Y. Shi. “Particle swarm optimization”. In: *IEEE connections* 2.1 (2004), pp. 8–13 (cit. on p. 140).

[23] D. Wang, D. Tan, and L. Liu. “Particle swarm optimization algorithm: an overview”. In: *Soft computing* 22 (2018), pp. 387–408 (cit. on p. 140).

[24] Z.-L. Gaing. “A particle swarm optimization approach for optimum design of PID controller in AVR system”. In: *IEEE transactions on energy conversion* 19.2 (2004), pp. 384–391 (cit. on p. 140).

[25] A. González-Suárez, E. Berjano, J. M. Guerra, and L. Gerardo-Giorda. “Computational Modeling of Open-Irrigated Electrodes for Radiofrequency Cardiac Ablation Including Blood Motion-Saline Flow Interaction”. In: *Plos One* 11 (2016), pp. 1–18 (cit. on p. 140).

[26] J. J. Pérez, A. D’Avila, A. Aryana, and E. Berjano. “Electrical and Thermal Effects of Esophageal Temperature Probes on Radiofrequency Catheter Ablation of Atrial Fibrillation: Results from a Computational Modeling Study”. In: *Journal of Cardiovascular Electrophysiology* 26 (2015), pp. 556–564 (cit. on p. 140).

[27] A. González-Suárez and E. Berjano. “Comparative Analysis of Different Methods of Modeling the Thermal Effect of Circulating Blood Flow During RF Cardiac Ablation”. In: *IEEE Transactions on Biomedical Engineering* 63 (2016), pp. 250–259 (cit. on p. 141).

[28] S. Mirjalili, S. M. Mirjalili, and A. Lewis. “Grey wolf optimizer”. In: *Advances in engineering software* 69 (2014), pp. 46–61 (cit. on p. 141).

[29] S. Khodadoost, M. Saraee, S. Talatahari, and P. Sareh. “Optimal design of fractional-order proportional integral derivative controllers for structural vibration suppression”. In: *Scientific Reports* 14.1 (2024), p. 17207 (cit. on p. 141).

APPENDIX B – Systematic Review - search string

("Experimental Model*") OR ("Mathematical Model*") OR ("Model*" AND "(Theoretical)") OR ("Model*" AND "Experimental") OR ("Model*" AND "Mathematical") OR ("Model*" AND "Theoretic*") OR ("Stud*" AND "Theoretical") OR ("Theoretical Model*") OR ("Theoretical Studies") OR ("Theoretical Study") OR ("Theoretical Studies Fibrillations" AND "Paroxysmal Atrial") OR ("Paroxysmal Atrial Fibrillations") AND ("Catheter Ablation") OR ("Ablation" AND "Catheter") OR ("Ablation" AND "Electric* Catheter") OR ("Ablation" AND "Percutaneous Catheter") OR ("Ablation" AND "Radiofrequency Catheter") OR ("Ablation" AND "Transvenous Catheter") OR ("Ablation" AND "Transvenous Electric*") OR ("Ablation" AND "Transvenous Electrical") OR ("Catheter Ablation" AND "Electric*") OR ("Catheter Ablation" AND "Percutaneous") OR ("Catheter Ablation" AND "Radiofrequency") OR ("Catheter Ablation" AND "Transvenous") OR ("Electric* Ablation" AND "Transvenous") OR ("Electric* Catheter Ablation") OR ("Percutaneous Catheter Ablation") OR ("Radiofrequency Catheter Ablation") OR ("Transvenous Catheter Ablation") OR ("Transvenous Electric* Ablation") OR ("Radiofrequency Ablation") OR ("Ablation" AND "Radio* Frequency") OR ("Radio* Frequency Ablation") OR ("RFA (radiofrequency ablation)") OR ("RFA therapy") OR ("Ablation Technique*") OR ("Technique*" AND "Ablation") OR ("Ablation therapy") OR ("ablation method*") OR ("ablation procedure*") OR ("ablation surgery") OR ("ablation treatmen") OR ("ablative method*") OR ("ablative procedure*") OR ("ablative surgery") OR ("ablative technique*") OR ("ablative therapy") OR ("ablative treatment") AND ("temperaturare*") OR ("differential temperature") OR ("Computer simulation*") OR ("Computer Model*") OR ("Computerized Model*") OR ("In Silico*") OR ("Model*" AND "computer*") OR ("Silico*" AND "In") ("Simulation*" AND "Computer") OR ("In silico Simulation") OR ("Simulation" AND "In sílico") OR ("In silico Model*") OR ("Model" AND "In sílico") OR ("Computational Model*") OR ("Model*" AND "Computational") OR ("computational simulation") OR ("computer-based simulation")

APPENDIX C – Systematic Review table results - In silico studies

Study	**In silico Assays**	**Intervention**		**Simulations**		**Outcomes**	
Author, Year/ Country	*Software*	*Objective*	*Methodology*	*Variable*	*Types of Analysis*	*Results*	*Limitations*
[41]	Minitab®, COMSOL® Multiphysics	Quantifying the effect of the tumor and the properties of the surrounding healthy tissue using the Taguchi experimental design.	Solution via FEM of a Simplified 2D Tumor Model in Occlusion with a PID Controller Constrained to a Temperature of 100°C.	Electrical conductivity, thermal conductivity, and blood perfusion rate.	Analyzing the relationship between the ablation volume and the variation of parameter values.	The variation in electrical and thermal properties of the tumor and healthy tissue affects ablation volume differently. Decreased blood perfusion increases the ablation volume. The studied variables do not exhibit a linear behavior concerning tumor size.	Simulations conducted employing simplistic geometries and a streamlined model.
[16]	MATLAB®, COMSOL® Multiphysics	Evaluate the capability of a simplified method to predict temperature distribution in blood/tissue and lesion dimensions in comparison with a validated comprehensive method.	Simulations were conducted using FEM along with the implementation of a PI controller on a small section of cardiac tissue through an irrigated open electrode, employing two methods: an approximate and a precise approach.	Density, enthalpy, time, electrical and thermal conductivity, temperature, and sources of metabolic heat and the active electrode part.	Simulation of two methods applied to a portion of cardiac tissue at 37°C with an irrigated open electrode at 22°C, utilizing a power of 10 W for 60 seconds.	The approximate method encounters challenges in accurately predicting the maximum blood temperature and thermal lesion size, exhibiting an overestimation of 5 mm compared to the precisely validated experimental method. Nonetheless, it demonstrates significant outcomes concerning lesion depth and tissue temperature.	The study does not present its limitations.

Continuue

Author, Year/ Country	*Software*	*Objective*	*Methodology*	*Variable*	*Types of Analysis*	*Results*	*Limitations*
[42]	Pro/ ENGINEER® COMSOL®	Propose a prototype of a multi-lumen open electrode catheter equipped with a helical antenna for temperature monitoring through microwave radiometry.	Ablative tests used agar gel phantoms filled with saline to mimic blood. Computational simulations via FEM. Experiments and simulations executed with the electrode oriented parallel and perpendicular to block surfaces.	Voltage, impedance, current density, electrical and thermal conductivity, electric field, dynamic viscosity, velocity, density, pressure, gravitational force and acceleration, temperature, heat and time.	Voltage, impedance, current density, electrical and thermal conductivity, electric field, dynamic viscosity, velocity, density, pressure, force, gravitational acceleration, temperature, heat, and time.	Experiments showed impedances of 157 and 136 ohms (parallel and perpendicular). Computational model had 167 and 173 ohms. Temperature varied (3.2 to 8.4°C), lesion width (0.2 to 1.1 mm) at depths (0 to 0.8 mm, perpendicular orientation) and (3.6 to 4.9°C), (0 to 0.1 mm), and (0.4 to 0.9 mm, parallel arrangement).	Agar tests had a microwave antenna, unused in experiments or the model. No analysis of electrode depth or tissue heterogeneity, phase changes, or consistent power implementation.
[43]	COMSOL® Multiphysics	The study aims to ascertain the impact of electrothermal parameters on liver tumor ablation via RFA. The goal is to analyze ablation temperature and lesion volume by assessing parameter sensitivity.	FEM-based RFA simulation model created in COMSOL® software. Analysis involved thermal and electrical parameters using RSM. CCD experimental design used to study parameter impact on ablation volume, considering electrode symmetry for computational efficiency.	Specific heat capacity, thermal conductivity, electrical conductivity, density, dielectric constant.	Thermal and electrical parameters.	The study examined parameter effects on temperature during RFA. Parameters R and Sigma had notable impact at distant points, whereas Cp and rho exhibited minor effects. Parameter sensitivities varied over time.	There are still limitations, such as not accounting for the cooling effect of blood vessels during RFA and the need for further studies with models that consider the presence of blood vessels.

Continuue

Author, Year/ Country	*Software*	*Objective*	*Methodology*	*Variable*	*Types of Analysis*	*Results*	*Limitations*
[15]	COMSOL® Multiphysics	This work reviews models in radiofrequency catheter ablation, highlighting their significance in understanding RFCA's physics and clinical implications. It discusses model types, validation, and outlines limitations and future research directions.	Study introduces 3D model for RF cardiac ablation simulation, including tissue, electrode, and blood. Model derived from clinical data, tested for resolution. Different saline irrigation methods considered. Model enables RF ablation simulation and impact assessment.	Maximum depth (D), maximum width (MW), depth at maximum width (DW), superficial width (SW), maximum temperature values reached in tissue and blood.	Thermal and electrical parameters.	The reduced model inadequately replicated the shape and width of thermal lesions created with irrigated-tip electrodes. Furthermore, it inaccurately predicted maximum width and lesion volume at low blood flow rates. It also overestimated blood temperature near the electrode-tissue interface.	Study limitations include: reduced model not reproducing lesion shape, overestimated width and volume under low blood flow, temperature errors near electrode-tissue interface. Caution needed when applying conclusions in clinical settings.
[44]	COMSOL® Multiphysics	Simulated hepatic RFA to analyze vessel wall heat transfer, blood's directional effect, and vessel impact on lesions. Results guide accurate multi-scale bio-heat model for predicting outcomes near liver blood vessels.	Study employed simulations, experiments to explore blood vessel impact on RF ablation. Assessed geometry, developed accurate multi-scale model. Metrics measured vessel effect, statistical analysis applied.	Density, specific heat capacity, thermal conductivity, and electrical conductivity.	Thermal and electrical parameters.	Study investigated effects of parameters like RF needle-vessel distance, vessel radius, active needle length on thermal lesions. Distance impacted lesion direction, blood coagulation affected size, especially in smaller vessels. Enhances comprehension of blood flow's lesion impact.	Study limitations: 1) Results specific to used RF needle; 2) Single vessel consideration may not capture multi-vessel interaction complexity; 3) Weak coupling of blood coagulation, flow, and energy models; 4) Vessel classification only based on radius; 5) Experimental validation needed for theoretical conclusions. Highlight the need for future research addressing these issues and enhancing RF ablation treatment understanding.

Continuue

Author, Year/ Country	*Software*	*Objective*	*Methodology*	*Variable*	*Types of Analysis*	*Results*	*Limitations*
[29]	COMSOL® Multiphysics	Study aims to investigate lesion contour, temperature field variations in atrial RFA using FEM.	Study used thermal dose to define tissue boundaries, compared 50°C isotherm results. Employed hyperbolic equation with relaxation time for temperature calculation, compared with Pennes' equation.	Lesion delineation via CEM43°C and 50°C isotherm, temperature distribution using hyperbolic and Pennes' equation, lesion size at different times/voltages, relaxation time's effect on max temperature. Insights into atrial RF ablation parameters and equations.	Thermal and electrical parameters.	Study compared methods for atrial RF ablation lesion delineation. CEM43°C and 50°C isotherm used, CEM43°C slightly smaller. Hyperbolic equation yielded higher temperatures than Pennes'. CEM43°C suited short ablations, hyperbolic equation reflected actual distribution better.	Use of simplified 2D model, reliance on empirical parameters, lack of experimental validation, simplified boundary conditions, and limitations of calculation methods. These factors may impact result accuracy and representativeness regarding actual cardiac ablation conditions.
[50]	COMSOL® Multiphysics	Externally irrigated RF electrodes widely used for tumor ablation lack a mathematical model for their electrical and thermal performance, including the role of the surrounding saline layer.	Numerical model developed for RF ablation prediction. Experiments validated it, showing good alignment. Considers tissue properties and saline. Offers potential for RF parameter optimization.	Study focused on RF electrode external irrigation, studying effects of surrounding saline layer. Analyzed variables: electrode geometry, saline layer, flow rate, and heating temp, aiming to understand impact on thermal lesion formation.	Thermal and electrical parameters.	A numerical model was created to predict impedance and thermal lesion size in RF ablation. Experimental and numerical outcomes aligned reasonably well. The model incorporated tissue properties and saline presence, yielding consistent lesion size and shape. This model holds potential for optimizing RF ablation parameters.	The study has limitations: ex-vivo bovine may not reflect in vivo, the numerical model is simplified and requires clinical validation. Simulated thermal lesions were larger than observed. Further research is needed to enhance and validate the model in real clinical scenarios.

Continuue

Author, Year/ Country	*Software*	*Objective*	*Methodology*	*Variable*	*Types of Analysis*	*Results*	*Limitations*
[45]	COMSOL® Multiphysics	The study examined how tissue size affects necrosis volume in RFA. Different tissue sizes were modeled using a two-compartment RFA model. Maximum necrosis volume was determined for each size with varying voltages, stopping at the first drop or after 12 minutes.	A finite element model was used to analyze RFA in tissue with temperature-dependent properties and blood perfusion. Different voltages were applied to determine the maximum necrosis volume per tissue size, emphasizing protocol adaptation according to the target size.	The study analyzed effects of factors (size, voltage, conductivity, blood flow, ablation time) on tissue during RFA. Temperature-dependent properties, including electrical conductivity, were considered.	Thermal and electrical parameters.	The study discusses computer simulations of RFA in tissues of different sizes. It was observed that the coagulated area/volume increases with voltage until a critical value, decreasing thereafter. RFA effectiveness decreases for tumors larger than 30 mm. Protocol adaptation is crucial. Comparison of RFA models and the need for more realism.	Study limitations: no experimental validation, no consideration of cooling effect by large blood vessels, no analysis of various tumor types. Need for future research to validate and enhance results. Also, suggested investigation of tissue size impact on pulsed RFA.
[46]	COMSOL® Multiphysics	Study examines boundary effects on liver cancer RFA models, especially near the edge. 3D liver models with artificial tumors from CT scans. Simulations show boundary conditions greatly impact potential, temperature, and coagulation. Emphasizes need for accurate boundary conditions in edge RFA simulations.	This study analyzed boundary effects on liver cancer RFA models using 3D liver models from CT scans. Various boundary conditions affected electric potential, temperature, and coagulation distribution. Proper boundary selection is crucial for accurate RFA simulations near the liver's edge.	The study tested diverse variables, including electric and thermal boundary conditions, ablation time, tissue impedance, temperature distribution, and thermal damage. Findings highlighted the crucial role of these conditions in shaping thermal ablation's effectiveness and extent over a 600-second protocol.	Thermal and electrical parameters.	Study examined effects of electrical and thermal boundary conditions on thermal ablation. Impedance profiles varied with conditions over time. Temperature distribution influenced by thermal conditions during heating and cooling. Incomplete ablation with body temperature, while insulation caused greater damage.	Study limitations include: 1) hypothetical ellipsoidal tumor shape; 2) not considering nearby organ's electrical and thermal effects near liver edge; 3) excluding larger blood vessel effects; 4) lack of experimental validation; 5) need for further investigation on appropriate boundary conditions. These might impact result generalization to real clinical cases.

Continuue

Author, Year/ Country	*Software*	*Objective*	*Methodology*	*Variable*	*Types of Analysis*	*Results*	*Limitations*
[47]	COMSOL® Multiphysics	This study assesses the impact of different electrode configurations in alternating bipolar RFA on liver cancer treatment. Computational modeling reveals that electrode arrangement, voltage, and ablation duration influence the size of the coagulation zone.	A computational model assessed bRFA efficacy for liver cancer treatment with different electrode setups. Varying operational conditions influenced thermal response and coagulation zone. Increasing input voltage or ablation duration expanded the coagulation zone, depending on electrode setup.	Study tested variables: electrode configurations (X, C, U, N, Z, O), input voltage (70 V, 90 V), ablation duration (5, 10 mins), and simultaneous ablation. Results showed electrode setup influenced thermal coagulation zone. Higher voltage and longer duration expanded coagulation. Simultaneous ablation increased coagulation compared to alternate.	Thermal and electrical parameters.	The study explored electrode configurations, input voltage, and ablation duration's effects on thermal coagulation zone in tumors. Voltage increased coagulation but led to more roll-offs. Prolonging ablation duration expanded the zone effectively. Simultaneous ablation with four needles showed promise but increased roll-offs. The findings stress these factors' importance in tumor RFA.	Study limitations: No in vivo validation; limited electrode configurations; spherical tumor focus, ignoring irregular shapes. Identical bipolar needles, no varied lengths; instant polarity changes without delays; further research needed for comprehensive clinical use.
[48]	COMSOL® Multiphysics	Study examined reversible and irreversible tissue conductivity effects on temperature distribution and coagulation zone in two-compartment RF ablation model. Irreversible changes had minimal impact on coagulation zone size, suggesting limited relevance.	Created two-compartment RF ablation model for liver tumors. Tested reversible/irreversible tissue conductivity changes due to temp/-coagulation. Simulations showed minimal impact on coagulation zone size from irreversible changes. Used controlled impedance protocol, verified models for accuracy.	Temperature distribution during RF ablation. Coagulation zone size concerning reversible/irreversible tissue conductivity changes. Tissue conductivity variations due to ablation-induced heating. Impact of tumor diameter on studied variables. RF ablation protocol involved constant voltage pulses with cooling periods.	Thermal and electrical parameters.	Comparison of two RFA models to evaluate reversible and irreversible tissue electrical conductivity changes. Similar results in coagulation zone and temperature distribution. Irreversible changes had minimal impact; conductivity equalized between healthy tissue and coagulated tumor in such models.	Study limitations: Speculated conductivity equalization, kidney data use, no experimental validation, limited thermal property consideration, Bioheat Equation assumptions. Model suited study's specific conditions.

Continuue

Author, Year/ Country	*Software*	*Objective*	*Methodology*	*Variable*	*Types of Analysis*	*Results*	*Limitations*
[2]	COMSOL® Multiphysics	Develop computational models to simulate impedance-controlled pulsing protocol in clinical RF generators for RFA. Evaluate model suitability by comparing computational results with previous experimental studies.	The study explored theoretical and computational models for radiofrequency catheter ablation. It investigated the impact of different parameters on coagulation zone formation, considering electrical, thermal properties, and boundary conditions, particularly with a cooled 17G electrode.	The study analyzed current, voltage, and tissue conditions' effects on coagulation zones during ablation. Vascular clamping impact was also assessed. Results emphasized parameter importance in procedure effectiveness.	Thermal and electrical parameters.	The study examined the impact of current and voltage pulses on tissue ablation, finding optimal protocols for each. Coagulation zone sizes varied with current, while voltage pulses up to 45 V were applied without impedance rise. Proper current and voltage selection proved crucial for effective tissue ablation.	Comparing computational and experimental results in clinical RFA is complex due to variable conditions and limited direct comparisons. Despite challenges, this study developed a model for simulating impedance-controlled pulses used in RFA practice.
[51]	COMSOL®	Evaluate systems based on their solution principles for RFA procedures using a theory known as axiomatic design.	RFA using an internally cooled cluster electrode to treat ellipsoidal-shaped hepatic tissue in a simulation environment with the FEM.	Temperature control system, timing, ellipsoid reproducibility, removed tissue.	Axiomatic design via FEM for tumor size and removal thoroughness.	By adding the internal cooling system to System 4, the maximum temperature during RFA is 99.451°C, preventing the Roll-off in this single RFA treatment. Otherwise, Roll-off would occur relatively early, resulting in generating only a small-sized TTN.	Diversification of the target tissue shape analyzed in the simulated ellipsoid. Case study, single assessment.

Continuue

Author, Year/ Country	*Software*	*Objective*	*Methodology*	*Variable*	*Types of Analysis*	*Results*	*Limitations*
[52]	COMSOL® e PYTHON®	Develop a mathematical model to assess the performance and variations of an esophageal-operated device.	Simulate RF ablation process in a simplified 2D axially symmetric model of a collapsed esophagus in contact with the left atrium, with and without the addition of a cooling device.	RF power, peak temperature, cooling device, time, lesion, and tissue depth.	FEM implemented in COMSOL® to analyze variables in the simulated organ model using governing equations.	Esophageal cooling reduced esophageal lesion depth, with cooling water acting as a thermal barrier. The device had a more pronounced effect on the esophagus than the myocardium, and temperature adjustment could optimize protection without impacting cardiac lesions.	Paving the way for computational models aimed at simulating RF ablation based on the ablation index, rather than fixed values for various parameters.
[58]	Mathematica® 6.0 software	Identifying under which circumstances of electrode geometry, electrode type, and blood perfusion the temperature reaches a steady state at any point within the tissue.	Compare the long-term thermal performance of the most commonly used electrode geometries (spherical/-cylindrical) in RF thermal ablation procedures.	All electrode geometries, electrode types, blood perfusion, tissue temperature.	Electrode geometry (needle vs. spherical tip), electrode type (dry vs. cooled), blood perfusion, and temperature.	Tissue temperature reaches a steady state in all cases except for cylindrical electrodes in non-perfused tissue. Spherical electrodes exhibited a more localized power distribution, while cooled electrodes displayed shifted temperature peaks, resulting in larger lesions.	The models didn't account for dynamic tissue characteristic changes. Electrical conductivity appears crucial, though not explicitly in the study's equations.
[53]	COMSOL® e MATLAB®	Investigate electric current transport, heat, boiling, and water diffusion within tissue during RF heating through a numerical model.	Simulate treatment process, investigate excessive water evaporation through a 2D symmetric cylindrical mathematical model.	Transport of electric currents and heat; water evaporation; RF energy deposition before or after charring.	2D symmetric cylindrical mathematical model numerical simulation for RF ablation mediated by mathematical equations.	Impedance variation during treatment indicates water evaporation. Internally cooled electrodes are beneficial in reducing evaporation. Impedance monitoring is crucial for enhancing thermal ablation outcomes.	The study employs a simplified mathematical model and assumes certain ideal conditions, such as tissue homogeneity and axial/radial symmetry.

Continuue

Author, Year/ Country	*Software*	*Objective*	*Methodology*	*Variable*	*Types of Analysis*	*Results*	*Limitations*
[54]	COMSOL® e ANYSIS®	Compare variable voltage calibration with temperature-dependent values against fixed voltage settings, and also compare the use of Pennes' Bioheat Equation (PBE) and Hyperbolic Bioheat Equation (HBE).	The symmetrical model was developed for a homogeneous tissue phantom prism of liver tissue, and a clinical multipolar electrode was incorporated.	Voltage calibration, temperature variation, fixed voltage, PBE (Pennes' Bioheat Equation), and HBE (hyperbolic bioheat equation).	Voltage calibration with temperature variation in four mathematical models using multipolar electrodes through FEM in COMSOL®.	Simulation results indicate higher temperature with the HBE method compared to the PBE method, but the difference is not significant.	Metallic thermocouples were employed, which might cause RF interference and impact temperature measurements.
[1]	COMSOL® e MATLAB®	Quantify the relationship between the ablation zone and the target tip temperature during RFA in various organs using a multi-tip electrode.	The computed simulation volume was compared with the coagulation volume from in vitro experimental studies during temperature-controlled RFA in a phantom gel mimicking tissue.	Tissue model; electrode; electrical conductivity; electrode tip target temperature; coagulation volume in target tissue.	A closed-loop PID controller was employed within the finite element model for conducting RFA. Coupling resolution for tissue necrosis.	A strong agreement was observed between computational and experimental outcomes regarding coagulation volume. The onset time of damage decreased with higher target temperatures, attributed to the applied input voltage.	The main limitation of the study is the consideration of a single-compartment model (i.e., a homogeneous model without tumor tissues).

Continuue

Author, Year/ Country	*Software*	*Objective*	*Methodology*	*Variable*	*Types of Analysis*	*Results*	*Limitations*
[36]	"COMSOL® and ANSYS®.	Developing a computational model for cardiac ablation with irrigated electrodes to study lesion size and blood temperature based on irrigation rate and electrode position.	A computational model simulates cardiac ablation with irrigated electrodes, validated against experimental data. It examines lesion size, blood temperature impact, saline irrigation rates, and electrode positions.	The study explored thermal lesion variations and blood temperature in cardiac tissue, considering various saline irrigation rates and electrode positions. A validated computational model was used, aligned with experimental data.	A model analyzed thermal lesion dimensions, variations, and peak blood temperature during ablation. It employed FEM, COMSOL® Multiphysics, and MATLAB for numerical solutions and power control. Validation was done by comparing with experimental data.	he study examined the impacts of irrigation rate and electrode position on RF ablation. Higher irrigation rates reduced lesion size and peak blood temperature. Electrode positioned parallel to the tissue led to larger lesions and higher blood temperature.	Limitations of the described computational model include simplified cardiac geometry, simplified properties of model elements, simplified boundary conditions, simplified governing equations, limited validation, and absence of dynamic interactions.
[24]	COMSOL® Multiphysics	The study aims to analyze temperature distribution and thermal coagulation size during RFA around an RF electrode in the liver, using a simplified geometric model and finite element approach.	A simplified liver model is created using finite elements. Equations are numerically solved with temperature-dependent electrical conductivity. The analysis includes temperature distribution, thermal coagulation around the RF electrode, and domain convergence study for model accuracy.	The study investigated how electrode length variables affect efficiency and heating speed in bipolar RFA, a medical procedure for treating tumors with controlled heat application.	The study analyzed electrode length variations, introduced parameter rl for quantifying effects, examined tissue impedance during ablation, and observed the relationship between electrode lengths and heating efficiency.	Reducing the active electrode length led to faster and more efficient tissue heating during bipolar RFA. This was evidenced by shorter time to the first roll-off and higher energy conversion into tissue heat.	Study limitations encompass geometric simplification of the liver, quasi-static approximation of Maxwell's equations, temperature-dependent electrical conductivity, finite element modeling simplifications, simplified boundary conditions, and lack of domain convergence study results.

Continuue

Author, Year/ Country	*Software*	*Objective*	*Methodology*	*Variable*	*Types of Analysis*	*Results*	*Limitations*
[169]	COMSOL®	The study aims to analyze the depth of lesions caused by ablation electrode in cardiac and esophageal tissues, using a 2D computational model and FEM. This aims to provide insights into the safety of the ablation procedure.	This study develops a 2D computational model to simulate the thermal and electrical behavior of cardiac and esophageal tissues. It examines the depth of lesions caused by the ablation electrode under various scenarios, offering insights into the procedure's safety.	Varied distances between electrode tip and esophagus wall (2.5 mm, 5 mm). Different tissue thickness scenarios for atrial and connective tissues (2.5 mm/2.5 mm and 1.5 mm/1 mm).	Modeling tissue responses, lesion depth measurement, analyzing cardiac tissues, and different distances between electrode and esophagus. Examining non-irrigated electrode, simulating lesions in various scenarios, evaluating commercial electrode's effective area.	Simulation results included electrode temperature (Te), control temperature (Tc), esophageal wall temperature (TPE), and lesion depth (D). Scenarios considered varying electrode-to-wall distance and tissue thickness, providing insights into esophageal wall temperature and lesion depth.	The model simplifies in 2D vs. 3D, assumes connective tissue as fat, and has constraints in electrode-wall distances. Uncertainties arise from CT measurements, structural aspects, lesion simulations, fixed electrode-tissue contact, varying commercial electrode area, and other assumptions.
[11]	COMSOL® Multiphysics	The study analyzes a non-irrigated ablation electrode's thermal effect and simulates temperature control during RFA. A coupled 2D computational model considers tissue properties to investigate lesion depth and scenario impacts.	A computational model simulates a non-irrigated electrode and temperature control using finite element analysis. Blood flow is considered through convective thermal coefficients. Boundary conditions are set, and simulations run for 60 seconds with a time step of 0.05 seconds.	Thermal conductivity, electrical conductivity, voltage, current, temperature, power, time, density, and electrode dimensions.	The study conducted temperature distribution analysis in tissue and blood, evaluated different ablation modes (constant voltage and constant temperature), compared results between methods, and investigated the effect of short ablations.	Results indicated that Method 4 (temperature control) achieved symmetric temperature distribution in blood and cardiac tissue. Methods 2 and 3 showed higher blood temperatures. All methods yielded similar lesion depths, but Method 3 had a wider lesion. Method 4 applied the most energy. Short-duration ablation had outcomes similar to 60-second ablation.	The model includes simplifications: no blood flow, neglect of key terms, and monopolar setup. Lack of experimental validation limits reliability. Applicability is restricted to specific geometry, may not cover all heat transfer aspects. No details on hardware or processing capabilities are provided.

Continuue

Author, Year/ Country	*Software*	*Objective*	*Methodology*	*Variable*	*Types of Analysis*	*Results*	*Limitations*
[56]	ANSYS®	Simulate RCFA, study thermal and mechanical responses linked to heartbeats, analyze various ablation depths and contact forces.	2D model, electrode in cardiac tissue, FEM with ANSYS, coupled electro-thermal-mechanical problem. Bioheat equation for heat, electrode movement in sine pattern. Defined electrical and thermal properties. Boundary conditions with initial temperature, constant RF power.	Thermal conductivity, electrical conductivity, voltage, current, temperature, power, time, density, procedure depth, and contact force.	Contact force analysis, insertion and removal analysis, thermal properties analysis, and comparative temperature analysis.	The model was verified and deemed suitable in terms of mesh and dimensions. There were no significant differences in lesions between static and dynamic contact force. Tissue hydration had a negligible effect on lesions. The model accurately predicted tissue depth and maximum temperature. Limitations must be considered when interpreting and applying results.	No modeling for high-temperature vapor explosions. Model limited to perpendicular catheter and 2D approach. Simplified blood thermal effect may overestimate lesion width. Basic electrode irrigation modeling. Limited contact force variation, only considering heartbeats. No viscous behavior in mechanical model, affecting accuracy in some scenarios.
[57]	COMSOL® Multiphysics	Assessing the impact of blood perfusion and saline injection during hepatic ablation.	Testing six different concentrations of saline solution.	Temperature; electrical dispersion; blood flow; saline solution flow.	Temperature variation.	Blood flow and saline perfusion have opposite influences on the ablation temperature.	No information.

Source: Own authorship

APPENDIX D – Systematic Review table results - ex vivo studies

Study	**Ex vivo Assays**	**Intervention**		**Ablation procedure**		**Outcomes**	
Author, Year/ Country	*Sample*	*Objective*	*Methodology*	*Variable analyzed*	*Laboratorial procedure*	*Results*	*Limitations*
[59]	Two freshly excised porcine hearts.	Developing an ex vivo experimental model of cardiac ablation.	Comparison between the ex vivo experimental model and the actual experiment.	Temperature	Porcine myocardium at 37°C; insertion of optical fibers with 2mm longitudinal spacing between them; section along the insertion after ablation.	Development of an experimentally calibrated finite element-based mathematical model for ex vivo cardiac ablation.	Experimental thickness variation and associated microstructure can introduce potential error in model fitting, and the material modeling lacks cardiac electromechanical couplings.
[60]	Porcine hepatic tissue	Provide relevant information about temperature distribution during RFA in liver tissue.	A semicylinder was carved from a single block of insulating material containing porcine liver tissue. Temperature was measured by thermal sensors on the electrodes and an infrared camera.	Temporal and spatial evolution of temperature within the electrode field and applied tissue. Tissue lesion, energy, and depth distribution.	Samples from pigs slaughtered within the last 2 days and refrigerated until testing.	Temperature distribution becomes more uniform as heating progresses, with peaks at the ends. The ends heat at different rates due to the asymmetry of spatial thermal source distributions and the electrode's heat sink.	The effects of the liquid-vapor phase change and to measure temperature distribution more accurately.

Continuue

Author, Year/ Country	*Sample*	*Objective*	*Methodology*	*Variable analyzed*	*Laboratorial procedure*	*Results*	*Limitations*
[61]	Porcine myocardium.	Developing a method using direct thermography for visualizing temperature kinetics without the need for intramyocardial thermoelectric elements.	Temperature was recorded using a thermal camera in an acrylic container with saline solution and an optical lens made of sapphire glass. An RFA generator was used as the energy source.	A total of n=50 coagulations were performed, each at 10, 20, 30, 40, and 50 W for 60 s, respectively. The neutral electrode is placed on the myocardial substrate with RFA conducted in monopolar mode.	The highest temperature is located at the myocardium surface, with an exponential decrease at increasing depths within the tissue.	Accurate and real-time temperature images of the myocardium were successfully obtained. The sapphire glass optical lens ensured reliable measurements. System calibration showed consistent results between temperature measurement methods.	The development should encompass a physiologically adjusted setup monitored by a conductivity meter, as well as a more distant position from the neutral electrode, incorporating three-dimensional thermographic detection.
[62]	Liver and neck veins of pigs.	Investigate the impact of blood flow on tissue cooling during RFA using the heat transfer parameter Nu and FEM.	FEM and the bioheat equation were employed to estimate temperature distribution using thermocouples in an experimental setup with a container of liver tissue-mimicking gel during RFA.	The positive voltage of the needle electrode was maintained at a constant 20 [V]. The flow rate was kept constant and controlled by a digital pump, similar to the flow conditions in the liver.	The specificity of the thermal properties of the tissues resulted in a variable cooling effect on the large blood vessel.	Given the individual tissue properties, the cooling effect of the vessel differed; in some samples, cooling became stronger with increasing temperature, while in others it was less pronounced.	Consideration of other factors beyond the cooling effect of the blood vessel, such as the diameter of the blood vessels.

Continuue

Author, Year/ Country	*Sample*	*Objective*	*Methodology*	*Variable analyzed*	*Laboratorial procedure*	*Results*	*Limitations*
[63]	The study was conducted on Landrace breed pigs. A total of 3 female pigs were used. Each pig underwent a total of 4 procedures, one in each hepatic lobe.	Study explored hybrid ablation with EP pulses preceding RFA to enhance coagulation volume by reducing blood perfusion's cooling effect.	Studied hybrid EP and RFA technique theoretically and in porcine experiments. Theoretical model considered materials and geometries. Results showed no added benefits of hybrid approach, as EP effects were masked by RFA. In vivo experiments found no significant differences, concluding hybrid technique didn't surpass standalone RFA.	Temperature, voltage and time.	Study conducted RFA and EP procedures in Landrace pigs using 3 cm Cool-tip catheters. Each pig had four treatments: RFA in one liver lobe, EP in another lobe, and combined EP and RFA in two lobes. RFA lasted 12 minutes with internal cooling. EP used eight 2000V, 100 ms pulses. Coagulation zones were assessed macroscopically after procedures.	Study examined hybrid EP and RFA ablation technique through simulations and in vivo pig experiments. Combined approach didn't outperform standalone RFA. EP's influence on blood flow during RFA was limited. Hybrid method showed no added benefits over RFA alone.	Study limitations include limited generalization to humans due to animal model use; small sample size impacting statistical reliability; short-term follow-up, limiting long-term effects assessment; primarily macroscopic analysis, excluding relevant clinical and histological parameters; specific parameters for EP and RFA combination were limited, missing other potential setups or parameter adjustments.

Source: Own authorship

APPENDIX E – PSO Flowchart

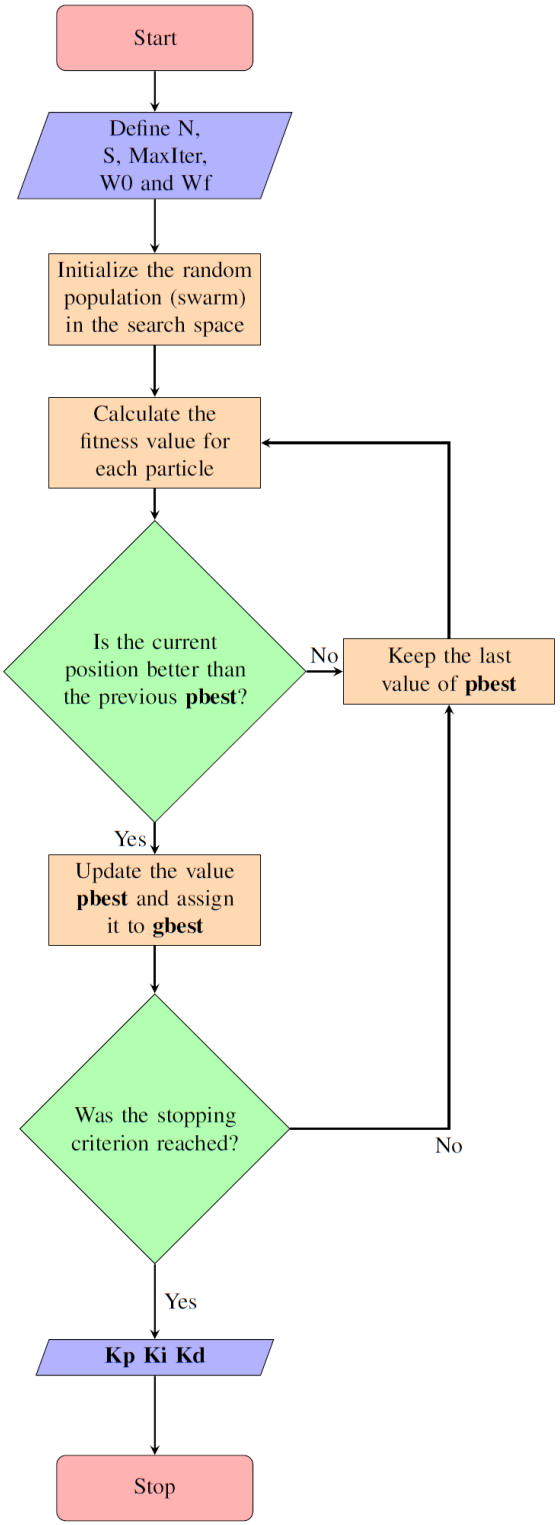

Figure 33 – PSO Flowchart
Source: Own authorship

APPENDIX F – GWO Flowchart

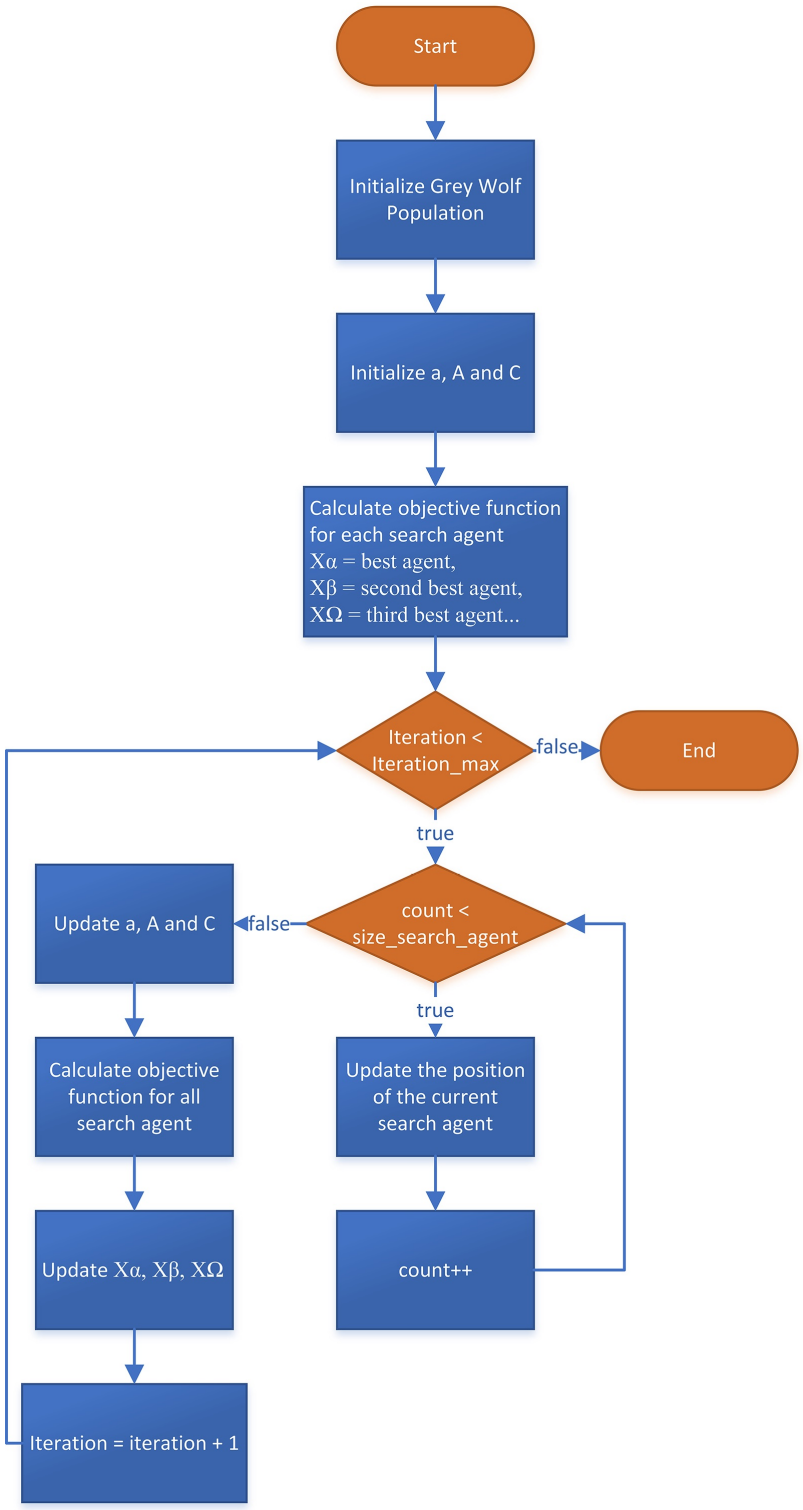

Figure 34 – GWO Flowchart
Source: [170]

APPENDIX G – Programming codes

ARX

Code G.1 – MATLAB Code: Main

```
% Bio-Inspired Solution for Roll-Off Control in Radiofrequency Ablation of Liver Tumors:
% A Particle Swarm Optimization Approach for PID Controller Tuning.
% ------------------------------------------------------------------------
% by Rafael Mendes Faria:
% Postgraduate Programme in Mechatronic Systems, Mechanical Engineering Department,
% University of Brasilia, Brasilia, Distrito Federal, 70910-900, Brazil;
% Federal Institute of Education, Science and Technology of Triângulo Mineiro,
% Paracatu, Minas Gerais, 38609-899, Brazil.
% June, 2023.
%%

clc
clear
close all
% ---- code begins
%% Estimation DATA
[EstimationData] = xlsread('rf_Estimation');
timeEST = EstimationData(:,1);
VoltageEST = EstimationData(:,2);
CurrentEST = EstimationData(:,3);
PowerEST = EstimationData(:,4);
ImpedanceEST = EstimationData(:,5);
[TimeEst,VoltageEstNew,ImpedanceEstNew] = ResampleEstimation(timeEST,ImpedanceEST,VoltageEST);

%% Validation DATA
[ValidationData] = xlsread('rf_Validation');
timeVAL = ValidationData(:,1);
VoltageVAL = ValidationData(:,2);
CurrentVAL = ValidationData(:,3);
PowerVAL = ValidationData(:,4);
ImpedanceVAL = ValidationData(:,5);
[TimeVal,VoltageValNew,ImpedanceValNew] = ResampleValidation(timeVAL,ImpedanceVAL,VoltageVAL);
%% Initial Plots
ExVivoElectricalQuantityPlot(timeEST,VoltageEST,CurrentEST, ...
PowerEST,timeVAL,VoltageVAL,CurrentVAL,PowerVAL)
```

```
%% ARX
na = 20;
nb = 20;
[yhat_TRA_OSA,yhat_VAL_OSA,Y1,Y2,p] =
ARX(VoltageEstNew,ImpedanceEstNew,VoltageValNew, ...
ImpedanceValNew,na,nb);

%% plot predictions
PlotPredictions(TimeEst,ImpedanceEstNew,TimeVal, ...
ImpedanceValNew,Y1,Y2,yhat_TRA_OSA,yhat_VAL_OSA)

%% Model Residuals OSA
[Residual] = ResidualsAnalyze(Y1,Y2,yhat_TRA_OSA,yhat_VAL_OSA)

%% Correlation Tests
plot_correlation(Y1-yhat_TRA_OSA,VoltageEstNew(p:end))
%% Plot Final Model - ARX --> FT
poles = 8; zeros = 6; % to descrete transfer function
[Discrete,Continuous,RouthHurwitzTable] =
PlotsARXtoTF(ImpedanceEstNew,VoltageEstNew,yhat_TRA_OSA, ...
VoltageValNew,ImpedanceValNew,poles,zeros,p)
```

The `rf-estimation.xlsx` and `rf-validation.xlsx` files are available in Fig 35.

Code G.2 – MATLAB Code: Resample Estimation Data

```
function [Ty7,Voltage7New,Impedance7New] =
   ResampleEstimation(time7,Impedance7,Voltage7)

[Impedance7New,Ty7] = resample(Impedance7,time7,1);
[Voltage7New,Ty7] = resample(Voltage7,time7,1);
Voltage7New = Voltage7New(1:end-3);
Ty7 = Ty7(1:end-3);
Impedance7New = Impedance7New(1:end-3);

end
```

Code G.3 – MATLAB Code: Resample Validation Data

```
function [Ty10,Voltage10New,Impedance10New] =
   ResampleValidation(time10,Impedance10,Voltage10)

[Impedance10New,Ty10] = resample(Impedance10,time10,1);
[Voltage10New,Ty10] = resample(Voltage10,time10,1);
Voltage10New = Voltage10New(1:end-4);
Ty10 = Ty10(1:end-4);
Impedance10New = Impedance10New(1:end-4);

end
```

Code G.4 – MATLAB Code: Ex-Vivo Electrical Quantities

```
function ExVivoEletricalQuantityPlot(time7,Tensao7,Corrente7, ...
Potencia7,time10,Tensao10,Corrente10,Potencia10)
figure;
subplot(3,2,1)
plot(time7,Tensao7,'LineWidth',2);
grid on
xlabel('Time(s)')
ylabel('Voltage (V)')
title('a) Voltage behavior - Estimation')
subplot(3,2,3)
plot(time7,Corrente7,'LineWidth',2);
grid on
xlabel('Time(s)')
ylabel('Current (A)')
title('b) Current behavior - Estimation')
time7 = time7(1:end-1);
Potencia7 = Potencia7(1:end-1);
subplot(3,2,5)
plot(time7,Potencia7,'LineWidth',2);
grid on
xlabel('Time(s)')
ylabel('Power (W)')
title('c) Power behavior - Estimation')
subplot(3,2,2)
plot(time10,Tensao10,'LineWidth',2);
grid on
xlabel('Time(s)')
ylabel('Voltage (V)')
title('d) Voltage behavior - Validation')
subplot(3,2,4)
plot(time10,Corrente10,'LineWidth',2);
grid on
xlabel('Time(s)')
ylabel('Current (A)')
title('e) Current behavior - Validation')
time10 = time10(1:end-1);
Potencia10 = Potencia10(1:end-1);
subplot(3,2,6)
plot(time10,Potencia10,'LineWidth',2);
grid on
xlabel('Time(s)')
ylabel('Power (W)')
title('f) Power behavior - Validation')
end
```

Code G.5 – MATLAB Code: ARX

```
function [yhat_TRA_OSA,yhat_VAL_OSA,Y1,Y2,p] =
   ARX(UTRA,YTRA,UVAL,YVAL,na,nb)
p = 1+max(na,nb);
[Phi, Y1] = matReg(YTRA,UTRA,na,nb,p);
```

```
[PhiVAL, Y2] = matReg(YVAL,UVAL,na,nb,p);

% estimate parameters:
th_hat = (Phi'*Phi)^(-1)*Phi'*Y1; % batch least squares

% one step ahead prediction
yhat_TRA_OSA = Phi*th_hat;
yhat_VAL_OSA = PhiVAL*th_hat;
end
```

Code G.6 – MATLAB Code: Regression matrix

```
function [phi, Y] = matReg(y,u,na,nb,p)

    N = length(y);
    Y = y(p:N);
    a=0;
    for i=1:(N-p+1)
        for j=1:na
            phiy(i,j) = -y(p+a-j);
        end
        a=a+1;
    end
    a=0;
    for i=1:(N-p+1)
        for j=1:nb
            phiu(i,j) = u(p+a-j);
        end
        a=a+1;
    end
    phi = [phiy phiu];

end
```

Code G.7 – MATLAB Code: Plot Predictions

```
function PlotPredictions(TimeEst,ImpedanceEstNew,TimeVal, ...
ImpedanceValNew,Y1,Y2,yhat_TRA_OSA,yhat_VAL_OSA)
figure
subplot(2,2,1)
plot(TimeEst,ImpedanceEstNew,'LineWidth',2);
grid on
xlabel('Time(s)')
ylabel('Impedance (\Omega)')
title('a) Measurements - Estimation')

subplot(2,2,2)
plot(TimeVal,ImpedanceValNew,'LineWidth',2);
grid on
xlabel('Time(s)')
ylabel('Impedance (\Omega)')
title('b) Measurements - Validation')
```

```
17
18 subplot(2,2,3)
19 plot([Y1 yhat_TRA_OSA],'LineWidth',2)
20 grid on
21 xlabel('Time(s)')
22 ylabel('Impedance (\Omega)')
23 title('c) Estimation phase - One-step-ahead prediction')
24 legend('Measured','One-step-ahead
      prediction','Location','Northwest')
25
26 subplot(2,2,4)
27 plot([Y2 yhat_VAL_OSA],'LineWidth',2)
28 grid on
29 xlabel('Time(s)')
30 ylabel('Impedance (\Omega)')
31 title('d) Validation phase - One-step-ahead prediction')
32 legend('Measured','One-step-ahead
      prediction','Location','Northwest')
33 end
```

Code G.8 – MATLAB Code: Residuals Analysis

```
1  function [Residual] =
      ResidualsAnalyze(Y1,Y2,yhat_TRA_OSA,yhat_VAL_OSA)
2
3  residual_OSA_TRA = Y1-yhat_TRA_OSA;
4  residual_OSA_VAL = Y2-yhat_VAL_OSA;
5  [MSE_OSA_TRA, R2_OSA_TRA, FITosa] = Residuals(residual_OSA_TRA,Y1);
6  [MSE_OSA_VAL, R2_OSA_VAL, FITval] = Residuals(residual_OSA_VAL,Y2);
7  %% calculate metrics
8  ErrorType = {'MSE';'R2';'Fit to estimation data'};
9  OSA_TRA = [MSE_OSA_TRA; R2_OSA_TRA; FITosa];
10 OSA_VAL = [MSE_OSA_VAL; R2_OSA_VAL; FITval];
11 Residual = table(ErrorType,OSA_TRA,OSA_VAL);
12
13 end
```

Code G.9 – MATLAB Code: Residuals

```
1  function [MSE, R2, FIT] = Residuals(erro,y)
2  N = length(y);
3  somaErro = 0;
4  somaY = 0;
5  for t=1:N
6      somaErro = somaErro+erro(t)^2;
7      somaY = somaY + (y(t)-mean(y))^2;
8  end
9  MSE = (1/N)*somaErro;
10 R2 = 1 - (somaErro/somaY);
11 NRMSE = sqrt(somaErro)/sqrt(somaY);
12 FIT = (1-NRMSE)*100;
13
```

```
end
```

Code G.10 – MATLAB Code: Correlations' Plots

```
function plot_correlation(error,inputs)
% --- plot correlation based tests
ml = 25;
N = length(inputs);

% --- plots
cf = 1.96/sqrt(N);
lv = -ml:ml;
conf = [ones(length(lv),1).*cf ones(length(lv),1).*-cf];

figure
subplot(5,1,1)
EE = crosscorrelation(error,error,ml);
plot(lv,EE,'k',lv,conf,'k:')
grid on
xlim([-ml ml]);
ylim([-1 1]);
ylabel('$\phi_{\xi\xi}(\tau)$','Interpreter','LaTex')
title('Correlation tests')

subplot(5,1,2)
UE = crosscorrelation(inputs,error,ml);
plot(lv,UE,'k',lv,conf,'k:')
grid on
xlim([-ml ml]);
ylim([-1 1]);
ylabel('$\phi_{u\xi}(\tau)$','Interpreter','LaTex')

subplot(5,1,3)
EEU =
crosscorrelation(error(1:end-1,1),error(2:end,1).*inputs(2:end,1),ml);
plot(lv,EEU,'k',lv,conf,'k:')
grid on
xlim([0 ml]);
ylim([-1 1]);
ylabel('$\phi_{\xi(\xi u)}(\tau)$','Interpreter','LaTex')

subplot(5,1,4)
U2E = crosscorrelation(inputs.^2 - mean(inputs.^2),error,ml);
plot(lv,U2E,'k',lv,conf,'k:')
grid on
xlim([-ml ml]);
ylim([-1 1]);
ylabel('$\phi_{(u^2)'' \xi}(\tau)$','Interpreter','LaTex')

subplot(5,1,5)
U2E2 = crosscorrelation(inputs.^2 - mean(inputs.^2),error.^2,ml);
plot(lv,U2E2,'k',lv,conf,'k:')
```

```
grid on
xlim([-ml ml]);
ylim([-1 1]);
ylabel('$\phi_{(u^2)'' \xi^2}(\tau)$','Interpreter','LaTex')
xlabel('$\tau$','Interpreter','LaTex')

end
```

Code G.11 – MATLAB Code: Cross Correlation

```
function coefs = crosscorrelation(x,y,ml)
% Calculate correlation coefficients.

if nargin>3 || nargin<2
   error('Wrong number of arguments');
elseif nargin==2,
   ml=25;
end

% Extract mean and make sure the vectors are column vectors
x = x(:)-mean(x);
y = y(:)-mean(y);
if length(x) ~= length(y)
   error('v and w must have the same length');
end
ml = min(ml,length(x)-1);   % Reduce maxlag if vectors are too
   short

normcoef=sqrt(sum(x.*x)*sum(y.*y));
coefs = zeros(ml+1,1);              % Allocate vector for
   correlation function
for k=0:ml,
   coefs(k+1) = sum(x(1:end-k).*y(k+1:end))/normcoef;
end

coefs2 = zeros(ml,1);              % Allocate vector for correlation
   function
for k=1:ml,
   coefs2(k) = sum(y(1:end-k).*x(k+1:end))/normcoef;
end

coefs = [flipud(coefs2);coefs];
```

Code G.12 – MATLAB Code: Plots: ARX to TF

```
function [Discrete,Continuous,RouthHurwitzTable] =
   PlotsARXtoTF(YTRA,UTRA,yhat_TRA_OSA,UVAL,YVAL,poles,zeros,p)

DadosInput = iddata(YTRA,UTRA,1);
DadosInputVAL = iddata(YVAL,UVAL,1);
DadosOutput = iddata(yhat_TRA_OSA,UTRA(p:end),1);
Discrete = tfest(DadosOutput, poles, zeros, 'Ts', 1)
```

```
Continuous = d2c(Discrete);

den = Continuous.Denominator;
num = Continuous.Numerator;
[RouthHurwitzTable] = RH(den);

figure
subplot(2,1,1)
compare(DadosInput,Continuous,'g-*')
grid on

subplot(2,1,2)
compare(DadosInputVAL,Continuous,'r-*')
grid on

figure
subplot(2,1,1)
step(Continuous)
grid on

subplot(2,1,2)
rlocus(Continuous)
grid on

end
```

Code G.13 – MATLAB Code: Routh-Hurwitz

```
function [TabelaRouthHurwitz] = RH(den)
%% Routh-Hurwitz Criterion
c = length(den);
S = zeros(c+1);
k=1;
K=1;
for i=1:c

    for j=1:c

        if i==1 && mod(j,2)==1
            S(i,k) = den(j);
            k=k+1;

        elseif i==2 && mod(j,2)==0
            S(i,K) = den(j);
            K=K+1;
        end
        if i>=3
            S(i,j) = -det(S([i-2 i-1],[1 j+1]))/S(i-1,1);
        end

    end
end
```

```
25
26 SignalTurn=0;
27 for i=1:c
28
29     if sign(S(i))*sign(S(i+1)) == -1
30         SignalTurn = SignalTurn+1;
31     end
32 end
33 if SignalTurn==0
34     fprintf('The system is stable.\n')
35 else
36     fprintf('The system is unstable and has %d roots (poles) in
       the right half-plane.\n', SignalTurn)
37 end
38 count=0;
39 for i=1:c
40     if S(1,i)==0
41         count = count+1;
42     end
43 end
44
45
46 TabelaRouthHurwitz = S(1:c,1:round((c)/2));
47 end
```

Particle Swarm Optimization

Code G.14 – MATLAB Code: Main

```
1  % Bio-Inspired Solution for Roll-Off Control in Radiofrequency
     Ablation of Liver Tumors:
2  % A Particle Swarm Optimization Approach for PID Controller Tuning.
3  %
     ------------------------------------------------------------------------
4  % by Rafael Mendes Faria:
5  % Postgraduate Programme in Mechatronic Systems, Mechanical
     Engineering Department,
6  % University of Brasilia, Brasilia, Distrito Federal, 70910-900,
     Brazil;
7  % Federal Institute of Education, Science and Technology of
     Triângulo Mineiro,
8  % Paracatu, Minas Gerais, 38609-899, Brazil.
9  % June, 2023.
10 %%
11 clear all
12 format short
13 close all
14 clc
15 tic
16 %% PSO PARAMETERS %%
```

```
Nparticles = 30;
Ndimensions = 3;
x_max = 10;
x_min = 0;
MaxIter = 10; % max number of iterations
w0 = 0.9;
wf = 0.1;
w=zeros(MaxIter,1);
w(1)= w0;
slope = (wf-w0)/MaxIter;
c1 = 2.05;
c2 = 2.05;
max_v =(x_max-x_min)*2 ;
ini_v = max_v/3;
%% PID TRANSFER FUNCTION - Provided on Identification
num = [32.43 135 510.3 925.7 1104 829.7 556.9 58.83 0.8122];
den = [1 2.119 15.76 21.61 55.28 46.8 49.14 24.45 7.278 0.5032];
%%
k = 1;  % index of iteration
%%
[Fbest,gBest,x,pBest,v] =
   Initialization(Nparticles,Ndimensions,x_min,x_max,ini_v);
%% ITERATIVE PROCESS
while k<= MaxIter

[Fbest,x,pBest] = PbestGbest(Nparticles,Fbest,x,pBest);
[bestfitness(k), p] = min(Fbest);
gBest = pBest(p,:);

[v,x] =
Update(Ndimensions,Nparticles,v,x,pBest,gBest,w,c1,c2,k,max_v,x_max);

k=k+1;
disp(k)
w(k) = w(k-1) + slope;
end
Kp = gBest(1); Ki = gBest(2); Kd = gBest(3);
PID = table(Kp,Ki,Kd)
[Routh_Hurwitz_Table] = ControlPlot(num,den,Kp,Ki,Kd,bestfitness)
%%
toc
```

Code G.15 – MATLAB Code: Initialization

```
function [Fbest,ys,x,y,v] =
   Initialization(Nparticles,Ndimentions,x_min,x_max,ini_v)

for j=1:Ndimentions
    for i=1:Nparticles
        x(i,j) = x_min + (x_max-x_min) * rand();
        y(i,j) = x_min + (x_max-x_min) * rand();
        v(i,j) = ini_v;
```

```
    end
end
    Fbest = 1e10*ones(Nparticles,1); % initialize best fitness
    ys = x_min + (x_max-x_min) * rand(1,Ndimentions);
end
```

Code G.16 – MATLAB Code: Pbest and Gbest

```
function [Fbest,x,y] = PbestGbest(Nparticles,Fbest,x,y)

for i = 1:Nparticles
    F(i,1) = PIDSimulation(x(i,:));
    if F(i) < Fbest(i)
        y(i,:) = x(i,:);
        Fbest(i) = F(i);
    end
end

end
```

Code G.17 – MATLAB Code: PID simulation - launch Simulink

```
function F = PIDSimulation(PID)
 Kp = PID(1);
 Ki = PID(2);
 Kd = PID(3);
 sp = 1;
 % Compute function value
 simopt = simset('solver','ode23','SrcWorkspace', ...
 'Current','DstWorkspace','Current');
 [tout,xout,yout] = sim('PIDSimulink',[0 10],simopt);
 sys_overshoot=abs(max(yout)-sp); % overshoot
 Alpha=0.5;Beta=0.6;Gamma=0.8;
 F=ISE*Beta+sys_overshoot*Alpha+Gamma*ITSE;

end
```

Code G.18 – MATLAB Code: Update positions and velocity

```
function [v,x] =
Update(Ndimensions,Nparticles,v,x,pBest,gBest,w,c1,c2,k,max_v,x_max)

for j = 1:Ndimensions
    for i=1:Nparticles
        r1 = rand();
        r2 = rand();
        v(i,j) = w(k)*v(i,j) + c1*r1*(pBest(i,j)-x(i,j)) +
           c2*r2*(gBest(j) - x(i,j));
        if abs(v(i,j)) > max_v
            if v(i,j) > 0
                v(i,j) = max_v;
```

```
            else
                v(i,j) = -max_v;
            end
        end
        x(i,j) = x(i,j) + v(i,j);
         if abs(x(i,j)) > x_max
            if x(i,j) > 0
                x(i,j) = x_max;
            else
                x(i,j) = -x_max;
            end
        end

    end
end

end
```

Code G.19 – MATLAB Code: Plots

```
function [Routh_Hurwitz_Table] =
   ControlPlot(num,den,Kp,Ki,Kd,bestfitness)

plant = tf(num,den);
control = tf([Kd Kp Ki],[1 0]);
Controled = control*plant;
sys = feedback(Controled,1);
[NUM DEN] = tfdata(sys, 'v');
[Routh_Hurwitz_Table] = RH(DEN);

figure
subplot(2,1,1)
step(plant)
grid on
subplot(2,1,2)
step(sys)
grid on

figure
subplot(2,1,1)
step(sys)
grid on
subplot(2,1,2)
rlocus(sys)
grid on
figure
semilogy(bestfitness,'-k');
grid on
xlabel('Iterations')
ylabel('Best Fitness')
title('Convergence')

```

```
end
```

Code G.20 – MATLAB Code: Routh-Hurwitz

```
function [TabelaRouthHurwitz] = RH(den)
%% Routh-Hurwitz Criterion
c = length(den);
S = zeros(c+1);
k=1;
K=1;
for i=1:c

    for j=1:c

        if i==1 && mod(j,2)==1
            S(i,k) = den(j);
            k=k+1;

        elseif i==2 && mod(j,2)==0
            S(i,K) = den(j);
            K=K+1;
        end
        if i>=3
            S(i,j) = -det(S([i-2 i-1],[1 j+1]))/S(i-1,1);
        end

    end
end

SignalTurn=0;
for i=1:c

    if sign(S(i))*sign(S(i+1)) == -1
        SignalTurn = SignalTurn+1;
    end
end
if SignalTurn==0
    fprintf('The system is stable.\n')
else
    fprintf('The system is unstable and has %d roots (poles) in
       the right half-plane.\n', SignalTurn)
end
count=0;
for i=1:c
    if S(1,i)==0
        count = count+1;
    end
end


TabelaRouthHurwitz = S(1:c,1:round((c)/2));
end
```

Grey Wolf Optimizer

Code G.21 – MATLAB Code: System Identification - thermocouple

```
clc
clear all
close all
format long

Data = xlsread('K');

k=1;
LineMinorZero = 27;
T = zeros(LineMinorZero,1);
V = zeros(LineMinorZero,1);
for i=1:length(Data)-4
    if i<=LineMinorZero
        for j=11:-1:2
            T(k,1) = Data(i+2,1)+Data(1,j);
            V(k,1) = Data(i+2,j);
            k=k+1;
        end
    else
%         pause()
        for j=2:11
            T(k,1) = Data(30+i-LineMinorZero,1)+Data(30,j);
            V(k,1) = Data(30+i-LineMinorZero,j);
            k=k+1;
        end
    end
end

FinalTable = [T V];

TermoparSys =
   iddata(V,T,'OutputName','Voltage','InputName','Temperature');
Transfer = tfest(TermoparSys,1,0)
compare(TermoparSys,Transfer)
grid on
[NUM DEN] = tfdata(Transfer, 'v');
[Routh_Hurwitz_Table] = RH(DEN)
```

Code G.22 – MATLAB Code: System Identification - Esophageal temperature

```
%% System Identification CETER
clc
clear all
close all
```

```
format long

Data = load('TempEsofago.txt');
Val = load('TempEsofago_Validation.txt');

SysID = iddata(Data(:,2),Data(:,3),0.1,'OutputName', ...
'Temperature','InputName','Voltage');
SysID_Val =
   iddata(Val(:,2),Val(:,3),0.1,'OutputName','Temperature', ...
'InputName','Voltage');

figure
plot(Data(:,1),Data(:,2))
title('Esophageal temperature')
xlabel('Time(s)')
ylabel('Temperature(degC)')
grid on
plant = tfest(SysID, 3)
figure
subplot(1,2,1)
compare(plant,SysID,'-g')
grid on
subplot(1,2,2)
compare(plant,SysID_Val,'-r')
grid on

[NUM DEN] = tfdata(plant, 'v');
[Routh_Hurwitz_Table] = RH(DEN)
```

The files `K.xlsx` [166], `TempEsofago.txt` and `TempEsofago-validation.txt` are available in Fig 35.

The GWO algorithm code used in this doctoral thesis was created by Mirjalili et. al. [161]. The code is available at: `https://seyedalimirjalili.com/gwo`

Figure 35 – Folder with files for system identification.

Annex

ANNEX A – Academic Productions

During this 37-month period in the Mechatronic Systems graduate program, all credits related to mandatory and elective courses were successfully completed. Additionally, academic productions were developed in parallel with the elaboration of the doctoral thesis.

Completed Productions:

- **Oliveira, R.H.d., Silva, M.d.S., Nunes, G.A.M.A. et al. Control engineering investigation of the effects of proliferative diabetic retinopathy on the crystalline lens and ciliary muscle dynamic behavior. Res. Biomed. Eng. (2023).** https://doi.org/10.1007/s42600-023-00297-5

- **Faria RM, Rosa SdSRF, Nunes GAMdA, Santos KS, de Souza RP, Benavides ADI, et al. (2024) Particle swarm optimization solution for roll-off control in radiofrequency ablation of liver tumors: Optimal search for PID controller tuning. PLoS ONE 19(6): e0300445.** https://doi.org/10.1371/journal.pone.0300445

- DYCAELS 2023 - Abstract and poster: **PID Controller Optimization Using the Grey Wolf Optimizer Algorithm for Roll-Off Displacement in Radiofrequency Ablation of Liver Tumors**

  Rafael Mendes Faria, Ana Karoline Almeida da Silva , Gustavo Adolfo Marcelino de Almeida Nunes,Klériston Silva Santos , Mário Fabrício Fleury Rosa , Suélia de Siqueira Rodrigues Fleury Rosa.

  https://dycaels2023.github.io/DYCAELS2023/accept.html

- **Understanding Acoustic Phenomena in Stenosed Coronary Arteries Through Bond Graph Modeling of Sound Generation**

  IEEE Engineering in Medicine and Biology Society : EMBS Student Paper Competition at the 46th Annual International Conference of Engineering in Medicine and Biology in Orlando, Florida.

  Loreto Rojas Sandoval, René Araya Ulloa, Ana Karoline Almeida da Silva, Gustavo Adolfo Marcelino de Almeida Nunes, Rafael Mendes Faria, José Parra Sepúlveda, Lindemberg Barreto Mota da Costa, Luca Rubilar Acevedo, Mário Fabrício Fleury Rosa, Esteban J. Pino, Suélia de Siqueira Rodrigues Fleury Rosa.

  https://epapers2.org/embc2024/ESR/paper_status.php - *paper 6334*.

- **Mathematical Modeling of the Impact of Diabetes Mellitus on a Neovascularized Human Blood Vessel**

  ICBGM 2024 - International conference on bond graph modeling and simulation.

  Marcos Augusto Moutinho Fonseca, Ana Karoline Almeida da Silva, Gustavo Adolfo Marcelino de Almeida Nunes, Luciana Alves Fernandes, Ronei Delfino da Fonseca Campos, Rafael Mendes Faria, Lindemberg Barreto Mota da Costa, Mário Fabrício Fleury Rosa, Suélia de Siqueira Rodrigues Fleury Rosa.

- **Mathematical Modeling in the Thermoregulation of Custom Organ-on-a-Chip Platform for Medical Equipment Testing**

  Mathematics in Science, Engineering, and Aerospace (ISSN 2041-3165) QUALIS CAPES B2

  Karoany M. M. Ibiapina, Christian F. Gonçalves, Ana K. A. da Silva, Gustavo A. M. A. Nunes, Mario F. F. Rosa, Rafael M. Faria, Harsson S. Santana, Adson F. da Rocha, Lindemberg B. M. da Costa, Kleriston S. S, Arthur C. Aguiar, Suélia S. R.F. Rosa.

  https://nonlinearstudies.com/index.php/mesa/index

Submitted Productions:

- **Optimizing temperature control with grey wolf optimizer to prevent esophageal fistula: a three-dimensional radiofrequency cardiac ablation model**
  PLoS ONE (ISSN 1932-6203).

  Rafael Faria, Sylvia Faria, Enrique Berjano, Ana Gonzáles-Suarez, Suélia Rosa, Ana Karoline Silva, Mayla Silva, Adson Rocha, Angélica Kathariny Alves, Gustavo Nunes, Mário Fabrício Rosa and Ícaro Santos.

  https://journals.plos.org/plosone/

- **Organ-on-a-Chip for diabetic wound foot neovascularization: a systematic review of preclinical studies and future directions**
  PLoS ONE (ISSN 1932-6203).

  Ana Karoline Almeida da Silva, Suelia de Siqueira Rodrigues Fleury Rosa, Gustavo Adolfo Marcelino de Almeida Nunes, Rafael Mendes Faria, Klériston Silva Santos, Rafael Pissinati de Souza, Lindemberg Barreto Mota da Costa, Marcos Augusto Moutinho Fonseca, Sheila Sousa Gomes Fortes, Amanda Maciel Lima, Isolda de Sousa Monteiro, Pedro Henrique Silva de Almeida, Ana Carolina Migliorini Figueira, Harsson Silva Santana, Marcella Lemos Brettas Carneiro, Glécia Virgolino da Silva Luza, Graziella Anselmo Joanitti, José Carlos Tatmatsu Rocha, Mário Fabrício Fleury Rosa, Paulo Sérgio França, Maria Alice Martins, Ícaro Santos, Emanuel Carrilho.

- **State-of-the-Art Organ-on-Chip Models and Designs for Medical Applications: A Systematic Review**
  PLoS ONE (ISSN 1932-6203).

  Gustavo Adolfo Marcelino de Almeida Nunes, Suélia de Siqueira Rodrigues Fleury Rosa Senior, IEEE, Ana Karoline Almeida da Silva, Rafael Mendes Faria Member, IEEE, Klériston Silva Santos, Lindemberg Barreto Mota da Costa, Arthur da Costa Aguiar, Glécia Virgolino da Silva Luz, Marcella Lemos Brettas Carneiro, Adson Ferreira da Rocha, Mário Fabrício Fleury Rosa, Graziella Anselmo Joanitti, José Carlos Tatmatsu Rocha, Emanuel Carrilho, Harsson Silva Santana.

- Book Chapter: **Engineering principles for organs-on-a-chip: a detailed exploration of design and construction**

  Book: Disruptive Technology: Maximizing Efficiency with Organ-on-a-Chip

  Ana Karoline Almeida da Silva, Gustavo Adolfo Marcelino de Almeida Nunes, Mário Fabrício Fleury Rosa, Rafael Mendes Faria, Newton de Faria, Lindemberg Barreto da Mota Costa, Suélia de Siqueira Rodrigues Fleury Rosa.

- **Modeling Capillaries in Diabetic Wound Foot with Bond Graph: Integrating Engineering and Health Using Ankle-Brachial Index**

  IEEE Transactions on Biomedical Engineering (ISSN 0018-9294) - QUALIS CAPES A1.

  Ana Karoline Almeida da Silva, Rafael Mendes Faria, Newton de Faria, Gustavo Adolfo Marcelino de Almeida Nunes, Lindemberg Barreto Mota da Costa, Mário Fabrício Fleury Rosa, Adson Ferreira da Rocha, José Carlos Tatmatsu Rocha and Suelia de Siqueira Rodrigues Fleury Rosa.

  https://ieeexplore.ieee.org/xpl/RecentIssue.jsp?punumber=10

- SOBENFeE - Abstract: **CHIP-Eny: Desenvolvendo uma alternativa inovadora para o Tratamento de Doenã dos Pés relacionada a Diabetes**

  Ana Karoline Almeida Da Silva, Gustavo Adolfo Marcelino De Almeida Nunes, Francisca Rayane Feitoza Lêdo, Mário Fabrício Fleury Rosa , Rafael Mendes Faria 3, Tiago Martins De Brito, Lindemberg Barreto Mota Da Costa, Suélia De Siqueira Rodrigues Fleury Rosa.

  https://www.sobenfee.org.br/trabalhos-cientificos

Ongoing Productions:

- **Advancements in Radiofrequency Ablation: A Systematic Analysis of Mathematical Modeling Techniques and Temperature Control Strategies**

Rafael Faria, Suelia Rosa, Ana Karoline Silva, Kléríston Santos, Arthur Aguiar, Rafael Pissinati, Gustavo Nunes, Lindemberg Barreto.

- **Modelling and dynamic responses of SARS-CoV-2 inactivation during chitosan nanoparticle interaction**

  M. A. M. Fonseca, M. G. Landim, L. A. Fernandes, R. M. Faria, R. D. Fonseca, M. S. Monteiro, M. F. Fleury Rosa, S. S. R. Fleury Rosa

- **Wearable respiratory change analyser to assess sequelae in patients with Covid-19 after discharge**

  Allisson Lopes Oliveira, João Pedro Castro de Souza, Kleriston Silva Santos, Rafael Mendes Faria, Gustavo Luiz Sandri, Suélia de Siqueira Rodrigues Fleury Rosa.

Patents Filed:

- Process SEI 23106.068727/2023-14 - "Firmware de testes dos módulos do circuito do equipamento ARFACTA - Ablação por Radiofrequência com Ajuste de Frequência e Controle de Temperatura para uma Ablação Abrangente e Eficiente". No: BR512023002028-1.

- ARFACTA - Ablação por Radiofrequência com Ajuste de Frequência e Controle de Temperatura para uma Ablação Abrangente e Eficiente". Demanda 78-1123-ARFACTA - Núcleo de Propriedade Intelectual (NUPITEC - UnB).